Proceedings of the First International Workshop on

FRONTIER SCIENCE 2002 – CHARM, BEAUTY and CP

FRASCATI PHYSICS SERIES

Series Editor
Stefano Bianco

Technical Editor
Luigina Invidia

Cover:

The cartoon in the front cover was made by our collegue Luca Lista, a physicist from INFN Naples, who was able to portrait in a few quite effective pencil strokes a true story! This is what really happened to one of the participants to the Conference while applying for a visa in the italian Consulate in Moscow. The qui pro quo was readily clarified, and she was then able to tell us this funny story in person. We found it worth sharing with all of you.

Volume XXXI

Istituto Nazionale di Fisica Nucleare – Laboratori Nazionali di Frascati
Divisione Ricerca – SIS – Ufficio Pubblicazioni
P.O. Box 13, I–00044 Frascati (Roma) Italy
email: sis.publications@lnf.infn.it

FRASCATI PHYSICS SERIES

Proceedings of the First International Workshop on
FRONTIER SCIENCE 2002 – CHARM, BEAUTY and CP

ISBN 88-86409-37-0

Printed in Italy
by Poligrafica Laziale
P.le della Stazione 4/6, 00044 Frascati

FRASCATI PHYSICS SERIES

Volume XXXI

Proceedings of the First International Workshop on

FRONTIER SCIENCE 2002 – CHARM, BEAUTY and CP

Editors
L. Benussi, R. de Sangro, F.L. Fabbri, P. Valente

Frascati, October 6 –11, 2002

International Advisory Committee

J.–J. Aubert	*IN2P3*
J. Butler	*Fermilab*
J. Dorfan	*SLAC*
E. Iarocci	*INFN*
L. Maiani	*CERN*
H. Sugawara	*KEK*
A.N. Skrinsky	*Novosibirsk*
A. Wagner	*DESY*
M. Witherell	*Fermilab*

Steering Committee

Permanent Members:

G. Casali	*Como University*
F.L. Fabbri	*INFN – Frascati*
G. Pancheri	*INFN – Frascati*
S. Ratti	*INFN – Pavia University*

2002 Scientific Secretary

S. Bianco	*INFN – Frascati*

Local Organizing Committee

L. Benussi	*INFN – Frascati*
M: Bertani	*INFN – Frascati*
S. Bianco	*INFN – Frascati*
O. Ciaffoni	*INFN – Frascati*
E. De Lucia	*INFN – Roma 1*
P. de Simone	*INFN – Frascati*
R. de Sangro	*INFN – Frascati*
F.L. Fabbri	*INFN – Frascati (Chair)*
S. Giromini	*INFN – Frascati*
F. Grancagnolo	*Lecce University*
G. Isidori	*INFN – Frascati*
A. La Monaca	*INFN – Frascati*
M. Moulson	*INFN– Frascati*
E. Pace	*INFN – Frascati*
G. Pancheri	*INFN – Frascati*
P. Valente	*INFN – Frascati*

Secretary

M. Legramante	*INFN – Frascati*

2002 Program Committee

H. Aihara	*Tokyo University*
J.A. Appel	*Fermilab*
I. Bigi	*Notre Dame University*
M. Calvetti	*INFN, Pisa University*
N. Ellis	*CERN*
B. Foster	*Bristol University*
R. Galik	*Cornell University*
A. Goshaw	*Duke University*
M. Kienzle	*Geneva University*
P. Laurelli	*INFN – Frascati*
A.J. Smith	*Princeton University*
S. Stone	*Cornell*

Scientific Secretary

M. Alfonsi	*Roma 1 University*
T. Capussella	*Napoli University*
C. Gatti	*Roma 1 University*
F. Perfetto	*Napoli University*
M. Plo Lener	*Roma 2 University*
S. Stone	*Cornell*

Secretariat

S. Colasanti	*INFN – Frascati*
L. Sabatini	*INFN – Frascati*

PREFACE

This volume contains the oral presentations of the first Frontier Science International Conference held at the Frascati Laboratory from 6 to 11 October 2002. About 150 people from 18 countries participated in the conference.

This new series of conferences is held in alternate years at Frascati and Pavia, Italy. Each conference focuses on one topic, selected from among the most dynamic in nuclear and sub-nuclear physics, astrophysics, mathematics, theoretical physics, earth science, instrumentation, electronics, computing, and others. The series is organised into plenary sessions, devoted partly to invited talks by senior scientists and partly to selected presentations by young researchers, and a poster session. Each year, special awards and credits are given to significant contributions presented at the conference by young researchers. A further mission of the series is to convey to the general public the importance of the field identified as a frontier in modern science.

This first conference was dedicated to the physics of charm, beauty and CP violation, with special emphasis on experimental results from operating facilities and on future projects and programs. The main topics were heavy-quark production and hadron decays, CP violation and mixing, heavy-flavour spectroscopy, leptonic and semileptonic decays, rare and forbidden decays, instrumentation and facilities.

The organisation of the conference had three challenging focal points. The first was obviously scientific. This was a time when physics at the meson facilities Bbar and Belle was provided exciting new results. A new era was beginning for the topics under discussion and, as John Ellis said in his remarkable concluding talk: "Providing a comprehensive and scientific programme has been a very exciting and motivating task". If this was so, as the success of the conference seems to show, most of the merit goes to the Programme Committee members, who helped us in suggesting excellent reviewers.

The second task was no less compelling The innovative format of the conference, that is, mixing distinguished senior physicists and young researchers, poses both organisational as well as scientific issues. From the young researchers, we received about 60 presentations, 90% of which presented at the plenary sessions as accepted contributions or short talks. Fifteen of these presentations were selected for the Frontier Science Awards by a jury chaired by Sergio Bertolucci and Brad Cox. Our sincere thanks

to Sergio and Brad for having accepted this difficult task. The best posters, instead, were selected on the basis of the votes cast by all the attendees at the poster session. The Award winners were: Tommaso Boccali, Tim Christiansen, Pasquale Di Nezza, Ulrik Egede, Marc Holfeld, Alexey Petrov, Marco Rovere, Paolo Rumerio, Ilaria Segoni.

The third task was to establish an outreach activity on the topics of the conference. A lecture open to the public was given in Italian by Antonino Zichichi and had an attendance of about 400 people. An educational Web site "ScienzaperTutti" http://www.lnf.infn.it was realized and started up by fthe Frontier Science Organising Committee. The site is now successfully operating .

The conference was a success in all these aspects and the new series has been well and solidly established.

On behalf of the organizers I would like to thank the International Advisory Committee members for their valuable advice and support all along the course of the conference organisation. Our gratitude goes to all our reviewers, who did an excellent job and inspired lively discussions on their subjects, to Marina Arturo and Clara Matteuzzi, who organised and chaired a stimulating round table on the "Future in Flavour", and to all the speakers for their contributions.

I personally would like to thank the Frascati Laboratory Director for his continuous support and for having assured the smooth running of the conference activities by providing help from the laboratory services, the people of the Servizio Informazione Scientifica for their constant support, Lia Sabatini, Rossana Centioni and Maddalena Legramante for their day-by-day assistance in all administrative and organisational issues, and Luigina Invidia for assistance in editing these proceedings.

Franco Luigi Fabbri

FrontierScience Awards

The Frontier Science Organizing Committee, to encourage and promote the participation of young researchers to the event, has presented a number of selected young physicists with a FrontierScience Award for the best oral contributions and posters.

An international jury of senior physicists participating at the conference has evaluated the young physicist oral contributions on the basis of the scientific relevance, clearness and originality, while the best posters have been selected based on the votes cast by all the attendees during the poster session.

The awarded researchers of the two categories are:

Best Oral Presentation by a Young Physicist

1° Pasquale Di Nezza
2° Alexey Petrov
3° Ulrik Egede
4° Paolo Rumerio

Best Poster by a Young Physicist

1° Ilaria Segoni
2° Marco Rovere
3° Tim Christiansen
4° (ex equo) Marc Holfeld
4° (ex equo) Tommaso Boccali

Frontier Science 2002 - Charm, Beauty and CP

The workshop is dedicated to heavy-quark production and spectroscopy, leptonic and semileptonic decays, CP violation, mixing, detectors and new facilities. Invited speakers will review key topics while young researchers will present recent scientific achievements.

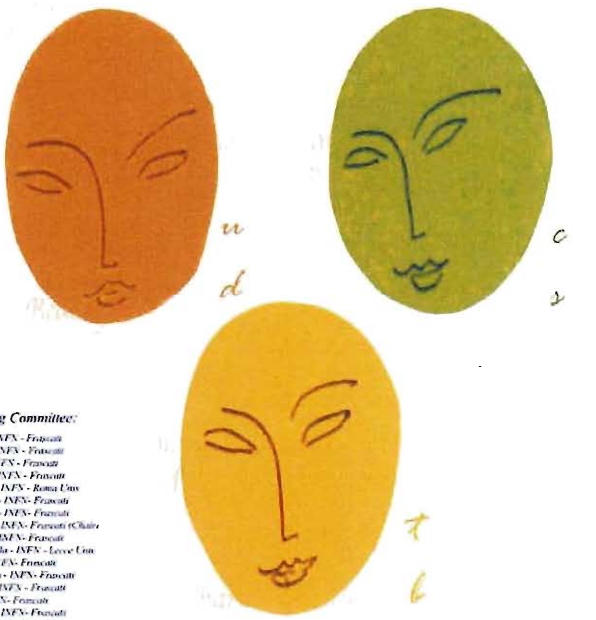

E_mail: FrontierScience@lnf.infn.it - http://FrontierScience.lnf.infn.it
Laboratori Nazionali di Frascati - Via E.Fermi 40, 00044 Frascati Italy - Phone: +390694032791 - Fax: +390694032900

36

CONTENTS

Heavy Flavour QCD – Session I

Chairpersons: F.L. Fabbri, B. Cox

D.H. Saxon	Heavy Quark Production
F.R. Spada	Charm Physics in the Neutrino Emulsions
T. Boccali	Model Independent Measurement of the Fragmentation of b Quarks into B Meson
P. Achard	Charm and Beauty Production in Two Photon Collisions at LEP
J.S. Russ	First Observation of a Family of Double-Charm Barions
P. Nason	Heavy Flavours Production

Frascati Physics Series Vol. XXXI (2003), pp. 3–10
FRONTIERSCIENCE 2002 – Frascati, October 6–11, 2002
Invited Review Talk in Plenary Session

HEAVY QUARK PRODUCTION

D H Saxon
Dept of Physics and Astronomy, University of Glasgow, Glasgow, G12 8QQ, Scotland

ABSTRACT

The quality of the data on charm and beauty production is improving fast, with new techniques reported at HERA and the TeVatron. Charm fragmentation at HERA looks the same as at LEP. There is evidence for charm content in the photon and fair agreement between theory and data in DIS. Beauty production at LEP agrees with astounding precision with theory, but at TeVatron and HERA there are 70% discrepancies between theory and results. Future accelerator running with the upgraded detectors will lead to a great improvement in understanding.

1 Introduction

This article is an experimental review of open heavy flavour production, principally in *ep* collisions, but with some reference to TeVatron and LEP results,

concentrating on results which are new since the review by Bussey [1]. (Theoretical aspects are dealt with in the talk by Nason in these proceedings.) There has been considerable progress in technique. In charm-finding H1 use decay length tagging as well as mass peaks, and the CDF two-track trigger will greatly increase charm samples. In beauty-finding results are available using muon impact parameter as well as p_T^{rel} of the muon relative to jets and for the first time also $D^*\mu$ correlations. The situation on charm measurements is relatively healthy. Comparison of the increasing number of beauty results to theory still leaves more questions than answers.

2 Charm production

The traditional method of identifying charm events is through the decay chain $D^{*+} \to D^0\pi_s^+, D^0 \to K^-\pi^+$, looking for a peak in the $K^-\pi^+$ mass spectrum in events with a tagged by $\Delta m = (m(K^-\pi^+\pi_s^+) - m(K^-\pi^+))$ close to 145 MeV. Charm signals are also seen in the $K^-\pi^+$ mass spectrum without the D^* tag. H1 see a modest peak in $D^+ \to K^-\pi^+\pi^+$ on a huge combinatorial background. This is massively improved using the H1 silicon tracker to add a decay length tag, and charm signals are seen for D^+, D^0, D_s and D^{*+} in DIS for $2 < Q^2 < 100$ GeV^2, typically for $p_T > 2.5$ GeV and $|\eta(D)| < 1.5$. Leading order plus parton shower Monte Carlos such as Aroma [2] provide a good description in normalisation and shape of the distributions in p_T, Q^2, η and y.(see figure 1.)

Having these four channels available allows one to compare charm fragmentation parameters in DIS with those found at LEP. H1 find $R(u/d) = 1.26 \pm 0.11 \pm 0.04$, $\gamma_s = 0.36 \pm 0.10 \pm 0.04$ and $V/(P+V) = 0.693 \pm 0.045 \pm 0.006$ or $0.613 \pm 0.061^{+0.033}_{-0.088}$, depending on the assumptions made about u/d universality. These are in reasonable agreement with the world averages of $1.00 \pm 0.09, 0.26 \pm 0.07$ and 0.601 ± 0.032 respectively. ZEUS have compared the distribution in $z = (E + p_\parallel)/2E_{jet}$ with LEP and CLEO data and find agreement within the modest errors on all these. [3] One concludes that charm fragmentation in DIS looks like charm fragmentation in e^+e^- annihilations.

The NLO-DGLAP model HVQDIS [4] (with the gluon ladder ordered in k_T) describes differential cross-section distributions well, but double differential distributions such as the rapidity spectrum of D^* for different p_T bins are less well described. HVQDIS lies below the forward D^* data. Cascade (using CCFM parton shower distributions, where the gluon ladder is ordered in

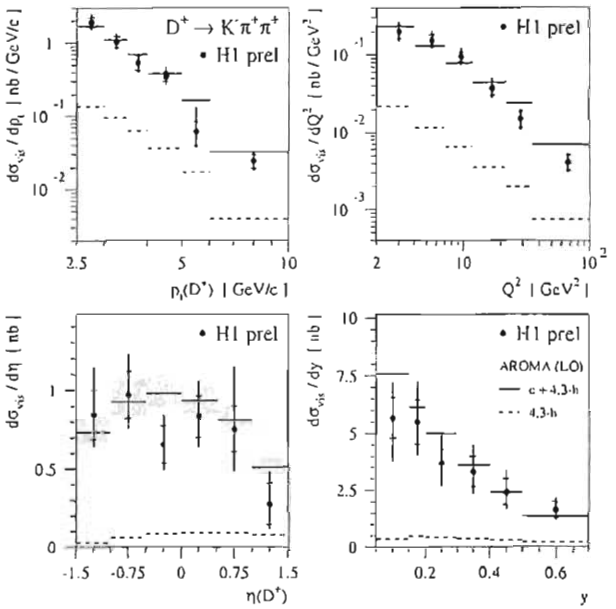

Figure 1: D^+ *inclusive distributions in deep inelastic scattering compared to Monte Carlo calculations*

rapidity) seems to do better. [5]

The structure function $F_2^{c\bar{c}}$ can be determined from the D^* rate. There is a large extrapolation to reach full acceptance, so one has to watch the model assumptions made in doing this. Both ZEUS and H1 have done this in the NLO DGLAP scheme. The scaling violations have a steeper Q^2 dependence than F_2, such that charm contributes about 50% of the scaling violation in F_2. One can make further assumptions and calculate the gluon distribution $xg(x)$ from D^* production in DIS and photoproduction. H1 find results very consistent with $xg(x)$ obtained from scaling violations in DIS. [6] H1 have also calculated $F_2^{c\bar{c}}$ in the CCFM scheme.The extrapolation factors are smaller (which is good) and the value of $F_2^{c\bar{c}}$ found tends to be lower. To understand this fully presumably needs a lot of work on F_2^{CCFM}, comparable to that over the years on F_2^{DGLAP}. Watch this space.

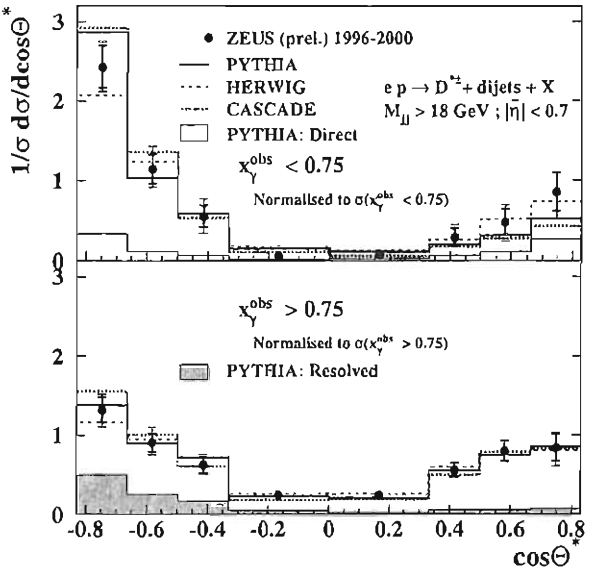

Figure 2: *Photoproduced D^* angular distribution in $\gamma^* p$ centre of mass*

ZEUS have studied D^{*+} photoproduction for $1.9 < p_T < 20$ GeV, $|\eta| < 1.6$ and $130 < W < 285$ GeV looking at distributions of p_T, η, W and $z(D^*)$. Theory (NLO or FONLL) agrees reasonably in shape but lies somewhat below the data in normalisation.

More information about the origin of charm in photoproduction is obtained by studying $\gamma p \to c\bar{c}X$ in events with two jets and a D^* tag. Experimentally one histograms the fraction of the energy in each event which is contained in the two highest-E_T jets, $(x_\gamma^{obs} = (\Sigma_{j=1,2} E_{T,j} e_j^{-\eta})/2yE_e)$. The region $x_\gamma^{obs} > 0.75$ is dominated by direct photon-gluon fusion with a hard quark exchange. In the γp centre-of-mass frame this leads to a jet angular distribution proportional to $1/(1 - \cos\theta^*)$. The $x_\gamma^{obs} < 0.75$ region includes the possibility of a $c\bar{c}$ pair being resolved within the structure of the photon. One of these is struck by a hard gluon and recoils from the photon with an angular distribution of $1/(1 + \cos\theta^*)^2$. A strong backward peak is found in the

data, providing clear evidence for charm content in the photon. [7] (see figure 2.) Monte Carlo calculations based on Pythia, Herwig or Cascade describe the distributions fairly well.

The ratio, $(R = \sigma(x_\gamma^{obs} < 0.75)/\sigma(x_\gamma^{obs} > 0.75))$, for $(\gamma p \rightarrow$ two jets) events is sensitive to the resolved photon structure. For all two-jet events this ratio exceeds 1 for photoproduction (rising to 2 for jets at lower E_T) and falls to around 0.3 (depending on E_T) for $Q^2 > 100$ GeV^2. For events with a charm tag the ratio is flat at about 0.6 independent of Q^2.This result is described by various approaches: SAS1D describe it in terms of γ^* structure. Cascade and Aroma avoid assumptions on γ^* structure and produce low values of x_γ^{obs} by parton shower evolution. Aroma, using DGLAP evolution, somewhat underpredicts this effect. Cascade, using CCFM evolution, lies closer to the data.

There is a curious anomaly reported by ZEUS in that D^* production in e^+p is less than in e^-p at the highest x and Q^2 values. The result (a factor of two over several bins) persists after checks for many types of experimental error. It is not understood. [7]

ZEUS report on D^* production in diffractive DIS, [7] selecting events on the basis of the most forward energy deposit, $(\eta_{max} < 3.0.)$ This includes $(6.3 \pm 0.6^{+0.3}_{-0.7} \pm 0.3)\%$ of all D^* in DIS. Seven distributions are studied and described by models either having a gluon structure within the Pomeron (where the result falls between the $c\bar{c}$ and the $c\bar{c}g$ models of BJLW,) or using gluon ladders or higher order processes instead of an explicit Pomeron.

CDF report first results from their new two-track trigger, which is producing a step increase in quality of data. beautiful signals are seen for $D^0 \rightarrow KK$, $D^0 \rightarrow \pi\pi$, $D^+ \rightarrow \phi\pi^+$ and $D_s \rightarrow \phi\pi^+$. Exclusive beauty hadronic decays such as $B^\pm \rightarrow D^0\pi \rightarrow K\pi\pi$ are found after selecting on the D^0 impact parameter. We may expect significant new physics results on charm and beauty production in the future. [8]

3 Beauty production

Beauty production in e^+e^- annihilation is extraordinarily precisely measured and agrees astoundingly well with theory and model predictions. The b-fraction and the b-fragmentation are exemplary, and 2% effects on gluon emission are used to measure precisely m_b. [9] It is therefore something of a shock to realise that in pp and ep collisions there are big discrepancies between theory and

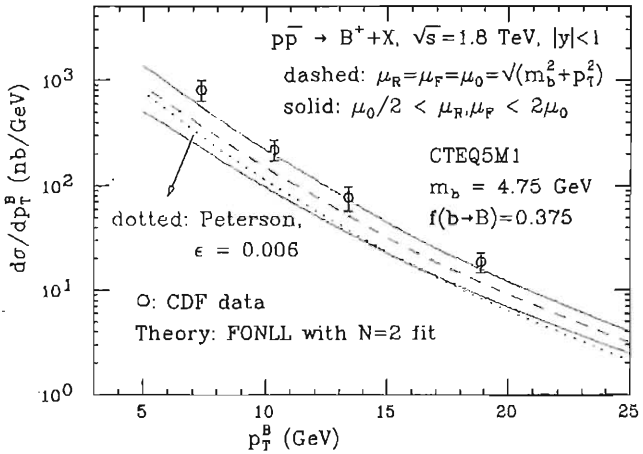

Figure 3: *CDF results on B^+ production compared to calculations*

data.

CDF run I measured b-production via $B^+ \rightarrow J/\psi K^+$ for $p_T < 20$ GeV and found a signal 2.9 times theory. Revisiting the theory, [8] with revised fragmentation functions and updating the calculation (FONLL) has reduced this ratio to 1.7. A similar story is found in D0. Jung reports a new fit using Cascade (CCFM-based) that goes well through the data points. [5] We can expect an improvement in the data with the upgrades to the TeVatron detectors. The high b-tagging efficiency means we can look at $b\bar{b}$ correlations. Studies of angular differences between two tagged jets will discriminate between different production mechanisms.

Beauty production at HERA has been studied using muons close to jets and using the p_T^{rel} of the muon relative to the jet. ZEUS and H1 report event samples which are (27±3)% beauty with a large fake muon component. H1 have shown results also using the muon impact parameter. The method is partially independent, and yields similar purity (26 ± 5)%. For photoproduction with $p_T^\mu > 2$ GeV, $35° < \theta < 130°$ and k_T-jets with $E_T > 5$ GeV, H1 report a cross section of $(160 \pm 16 \pm 29)$ pb, which is a factor 2.4 to 4 times higher than NLOQCD(FMNR), Cascade, or Aroma prediction. ZEUS show differential

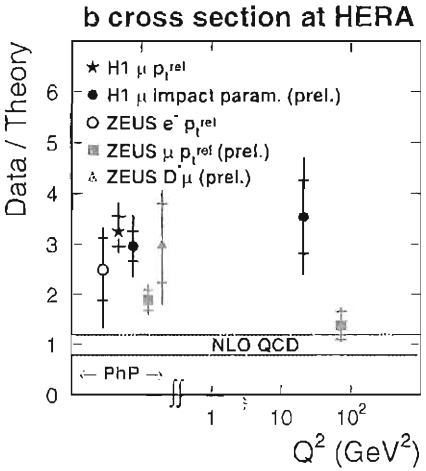

Figure 4: *Summary of b-production comparisons of data and theory*

cross-sections in rapidity (range -1.6 to 2.3) and p_T^μ (range 3 to 10 GeV), and find a cross-section 1.9 times FMNR and well outside the errors. [10]

In deep inelastic scattering H1, (using p_T^{rel} and impact parameters,) again find a value exceeding various calculations by a factor 2.6 to 4.3. ZEUS studied a sample of 836 events from 60 pb^{-1} of data with a $(25 \pm 5)\%$ purity. They find the spectra $p_\mu, \eta, E_{T\,jet}^{Breit}$, well described by Monte Carlo. Their result for $\sigma(ep \to eb\bar{b}X \to e \text{ jet } \mu X)$ is 1.4 times HVQDIS and only 1.0 S.D. high. [11]

First results are reported from a new technique of looking for events containing both D^* and muon. $c\bar{c}$ production produces these with opposite charge and in opposite hemispheres in the γg rest frame. $b\bar{b}$ production also produces opposite charges in the same hemisphere, same charge in opposite hemisphere. The statistics are modest but the background suppression is impressive (34 beauty events in the same hemisphere opposite charge, on a background of only 3). Results again lie above theory. [12] Figure 4 summarises the state of our knowledge.

In all these beauty studies the efficiencies are low and acceptance corrections large. Measurements are made in different kinematic regions and model assumptions are needed to reconcile them. Most of the results lie well above

the theoretical expectation. All will benefit from detector upgrades to H1 and to ZEUS for HERA-II.

Results [13] have been reported by L3 and by OPAL on $\gamma\gamma \to c\bar{c}X$, $b\bar{b}X$. L3 use both electron and muon signatures and have lower false-lepton backgrounds. The result is reminiscent of HERA. There is good agreement with QCD calculations for charm, but for beauty the data lie a factor of about three above the predictions. Clearly beauty production is fertile ground for future study both experimentally and theoretically.

References

1. P.J. Bussey, Int. J. Mod. Phys. **A17**, 1065 (2002)
2. G. Ingelman, J. Rathsman and G.A. Schuler, Comput. Phys. Commun. **101**, 135 (1997)
3. ZEUS collab. paper 778, ICHEP02. See www.ichep02.nl for papers
4. B.W. Harris and J. Smith, Phys. Rev. **D57**,2806 (1998)
5. H. Jung, hep-ph/0109146, hep-ph/0110034 G. Marchesini, Nucl. Phys. **B445**, 49 (1995) and refs therein S.P. Baranov *et.al.*, Eur. Phys. J. C24, 425 (2002)
6. C.Adloff *et.al.*, H1 collab., Nucl. Phys. B545, 21 (1999), paper 984, ICHEP00 (Osaka, 2000)
7. ZEUS collab, papers 780,781,786 ICHEP02
8. A. Cerri, Proc. ICHEP02 (Amsterdam, 2002, in press), C.M.S. Paus, *ibid.*
9. OPAL collab, paper 323, ICHEP02, DELPHI collab, paper 157, ICHEP02
10. ZEUS collab. paper 785, ICHEP02, C. Adloff *et.al.*, H1 collab., Phys. Lett. **B467**, 156 (1999) and erratum, *ibid.* **B518**, 330 (2001)
11. H1 collab., paper 1013, ICHEP02, ZEUS collab, paper 783, ICHEP02
12. ZEUS collab., paper 784, ICHEP02, H1 collab, paper 1016, ICHEP02
13. C. Acciari *et.al.*, L3 collab., Phys. Lett. **B503**, 10 (2001), OPAL collab., paper 366, ICHEP02

Frascati Physics Series Vol. XXXI (2003), pp. 11–16
FRONTIERSCIENCE 2002 – Frascati, October 6–11, 2002
Invited Contribution in Plenary Session

CHARM PHYSICS IN THE NEUTRINO EMULSIONS

Francesca R. Spada*
NIKHEF and INFN Rome 1

ABSTRACT

The CHORUS emulsion target was exposed during the years 1994–1997 to the CERN SPS wide band neutrino beam. About 840,000 ν_μ charged current interactions were collected, out of which 140,000 were located in emulsion. Significant improvements in the past few years in the automatic scanning systems allowed a sample of events located in emulsion to be used for studies of charm production. Here we present a determination of the semi-leptonic branching fraction of charm hadrons based on a sample of 56,172 ν_μ charged-current interactions. We find $B_\mu = (9.3 \pm 0.9\ (stat) \pm 0.9\ (syst)) \cdot 10^{-2}$. We also present a preliminary measurement of the production of Λ_c^+ baryon, based on 50,143 events, giving $\sigma(\Lambda_c^+)/\sigma(CC) = (1.99 \pm 0.13\ (stat) \pm 0.27\ (syst)) \cdot 10^{-2}$.

* On behalf of the CHORUS Collaboration

1 Introduction

CHORUS is a hybrid experimental setup, with a target/detector of nuclear emulsion which provides the resolution at vertex needed to directly observe production and decay of charmed hadrons.

Charm production in neutrino charged-current interactions has been studied in several experiments, in particular, CDHS [1], CCFR [2], CHARM [3], CHARM-II [4], NOMAD [5] and NuTeV [6] by means of electronic detectors and through the analysis of dimuon events. Dimuon experiments suffer from significant background (~30%) in which the second muon originates from an undetected decay in flight of a pion or a kaon rather than from a charm decay, and moreover the type of charmed particle and its decay topology cannot be identified in these experiments. This is instead possible in emulsion experiments which then guarantee a much lower level of background: this technique has already been used in FNAL E531, that collected a statistics of 125 events containing a charmed hadron.

2 The CHORUS experiment

The CHORUS event sample consists of about 840,000 ν_μ CC interactions, collected in the years 1994–1997. The SPS Wide Band neutrino beam is an almost pure ν_μ beam with an average energy of about 25 GeV with small contaminations from $\bar{\nu}_\mu$ (5%) and from ν_e and $\bar{\nu}_e$ (about 1%).

2.1 Experimental setup

The spatial resolution of nuclear emulsion (~1 μm with 300 three-dimensional hits/mm) allows the identifcation of the charmed hadron decay signature, which consists of the neutrino interaction followed by the charm path (visible for charged hadrons, invisible for neutrals) and by the charm decay, showing an odd number of tracks in the case of charged and even for neutrals.

The experimental setup is *hybrid* [7]: the emulsion target is followed by an electronic detector that reconstructs the kinematics of the event. The target is composed by 770 kg of emulsion divided into 4 stacks subdivided in 36 plates each. Scintillating fibre trackers are used to predict the vertex position and drive the event search in emulsion. Downstream the fiber tracker a hexagonal air-core spectrometer measures charge and momentum of hadrons with a

30% resolution for 5 GeV/c particles. A lead and fibre calorimeter built with the *spaghetti* technique measures energy and direction of electromagnetic and hadronic showers. The end system is an iron-core spectrometer which measures the momentum of muons with a resolution of 19%.

2.2 Emulsion scanning and event reconstruction

The charm decay search is performed using the *netscan* method, originally developed for the DONUT experiment [8]. It consists in recording all track segments within a 400 mrad angular acceptance in a volume surrounding the assumed vertex position (6.3 mm longitudinally, corresponding to 8 plates, and 1.5 × 1.5 mm^2 transversely). The parameters of all track segments found in this volume are stored in a database. Typically, five thousand track segments are recorded per event. Alignment, tracking and a first rejection of tracks not belonging to the event are then performed offline, giving on average 40 tracks per event. The track sample is redundant: optimized event selections must be developed for each specific analysis.

3 The semileptonic branching fraction masurement

The charm production cross section is relevant for the determination of several quantities such as the strange quark content of the nucleon, the charm mass and the CKM matrix elements $|V_{cd}|$ and $|V_{cs}|$. Counter experiments can only measure the dimuon production rate, which is correlated to the charm production cross section through the average charm branching ration into muons B_μ. The only existing measurement of this quantity is due to FNAL E531, which measured fragmentation fractions and combined them to the already known individual semileptonic branching fractions and found $B_\mu = 0.099 \pm 0.012$. CHORUS has the statistics sufficient to determine B_μ directly from the number of charm events with a secondary muon in the final state with an error comparable to that of the indirect measurement. The starting sample consists of 56,172 events analyzed with the *netscan*.

3.1 Event selection

The selection of events containing a charm decay is based on the evidence of a secondary signal: either a vertex or an isolated track stopping in the fiducial

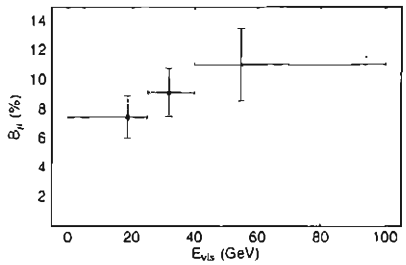

Figure 1: *The semileptonic branching fraction behaviour with visible energy.*

volume must have been reconstructed in addition to the primary vertex. The matching with a detector track guarantees that the vertices do belong to the event. Thus 1055 events are selected. To evaluate the purity a subsample of 244 events was visually inspected, and 11 events did not show secondary vertex (primary tracks wrongly tagged as secondary, passing-through tracks identified as stopping) while 12 events contained secondary interactions. This results in a selection purity of 0.91 ± 0.02 and in a corrected number of selected events $N_{sel} = 956 \pm 35$.

Efficiencies were evaluated with a Monte Carlo in which simulated interactions are superimposed onto real *netscan* acquisitions in order to have a realistic track background, then processed as real data.

3.2 Secondary muon identification

Muons can be identified in calorimeter and spectrometer. Above 4 GeV, where all muons reach the latter, the efficiency is above 95%, while it is much lower where only a calorimeter measurement is available. Integrated over the momentum spectrum, the average μ identification efficiency is 55%. The number of events in which a secondary muon was identified is $N^{2\mu}_{sel} = 88 \pm 10\ (stat) \pm 8\ (syst)$. The semileptonic branching fraction is then given by $B_\mu = R \cdot N^{2\mu}_{sel}/N_{sel}$ where $R = 1.01 \pm 0.05$ is a correction factor that takes into account the efficiencies. CHORUS then measures $B_\mu = (9.3 \pm 0.9\ (stat) \pm 0.9\ (syst)) \cdot 10^{-2}$. Dividing the sample into three bins, the energy dependence of B_μ shown in figure 1 has been obtained.

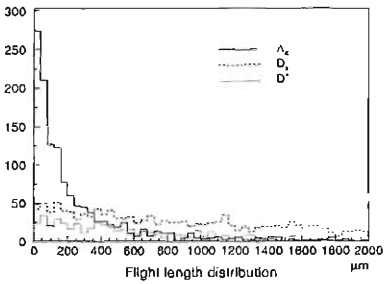

Figure 2: *Flight length distribution for D^+, D_s^+ and Λ_c^+ (Monte Carlo).*

4 The Λ_c^+ production measurement

The resolution on hadron momentum does not allow particle identification on an event-by-event basis, thus the Λ_c^+ production has been studied with statistical methods using the particle flight length distribution. As shown in figure 2, the sample of events with flight length below 400 μm is dominated by Λ_c^+. The event selection is then based on the requirement that the the primary muon and some other track of the event originate in the same emulsion plate. The starting sample consists of 50,143 events analyzed with the *netscan*. To optimize the efficiency no track matching with the detector is required, but this disfavours the purity which is about 20%: all 1605 selected events were then visually inspected. Of the confirmed charm events, those with flight length between 40 and 400 μm are kept (125 events). To estimate the contamination from D^+ and D_s^+, another charm search is performed on events selected requiring that the secondary vertex (or track) is not in the same plate as the primary, and 582 events are selected and visually inspected. Of the confirmed charm events, those with flight length above 400 μm are used in the analysis (227 events).

The background mainly comes from *white* interactions, i.e. in which the nuclear activity is not visible, and 6 ± 1 events are expected. Efficiencies are evaluated with the Monte Carlo simulation described in section 3.1

Combining short and long decay search after dividing decays in 1 prong

from decays in 3 prongs, the number of Λ_c^+ produced can be evaluated solving the system of equations

$$N_{S1} = n_D f_{S1}^{D^+} \varepsilon_{S1}^{D^+} + k n_D f_{S1}^{D_s^+} \varepsilon_{S1}^{D_s^+} + n_{\Lambda_c^+}(1 - f_3^{\Lambda_c^+}) \varepsilon_{S1}^{\Lambda_c^+}$$
$$N_{S3} = n_D f_{S3}^{D^+} \varepsilon_{S3}^{D^+} + k n_D f_{S3}^{D_s^+} \varepsilon_{S3}^{D_s^+} + n_{\Lambda_c^+} f_3^{\Lambda_c^+} \varepsilon_{S3}^{\Lambda_c^+}$$
$$N_{L3} = n_D f_{L3}^{D^+} \varepsilon_{L3}^{D^+} + k n_D f_{L3}^{D_s^+} \varepsilon_{L3}^{D_s^+} + n_{\Lambda_c^+} f_3^{\Lambda_c^+} \varepsilon_{L3}^{\Lambda_c^+}$$

where $N_{S1\,(S3,\,L3)}$ is the number of events in the short–1 prong (short–3 prong, long–3 prong) sample, $\varepsilon_{S1\,(S3,\,L3)}^{D^+\,(D_s^+,\,\Lambda_c^+)}$ are the efficiencies evaluated with the simulation, $f_{S1\,(S3,\,L3)}^{D^+\,(D_s^+)}$ and $f_3^{\Lambda_c^+}$ are the production fractions taken from existing measurements, the ratio $k = n_{D_s^+}/n_{D^+} = 0.13$ is taken from E531, and $n_D = n_{D^+} + n_{D_s^+}$ and $n_{\Lambda_c^+}$ are free parameters to be determined from the equations. Taking into account the background, CHORUS measures $\sigma(\Lambda_c^+)/\sigma(CC) = (1.39 \pm 0.02\,(stat) \pm 0.27\,(syst)) \cdot 10^{-2}$. This result must be considered preliminary as systematics and other background sources are being further evaluated.

References

1. H. Abramowicz *et al.*, Z. Phys. C **15**, 19–31 (1982).
2. S.A. Rabinowitz, Phys. Rev. Lett. **2**, 134–137 (1993).
3. M. Jonker *et al.*, Phys. Lett. B **107** , 241 (1981).
4. P. Vilain *et al.*, Eur. Phys. J. C **11**, 19–34 (1999).
5. P. Astier *et al.*, Phys. Lett. B **486**, 35–48 (2000).
6. M. Goncharov *et al.*, Phys. Rev. D **64**, 112006 (2001).
7. E. Eskut *et al.*, Nucl. Inst. Meth. A **401**, 7 (1997).
8. K. Kodama *et al.*, Phys. Lett. B **504**, 218–224 (2001).

Frascati Physics Series Vol. XXXI (2003), pp. 17–20
FRONTIERSCIENCE 2002 – Frascati, October 6–11, 2002
Invited Contribution in Plenary Session

MODEL INDEPENDENT MEASUREMENT OF THE FRAGMENTATION OF b-QUARKS INTO B MESONS

Tommaso Boccali
Scuola Normale Superiore, Piazza dei Cavalieri 7, Pisa, Italy

ABSTRACT

The new results about b quark fragmentation function at the Z peak are reviewed. Different methods and strategies lead to compatible results, which are substantially higher than older results.

1 Introduction

In high energy processes which involve strong interactions the quarks are not observed as free particles, but appear as jets of colourless hadrons. The process of hadron production is usually described as the convolution of a perturbative part (photon and gluon radiation with $Q^2 > 1$ GeV) and the non-perturbative fragmentation process itself, which is parametrised in terms of the variable $z \equiv \frac{(E+p_{\parallel})_{\text{hadron}}}{(E+p)_{\text{quark}}}$, where the numerator refers to the hadron after fragmentation, and

the denominator to the quark just before fragmentation, i.e. taking into account initial and final state radiation and hard gluon emission. The fragmentation is described in terms of the probability of a B hadron to be generated with a given z, called $f(z)$. Many phenomenological models are present in literature for $f(z)$, amongst the most popular Peterson [1], Kartvelishvili [2], Collins [3] and Bowler [4] can be cited. Unfortunately z is not accessible experimentally, and hence a direct reconstruction of $f(z)$ is not possible. The energy spectrum of B hadrons can instead be described in terms of the *scaled mean energy* x_B, defined as the ratio of the heavy hadron energy to the beam energy $x_B \equiv \frac{E_{\rm had}}{E_{\rm beam}}$. The main difference between the z and x_B variables is in the denominator, because $E_{\rm beam}$ does not unfold the effects of initial and final state radiation and hard gluon emission. Together with x, a distribution $F(x)$ analogous to $f(z)$ can be defined. It is also often better to consider not the first generated B hadron, but *weakly-decaying* B hadron, whose scaled energy is denoted $x_B^{\rm wd}$. The differences are due to higher resonant states which decay heavily, as in $B^{**} \to B\pi$ or in $B^* \to B\gamma$.

2 Experimental methods

Different methods have been used so far to directly measure $F(x)$ fragmentation functions. Inclusive variables like semileptonic $b \to \ell\nu X$ lepton momenta and B jet energies are correlated with the energy of the B hadron. Otherwise, one can select inclusively jets coming from B decays using their lifetime information; then, a wise choice of the tracks in the jet which are supposed to come from heavy quark decays allows a direct reconstruction of the energy of the leading B hadron. Finally, one can also *semi-exclusively* reconstruct the energy of a B meson by looking at the semileptonic decays $B \to \ell\nu D^{(*)}$; the charmed meson can be identified in a number of decay channels, while the neutrino energy has to be estimated using missing energy techniques or directly correcting with Monte Carlo simulation. In the first method one basically reconstructs only the lepton track, and Monte Carlo simulation has to be used to derive the true B hadron energy; in the last one, instead, almost all of the energy of the B hadron is directly reconstructed, thus depending less on the simulation.

Older LEP measurements [5] were using the first method, and a functional shape for $f(z)$ (usually Peterson [1]) was imposed since the analysing power is not good enough to retrieve a real spectrum. The average value for $\langle x_B^{\rm wd} \rangle$ was

0.702 ± 0.008. The newest measurements by ALEPH [6], SLD [7], DELPHI [8] and OPAL [9], instead, use the second and the third methods.

ALEPH [6] selects B mesons exclusively in $B \to \ell\nu D^{(*)}$ decay channels, with the D^* and D mesons are reconstructed exclusively in five channels. Neutrino energy is recovered using missing energy techniques. In this way, 3400 candidates are selected with an expected B energy resolution of 4%.

DELPHI [8] and OPAL [9] select charged and neutral decay B products with artificial neural networks. Information like track impact parameter significance, the presence of displaced vertices and rapidity information are used as inputs. The B hadron energy is either estimated again by neural networks (DELPHI), or obtained from a weighted sum of all track and cluster energies, where the weights are again from neural networks (OPAL). This inclusive selection allows a greater statistical sample ($\approx$200000 B decays reconstructed), but with a resolution on B energy of about 10%.

SLD [7] achieves an inclusive B hadron reconstruction using only charged tracks from B decays, making use of their excellent vertexing system and of the very small interaction region of SLC. Neutral track information is retrieved using B flight direction from the decay vertex and assuming the B average mass for the vertex. In this way, using hard cuts to select a subsample with good resolution, SLD selects $\approx$4000 events with an energy resolution of $\approx$10%.

Two different kinds of analysis are possible once the reconstructed B energy is available:

- a fit to various $f(z)$ distributions, to check compatibility with data
- a model independent deconvolution of detector effects to get a $F(x)$ shape

The general trends is, consistently among the measurements, that Bowler and Kartvelishvili $f(z)$ parameterisations describe quite well the data; Peterson is disfavoured and Collins ruled out. Note also that the results using Peterson are consistently lower than the best ones.

The model-independent studies result in values for $\langle x_B^{\rm wd} \rangle$

ALEPH [6] $0.7163 \pm 0.0061 \pm 0.0056$ SLD [7] $0.709 \pm 0.003 \pm 0.003 \pm 0.002$

DELPHI [8] $0.7153 \pm 0.0007^{+0.0049}_{-0.0052}$ OPAL [9] $0.7193 \pm 0.0016^{+0.0036}_{-0.0031}$

and in full $F(x)$ shapes as in fig.1.

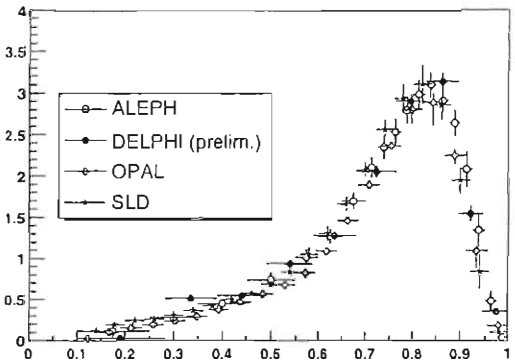

Figure 1: *Reconstructed spectrum for* $F\left(x_B^{\mathrm{wd}}\right)$

3 Conclusions

The newest results by LEP and SLD Collaborations agree well in setting an average value for b quark fragmentation function higher than previously measured [5]. This is explained since the older measurements were assuming a Peterson [1] shape for $f(z)$, while now this seems disfavoured.

References

1. C. Peterson *et al*, Phys. Rev. **D27** (1983) 105.
2. V.G. Kartvelishvili *et al*, Phys. Lett. **B78** (1978) 615.
3. P. Collins *et al*, J. Phys. **G11** (1985) 1289.
4. M.G. Bowler, Z. Phys. **C11** (1981) 169.
5. Lep ElectroWeak Working Group, LEPHF 2001-01.
6. ALEPH Coll., Phys. Lett. **B357** (1995) 699.
7. SLD Coll., ICHEP 2002 Abstract 967.
8. DELPHI Coll., ICHEP 2002 Abstract 583.
9. OPAL Coll., CERN-EP-2002-051, Submitted to Eur. Phys. J. C.

Frascati Physics Series Vol. XXXI (2003), pp. 21–24
FRONTIERSCIENCE 2002 – Frascati, October 6–11, 2002
Invited Contribution in Plenary Session

CHARM AND BEAUTY PRODUCTION IN TWO PHOTON COLLISIONS AT LEP

Achard Pablo*
Geneva University, DPNC, 24 quai E. Ansermet, 1211 Genève 4

ABSTRACT

Heavy quark production is widely studied in two-photon collisions at LEP and is a very fruitful laboratory for testing perturbative QCD. Clear evidence for the gluon content of the photon is obtained. The data favour low values of the charm mass. The $b\bar{b}$ production is found to be three times higher than the NLO QCD predictions.

Two photon collisions are the main source of hadrons at LEP. The study of charm and beauty production in two-photon collisions, introducing a large physical scale, provides a means of testing pertubative QCD and of probing the partonic structure of the photon. At LEP energies, the direct and single resolved processes, sketched in Figure 1, are predicted to give comparable contributions to the cross section $\sigma(\gamma\gamma \to c\bar{c}, b\bar{b})$. The resolved photon cross

* On behalf of the L3 Collaboration

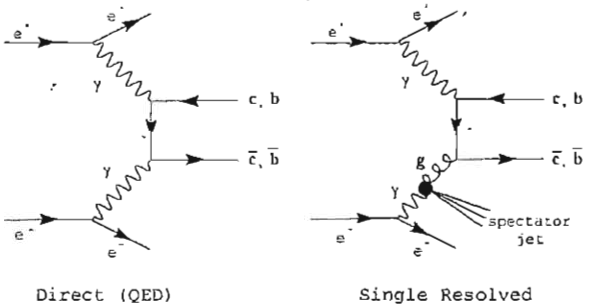

Figure 1: *Feynman diagrams of the two main* $\gamma\gamma \to c\bar{c}, b\bar{b}$ *processes*

section is dominated by the photon-gluon fusion process $\gamma g \to q\bar{q}$. This talk is a short survey of recent LEP results [1].

The event selection follows two steps: first hadronic final states from two-photon collisions are selected, then an heavy quark is tagged. A cut on the calorimetric energy deposited in the detector provides a clean separation between two-photon collisions and e^+e^- annihilation processes. The charm is

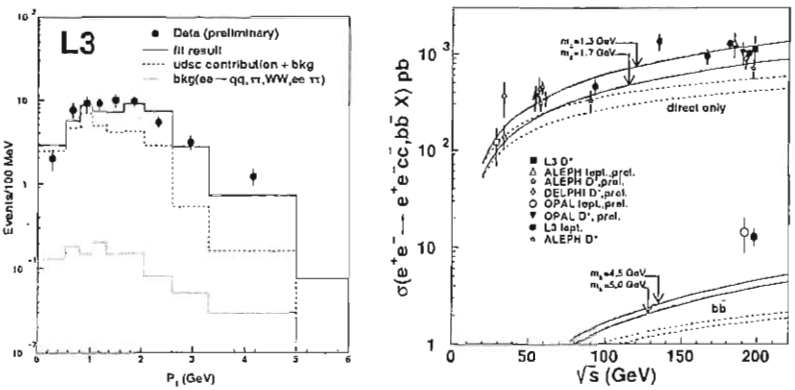

Figure 2: *Left: transverse momentum of the electron with respect to the nearest jet. Right: total cross section of* $c\bar{c}$ *and* $b\bar{b}$ *productions with respect to* $\sqrt{s}$.

tagged either by the presence of a D^* resonance or by the presence of a lepton (electron or muon). The $D^{*\pm}$ meson is studied via its decay into a D^0 meson and a low energy $\pi^{\pm}$. $D^0 \to K^-\pi^+$, $D^0 \to K^-\pi^+\pi^0$ and $D^0 \to K^-\pi^+\pi^-\pi^+$ decay channels are analysed. The beauty is tagged with high momentum leptons. The transverse momentum distribution of the lepton with respect to the nearest jet is fitted with uds, c and b content as free parameters as shown in Figure 2(left).

The total cross section of charm production, $e^+e^- \to e^+e^-c\bar{c}X$, shown in Figure 2(right) is in good agreement with NLO QCD predictions [2]. The direct process alone is insufficient to describe the data. This is an evidence of the importance of the gluon-photon fusion process and of the gluon content of the photon.

The L3 and OPAL measurements of the total cross section of beauty production are in good agreement with each other, but data are more than three times higher than NLO QCD predictions [2].

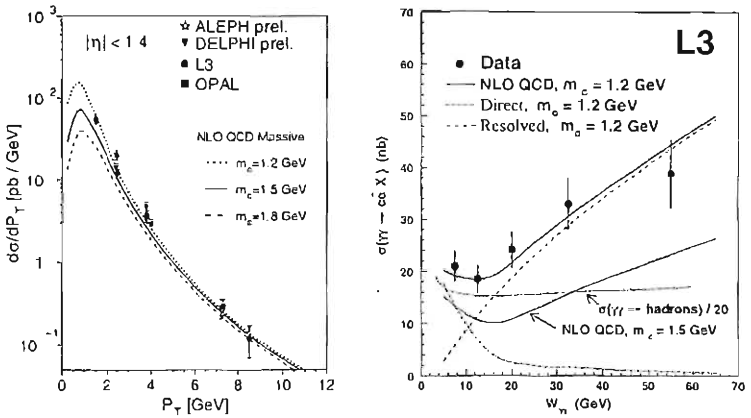

Figure 3: *Left: differential cross section of the charm production with respect to the transverse momentum of the D^*. Right: total cross section with respect to the mass of the $\gamma\gamma$ system.*

The differential cross section of the charm production as a function of the transverse momentum and the total cross section $\gamma\gamma \to c\bar{c}X$ as a function of the mass of the $\gamma\gamma$ system $W_{\gamma\gamma}$ are also measured. In Figure 3, one can see that

these measurements favour a low value of the charm mass. The rise of the $\gamma\gamma$ cross section at high $W_{\gamma\gamma}$ values is characteristic of the resolved processes [3]. The separation between the direct and the resolved processes has also been studied with kinematic variables of the jets.

As shown in Figure 4, the charm structure function of the photon exhibits at low x higher values than predicted [4]. The gluon component of the photon is therefore probably underestimated.

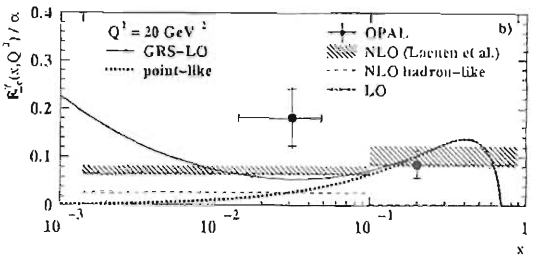

Figure 4: *Charm structure function of the photon.*

References

1. M. Acciarri *et al.* [L3 Collaboration], Phys. Lett. B **453**, 83 (1999);
   M. Acciarri *et al.* [L3 Collaboration], Phys. Lett. B **467**, 137 (1999);
   A. Bohrer and O. Krasel [ALEPH Collaboration], ALEPH-2000-031;
   A. Csilling [OPAL Collaboration], hep-ex/0010060;
   M. Acciarri *et al.* [L3 Collaboration], Phys. Lett. B **514**, 19 (2001);
   M. Acciarri *et al.* [L3 Collaboration], Phys. Lett. B **503**, 10 (2001);
   P. Achard *et al.* [L3 Collaboration], Phys. Lett. B **535**, 59 (2002);
   G. Abbiendi *et al.* [OPAL Collaboration], Phys. Lett. B **539**, 13 (2002).

2. M. Drees *et al.* , Phys. Lett. B **306**, 371 (1993).

3. S. Frixione *et al.*, J. Phys. G **26**, 723 (2000).

4. E. Laenen and S. Riemersma, Phys. Lett. B **376**, 169 (1996).

Frascati Physics Series Vol. XXXI (2003), pp. 25–28
FRONTIERSCIENCE 2002 – Frascati, October 6–11, 2002
Invited Contribution in Plenary Session

FIRST OBSERVATION OF A FAMILY OF DOUBLE-CHARM BARYONS

J. S. Russ
Carnegie Mellon University, Pittsburgh, PA 15213 USA *

ABSTRACT

The SELEX experiment (E781) at Fermilab observes high mass states decaying to $\Lambda_c^+ K^- \pi^+$ and $\Lambda_c^+ K^-$ pi$^+ \pi^+$, possible decay modes of doubly-charmed baryons Ξ_{cc}^+ and Ξ_{cc}^{++}. The masses are consistent with theoretical predictions for double-charm baryons.

---

*On behalf of the SELEX Collaboration: Ball State University, Bogazici University, Carnegie Mellon University, Centro Brasileiro de Pesquisas Fisicas (Rio de Janeiro), Fermi National Accelerator Laboratory, Petersburg Nuclear Physics Institute, IHEP (Beijing), IHEP (Protvino), ITEP (Moscow), Moscow State University, Max-Planck-Institut für Kernphysik (Heidelberg), Tel Aviv University, Universidad Autónoma de San Luis Potosí, University of Bristol, Universidade Federal da Paraiba, University of Iowa, University of Michigan–Flint, University of Rome "La Sapienza", INFN, University of São Paulo, University of Trieste.

1 Introduction

The existence of baryons with two and three charm quarks is expected from our present understanding of hadronic structure. In the double-charm system one expects a J=1/2 ground state iso-doublet, termed $\Xi_{cc}^{+,++}$ in PDG notation [1]. Most predictions for the masses of the J=1/2 states and the J=3/2 hyperfine excitations expect the ground state near 3.6 GeV/c^2 and a hyperfine split of 60 MeV/c^2 [2].

2 Features of the Selex spectrometer

The SELEX experiment at Fermilab used a magnetic spectrometer and a high resolution silicon vertex detector with 600 GeV Σ^- and π^- beams and a 570 GeV proton beam to study large-x_F charm production ($< x_F > \sim 0.35$). [3] A RICH detector identified secondaries above 25 GeV/c. [4] Details of single-charm analyses involving $\Lambda_c^+ \to pK^-\pi^+$ reconstructions can be found in [5, 6]. The double-charm search discussed here began with the sample of 1630 Λ_c^+ events used in the lifetime analysis [5].

3 Double-charm Analysis

Our topological search looked for double-charm baryons decaying via a Cabibbo-favored decay to an s-quark plus a daughter Λ_c^+ baryon. A double-charm candidate formed a vertex having the Λ_c^+ along with 2 more tracks (Q=1) or 3 more tracks (Q=2). We called the negative track a kaon in the right-sign reconstruction, then reanalyzed the same events calling the negative track a pion to study wrong-sign backgrounds. Event selection cuts required vertex separation significance $L_1/\sigma_1 \geq 1$. The Λ_c^+ momentum vector must point back to the primary vertex within a χ^2 cut of 4. The signal significance does not depend critically on any cut value.

3.1 Q = 1 reconstruction

For single-charged baryons, the $K^-\pi^+\Lambda_c^+$ mass distribution shows a Ξ_{cc}^+ candidate at 3520 MeV/c^2, consistent with most model calculations. The peak is narrow but consistent with simulation. The signal region contains 22 events with a background of 6.1 $\pm$ 0.51 events, for a single-bin significance of 6.3 σ.

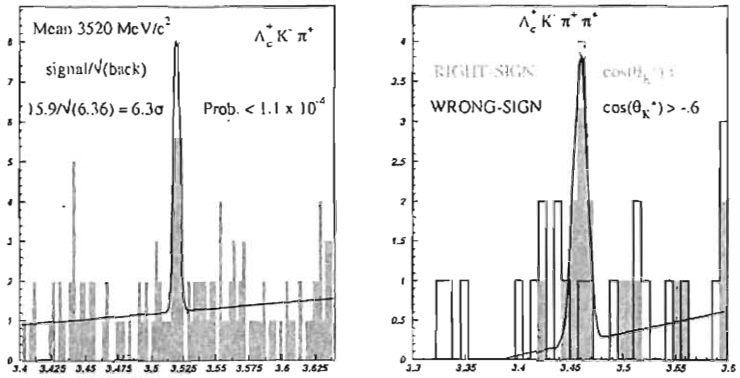

Figure 1: (a) The $\Lambda_c^+ K^- \pi^+$ mass distribution in 2.5 MeV/c^2 bins. (b)The $\Lambda_c^+ K^- \pi^+ \pi^+$ mass distribution in 7.5 MeV/c^2 bins.

The probability of such an excess is less than 10^{-6} for a single bin. The probability of such a fluctuation anywhere in the mass range is $< 1.1 \times 10^{-4}$. SELEX has reported this as the first observation of a doubly-charmed baryon [7].

3.2 Q=2 Reconstruction

For double-charged baryons, we look for an isospin partner of the $\Xi_{cc}^+(3520)$. The $K^- \pi^+ \pi^+ \Lambda_c^+$ mass distribution in the vicinity of 3520 MeV/c^2 is shown at right in Fig. 1, along with the wrong-sign background. There is a Ξ_{cc}^{++} candidate at 3460 MeV/c^2. The observed width (6 $\pm$ 1 MeV/c^2) matches simulation. Events outside the signal region show a strong preference for the center-of-mass (CM) angle of the negative track to be near 180 degrees. Simulation indicates that a cut to remove such events should have very little effect on the signal region for a phase-space decay distribution. That is indeed the case in the data. With the selection shown, we find 9 events in the peak, compared to an expected background of 1 event. The Poisson probability that there is an excess of 8 events or more anywhere on the plot is 10^{-5}.

3.3 Production

Both Ξ_{cc}^+ and Ξ_{cc}^{++} states are produced only by baryon beams in SELEX data. There are no signal candidates from the pion beam. Simulation studies sug-

gest that the double-charm states may account for as much as 40% of the Λ_c^+ sample seen in this experiment, a surprisingly high fraction. The FOCUS photoproduction experiment at Fermilab (230 GeV) has looked for these states using 20,000 Λ_c^+ events and sees no signal peaks [9]. If SELEX is correct, the hadroproduction mechanism is unusual. This situation is reminiscent of the discovery of the Ξ_c^+ baryon in the WA62 experiment at CERN. That experiment observed enormous large-x_F production: $\sigma \cdot \mathrm{B} = 0.6\ \mu$b for $x_F > 0.6$ from 135 GeV hyperons [8].

4 Summary

SELEX has introduced two statistically-compelling new high-mass states that decay into a final state Λ_c^+, K^- and one or two π^+, as expected for double-charm baryon decays. It is difficult to understand the 60 MeV/c^2 mass difference between the Q=1 and Q=2 states if they are members of the ground state isodoublet. However, any other interpretation of these states is also problematic.

References

1. Particle Data Group, D.E. Groom, *et al.*, Eur. Phys. J.C15,1 (2000)
2. see references 111-124 in hep/ph0201071, B Physics at the Tevatron.
3. J. Russ, *et al.* , *in Proceedings of the 29th International Conference on High Energy Physics,* edited by A. Astbury *et al.* (World Scientific, Singapore, 1999) VolII, p. 1259;hep-ex/9812031.
4. J. Engelfried, *et al.*, Nucl.Instr.and Methods A431, 53, 1999
5. A. Kushnirenko *et al.* Phys. Rev. Lett. **86**, 5243 (2001), hep-ex/0010014.
6. F. Garcia *et al.* Phys. Lett. **B528**, 49 (2002), hep-ex/0109017.
7. M. Mattson *et al.* Phys. Rev. Lett. **89**, 112001 (2002)
8. S. Biagi, *et al.*, Phys. Lett. **B122**, 455 (1983)
9. C. Riccardi, ICHEP02. See also http://www.hep.vanderbilt.edu/~stenson/xicc/xicc_focus.html

Frascati Physics Series Vol. XXXI (2003), pp. 29–37
FRONTIERSCIENCE 2002 – Frascati, October 6–11, 2002
Invited Review Talk in Plenary Session

HEAVY FLAVOUR PRODUCTION

P. Nason
INFN, Sez. di Milano, Milan, Italy

ABSTRACT

I discuss few recent developments in Heavy Flavour Production phenomenology.

1 Introduction

The phenomenology of Heavy flavour production attracts considerable theoretical and experimental interest.

The theoretical framework for the description of heavy flavour production is the QCD improved parton model. Besides the well-established NLO corrections to the inclusive production of heavy quark in hadron-hadron [1, 2, 3, 4], hadron-photon [5, 6, 7], and photon-photon collisions [8], much theoretical work has been done in the resummation of contributions enhanced in certain regions of phase space: the Sudakov region, the large transverse momentum region and the small-x region.

The theoretical effort involved is justified by the large variety of applications that heavy quark production physics has, in top, bottom and charm production. Besides the need of modeling these processes, heavy quark production is an important benchmark for testing QCD and parton model ideas, due to the relative complexity of the production process, the large range of masses available, and the existence of different production environments, like e^+e^- annihilation, hadron-hadron, photon-hadron and photon-photon collisions. Although the order of magnitude of the total cross sections, and the shape of differential distribution is reasonably predicted, in some areas large discrepancy are present, especially for b production.

2 Total cross section for top and bottom

Top production [9, 10] has been a most remarkable success of the theoretical model. The measured cross section has been found in good agreement with theoretical calculations, as shown in fig. 1. Resummation of soft gluon ef-

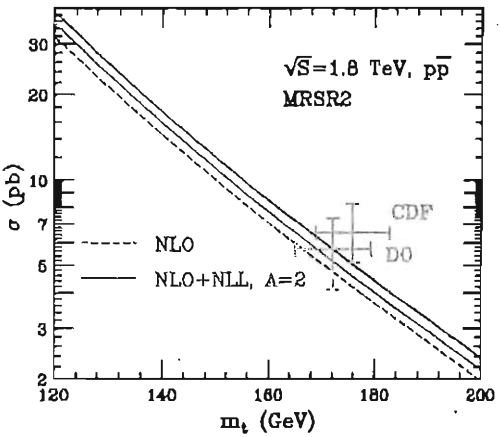

Figure 1: *Results on top cross sections at the Tevatron.*

fects [11] reduces the theoretical uncertainty in the cross section, pushing it toward the high side of the theoretical band. It remains, however, inside the theoretical band of the fixed order calculation, thus showing consistency with

the estimated error.

Recently, the HERA-B experiment has provided a new measurement of the $b\bar{b}$ total cross section [12]. Their result is in good agreement with previous findings [13, 14]. More details on this measurement have been given in Saxon's talk [15]. Here I will only make some remarks on the theoretical aspects. This experiment is sensitive to the moderate transverse momentum region, where the bulk of the total cross section is concentrated. Since the production is (in a certain sense) close to threshold, resummation of Sudakov effects is important also in this case, and brings about a considerable reduction of the theoretical uncertainty [11]. The HERA-b result is compatible with the central value prediction, with the b pole mass around 4.75 GeV. Higher precision may constrain further the b quark mass.

3 Differential distributions

The Tevatron has had a longstanding disagreement with QCD in the b transverse momentum spectrum. A recent publication of the B^+ differential cross section by CDF [16] has quantified the disagreement as a factor of $2.9 \pm 0.2 \pm 0.4$ in the ratio of the measured cross section over the theoretical prediction. This discrepancy has been present since a long time, and it has been observed both in CDF and D0. Some authors [17] have argued that the discrepancy could be interpreted as a signal for Supersimmetry.

Because of the large theoretical uncertainties, this discrepancy has been often downplayed. In fact, several effects may conspire to raise the b cross section to an appropriate value: small-x effects [1, 18, 19], threshold effects [11] and resummation of large $\log p_T$. It is not however clear whether these effect can be added up without overcounting. Furthermore, they are all higher order effects, and thus should not push the cross section too far out of the theoretical band, which includes estimates of unknown higher order effects.

Recently, a small-x formalism [20, 21, 22, 23] has been implemented in a Monte Carlo program [24] (the CASCADE Monte Carlo), and it has been claimed that this programs correctly predicts the b spectrum at the Tevatron [25]. Although encouraging, this result should be regarded with a word of caution. The formalism involved only accounts for leading small x effects, and does not correct for the lack of leading terms, that are known to be important for heavy flavour production at the Tevatron regime. Experience with other

contexts where resummation techniques have been applied has taught us that it is not difficult to overestimate the importance of resummation effects, and much study is needed to reliably assess their importance [26].

It has been observed since some time that an improper understanding of fragmentation effects may be one of the causes of the Tevatron discrepancy. This possibility stems from the fact that b quark cross sections are in reasonable agreement with the Tevatron measurements of the B meson spectrum, while the cross section obtained by applying a standard fragmentation function of the Peterson form [27] with $\epsilon = 0.006$ to the quark cross section yields too soft a spectrum. It was suggested [28] to study b quark jets rather than B meson's distributions. In fact, the jet momentum should be less sensitive to fragmentation effects than the hadron momentum. A D0 study [29] has demonstrated that by considering b jets instead of B hadrons the agreement between theory and data improves considerably.

It was recently shown [30] that an accurate assessment of fragmentation effects brings about a reduction of the discrepancy from the factor of 2.9 quoted by CDF to a factor of 1.7. This remarkable reduction is essentially due to recent progress in fragmentation function measurements by LEP experiments and the SLD [31, 32, 33, 34] (the current status of fragmentation measurements has been reviewed in Boccali's talk [35]), and by a particular method for extracting the relevant information about non-perturbative fragmentation effects from the e^+e^- data. Here I will not enter in the details of the method, that have been described in [30]. I will instead try to give an overall illustration of the main features of the method. First of all, strictly speaking, the description of fragmentation effects in terms of a fragmentation function (i.e., a probability distribution for an initial quark to hadronize into a hadron with a given fraction of its momentum) is only valid at very large transverse momenta. One could then extract the fragmentation function from LEP data, and use it in high p_T B production at the Tevatron. Unfortunately, the regime of large transverse momenta is not quite reached at the Tevatron. For example, the differential cross section $d\sigma/dp_T^2 dy$ at the Tevatron, for $p_T = 10, y = 0$, computed at the NLO level including mass effects is 12.1 nb/GeV^2, while in the massless approximation (i.e., neglecting terms suppressed as powers of m/p_T) is 1.78 nb/GeV^2. At $p_T = 20$ we have 0.372 nb/GeV^2 for the full massive, and 0.220 nb/GeV^2 for the massless limit, which starts to approach the asymptotic value. As a

rule of thumb, the massless approximation starts to approach the massive one around $p_T \approx 5m$[1]. It does therefore make no sense to use any massless approach for $p_T < 5m$. In earlier work on heavy quark production at large transverse momentum [37], this fact went unnoticed, since large higher order terms (i.e. beyond the NLO level) in the fragmentation function approach accidentally compensated for the lack of mass terms, thus giving the impression that the massless approach is good down to $p_T \approx 2m$.

In order to perform a calculation that is reliable in both the low and the high transverse momentum regime, we have thus to merge the massive NLO calculation with the fragmentation function approach. The merging point must therefore be around $pt \approx 5m$. A summary of the theoretical tools that have lead to the matched (so called FONLL) approach are summarised as follows:

1 Single inclusive particle production in hadronic collisions [38]. Single hadron production are described in term of NLO single parton cross section convoluted with a NLL fragmentation function;

2 Heavy quark Fragmentation Function [39]; a method for the computation of the heavy quark fragmentation function at all orders in perturbation theory is developed, and applied at NLL. Several applications in e^+e^- physics have appeared [40, 41, 42, 43].

3 Single inclusive heavy quark production at large p_T [37]; item 1 and 2 are combined to give a NLL resummation of transverse momentum logarithms in heavy quark production;

4 FONLL calculation of single inclusive heavy quark production; item 3 is merged without overcounting with standard NLO calculations. This procedure has been implemented both in hadroproduction [44] and in photoproduction [45, 46].

A summary of comparison of the FONLL calculation with data is given in fig. 2. More details on the CDF measurement have been given in Saxon's talk. The comparison with D0 data (still preliminary) shows very good agreement, compared to the discrepancy of a factor of order 3 found in the D0 publication.

[1]This elementary fact has been known for more than five years, although, surprisingly enough, some authors prefer to ignore it even now [36]

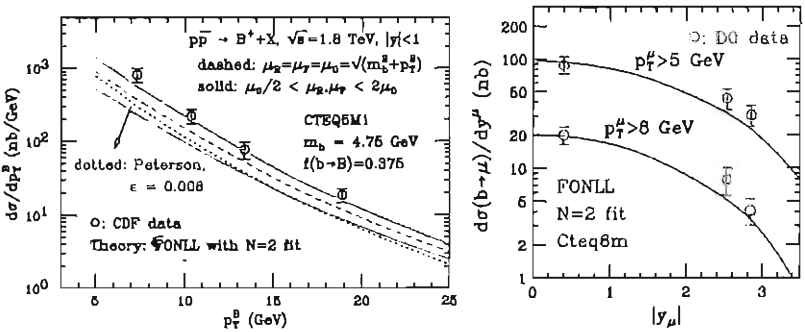

Figure 2: *Comparison of CDF* [16] *and D0* [47] *data with the FONLL calculation* [30].

4 Conclusions

The theory of heavy flavour production seems to give a good qualitative description of the available data. In the case of top production, the comparison between theory and experiment is satisfactory also at a quantitative level.

Recent progress has taken place in the field of b hadroproduction. The HERA-b experiment has provided a cross section for b production at relatively low CM energy. Some progress in understanding the role of fragmentation has considerably reduced the longstanding problem of the b momentum spectrum at the Tevatron.

Major problems do remain in the (perhaps less developed) areas of bottom production in $\gamma\gamma$ and γp collisions. Discussion of these problems were reported in Saxon's and Achard's talk in this conference [15, 48]. In both contexts, while charm production seems to be reasonably well described by QCD, there is an excess of bottom production, which seems to be far out of the theoretical uncertainty band. These problems have been around for sometimes now. On the positive side, the recent Zeus measurements presented in [15] seem to show a smaller discrepancy than previously found.

References

1. P. Nason, S. Dawson and R. K. Ellis, *Nucl. Phys.* **B303** (1988) 607.

2. P. Nason, S. Dawson and R. K. Ellis, *Nucl. Phys.* **B327** (1989) 49–92.

3. W. Beenakker, W. L. van Neerven, R. Meng, G. A. Schuler and J. Smith, *Nucl. Phys.* **B351** (1991) 507–560.

4. M. L. Mangano, P. Nason and G. Ridolfi, *Nucl. Phys.* **B373** (1992) 295–345.

5. R. K. Ellis and P. Nason, *Nucl. Phys.* **B312** (1989) 551.

6. J. Smith and W. L. van Neerven, *Nucl. Phys.* **B374** (1992) 36–82.

7. S. Frixione, M. L. Mangano, P. Nason and G. Ridolfi, *Nucl. Phys.* **B412** (1994) 225–259, [hep-ph/9306337].

8. M. Drees, M. Kramer, J. Zunft and P. M. Zerwas, *Phys. Lett.* **B306** (1993) 371–378.

9. **CDF** Collaboration, T. Affolder *et. al.*, *Phys. Rev.* **D64** (2001) 032002, [hep-ex/0101036].

10. **D0** Collaboration, V. M. Abazov *et. al.*, [hep-ex/0205019].

11. R. Bonciani, S. Catani, M. L. Mangano and P. Nason, *Nucl. Phys.* **B529** (1998) 424–450, [hep-ph/9801375].

12. **HERA-B** Collaboration, I. Abt *et. al.*, [hep-ex/0205106].

13. D. M. Jansen *et. al.*, *Phys. Rev. Lett.* **74** (1995) 3118–3121.

14. **E771** Collaboration, T. Alexopoulos *et. al.*, *Phys. Rev. Lett.* **82** (1999) 41–44.

15. D. H. Saxon, this proceedings.

16. **CDF** Collaboration, D. Acosta *et. al.*, *Phys. Rev.* **D65** (2002) 052005, [hep-ph/0111359].

17. E. L. Berger *et. al.*, *Phys. Rev. Lett.* **86** (2001) 4231–4234, [hep-ph/0012001].

18. S. Catani, M. Ciafaloni and F. Hautmann, *Nucl. Phys.* **B366** (1991) 135–188.

19. J. C. Collins and R. K. Ellis, *Nucl. Phys.* **B360** (1991) 3–30.

20. M. Ciafaloni, *Nucl. Phys.* **B296** (1988) 49.

21. S. Catani, F. Fiorani and G. Marchesini, *Phys. Lett.* **B234** (1990) 339.

22. S. Catani, F. Fiorani and G. Marchesini, *Nucl. Phys.* **B336** (1990) 18.

23. G. Marchesini, *Nucl. Phys.* **B445** (1995) 49–80, [hep-ph/9412327].

24. H. Jung, *Comput. Phys. Commun.* **143** (2002) 100–111, [hep-ph/0109102].

25. H. Jung, *Phys. Rev.* **D65** (2002) 034015, [hep-ph/0110034].

26. S. Catani, M. L. Mangano, P. Nason and L. Trentadue, *Nucl. Phys.* **B478** (1996) 273–310, [hep-ph/9604351].

27. C. Peterson, D. Schlatter, I. Schmitt and P. M. Zerwas, *Phys. Rev.* **D27** (1983) 105.

28. S. Frixione and M. L. Mangano, *Nucl. Phys.* **B483** (1997) 321–338, [hep-ph/9605270].

29. **D0** Collaboration, B. Abbott *et. al.*, *Phys. Rev. Lett.* **85** (2000) 5068–5073, [hep-ex/0008021].

30. M. Cacciari and P. Nason, Phys. Rev. Lett. **89** (2002) 122003 [hep-ph/0204025].

31. **ALEPH** Collaboration, A. Heister *et. al.*, *Phys. Lett.* **B512** (2001) 30–48, [hep-ex/0106051].

32. **SLD** Collaboration, K. Abe *et. al.*, [hep-ex/0202031].

33. **OPAL** Collaboration, G. Abbiendi *et. al.*, [hep-ex/0210031].

34. DELPHI Coll., ICHEP 2002 Abstract 583.

35. T. Boccali, this conference proceedings.

36. B. A. Kniehl, [hep-ph/0211008].

37. M. Cacciari and M. Greco, *Nucl. Phys.* **B421** (1994) 530–544, [hep-ph/9311260].

38. F. Aversa, M. Greco, P. Chiappetta and J. P. Guillet, *Phys. Rev. Lett.* **65** (1990) 401–403.

39. B. Mele and P. Nason, *Nucl. Phys.* **B361** (1991) 626–644.

40. G. Colangelo and P. Nason, *Phys. Lett.* **B285** (1992) 167–171.

41. M. Cacciari, M. Greco, S. Rolli and A. Tanzini, *Phys. Rev.* **D55** (1997) 2736–2740, [hep-ph/9608213].

42. M. Cacciari and M. Greco, *Phys. Rev.* **D55** (1997) 7134–7143, [hep-ph/9702389].

43. P. Nason and C. Oleari, *Nucl. Phys.* **B565** (2000) 245–266, [hep-ph/9903541].

44. M. Cacciari, M. Greco and P. Nason, *JHEP* **05** (1998) 007, [hep-ph/9803400].

45. M. Cacciari, S. Frixione and P. Nason, *JHEP* **03** (2001) 006, [hep-ph/0102134].

46. S. Frixione and P. Nason, *JHEP* **03** (2002) 053, [hep-ph/0201281].

47. **D0** Collaboration, B. Abbott *et. al.*, *Phys. Rev. Lett.* **84** (2000) 5478–5483, [hep-ex/9907029].

48. P. Achard, this conference proceedings.

Heavy Flavour QCD – Session II

Chairpersons: G. Pancheri, L. Votano

R. Cester	Quarkonium Production and Decays
P. Rumerio	The Exclusive Reaction $p\bar{p} \rightarrow \chi_{c0}(1^3P_0) \rightarrow \pi^0\pi^0$ (and $\eta\eta$) $\rightarrow \gamma\gamma\gamma\gamma$
A. Meyer	Charmonium Production at HERA
B. Giacobbe	Measurement of the $b\bar{b}$ Production Cross Section in 920 GeV p–N Collisions with HERA-B
P.D. Sheldon	Charm and Beauty Spectroscopy
M. Levtchenko	Search for η_b in Two–Photon Collisions with the L3 Detector at LEP
O. Schneider	Charm and Beauty Lifetimes
L. Agostino	Λ_c^+ and Ξ_c^+ Branching Ratios in the FOCUS Experiment

Frascati Physics Series Vol. XXXI (2003), pp. 41–61
FRONTIERSCIENCE 2002 – Frascati, October 6–11, 2002
Invited Review Talk in Plenary Session

QUARKONIUM PRODUCTION AND DECAYS

Rosanna Cester
University of Torino - Italy

ABSTRACT

Recent experiments on heavy quarkonium production performed at high energy colliders (HERA and the TEVATRON) and at e^+e^- machines, are presented and discussed within the framework of the NRQCD/factorization formalism.

Experiments at the new high luminosity e^+e^- beauty factories (BABAR and BELLE) and the upgraded versions of CLEO and BES are producing a wealth of new data on heavy quarkonium decays. Here the discussion is restricted to the most recent results on radiative cascade decays $(\bar{Q}Q) \rightarrow (\bar{Q}Q)' + \gamma)$ and on the electromagnetic decays $(\bar{Q}Q) \rightarrow \gamma\gamma)$. The results from e^+e^- machines are compared to those obtained with a different technique by E835 at Fermilab.

New evidence for the 2^1S_0 state of Charmonium , the $\eta_c(2S)$, and for a 1D state of Bottomonium, announced respectively by the CLEO-III and BELLE collaborations, is also presented.

1 Introduction

After a few years of relative quiet, the field of Quarkonium (= heavy quarkonium) is now again bursting with activity. New results on spectroscopy, production and decay are coming in and more are expected given the large data samples available. Moreover failures in past attempts of explaining some of the experimental results have stimulated theoretical investigations leading to improved tools to deal with the boundary domain between perturbative and non perturbative QCD.

In this paper I will introduce briefly the theoretical formalism currently used to discuss Quarkonium (section 2), review significant experimental results elucidating the mechanism of Quarkonium production (section 3), and present new results on a subset of interesting Quarkonium decay channels (section 4).

2 The NRQCD/factorization formalism

At the beginning of the past decade Bodwin, Braaten and Lepage [1] introduced the Non Relativistic QCD/factorization formalism, an effective field theory based on a double series expansion on α_s and v, where v is the velocity of the quarks relative motion within the hadronic states partaking in a reaction. Since obviously this formalism applies when both α_s and v are small, Quarkonium is an ideal test ground.
In this formalism the cross-section for Quarkonium production is written as:

$$\sigma(a+b \rightarrow (\bar{Q}Q)+...) = \Sigma \sigma_{SD}(p_a + p_b \rightarrow (\bar{Q}+Q)[n]+....) \times LDME[n]$$

where a and b are the incoming particles and p_a, p_b are point-like probe and target for the short distance elementary process. σ_{SD} is the cross section for the short distance process, calculated with standard perturbative techniques. The perturbative series runs over intermediate Fock states [n(colour,$^{(2S+1)}l_J$))], characterized by their color and angular momentum degrees of freedom.

LDME[n] are long distance matrix elements that are assumed to be universal (that is independent of the short distance process) and factorizable. It is hoped that eventually the LDME[n] will be computed by Lattice techniques. At present they are derived from fits to experiments. Results should depend only on [n] and be consistent with a prescribed NRQCD scaling order (for example,

for[n] = $[1,^3S_1]$ they should contribute a factor $\propto M_Q^3 v_Q^3$ and for [n] = $[8,^3P_1]$ a factor $\propto M_Q^5 v_Q^5$). For $^3S_1$ states (ψ 's and Υ 's), in the limit $v \to 0$ this formalism, at lowest order, reduces to the more familiar Color Singlet Model (CSM) where only intermediate colorless states are allowed and where the soft processes are described in terms of $\bar{Q}Q$ state wave-functions calculated from potential models.

Early results from the measurement of the:

$$\bar{p} + p \to (\bar{Q}Q) + ...$$

cross-section [2], performed in Run I at the Tevatron, encouraged optimism. As shown in Fig.1, while Lowest Order (LO) CSM fails to reproduce the data, LO NRQCD, which allows for a significant contribution of octet terms (CO) $[8,^{2S+1}l_J]$, describes well the experimental results. In the next section I will show how the situation evolved in the light of recent experiments.

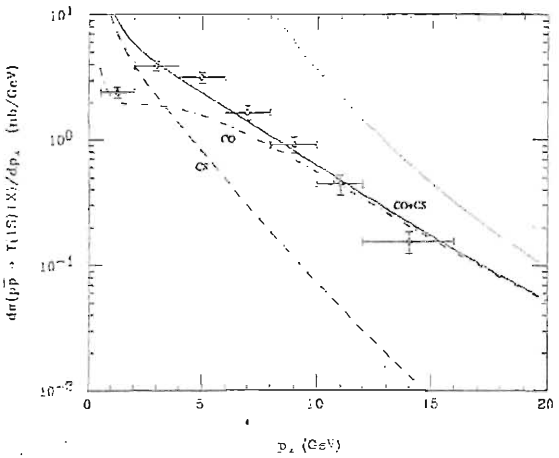

Figure 1: *Transverse momentum distribution of $\Upsilon(1S)$ from prompt production channels*

3 $\bar{Q}Q$ production mechanism

I will discuss first production mechanisms on a proton target. This will include results from experiments performed at HERA (ZEUS and H1) to study

$$e^{\pm} + p \rightarrow (\bar{Q}Q) + ...$$

and results of recent measurements performed at the Tevatron (CDF and D0) where the reaction studied is:

$$\bar{p} + p \rightarrow (\bar{Q}Q) + ...$$

The available data samples are listed in Table 1. New results are expected soon from the current data taking (Run II) at the Tevatron.

Experiment	Year	Luminosity
ZEUS + H1 (e^+)	94 -97; mid 99- 00	60;120 pb^{-1}
ZEUS + H1 (e^-)	98 - mid 99	15 pb^{-1}
CDF and D0	1992-95	110 pb^{-1}

Table 1: Integrated Luminosities for high energy experiments on a proton target

3.1 ZEUS and H1 at HERA

Variables used are: transverse momentum, p_T, $W^2_{\gamma p} = (q + P)^2$, (with q,P the four momenta of γ and proton respectively), rapidity, and $z = \frac{q.P_\psi}{q.P} = \frac{E^*_\psi}{E^*_\gamma}$ (with E^* in the proton rest frame). The variable z is used to distinguish diffractive processes, where $z \approx 1.0$, from inelastic processes, where $z \leq 0.9$. In what follows I will only discuss inelastic processes.

In Fig.2 are drawn the NRQCD lowest order photon-gluon fusion graphs that are thought to give the largest contributions. In (a) the intermediate state is a singlet and the emitted gluon is a hard one. In (b) the intermediate state is an octet that transforms into a singlet by bleeding off a soft gluon.

A good example of the ambiguities that can arise in the interpretation of experimental results is given in Fig.3, left [3] were the p^2_T distribution of inelastic J/ψ photoproduction, is compared to CS LO, to (CS + CO) LO and to CSM NLO. It is apparent that to describe the experimental results a

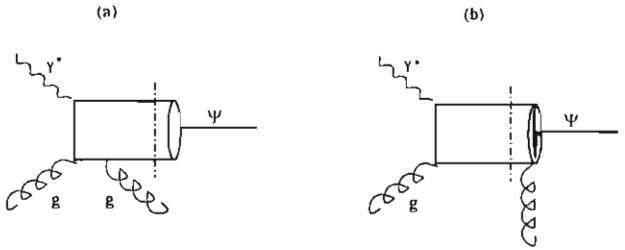

Figure 2: *Lowest Order graphs for Quarkonium production in electron proton interactions. The dash-dotted line is drawn to separate hard and soft processes.*

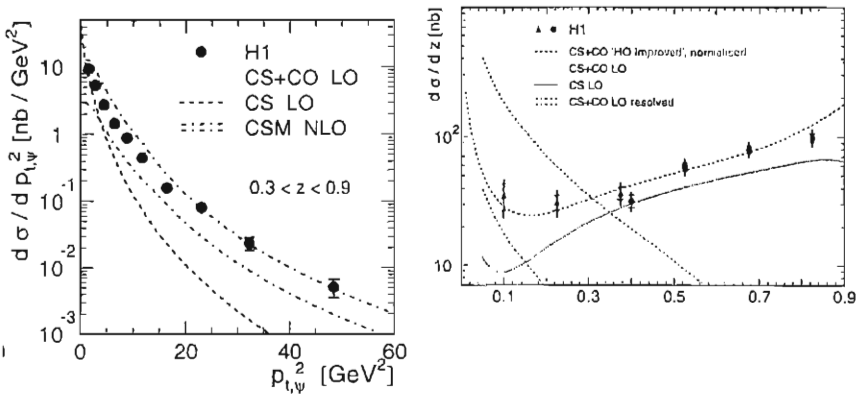

Figure 3: *Comparison of p_T^2 (left) and z (right) distributions with theoretical estimates*

lowest order calculations would require a CO contribution, which seems to be unnecessary when CSM calculations are performed at NLO. In Fig.3, right [3] the z distribution is compared to theoretical predictions. The dotted curve going through the data is the result of a NRQCD calculation and includes contributions of singlet and octet terms. The apparent agreement is misleading since it was obtained modifying the values of the LDME obtained by CDF for the same intermediate states.

3.2 CDF and D0 at the Tevatron

The interpretation of experimental results is more complicated in this case due to the complex nature of the probe. In $\bar{p}p$ collisions the dominant contributions to $\bar{Q}Q$ production are expected to come from the lowest order gluon-gluon fusion diagrams (the diagrams of Fig.2 where a gluon is substituted to the incoming γ^*). At present results are available both for $(\bar{c}c)$ and $(\bar{b}b)$ production however, since $(\bar{c}c)$ data are much more abundant and since the data on $(\bar{b}b)$ seem to follow closely the pattern of $(\bar{c}c)$ production, I will discuss only production of $(\bar{c}c)$ states

The experiments detect J/ψ and $\psi(2S)$ states through their decay into a $\mu^+\mu^-$ final states. J/ψ can come from three different sources: (a) directly produced in the $\bar{p}p$ reaction, (b) from the decay of heavier $(\bar{c}c)$ states,$\psi(2S)$ and χ_c, and (c) from the decay of b-flavored hadrons. The CDF collaboration estimated the fraction of J/ψ's from χ_c by reconstructing the χ_c decays to $J/\psi + \gamma$, while the (c) component was separated from the prompt ((a) + (b)) components reconstructing the displaced vertex of B decay.
CDF has recently measured the polarization of J/ψ and $\psi(2S)$ produced in $\bar{p}p$ interactions [4]. At large p_T one expects the $\psi's$ to be increasingly transversely polarized if their production is dominated by gluon fragmentation. This follows from the fact that the polarization of the gluon, close to being on shell in this kinematic regime, is preserved when the $\bar{c}c$ state evolves into a bound state.

The measurement of the polarization of ψ mesons is performed by studying the differential cross section as a function of the angle θ^* between the μ^+ direction in the ψ rest frame and the ψ direction in the $\bar{p}p$ center of mass frame. The angular distribution $I(cos\theta^*)$ is proportional to $(1 + \alpha \times cos^2\theta^*)$ where α = +1 (-1) for full transverse (longitudinal) polarization and 0 for unpolarized ψ's. Fig.4 shows the comparison of the experimental results to the predictions of the NRQCD/factorization model. As seen in Fig.4 the polarization fails to increase with p_T as would be expected from the theory .

3.3 Direct Quarkonium production at e^+e^- colliders

Prompt production of Quarkonium has also been extensively studied at e^+e^- colliders: at LEP where Z$\rightarrow$ J/ψ, Z$\rightarrow$ $\psi(2S)$ and Z$\rightarrow$ Υ, cross sections have been measured and, at low energy, by CLEO, BABAR and BELLE.
The most recent results come from BABAR [5] and BELLE [6] that have stud-

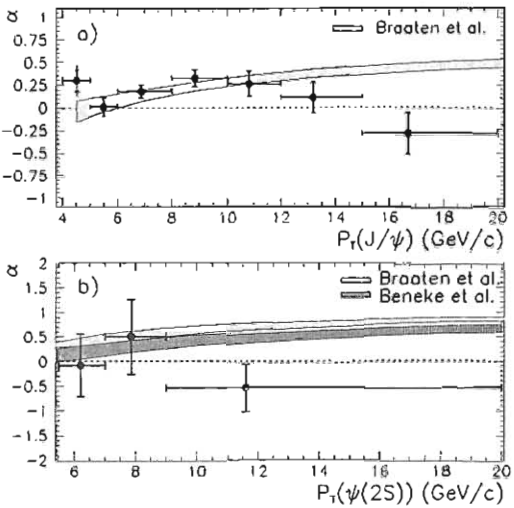

Figure 4: *CDF Polarization Measurements*

ied prompt production of J/ψ at and just below the $\Upsilon(4S)$ with the largest integrated luminosities ever obtained so far (see Table 2).

In the NRQCD formalism one expects the graphs given in Fig.5 to contribute

Exper.	J/Ψ	$\Psi(2S)$	$\Upsilon(1S)$	$\Upsilon(2S)$	$\Upsilon(3S)$	$\Upsilon(4S)$
BES	5.8×10^7	1.5×10^7				
CLEO-III			2.9×10^7	3.6×10^7	$4.7\ 10^6$	
BELLE						91. fb^{-1}
BABAR						95. fb^{-1}

Table 2: Experiments with large data samples, in part still to be analyzed

to prompt production in e^+e^- annihilations. Theoretical calculations [7), 8), 9)] predict graph (a), with an intermediate $^3S_1$ singlet state, to give the dominant contribution. The other $^3S_1$ singlet contribution (c), leading to a final state with two ($\bar{c}c$) pairs, is expected to be of order 10%. The octet terms (b), was predicted to be small over the range of J/ψ (and $\psi(2S)$) momenta in the center of mass system (p^*) except at the end point where some calculation predicted a dramatic increase.

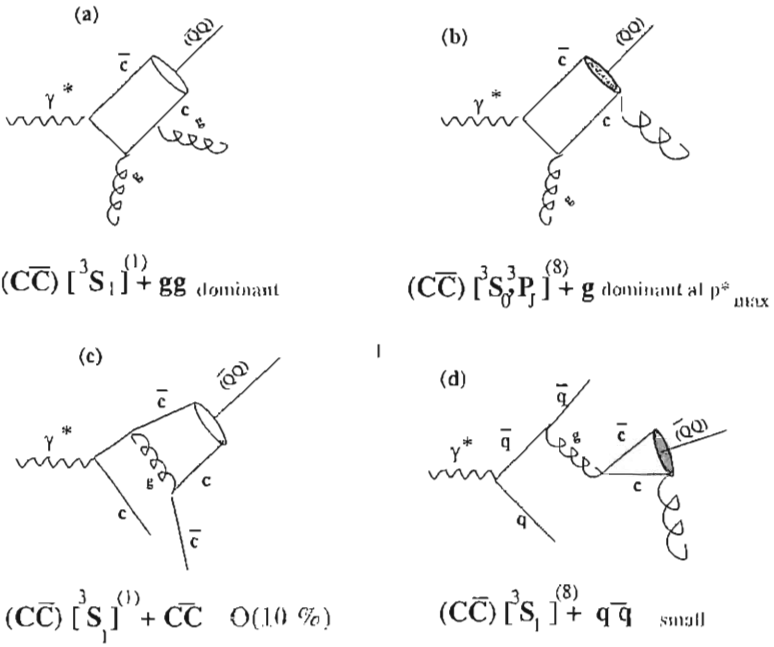

Figure 5: *Lowest order graphs contributing to the process of Quarkonium production in e^+e^- collisions*

The parameter $A(p^*)$ in the angular distribution $I(cos\theta^*) \propto (1 + A(p^*) \times cos^2(\theta^*))$ is predicted in the range $0.6 < A < 1.0$ by NRQCD while CSM predicts A = -0.8. Finally, J/ψ (and $\psi(2S)$) are expected to be longitudinally polarized only if Fig.5(b) contributes significantly to the production process. BABAR and BELLE have performed similar analysis of their data, measuring (a) the cross-section for production of J/ψ for $p^* > 2.GeV/c$ where backgrounds from Υ decays are small, (b) angular distributions determining the value of A(p^*) and (c) polarization measurements, determining the value of the parameter α which is +1 (-1) for transverse (longitudinal) polarization and 0 for unpolarized J/ψ's. BELLE, that reported results from 41.8 fb^{-1} taken at the Υ formation energy and 4.4 fb^{-1} taken 60 MeV below the resonance, also quotes results for the $\psi(2S)$. The two experiments give results that are in fair agreement, except for the value of the cross section which is measured to be (1.87 ± 0.10 ± 0.15) pb by BABAR and (1.05 ± 0.04 ± 0.09) pb by BELLE.

In Fig.6 we give the center of mass momentum (p*) distributions as measured

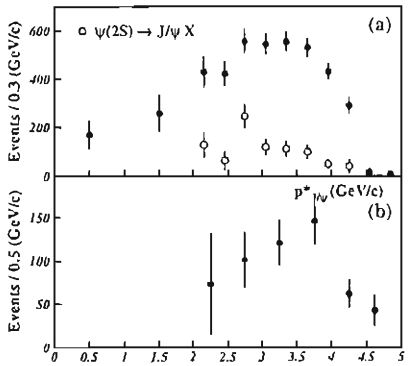

Figure 6: *J/ψ (a) and $\psi(2S)$ (b) center of mass momentum (p*) distributions*

by BELLE; the absence of an increase near the end point suggests that the contribution of the octet term Fig.5(b) is small . The value of A for $p^* > 2.$ GeV/c is found to be large and positive, in both experiments, favoring NRQCD vs the CSM. The value of α is approximately 0.5 and negative, as expected if the graph of Fig.5 (a) dominates.

The most recent result comes from a study by the BELLE collaboration [10] of the mass (m_R) spectrum of the object recoiling against the J/ψ. In the mass range $M_{\eta_c} < m_R < 2 \times m_{D0}$ they observe structures corresponding to the production, in association with the J/ψ, of charmonium states, with a significant ($\sim 5\sigma$) η_c signal and a good hint ($\sim 3.5\sigma$) of χ_0 and $\eta_c(2S)$ (Fig.7).

Above the open charm thresbold they observe the reactions:

$e^+ + e^- \rightarrow J/\psi + D^* + X$ *and* $e^+ + e^- \rightarrow J/\psi + D^0 + X$

The surprising results is that the $(2 \times \bar{c}c)$, component, which according to calculations should be of order 10%, has been measured to be $(59^{+15}_{-13} \pm 12)\%$, if one sums over charmonium and open charm production. A very interesting byproduct of this measurement is , of course, the siting of the $\eta_c(2S)$ (with $m_{\eta_c(2S)} = (3.622 \pm 0.012)\ GeV/c^2$) recoiling against the J/ψ.

In conclusion these measurements favour NRQCD over CSM, but indicate that some adjustment needs to be made to understand the relative weight of

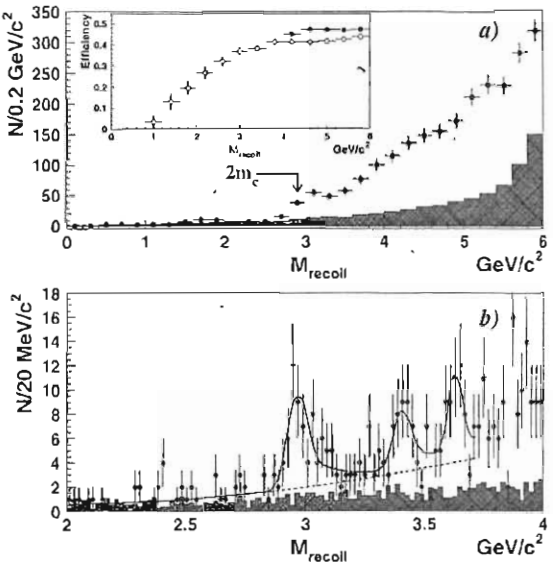

Figure 7: *Recoil mass (M_{recoil}) distribution in the reaction $e^+e^- \rightarrow J/\psi +$ recoil; (a) and (b) are without and with a constrain on the value of J/ψ mass*

the four graphs in Fig.5.

4 Quarkonium decays

$(\bar{Q}Q)$ decays can be divided in three groups:

- Electromagnetic decays: $(\bar{Q}Q) \rightarrow \gamma^* \rightarrow l^+l^- and (\bar{Q}Q) \rightarrow \gamma\gamma$
- Radiative decays to a lower mass charmonium state: $(\bar{Q}Q) \rightarrow \gamma + (\bar{Q}Q)$ or to light hadrons; $(\bar{Q}Q) \rightarrow \gamma + LH$
- Hadronic decays to a lower mass charmonium state: $(\bar{Q}Q) \rightarrow LH + (\bar{Q}Q)$ or to light hadrons: $\bar{Q}Q \rightarrow LH$

The field is too wide to be covered in this short review. I will restrict the discussion to few channels guided in the choice by the level of present activity and understanding and by personal taste.

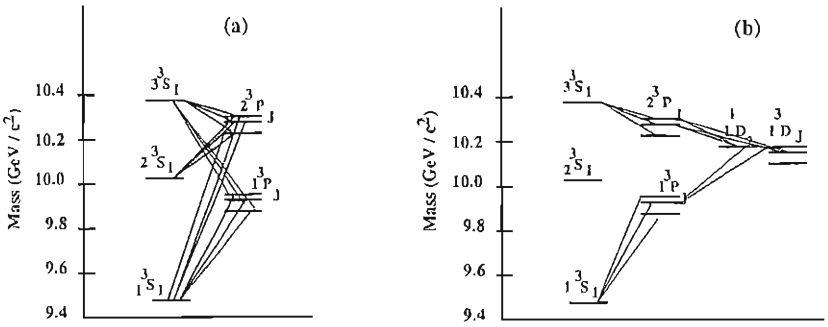

Figure 8: *Radiative* $\Upsilon(3S)$ *Cascade Decays: (a) to Final State* $2\gamma l^+l^-$ *and (b) to Final State* $4\gamma l^+l^-$

4.1 Radiative $(\bar{b}b)$ decays

CLEO-III [11] has recently studied $\Upsilon(3S)$ decays into a $l^+l^-\gamma\gamma$ final state with a data sample of 4.7×10^6 $\Upsilon(3S)$ events.

The decay chains observed (Fig.8 (a)), are:

$$3^3S_1 \to 2^3P_j + \gamma \to 2^3S_1 + \gamma; \quad j = 1,2$$

$$3^3S_1 \to 2^3P_j + \gamma \to 1^3S_1 + \gamma; \quad j = 1,2$$

$$3^3S_1 \to 1^3P_j + \gamma \to 1^3S_1 + \gamma; \quad j = 1,2$$

(The $^3P_0$ states decay predominantly to light hadrons, the Branching Ratio for radiative decays is small and therefore hard to measure.)
In the non relativistic limit, the decay rates for E1 radiative transitions scale with E_γ^3:

$$\Gamma_{E1} \propto e_b^2 \times | < n_f, l_f|r|n_i, l_i > |^2 \times E_\gamma^3$$

were $< n_f, l_f|r|n_i, l_i >$ decreases as the radial quantum number difference between initial and final states , $\Delta n = (n_i - n_f)$, increases. Deviation from this rule probe non relativistic effects (that in the case of $(\bar{b}b)$ states should be small). The results of the CLEO-III measurement are:

$$\frac{| < 2P_j|r|1S > |}{| < 2P_j|r|2S > |} = \sqrt{\frac{BR(3S \to \gamma 2P_j) \times BR(2P_j \to \gamma 1S) \times E_\gamma(2P_j \to 2S)^3}{BR(3S \to \gamma 2P_j) \times BR(2P_j \to \gamma 2S) \times E_\gamma(2P_j \to 1S)^3}} =$$

$= 0.105 \pm 0.004 \pm 0.006$ *for* $j = 2$ *and* $= 0.087 \pm 0.002 \pm 0.005$ *for* $j = 1$

with a ratio of 1.21 ± 0.06, 3.5 standard deviations from unity.
From their measured value of $BR(3^3S_1 \to \gamma 1^3P) \times BR(1^3P_j \to \gamma 1^3S_1)$ using

the world average for $BR(1^3P_j \to 1^3S_1 + \gamma)$, and assuming the matrix element to be spin independent, they succeed in extracting a new value for the $\Delta n = 2$ matrix element:

$$| < 1P_j|r|3S > | = (0.050 \pm 0.006)\ GeV^{-1}$$

Using the same data sample they also studied $l^+l^-4\gamma$ final states [12] searching for $\Upsilon(1^3D_j)$ production in the cascade reactions shown in Fig.8 (b). They claim a signal of $9.7\sigma's$ and measure:

$$BR(\Upsilon(3S) \to \gamma\gamma\Upsilon(1D) \to \gamma\gamma\gamma\gamma\Upsilon(1S) \to \gamma\gamma\gamma\gamma l^+l^-) = (3.3 \pm 0.6 \pm 0.5) \times 10^{-5}$$

in good agreement with the predicted value: 3.8×10^{-5} [13].

4.2 $(\bar{c}c)$ radiative cascade decays

The **BES** collaboration [14] has in hand data samples of 5.8×10^7 $\psi(2S)$ and 1.5×10^7 J/ψ and is presenting preliminary results on the decay:

$$J/\psi \to \eta_c + \gamma \to \gamma + LH$$

detected by reconstructing exclusive light hadrons final states. In the near future they should be able to resolve the $\eta_c(2S)$ puzzle; the $\eta_c(2S)$ was first detected by the Crystal Ball experiment in the $\psi(2S) \to \gamma + \eta_c(2S)$ inclusive decay channel at a mass of $(3594 \pm 5)\ GeV/c^2$ [15] and recently spotted in the $e^+ + e^- \to J/\psi + X$ reaction at $m_{\eta_c(2S)} = m_X = (3.622 \pm 0.012)\ GeV/c^2$ (see section 3.3).

	M [MeV/c^2]	Γ_{tot} [MeV]	$B_{in} \times \Gamma(\chi_c \to J/\psi + \gamma)$ [eV]
χ_{c0}	$3415.4 \pm 0.4 \pm 0.2$	$9.8 \pm 1.0 \pm 0.1$	$26.6 \pm 2.5 \pm 1.3$
χ_{c1}	$3510.60 \pm 0.02 \pm 0.13$	$0.88 \pm 0.06 \pm 0.06$	$19.3 \pm 0.8 \pm 1.2$
χ_{c2}	$3556.13 \pm 0.06 \pm 0.13$	$1.96 \pm 0.13 \pm 0.06$	$26.2 \pm 1.0 \pm 1.4$

Table 3: Preliminary values of the χ_c parameters from the Fermilab Experiments E760 and E835. The last column is obtained dividing the measured values by $BR(J/\psi \to e^+e^-) = (5.93 \pm 0.10) \times 10^{-2}$

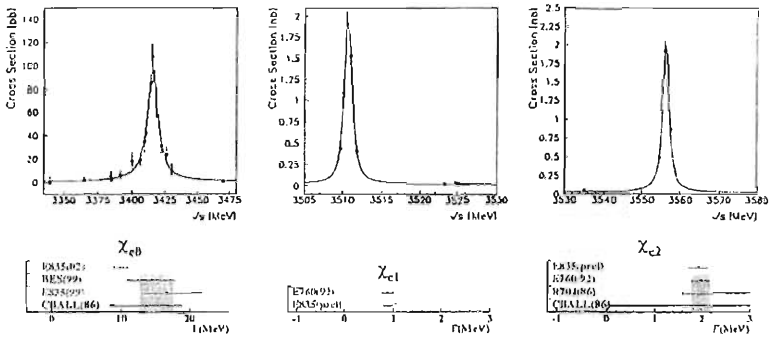

Figure 9: *E835* $\bar{p}p \to 1^3P_j \to J/\psi + \gamma \to e^+ + e^- + \gamma$ *excitation curves*

The E835 collaboration has recently completed [16] the study of the reactions: $\bar{p}p \to 1^3P_j \to J/\psi + \gamma \to e^+ + e^- + \gamma$ *with* $j = 0, 1, 2$. In this experiment the mass $m(\chi_{cj})$ the total width $\Gamma(\chi_{cj})$ and the product

$$\Gamma(\chi_{cj} \to J/\psi + \gamma) \times BR(J/\psi \to e^+ + e^-) \times BR(\chi_{cj} \to \bar{p}p)$$

are determined directly from the study of the resonance excitation curve. The quality of the data is demonstrated in Fig.9, were the results for the total widths are also compared with those of the predecessor experiment (E760) [17] and with those obtained by other experiments with different techniques.
In Tab.3 are reported the values obtained by combining the results of E835 and E760. The branching ratios for $\chi_{cj} \to J/\psi + \gamma$ and $\chi_{cj} \to \bar{p}p$ (Table 4) have been recalculated [18], [19] with a global refitting of existing data that uses as inputs measured combinations of branching fractions and partial widths, in an attempt to resolve the issue of correlations in the derivation of the values quoted . The calculation has been recently updated [20] to include new results published but not included in the 2002 issue of PDG [21, 22] or presented at the summer conferences [23, 24]. The results are still not sufficiently accurate to test the E_γ^3 scaling law (see section 4.1) and determine the effect of relativistic corrections that should be larger for $(\bar{c}c)$ than for $(\bar{b}b)$ states. Indeed the ratios of scaled widths for χ_{c2}, χ_{c1} and χ_{c0} are all compatible with 1, within errors.

The inclusive partial widths to light hadrons, $\Gamma(\chi_{cj} \to LH)$, also listed

	χ_{c0}	χ_{c1}	χ_{c2}
$B(\chi_c \to \bar{p}p) \times 10^4$	2.23 ± 0.26	0.72 ± 0.14	0.68 ± 0.07
$B(\chi_c \to J/\psi + \gamma) \times 10^2$	1.19 ± 0.14	31.7 ± 3.1	20.4 ± 0.6
$\Gamma(\chi_c \to J/\psi + \gamma)(keV)$	$126. \pm 17.$	291 ± 46	$428 \pm 37.$
$E_\gamma(MeV)$	303.6	389.2	429.6
$\frac{\Gamma(\chi_c \to J/\psi+\gamma)}{E_\gamma^3} \times 10^8(MeV^{-2})$	(4.5 ± 0.6)	(4.8 ± 0.9)	(5.4 ± 0.5)
$\Gamma_{LH}(MeV)$	9.7 ± 1.0	0.6 ± 0.1	1.58 ± 0.14

Table 4: Branching Ratios and Partial Widths as recalculated with global fitting (see text). Γ_{LH} are computed subtracting radiative widths from Γ_{tot}

in Table 4, were obtained by subtracting from the total widths given in Table 3 the radiative decay widths given in Table 4. The contribution of non electromagnetic cascade decays are negligible.

4.3 $(\bar{c}c)$ partial widths to $\gamma\gamma$

The $(\bar{c}c)$ partial widths to $\gamma\gamma$ have been measured by two different methods:

(a) Two-photon collisions at e^+e^- colliders.
These experiments measure the cross-section for exclusive resonance production:

$$\sigma(e^+e^- \to e^+e^-\gamma\gamma \to e^+e^-R) = \int L_{\gamma\gamma} \times \sigma(\gamma + \gamma \to R)dW$$

$\sigma(\gamma + \gamma \to R)$ is the Breit Wigner cross-section from which the partial width $\Gamma_{\gamma\gamma}$ can be extracted if the value of the total width Γ_{tot} is known.

Recent measurements come from **DELPHI** [25], on η_c production and from **BELLE** [22], on χ_{c2} production.

(b) Resonance formation in : $\bar{p}p \to R \to \gamma\gamma$
These experiments measure the product:

$$BR(R \to \bar{p}p) \times \Gamma(R \to \gamma\gamma)$$

E835 has presented recently new results on η_c and on χ_{c0}.

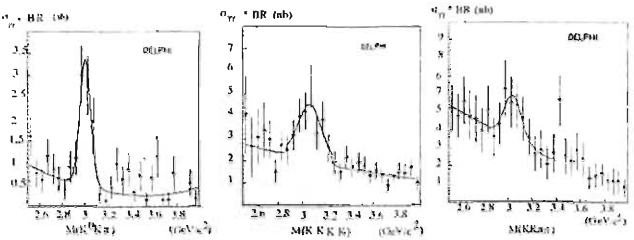

$\eta_c \to X$	$\Gamma_{\gamma\gamma}$ · BR(X) [keV]
$K^0_S K^+\pi^-$	$0.198 \pm 0.038(stat.) \pm 0.030(syst.)$
$K^+K^-K^+K^-$	$0.346 \pm 0.090(stat.) \pm 0.057(syst.)$
$K^+K^-\pi^+\pi^-$	$0.283 \pm 0.095(stat.) \pm 0.059(syst.)$

Figure 10: *Measurements of* $\Gamma(\eta_c \to \gamma\gamma)$ *by the* **DELPHI** *collaboration*

Measurement of $\Gamma(\eta_c \to \gamma\gamma)$

The **DELPHI** collaboration using method (a) detects the η_c through its exclusive decay to light hadrons (Fig.10) and measures the products of $\Gamma_{\gamma\gamma} \times BR(\eta_c \to X)$, (with X the detected final state), also given in Fig.10. From these results they extract the value: $\Gamma(\eta_c \to \gamma\gamma) = (13.9 \pm 2.0 \pm 1.4 \pm 2.7)\ keV$, where the last error reflects the uncertainties in the $\eta_c \to X$ branching ratios. A set of theoretical predictions is listed in Fig.11.

A recent calculation [27] gives: $\Gamma(\eta_c \to \gamma\gamma) = (7.6 \pm 1.5)\ keV$.

E835 uses method (b) [26]. Fig.12 shows the experimental cross section for the reaction $\bar{p}p \to \gamma\gamma$ measured at the η_c formation energy . From the measured value of $BR(\eta_c \to \bar{p}p) \times \Gamma(\eta_c \to \gamma\gamma)$ they derive:

$\Gamma(\eta_c \to \gamma\gamma) = 3.8^{+1.1+1.9}_{-1.0-1.0}\ keV$

The disagreement between the **DELPHI** and **E835** results is most probably due to the different ingredients used to go from the experimental result to the final value, pointing to the necessity of implementing a global fitting procedure also for the η_c state.

Measurement of $\Gamma(\chi_{c2} \to \gamma\gamma)$

The **BELLE** collaboration [22] has recently presented results of a determination

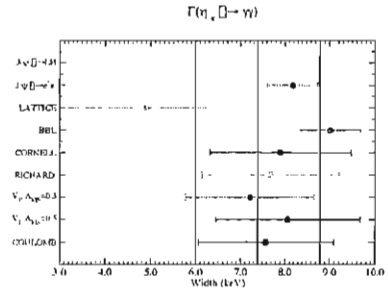

Figure 11: *Theoretical Predictions for* $\Gamma(\eta_c \to \gamma\gamma)$

of $\Gamma(\chi_{c2} \to \gamma\gamma)$ performed by measuring the cross section for the process:

$$e^+e^- \to e^+e^-\gamma\gamma \to e^+e^- + \chi_{c2} \to e^+e^- + J/\psi + \gamma \to e^+e^- + l^+ + l^- + \gamma$$

From this measurement they derive:

$$\Gamma(\chi_{c2} \to \gamma\gamma) \times BR(\chi_{c2} \to J/\psi + \gamma) = (114 \pm 11 \pm 9)\ eV$$

It is interesting to compare this result with that obtained by **E835** [28] measuring the cross section for $\bar{p}p \to \gamma\gamma$ at the χ_{c2} formation energy (Fig.13). In this case the quantity measured directly is:

$$\frac{\Gamma(\chi_{c2} \to \gamma\gamma)}{BR(\chi_{c2} \to J/\psi + \gamma) \times BR(J/\psi \to e^+ + e^-)}$$

from which one derives:

$$\frac{\Gamma(\chi_{c2} \to \gamma\gamma)}{BR(\chi_{c2} \to J/\psi + \gamma)} = (1.94 \pm 0.35)\ keV$$

Combining the BELLE and E835 measurements one could extract both the $BR(\chi_{c2} \to J/\psi + \gamma)$ and $\Gamma(\chi_{c2} \to \gamma\gamma)$. I prefer here to use the values of $BR(\chi_{c2} \to J/\psi + \gamma)$ obtained from the global refitting (see Table 4) and compare the values of $\Gamma(\chi_{c2} \to \gamma\gamma)$ obtained from the two experiments:
BELLE $\Gamma(\chi_{c2} \to \gamma\gamma) = (0.56 \pm 0.07)\ keV$
E835 $\Gamma(\chi_{c2} \to \gamma\gamma) = (0.40 \pm 0.07)\ keV$.
E835 has also recently presented preliminary results [24] on the measurement

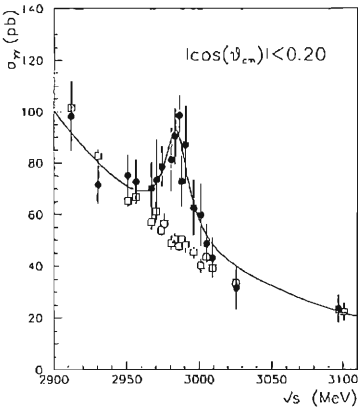

Figure 12: *E835* $\eta_c \to \gamma\gamma$ *excitation curve*

of the $\bar{p}p \to \gamma\gamma$ cross section at the χ_{c0} formation energy (Fig.14). In this case the quantity measured directly is: $\Gamma(\chi_{c0} \to \gamma\gamma) \times BR(\chi_{c0} \to \bar{p}p)$ from which, using the branching ratio to $\bar{p}p$ given in Table 4 one derives:

$$\Gamma(\chi_{c0} \to \gamma\gamma) = (2.9 \pm 0.9)\ keV$$

4.4 NRQCD predictions for χ_{cj} decays to light hadrons and to $\gamma\gamma$

Expressions for partial χ_{cj} widths to light hadrons have been calculated in the framework of NRQCD [29] to 3rd order in α_s. According to the authors the accuracy of the calculation is of $\approx 12\%$ [30]. In this formalism the expressions for $\chi_{cj} \to LH$ are given in term of a singlet ($H_1(m_c)$) and an octet ($H_8(m_c)$) matrix element. Color octet contributions do not depend on the spin of the χ state and, for the j=1 state, only appear at order α_s^3.

Partial χ_{cj} widths to $\gamma\gamma$ have been calculated to first order in α_s [29].

Using the existing formulas and the new experimental data it is possible to obtain a new determination of $H_1(m_c)$ and $H_8(m_c)$, and, more interesting, a new value for of α_s at the charmonium mass.

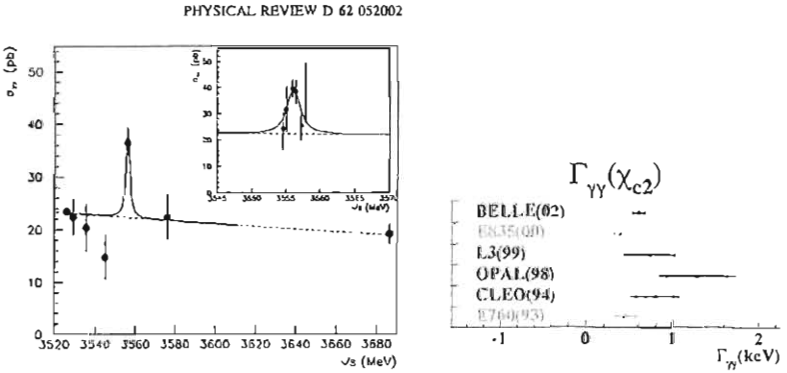

Figure 13: *E835* $\chi_{c2} \to \gamma\gamma$ *excitation curve*

5 Conclusions

The data on heavy quarkonium production are rich and accurate. New results are expected soon from Run II at the Tevatron and from the continuous flow of data at the B factories. The interpretation of the data with the current models is still ambiguous and contradictory but there are signs of renewed interest and theoretical effort to clarify the picture.

In this review I have limited the discussion to few decay channels omitting areas (for example that of glueball searches in J/ψ decays) of great interest.

New results on Quarkonium radiative cascade decays are approaching the level of directly measuring the effect of non-relativistic corrections both for the $(\bar{b}b)$ and the $(\bar{c}c)$ systems and suggest that such corrections are not very large.

New results on Quarkonium decays to two photons, coupled to measurements of decay widths to light hadrons will hopefully stimulate attempts to extend to higher orders the calculations of these processes.

Finally, a new, more rigorous, method (the global refitting procedure) of combining the data from different experiments shows the promise of reconciling results that had so far disagreed embarassingly.

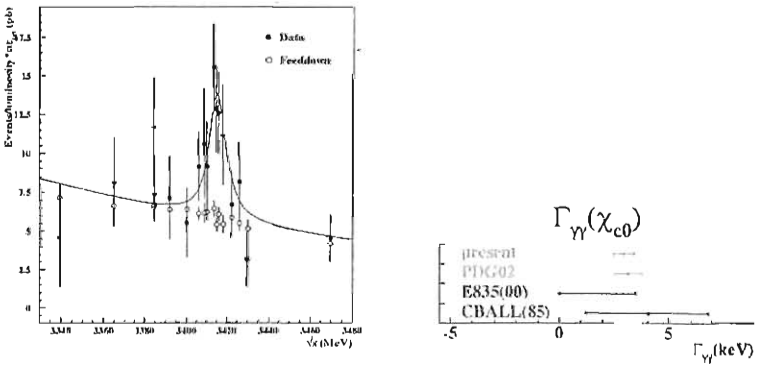

Figure 14: *E835* $\chi_{c0} \to \gamma\gamma$ *excitation curve*

References

1. G.T.Bodwin, E Braaten and G.P.Lepage, Phys. Rev.D. **51**,(1995) 1125
2. CDF collaboratio, F.Abe *et al.*, Fermilab-conf-94/221-E (1994) (unpublished)
3. Christoph Grab (for the H1 and ZEUS collaborations) ICHEP 02, July 2002 (to be published)
4. T.Affolder *et al.*, hep-ex/0004027 v2 17 Aug 2000
5. B.Aubert *et al.*, Phys.ReV. Lett. **87**, 162002 (2001)
6. K.Abe *et al.* Phys.ReV. Lett. **88**, 052001 (2002)
7. S.Baek,P.Ko,J.Lee and H.S. Song, Korean Phys. Soc. **33**, 97 (1998); hep-ph/9804455
8. P.Cho and A.K. Leibovich, Phys. Rev.D. **54**,6690 (1996)
9. E.Braaten and Yu-QiChen Phys.ReV. Lett. **76**, 730 (1996)
10. K.Abe *et al.* hep-ex/0205104 (2002) to be published in PRL Henryk Palka ICHEP 02, Amsterdam July 2002 (to be published)

11. D.Cinabro *et al.* hep-ex/0207062 v2 29 Aug 2002

12. S.E.Csorna *et al.* ICHEP 02, Amsterdam ABS948, CLEO CONF 02-06

13. Godfrey and Rosner Phys. Rev.D. **54**, 097501 (2001)

14. X.Shen (for the BES collaboration) XXII Physics in Collision Conference, SLAC, Stanford USA, June 2002

15. C.Edwards *et al.* [Crystal Ball collaboration] Phys.Rev.Lett.**48** 70 (1982)

16. W.Baldini *et al.* - to be published in Phys.ReV.D

17. T.A.Armstrong *et al.* Nucl.Phys B 373 (1992) 35

18. C.Patrignani, Phys.Rev.D 64(2001) 034017

19. K. Hagivara *et al.* [Particle Data Book collaboration] Phys.Rev.D 66(2002) 010001

20. C.Patrignani, private communication

21. S.Bagnasco *et al.* [E835 collaboration], Phys.Lett.B 533 (2002) 237

22. K.Abe [Belle Collaboration], Phys.Lett.B 540 (2002) 33

23. P.Rumerio [for the E835 collaboration] The Exclusive Reaction $\bar{p}p \rightarrow chi_{c0} \rightarrow \pi^0\pi^0 \quad (\eta\eta) \quad \rightarrow 4\gamma$. Presented at the BEACH02, Vancouver, June 2002, and at this Conference; to be published.
J.Z.Bai *et al.* [BES Collaboration], hep-ex/0109040v1, 26 Sep 2001

24. M. Graham [for the E835 collaboration] Measurement of the Two Photon Partial Width of the χ_{c0} at Fermilab E835. Presented at the 5th Int. Conf. on Quark Confinement and the Hadron Spectrum, Gargano, Sept. 2002, and to be published

25. A.Oblakowska-Mucha, B.Muryn and G. Polok, DELPHI 2002-080 CONF 614, June 2002, contributed paper for ICHEP02, Amsterdam, July 2002

26. M.Ambrogiani *et al.* [E825 collaboration], to be published

27. N.Fabiano and G. Pancheri, hep-ph/0204214 18 Apr 2002

28. M.Ambrogiani *et al.* [E825 collaboration],Phys.Rev.D **65**(2002)052002

29. H.Huang and K Chao hep-ph/960606220v3 29 Dec 1996

30. H.Huang and H. Hu and X. Zhang, Phys.Rev.D **56** (1997) 5816

Frascati Physics Series Vol. XXXI (2003), pp. 63–68
FRONTIERSCIENCE 2002 – Frascati, October 6–11, 2002
Invited Contribution in Plenary Session

THE EXCLUSIVE REACTION $p\bar{p} \to \chi_{c0}(1^3P_0) \to \pi^0\pi^0$ (and $\eta\eta$) $\to \gamma\gamma\gamma\gamma$

Paolo Rumerio *†
Northwestern University, Department of Physics and Astronomy,
2145 Sheridan Road, Evanston, IL 60208-3112, USA

ABSTRACT

For the first time in hadronic Charmonium production, hadronic annihilation channels have been clearly identified: $\pi^0\pi^0$ and $\eta\eta$ at the χ_{c0} resonance. This has required a parameterization of the non-resonant partially interfering final state channels. Preliminary results for $B(p\bar{p}) \times B(\pi^0\pi^0)$ and $B(p\bar{p}) \times B(\eta\eta)$ are reported.

1 Introduction

The Fermilab E835 Collaboration has studied Charmonium production using a gas jet hydrogen target, the virtually monoenergetic stochastically cooled

* On behalf of the Fermilab E835 Collaboration
† Email address: rumerio@fnal.gov

antiproton beam and a large acceptance shower spectrometer. A description of the experiment technique can be find in [1].

New data were collected in the year 2000, to continue the charmonium spectroscopy studies of 1996/97 and 1990/91 (E760). In particular, 33 pb^{-1} of luminosity were taken at the χ_{c0} energy, divided in 17 energy points.

2 $\pi^0\pi^0$ and $\eta\eta$ Angular Distribution

The angular distribution for $p\bar{p} \to \pi^0\pi^0$ and $p\bar{p} \to \eta\eta$ is:

$$\frac{d\sigma}{dz} = \left| \frac{-A_R}{x+i} + \underbrace{\sum_{J=0}^{even} C_J(x)\ e^{i\delta_J(x)}\ P_J(z)}_{\equiv A_I\ e^{i\delta_I}} \right|^2 + \left| \underbrace{\sum_{J=2}^{even} C_J^1(x)\ e^{i\delta_J^1(x)}\ P_J^1(z)}_{\equiv A_N\ e^{i\delta_N}} \right|^2 \quad (1)$$

where $x \equiv \frac{E_{CM} - M_{\chi_{c0}}}{\Gamma_{\chi_{c0}}/2}$ and $z \equiv |\cos\theta^*|$, with θ^* defined as the angle between the beam and the π^0 (or η) axes in the center of mass frame. $P_J(z)$ and $P_J^1(z)$ are the Legendre Polynomials and Associate Functions, respectively.

The term $-A_R/(x+i)$ is the parameterization of a Breit-Wigner resonant amplitude. No z-dependence is included since the χ_{c0} is a spin zero state. We can distinguish two contributions to the *non-resonant* cross section: $A_I e^{i\delta_I}$, which *interferes* with the resonance, and $A_N e^{i\delta_N}$, which does not. No matter how many partial waves play a role, $A_I e^{i\delta_I}$ and $A_N e^{i\delta_N}$ do not change markedly when the energy varies across the resonance.

Eq.1 can also be written as:

$$\frac{d\sigma}{dz} = \frac{A_R^2}{x^2+1} + A_I^2 + \underbrace{2A_R A_I \frac{\sin\delta_I - x\cos\delta_I}{x^2+1}}_{cross-term} + A_N^2 \quad (2)$$

For fixed values of z, as the energy varies across the resonance (x passes through zero), even a very small A_R^2 (relatively to the non-resonant cross section) can give rise to a detectable signal thanks to the *cross-term* of eq.2.

3 $\pi^0\pi^0$ Cross Section, Data and Fit

In fig.1 the measured cross section is plotted versus z and versus the energy in the center of mass, E_{CM}. At off-resonance energy points, the cross section is *non-resonant* production $p\bar{p} \to \pi^0\pi^0$ with a smooth dependence on the energy.

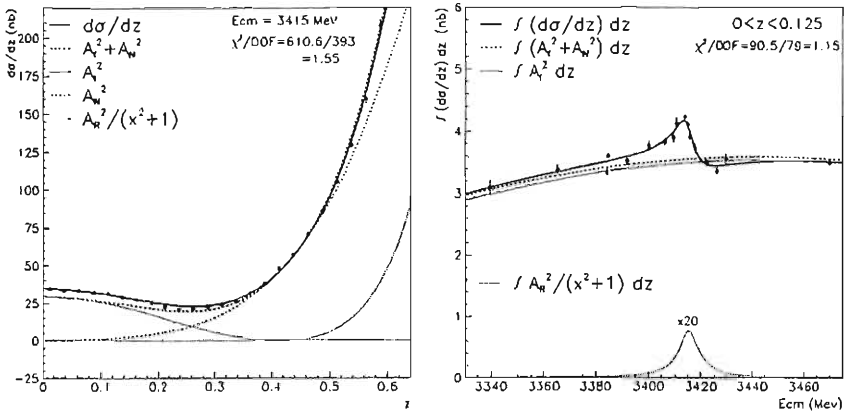

Figure 1: *Measured $\pi^0\pi^0$ cross section versus z at $E_{CM} = 3415$ MeV (left) and versus E_{CM} integrated over $0 < z < 0.125$ (right). Fits (described in the text) and their components are also shown.*

The instrumental background (events from different channels, such as $\pi^0\pi^0\pi^0$ and $\pi^0\omega$, that are misidentified as $\pi^0\pi^0$) is $\sim 1.5\%$ at all energies and it has been subtracted.

A maximum likelihood fit with the parameterization of eq.1, including partial waves up to $J = 4$, has been performed simultaneously on all energy points[1] (fig.1-left). The total number of bins is 17 (energy points) $\times 24$ (bins in z, from 0 to 0.6) $= 408$. The number of free parameters is 15: the resonance amplitude A_R, the coefficients $C_{0,2,4}$ and $C^1_{2,4}$ (each of them is given a linear dependence on the energy), and the phases $\delta_{0,2,4}$ and[2] $(\delta^1_4 - \delta^1_2)$.

The line $A_I^2 + A_N^2$ shows the sum of the two contributions to the non-resonant cross section. The effect of the resonance, amplified by the interference, is seen in the gap (evident at small z) between $d\sigma/dz$ and $A_I^2 + A_N^2$ and is

[1] E835 has recently studied the reaction [2)] $p\bar{p} \to \chi_{c0} \to J/\psi\,\gamma$; $J/\psi \to e^+e^-$. This channel has a virtually zero instrumental background and non-resonant cross section (optimal experimental conditions to fully exploit the superior mass resolution of the $p\bar{p}$ technique). The values $M_{\chi_{c0}} = (3415.4 \pm 0.4 \pm 0.2)$ MeV/c^2 and $\Gamma_{\chi_{c0}} = (9.8 \pm 1.0 \pm 0.1)$ MeV/c^2 thereby measured are used here to fit the cross section of the $\pi^0\pi^0$ channel.

[2] Only the difference between δ^1_4 and δ^1_2 is measurable.

due almost entirely to the cross-term of eq.2. The gap decreases as z increases, following the trend of A_I. The term A_N^2 is small at small values of z, due to a factor z present in all the associate functions $P_J^1(z)$. The net suppression factor of A_N^2 with respect to A_I^2 is z^2 at small z-values. The contribution of the *pure* resonance $A_R^2/(x^2+1)$ is negligible.

The fit in fig.1-left is very instructive. However, due to the limited available z-range and the necessity to contain the number of free parameters, we cannot further investigate the possible contribution of higher partial waves and affirm that only $J = 0, 2, 4$ are significant (although with just $J = 0, 2$ the fit gives an adequate description of the cross section in the available range). Considering also that the fit is dominated by the high statistics of the forward peak, where the resonant signal is not significant, we do not rely on it to estimate the magnitude of the resonance amplitude A_R.

A more reliable approach is to perform a different fit on a reduced range at small z (fig.1-right). In this range the resonance signal has a substantial size and, as observed above, the non-interfering part is very small (reducing therefore the uncertainty on the estimate of the ratio A_I^2/A_N^2, critical in determining the amplification effect of the interference). The expression used is:

$$\sigma = \int_0^{0.125} \left| \frac{-A_R}{x+i} + A_I \, e^{i\delta_I} \right|^2 dz + \int_0^{0.125} A_N^2 \, dz$$

where $A_I^2 \equiv A + Bx + Cx^2 + Dz^2$. A_N^2 is set to the values estimated by the fit in fig.1-left and corresponds to the gap between the lines $A_I^2 + A_N^2$ and A_I^2. Notice that in this case we do not need to make any assumption on the number of partial waves involved in the reaction. We just perform a polynomial expansion on z about $z = 0$, exploiting the small extension of the range. A polynomial expansion is used for the energy dependence as well. There are 6 free parameters (A_R, A, B, C, D, and δ_I), while the number of bins is 17 (energy points) $\times 5$ (bins in z) $= 85$. By searching for improvements in the χ^2 we find that the phase δ_I does not exhibit any dependence on z (in this small z-range) nor on the energy.

It has to be stressed that the *pure* Breit-Wigner (the fictional cross section that would result if the non-resonant amplitudes could be turned off) is very small. In fig.1-right it is shown multiplied by 20 to make it comparable to the signal that we detect.

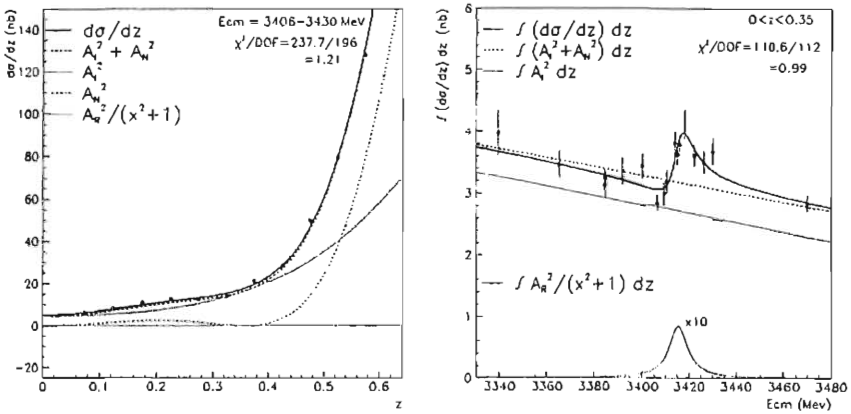

Figure 2: *Measured $\eta\eta$ cross section versus z at E_{CM} = 3406 − 3430 MeV (left) and versus E_{CM} integrated over $0 < z < 0.35$ (right). Preliminary fits and their components are also shown.*

Our preliminary result (with statistical and systematic errors, respectively) is:

$$B(\chi_{c0} \to p\bar{p}) \times B(\chi_{c0} \to \pi^0\pi^0) = (5.09 \pm 0.81 \pm 0.25) \times 10^{-7} \qquad (3)$$

4 The $\eta\eta$ and $\pi^0\eta$ channels

In addition to the data presented above, we are also analyzing the $\eta\eta$ and $\pi^0\eta$ final states. Fig.2 and fig.3 show the measured cross sections and the preliminary fits.

We observe a signal from the χ_{c0} in the $\eta\eta$ channel, as well, as shown in fig.2-right. The fitting procedure is similar to the one of the $\pi^0\pi^0$ analysis. Our preliminary result is:

$$B(\chi_{c0} \to p\bar{p}) \times B(\chi_{c0} \to \eta\eta) = (4.0 \pm 1.2) \times 10^{-7} \qquad (4)$$

The error is statistical. A study of the systematic error is ongoing.

No signal from the χ_{c0} is observed in $p\bar{p} \to \pi^0\eta$ ($c\bar{c}$ is isospin-suppressed) and the fit shown in fig.3 is performed using eq.1 with A_R set to zero[3]. The $\pi^0\eta$ channel provides a check on the systematics of the experiment.

[3]Removing the constraint, the fit estimate of A_R is consistent with zero.

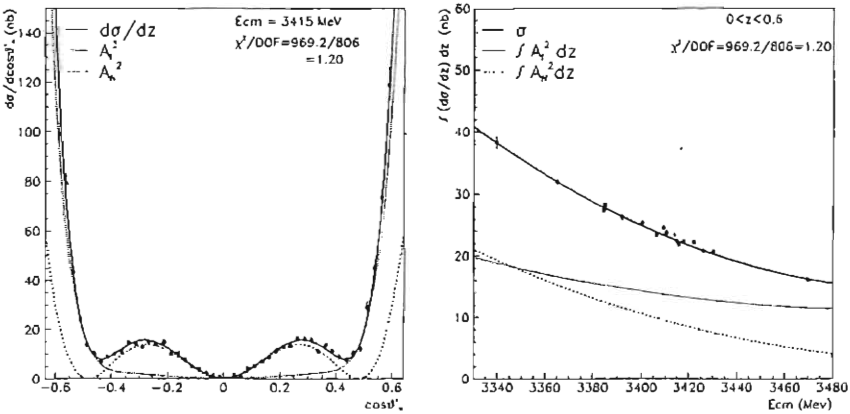

Figure 3: *Measured $\pi^0\eta$ cross section versus $\cos\theta^*_{\pi^0}$ at $E_{CM} = 3415$ MeV (left) and versus E_{CM} integrated over $0 < z \equiv |\cos\theta^*_{\pi^0}| < 0.6$ (right). A preliminary fit and its components are also shown.*

5 Conclusions

We have improved our knowledge of the χ_{c0} state. Combining our results, eq.3 and eq.4, with measurements from other experiments, improvements in $B(p\bar{p})$, $B(J/\psi\,\gamma)$, $B(\pi^0\pi^0)$, and $B(\eta\eta)$ will be obtained.

We have developed and proved the effectiveness of a technique for dealing with resonant/non-resonant interference and detecting a resonant signal in channels dominated by order-of-magnitude larger non-resonant cross section.

Finally, we have gained insights into possible future strategies for attacking outstanding problems, namely the poor knowledge of the singlet $c\bar{c}$ states and the existence of hadromolecular $c\bar{c}q\bar{q}$ states.

References

1. M. Ambrogiani *et al.* [E835 Collab.], Phys. Rev. D **62**, 052002 (2000).

2. S. Bagnasco *et al.* [E835 Collab.], Phys. Lett. B **533**, 237 (2002).

Frascati Physics Series Vol. XXXI (2003), pp. 69–72
FRONTIERSCIENCE 2002 – Frascati, October 6–11, 2002
Invited Contribution in Plenary Session

CHARMOMIUM PRODUCTION AT HERA

Andreas Meyer
Inst. f. Experimentalphysik, Universität Hamburg, Luruper Chaussee 149, 22761 Hamburg, Germany

ABSTRACT

Recent measurements on inelastic J/ψ production in ep collisions at HERA are presented. The data from the H1 and ZEUS experiments are compared to model predictions of the Colour Singlet Model and of non–relativistic QCD.

1 Introduction

Inelastic J/ψ production in ep collisions is dominated by the process of photon–gluon–gluon fusion where a photon from the incoming electron and a gluon from the proton produce a $c\bar{c}$ pair. The process can be calculated within the framework of non–relativistic QCD (NRQCD) where the cross section is a sum over all possible intermediate $c\bar{c}$ states, including colour singlet (CS) and also colour octet (CO) states. The amplitude for each $c\bar{c}$ state with definite colour and

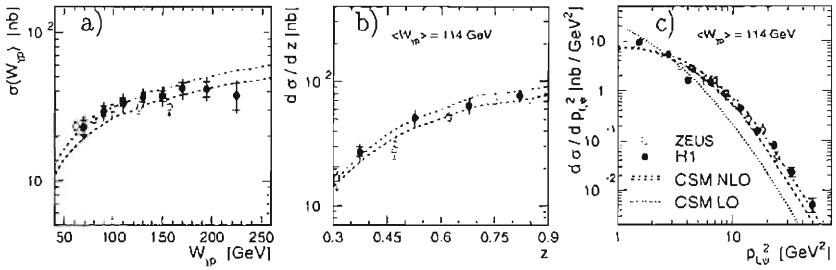

Figure 1: a) Total J/ψ photoproduction cross section as a function of $W_{\gamma p}$ and differential cross sections as functions of b) $p^2_{t,\psi}$ and c) z. The ZEUS points [3] are shifted by up to 12% to account for differences in the covered kinematic range. The CSM calculations in NLO is shown by the band. The normalization uncertainties are due to variations of α_s and the charm mass m_c.

angular momentum factorises into a short distance term which can be calculated in NRQCD and a long distance matrix element (LDME) describing the transition to a J/ψ. The LDME are not calculable and have been determined from J/ψ production data in $p\bar{p}$ collisions [1] where the CO contributions were found to be sizable. Previous HERA measurements show good agreement with the colour singlet term alone, which is the only term taken into account in the Colour Singlet Model (CSM), but small colour octet contributions could not be excluded. At HERA two kinematic domains are distinguished: In photoproduction ($Q^2 < 1\,\mathrm{GeV}^2$) the exchanged photons are quasi–real, in electroproduction they have a higher virtuality ($Q^2 > 2\,\mathrm{GeV}^2$).

2 Photoproduction Cross Sections

The H1 photoproduction data [2] are studied in the elasticity range $0.05 < z < 0.9$ and transverse momentum squared of the J/ψ meson $p^2_{t,\psi} > 1\,\mathrm{GeV}^2$. Remaining backgrounds to prompt J/ψ production coming from decays of B, ψ' or χ_c and mainly contributing at low values of z are not subtracted from the data. Figure 1 shows the H1 data in comparison with the ZEUS results [3]. Good agreement is found between the two experiments. The data are well described by a next–to leading order (NLO) calculation [4] in the Colour Singlet Model. In contrast, the LO calculation is much too steep in $p^2_{t,\psi}$. The elasticity distribution (Fig. 2 a) can also be described in the whole range by leading order

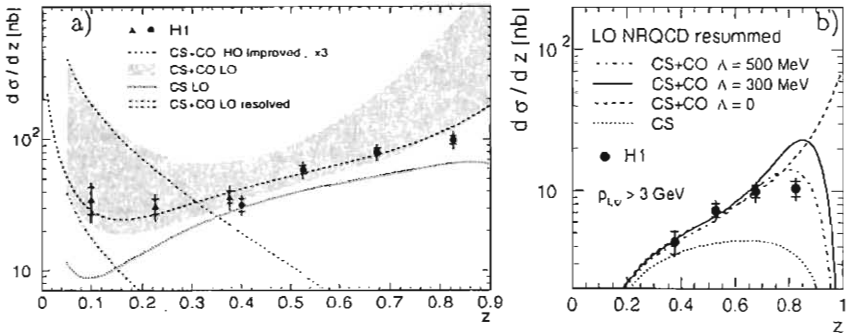

Figure 2: Differential J/ψ photoproduction cross section as a function of z a) in comparison to NRQCD calculations [5]; b) for $p_{t,\psi} > 3\,\mathrm{GeV}$ in comparison with a resummed NRQCD calculation [6] (scaled by a factor 3). The parameter Λ describes the energy loss of the J/ψ due to soft gluon emission.

NRQCD calculations [5] with LDMEs for the colour octet contributions at the lower end of the range allowed by the Tevatron data. The steeper rise of the NRQCD calculations towards high z than that in the data may be due to phase space limitations for the emission of soft gluons in the transition from the $c\bar{c}$ state to the J/ψ meson which are not considered in [5]. A resummation [6] of the non-relativistic expansion, which is valid at large $p_{t,\psi}$, leads to a considerable reduction of the increase and better agreement with the data (Fig. 2 b).

3 Electroproduction Cross Sections

The inelastic electroproduction of J/ψ mesons [2] is studied in the region $2 < Q^2 < 100\,\mathrm{GeV}^2$ for medium elasticities $0.3 < z < 0.9$ and the squared transverse momentum of the J/ψ meson in the photon–proton center-of-mass system $p^{*2}_{t,\psi} > 1\,\mathrm{GeV}^2$. Neither the full NRQCD calculation [7] nor the colour singlet part can describe the data in normalisation (Fig. 3 a,b). At high Q^2 and $p^{*2}_{t,\psi}$ agreement with the full NRQCD prediction is found. The CSM prediction falls too steeply in $p^{*2}_{t,\psi}$. This may be due to missing higher order contributions in this LO calculation (cf. Fig. 1 c) in photoproduction). The dependence of the cross section on z, however, is well described by the CS contribution. The calculation including the CO contributions rises too strongly towards large z.

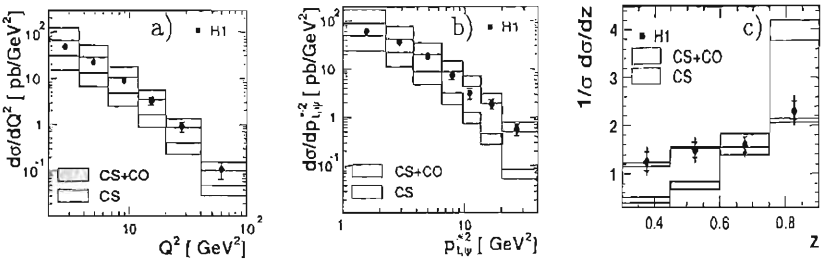

Figure 3: Differential J/ψ electroproduction cross section as a function of a) Q^2 and b) $p^{*2}_{t,\psi}$. c) Normalized differential cross section as a function of z. The data are compared to a full NRQCD calculation [7] (dark band) and to the colour singlet contribution alone (light band).

4 Summary

New results on inelastic J/ψ photo- and electroproduction have been presented. In photoproduction agreement is found with the CSM in next-to leading order and also with NRQCD calculations in leading order with small colour octet contributions. In electroproduction the leading order CSM does not describe the normalisation of the data. The full NRQCD calculation is in agreement with the data at large Q^2 and $p^{*2}_{t,\psi}$, but fails to describe the elasticity distribution.

References

1. F. Abe *et al.* [CDF Coll.], Phys. Rev. Lett. **79** (1997) 572.

2. C. Adloff *et al.* [H1 Coll.], Eur. Phys. J. C**25** (2002) 1, 25-39.;
   C. Adloff *et al.* [H1 Coll.], Eur. Phys. J. C**25** (2002) 1, 41-53.

3. S. Chekanov *et al.* [ZEUS Collaboration], arXiv:hep-ex/0211011.

4. M. Krämer, Nucl. Phys. B **459** (1996) 3.

5. M. Krämer, Prog. Part. Nucl. Phys. **47** (2001) 141. ;
   B.A. Kniehl and G. Kramer, Eur. Phys. J. C **6** (1999) 493.

6. M. Beneke, G.A. Schuler and S. Wolf, Phys. Rev. D **62** (2000) 034004.

7. B.A. Kniehl and L. Zwirner, Nucl. Phys. B **621** (2000) 337.

Frascati Physics Series Vol. XXXI (2003), pp. 73–77
FRONTIERSCIENCE 2002 – Frascati, October 6–11, 2002
Invited Contribution in Plenary Session

MEASUREMENT OF THE $b\bar{b}$ PRODUCTION CROSS SECTION IN 920 GeV p-N COLLISIONS WITH HERA-B

Benedetto Giacobbe
University and I.N.F.N Bologna, via Irnerio 46, 40127 Bologna, Italy

ABSTRACT

A measurement of the $b\bar{b}$ production cross section ($\sigma(b\bar{b})$) was performed by HERA-B in p-C and p-Ti collisions at 920 GeV. Delayed $J/\psi \to l^+l^-$ events from b decays were observed both in the muon and electron channels in the kinematic range $-0.25 < x_F < 0.15$ and a combined measurement was performed leading to a full x_F range value $\sigma(b\bar{b}) = 32^{+14}_{-12}(\text{stat})^{+6}_{-7}(\text{sys})$ nb/nucleon [1], in good agreement with the most recent theoretical calculations. The perspectives on an ongoing high statistics measurement will also be discussed.

1 Introduction

Due to the still large theoretical uncertainties in the description of b hadroproduction [2], a precise measurement of the $b\bar{b}$ cross section in proton-nucleus interactions is of high interest. Only two experiments at fixed target have measured $\sigma(b\bar{b})$ so far [3], their results showing a poor compatibility despite the large experimental errors. Thanks to its large coverage, its fast trigger and its high resolution Silicon Vertex Detector, HERA – B [4] appears to be the best candidate to provide a high precision measurement extending also in the non

explored negative x_F region. A clean and efficient separation of the b decays from the background is possible in HERA - B thanks to the excellent vertex resolution (≈ 500 μm along the beam direction and ≈ 40 μm in the transverse plane) compared to the large average b decay length (≈ 8000 μm).

During the year 2000 commissioning phase of the experiment, a small sample of dilepton triggered events were acquired in a reduced detector and trigger configuration at 5 MHz interaction rate. Electron candidates were selected by the Electromagnetic Calorimeter pretrigger as clusters with a transverse energy $E_T > 1.0$ GeV, while muon candidates were defined by the MUON pretrigger as double pad chambers coincidences. Double candidate events were acceted by the First Level Trigger, further confirmed by the Second Level software Trigger applying a simplified Kalman filter in the Main Tracker and the Vertex Detector System (an additional e^+e^- invariant mass trigger cut > 2 GeV/c^2 was applied) resulting in an overall rate reduction of about 10^5. About 900 k and 450 k events were acquired in the dielectron and dimuon channels respectively in about one week of data taking.

2 The measurement

We measured [1] the $b\bar{b}$ production cross section exploiting the inclusive reaction $pA \to b\bar{b}X$ with $b\bar{b} \to J/\psi Y \to (e^+e^-/\mu^+\mu^-)Y$. The $b \to J/\psi$ production cross section per nucleon in the measured range, containing a fraction f ($\approx 72\%$) of prompt J/ψ, is:

$$\Delta\sigma(b\bar{b}) = \sigma_r \, f \, \frac{N_B}{N_P} \, \frac{1}{\varepsilon_R \, \varepsilon_B^{\Delta z} \, \mathrm{Br}(b\bar{b} \to \mathrm{J}/\psi X)} \qquad (1)$$

We first select a clean prompt J/ψ sample (N_P), then isolating the $b \to J/\psi$ events (N_B) via a detached vertex selection with efficiency $\varepsilon_B^{\Delta z}$. Apart from $\varepsilon_B^{\Delta z}$, only the $b \to J/\psi$ to prompt J/ψ relative trigger and reconstruction efficiency ε_R has to be evaluated with the Monte Carlo including the J/ψ and $b \to J/\psi$ production models [1] and a detailed detector simulation. The branching ratio $\mathrm{Br}(b\bar{b} \to \mathrm{J}/\psi X)$ is $2 \cdot (1.16 \pm 0.10)\%$ [5], while the reference prompt J/ψ production cross section $\sigma_r = 314 \pm 7(\mathrm{stat}) \pm 31(\mathrm{sys})$ nb/nucleon is obtained by averaging and rescaling the existing E789 and E771 [6] results to the HERA - B kinematics [1]. The procedure is aimed to minimize systematic errors related to the detector and trigger simulation, which mostly cancel out in the ratio ε_R, and to remove the dependence on the absolute luminosity.

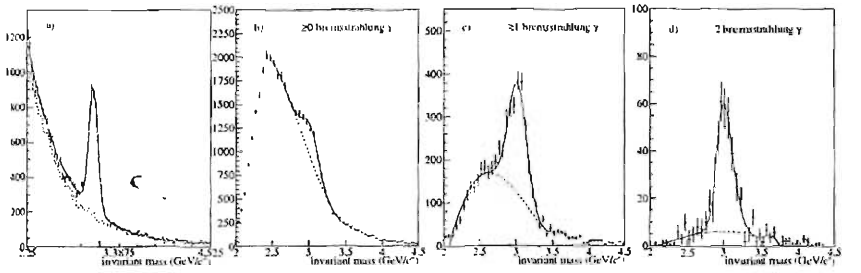

Figure 1: *a) $\mu^+\mu^-$ invariant mass with same sign background (25 MeV/c^2 bins). b-c-d) e^+e^- invariant mass with different bremsstrahlung requirements and combinatorial background (50 MeV/c^2 bins).*

3 Prompt J/ψ Selection

Events with two fully reconstructed trigger tracks and dilepton vertex requirement ($\chi^2 < 5$) are selected. A standard muon identification procedure, based on likelihood cuts in the MUON and RICH systems, is performed resulting in the dimuon mass spectrum of Fig. 1a) corresponding to $N_P = 2880 \pm 60$ prompt $J/\psi \to \mu^+\mu^-$ decays. Additional identification criteria for the $J/\psi \to e^+e^-$ signal are needed in order to reduce the large hadronic background, based on the electron energy-to-momentum (E/p) ratio and on the search for accompanying bremsstrahlung photons emitted upstream the magnet (i.e. maintaining the original electron direction). Fig 1b)-d) show the signal purity for various bremsstrahlung requirements and a 1 σ E/p cut. The careful evaluation of the efficiency for such cuts, confirmed by the simulation, allows to infer the number of prompt J/ψ present in a sample with looser identification cuts, in order to have sufficient statistics for the detached vertex analysis. A total number of prompt $J/\psi \to e^+e^-$ $N_P = 5710 \pm 380(\text{stat}) \pm 280(\text{sys})$ is found.

4 Detached J/ψ Selection

For the $b \to J/\psi$ event selection, detached vertex cuts are applied on the decay length (Δz), defined as the distance along the beam axis between the J/ψ decay vertex and the primary interaction wire, and on the impact parameter to the primary vertex (I_{vert}) and to the wire (I_w) or to any other track in the event (I_{iso}). These cuts allow to reject tracks compatible with coming from the primary vertex and from anywhere along the interaction wire. The

resulting mass versus Δz distribution of the dielectron sample is shown in Fig. 2a): 19 events downstream the primary interaction region (of which 10 in the J/ψ mass window 2.8 $GeV/c^2 < m_{e^+e^-} < 3.3$ GeV/c^2), and 8 upstream (pure combinatorial background) survive the requirements $\Delta z > 0.5$ cm, $I_w > 200\,\mu$m OR $I_{iso} > 250\,\mu$m. The mass distribution of the downstream events is submitted to an unbinned likelihood fit where the yields are left free, the $b \to J/\psi \to e^+e^-$ signal shape is taken from simulation and the background shape is a combination of the simulated main physical contribution (double semileptonic b decays) and the pure combinatorial events. The result of the fit yields $8.6^{+3.9}_{-3.2}$ $b \to J/\psi \to e^+e^-$ events. Varying the cuts in order to verify the stability of the result, a J/ψ signal is always observed with significance greater than 2 σ in the downstream spectrum, but never upstream. Moreover, the b assignment of the candidates is confirmed by an unbinned maximum likelihood fit of their Δz values, as opposed to the result obtained on the upstream pure background. A similar analysis with slightly looser cuts, due to the smaller available statistics, was applied on the dimuon sample, leading to $1.9^{+2.2}_{-1.5}$ $b \to J/\psi \to \mu^+\mu^-$ events.

5 Results and Conclusions

A combined analysis in the muon and electron channels was performed from Eq. 1 by applying a four parameter likelihood maximization ($\Delta\sigma(b\bar{b})$, $\mu^+\mu^-$ background slope, e^+e^- and $\mu^+\mu^-$ background yields) and using the computed efficiencies $\varepsilon_B^{\Delta z}$ and ε_R. The result obtained for the $b\bar{b}$ production cross section in the full x_F range is [1]:

$$\sigma(b\bar{b}) = 32^{+14}_{-12}(\text{stat})\,^{+6}_{-7}(\text{sys})\ \text{nb/nucleon}. \qquad (2)$$

where the quoted statistical uncertainty has been estimated directly from the fit. A detailed discussion of the systematic errors can be found in [1] and include contributions both external to the present analysis, statistics related terms and factors arising from the Monte Carlo simulation including prompt J/ψ and b production models. It has to be noted that more than 90% of b are produced in the HERA – B x_F acceptance, thus minimizing the uncertainties in the extrapolation to the full range.

The obtained result shows a satisfactory consistence with the most recent QCD calculations [2], as shown in Fig. 2b). During the year 2001 HERA

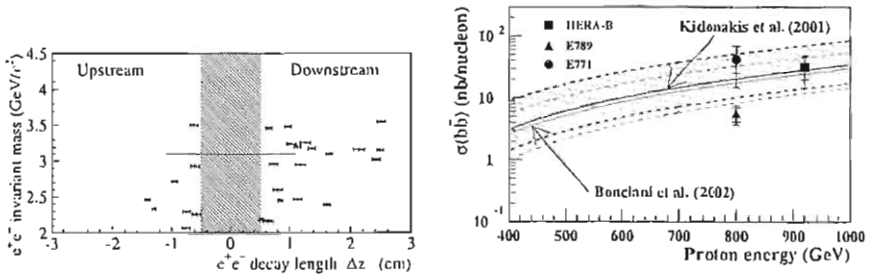

Figure 2: *a)* e^+e^- *invariant mass versus* Δz. *b)* $\sigma(b\bar{b})$ *measurements compared with theoretical calculations (see text).*

shutdown, HERA - B underwent a substantial improvement, resulting in an increased trigger efficiency, acceptance and resolution, which will allow the detector to acquire $O(10^6)$ prompt J/ψ events and $O(10^3)$ b events during the ongoing physics run, resulting in a $\leq 15\%$ error (systematic limited). This will be the by far most precise $\sigma(b\bar{b})$ measurement at fixed target energies.

References

1. HERA - B Collaboration, I. Abt *et al.*, Eur. Phys. J. C (2002) 10.1140/epjc/s2002-01071-8

2. P. Nason, Proc. of the XX International Symposium on Lepton and Photon Interactions at High Energies, hep-ph/0111024; S. Frixione *et al.*, Adv. Ser. Direct. High Energy Phys. **15** (1998), 609; R. Bonciani *et al.*, Nucl. Phys. **B529** (1998) 424; N. Kidonakis *et al.*, Phys. Rev. **D64** (2001) 114001.

3. D. M. Jansen *et al.*, Phys. Rev. Lett. **74** (1995) 3118; T. Alexopoulos *et al.*, Phys. Rev. Lett. **82** (1999) 41.

4. E. Hartouni *et al.*, HERA - B Design Report, DESY-PRC-95-01 (1995).

5. D. E. Groom *et al.*, Eur. Phys. J. **C15** (2000) 1.

6. M. H. Schub *et al.*, Phys. Rev. **D52** (1995) 1307; T. Alexopoulos *et al.*, Phys. Rev. **D55** (1997) 3927.

Frascati Physics Series Vol. XXXI (2003), pp. 79–87
FRONTIERSCIENCE 2002 – Frascati, October 6–11, 2002
Invited Review Talk in Plenary Session

CHARM AND BEAUTY SPECTROSCOPY

Paul D. Sheldon
Vanderbilt University, Nashville, TN, USA

ABSTRACT

Recent results in charm spectroscopy are discussed. Emphasis is given to the recent results on the wide L=1 charm mesons and to the possible observation of doubly charmed baryons.

1 Introduction

Charm hadron spectroscopy continues to be a vigorous and productive field, with the ground states well mapped out. Recently, significant forays have been made into the domain of higher angular momentum states.

For brevity, I will concentrate on recent results on the wide L=1 charm mesons and the possible observation of doubly charmed baryons.

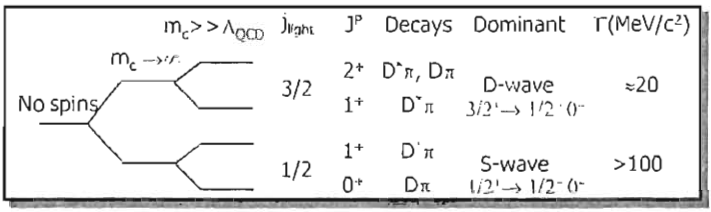

Figure 1: *Expected L=1 charm mesons.*

2 Charm Meson Spectroscopy

In Heavy Quark Effective Theory (HQET), mesons with one very heavy quark can be thought of as an atom where the spin of the heavy quark is decoupled from that of the light quark. The spectroscopy of states can be described by j_{light}, which is the sum of the spin of the light quark and the angular momentum of the light quark "orbit" around the heavy central quark. This model works suprisingly well for charm mesons. The expected L=1 states are illustrated in Fig 1. The six $j_{light} = 3/2$ states (two each for $c\bar{d}$, $c\bar{u}$, and $c\bar{s}$) are expected to be narrow because their decays must be D-wave. Mesons consistent with these states have all been observed and their properties, taken from the particle data book [2], are summarized in Table 1. The six $j_{light} = 1/2$ states states, on the other hand, are all expected to be very broad (hundreds of MeV) and it was assumed these states would be difficult if not impossible to observe. However, Belle and CLEO have recently presented what may be evidence for the D^0 $(c\bar{u})$ version of these states. More tenuous evidence for one of the wide D^+ $(c\bar{d})$ states has been shown in preliminary results from the FOCUS collaboration.

2.1 Wide L=1 D^0 States

Belle, the first generation B-factory at KEK, finds [1] possible evidence for the wide L=1 D^0 states using B^- decays: $B^- \to D^{**0}\pi^-$; $D^{**0} \to D^{(*)+}\pi^-$. They reconstruct D^+ candidates via the decay mode $K^-\pi^+\pi^+$, and D^{*+} candidates via $D^0\pi^+$; $D^0 \to K^-\pi^+$ or $D^0 \to K^-\pi^+\pi^-\pi^+$. They make a cut on the candidate D^+ mass or the D^0 mass and $D^{*+} - D^0$ mass difference, then use a beam energy constraint to eliminate feed down due to partially reconstructed decays of other states. The difference (ΔE) in the reconstructed energy of the B^- candidates and the beam energy is plotted in Fig. 2 for candidates

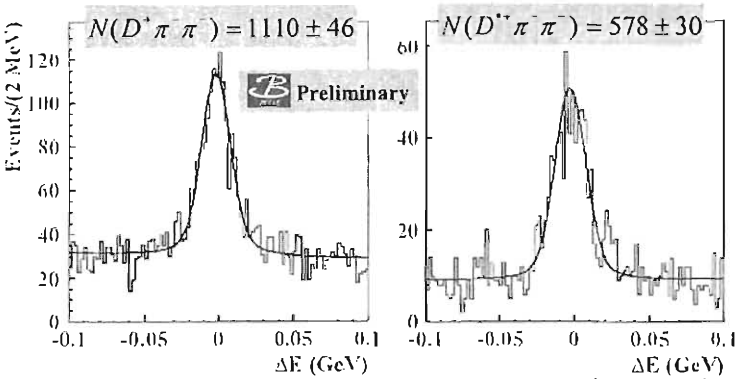

Figure 2: *ΔE for B^- candidates reconstructed via the D^+ and D^{*+} chains described in text.*

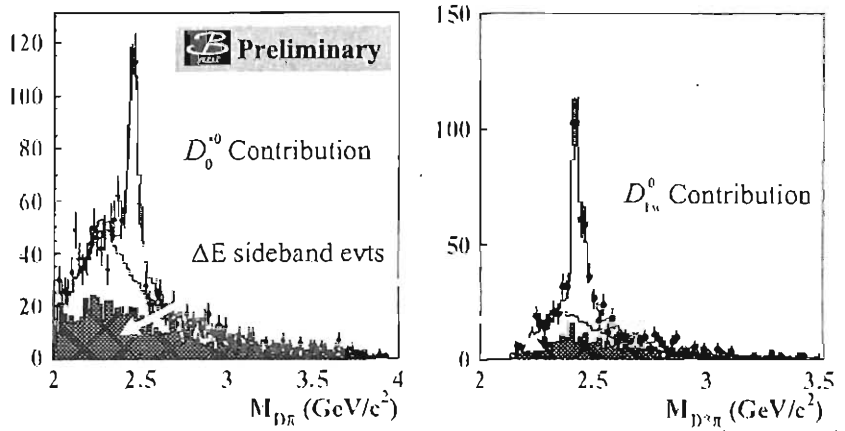

Figure 3: *$D\pi$ mass projections for candidates found via the D^+ and D^{*+} chains.*

reconstructed through the D^+ and D^{*+} chains.

$D\pi$ mass projections for these candidates (Fig. 3) show broad and narrow peaks. Belle fits the $D\pi\pi$ Dalitz plots for these events to a coherent sum of Breit-Wigner amplitudes, and try a variety of models for the wide contributions. For the candidates in the D^+ chain, they always include contributions from the narrow D_2^{*0} L=1 state as well as the L=0 D^*. For the wide contribution they try amplitudes with $J^p = 0^+$, 1^-, and 2^+. The likelihood for the fit with a

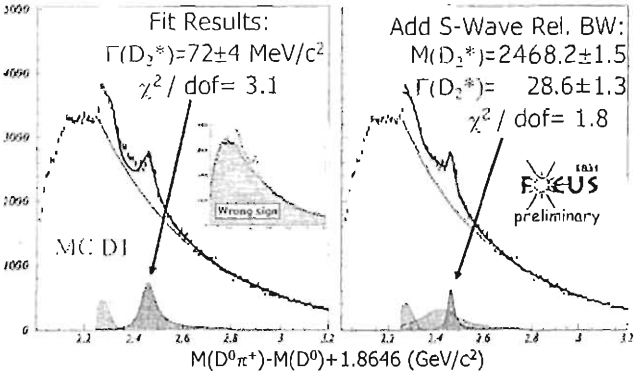

Figure 4: *Fits to $D^0\pi^+$ spectra with and without a broad S-wave contribution. The inset shows the combinatoric backgroup estimated using a wrong sign sample.*

0^+ contribution (assumed to be the D_0^{*0}) is significantly better than the other models. The mass and width that they get from this fit for the D_0^{*0} and D_2^{*0} are listed in Table 1.

Belle carries out a similar analysis for the D^{*+} chain, and find the likelihood is best when they include contributions from the wide L=1 states D_{1w}^0 and D_2^{*0} (they fix the mass and width of the D_2^{*0} from their D^+ fit above). They extract the masses and widths of the D_{1w}^0 and the D_1^0; these are listed in Table 1. CLEO, in a conference talk, has previously reported an observation of the D_{1w}^0 with similar parameters, and this result is also included in Table 1.

2.2 Wide L=1 D^+ States

FOCUS, a fixed-target photoproduction experiment at Fermilab, searches for the wide L=1 D_0^{*+} state through its decay to $D^0\pi^+$. Candidates for this decay are shown in Fig. 4. There is a large combinatoric background in these plots, see the "wrong sign" versus "right sign" comparison in the inset of the figure. This background is well modeled by an exponential beyond the signal region. There are also feeddown contributions from partially reconstructed D_1^+ and D_2^{*+} decays, the shapes of these are derived from Monte Carlo and included in the fit. They fit the candidate mass spectrum, including the three contributions above and a D-wave Breit-Wigner contribution from the D_2^{*+}. When they do,

Table 1: *Summary of the properties of the L=1 Charm Mesons.*

MeV/c²		Mass	Width	
D^0	D_2^{*0}	2458.9 ± 2.0	23 ± 5	PDG
		2461 ± 2 ± 3	46.4 ± 4.4 ± 3.1	Belle
	D_1^0	2422.2 ± 1.8	18.9+4.6-3.5	PDG
		2423.9 ± 1.7 ± 0.2	26.7 ± 3.1 ± 2.2	Belle
	D_{1w}^0	2400 ± 30 ± 20	380 ± 100 ± 100	Belle
		2461+48-42	290+110-90	CLEO
	D_{0}^{*0}	2290 ± 22 ± 20	300 ± 30 ± 30	Belle
D^+	D_2^{*+}	2459 ± 4	25+8-7	PDG
	D_1^+	2427 ± 5	28 ± 8	PDG
	D_{1w}^+	unseen		
	D_0^{*+}	??? seen by	FOCUS???	
D_S	D_{s2}^{*+}	2572.4 ± 1.5	15 + 5 − 4	PDG
	D_{s1}^+	2535.35 ± 0.34 ± 0.5	<2.3	PDG
	D_{s1w}^+	unseen		
	D_{s0}^{*+}	unseen		

the width they get for the D_2^{*+} is too wide by a factor of three. If they include an S-wave contribution (presumably from a D_0^{*+}) the χ^2 of their fit gets much better and the width of the D_2^{*+} agrees with previous measurements. Whether or not this truely is evidence for the D_0^{*+} remains to be seen.

2.3 L=1 Charm Meson Summary

A summary of the properties of the L=1 charm meson states is given in Table 1.

3 Charm Baryon Spectroscopy

The ground state charm baryons present a rich spectroscopy. The observed states seem to be consistent with those predicted by SU(4): candidates for all of the ground state (L=0) singly charmed baryons have been observed (although J^p has not been determined for any of them).

The SELEX collaboration has recently presented evidence [3] for one, and possibly two, doubly charmed baryons. SELEX is a fixed-target hadroproduction experiment at Fermilab. It took data with 600 GeV π^-, p, and Σ^- beams.

Doubly charmed baryons should have two secondary decay vertices, one

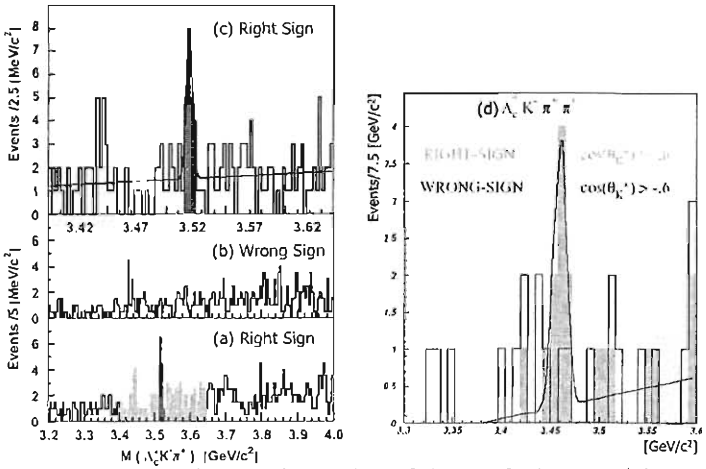

Figure 5: *Mass spectra for the SELEX candidates. Right sign (a) and wrong sign (b) Ξ_{cc}^{+} candidates. (c) Right sign plot in finer detail. (d) Right and wrong sign Ξ_{cc}^{++} candidates.*

for each charm quark. SELEX searched for deacys in which the second (most downstream) vertex was from the decay of a Λ_c^+ (such as $\Xi_{cc}^+ \to \Lambda_c^+ K^- \pi^+$; $\Lambda_c^+ \to pK^-\pi^+$). Starting with a sample of ~1600 Λ_c^+ candidates, they look for evidence of an additional decay vertex between the Λ_c^+ vertex and the primary (production) vertex. If the first charm quark decays to a strange quark (Cabibbo favored) then this vertex will likely contain a K^-; they use this to define a "right sign" and "wrong sign" (K^+) sample. Their resulting spectra for $\Xi_{cc}^+ \to \Lambda_c^+ K^- \pi^+$ candidates are shown in Fig. 5 (a) and (b), and the right sign spectrum is shown in finer detail in Fig. 5 (c). They observe a peak in the right sign distribution at a mass of 3520 MeV/c^2 and a width of 3 MeV/c^2. There are 15.9 background subtracted events in the signal region, with an expected background of 6.1 events. They are unable to determine the lifetime of the state, and can only say that it is < 33 fs. They find the probability that this peak is a fluctuation is $< 1.1 \times 10^{-4}$, and note that all 22 events in the signal region were produced by baryon beams (p or Σ^-).

SELEX has also shown a candidate signal (Fig. 5 (d)) for Ξ_{cc}^{++} in the decay mode $\Lambda_c^+ K^- \pi^+ \pi^+$. The peak in their right sign distribution is at a mass of 3460 MeV/c^2, with a width of 5 MeV/c^2. They observe 9 background sub-

Table 2: *Decay modes used in the FOCUS search for Ξ_{cc}^{+} and Ξ_{cc}^{++}. Expected signals are based on a simple model, and are not based on the SELEX result.*

Parent	Decay mode	BR(D or Λ_c)	BR(Ξ_{cc})	Signal
Ξ^{++}	$D^0(K\pi)\,\Lambda^0\,\pi^+\,\pi^+$	3.83%	3.2%	1.0
Ξ^{++}	$D^0(K3\pi)\,\Lambda^0\,\pi^+\,\pi^+$	7.5%	3.2%	0.5
Ξ^{++}	$D^0(K\pi)\,K_s^0\,p\,\pi^+$	3.83%	0.69%	0.2
Ξ^{++}	$D^0(K3\pi)\,K_s^0\,p\,\pi^+$	7.5%	0.69%	0.1
Ξ^{++}	$D^+\,K^-\,\pi^+\,p$	9.0%	1.0%	0.2
Ξ^{++}	$D^+\,\Lambda^0\,\pi^+$	9.0%	1.92%	0.8
Ξ^{++}	$D^+\,\Lambda^0\,\pi^+\,\pi^-\,\pi^+$	9.0%	0.32%	0.1
Ξ^{++}	$D^+\,K_s^0\,p$	9.0%	1.03%	0.5
Ξ^{++}	$\Lambda_c^+\,K^-\,\pi^+\,\pi^+$	5.0%	5.0%	1.0
Ξ^{++}	$\Lambda_c^+\,K^0\,\pi^+$	5.0%	1.72%	0.4
Ξ^{++}	$\Lambda_c^+\,K_s^0\,\pi^+\,\pi^-\,\pi^+$	5.0%	1.72%	0.2
Ξ_{cc}				
Total				5.0

Parent	Decay mode	BR(D or Λ_c)	BR(Ξ_{cc})	Signal
Ξ^{+}	$D^0(K\pi)\,K^-\,p\,\pi^+$	3.83%	1.0%	0.1
Ξ^{+}	$D^0(K3\pi)\,K^-\,p\,\pi^+$	7.5%	1.0%	0.1
Ξ^{+}	$D^0(K\pi)\,\Lambda^0\,\pi^+$	3.83%	4.47%	0.5
Ξ^{+}	$D^0(K3\pi)\,\Lambda^0\,\pi^+$	7.5%	4.47%	0.4
Ξ^{+}	$D^0(K\pi)\,\Lambda^0\,\pi^+\,\pi^-\,\pi^+$	3.83%	0.32%	0.0
Ξ^{+}	$D^0(K3\pi)\,\Lambda^0\,\pi^+\,\pi^-\,\pi^+$	7.5%	0.32%	0.0
Ξ^{+}	$D^0(K\pi)\,K_s^0\,p$	3.83%	1.03%	0.1
Ξ^{+}	$D^0(K3\pi)\,K_s^0\,p$	7.5%	1.03%	0.1
Ξ^{+}	$D^+\,K^-\,p$	9.0%	1.0%	0.5
Ξ^{+}	$D^+\,\Lambda^0$	9.0%	1.6%	0.4
Ξ^{+}	$D^+\,\Lambda^0\,\pi^+\pi^-$	9.0%	0.96%	0.2
Ξ^{+}	$D^+\,K_s^0\,p\,\pi^-$	9.0%	0.69%	0.1
Ξ^{+}	$\Lambda_c^+\,K^-\,\pi^+$	5.0%	3.0%	0.3
Ξ^{+}	$\Lambda_c^+\,K^-\,\pi^+\,\pi^-\,\pi^+$	5.0%	0.1%	0.0
Ξ^{+}	$\Lambda_c^+\,K^0$	5.0%	0.69%	0.1
Ξ^{+}	$\Lambda_c^+\,K_s^0\,\pi^-\,\pi^+$	5.0%	0.69%	0.0
Ξ_{cc}				
Total				2.8

tracted signal events, with an expected background of 1 event, and determine that the probability of such a fluctuation is $< 10^{-5}$.

There are some concerns with these signals, however. The mass difference between these two isospin partners is too large (60 GeV/c^2, the largest such splitting in singly charmed baryons is ~10 MeV/c^2). Double charm baryons would have to account for roughly 40% of SELEX's Λ_c^+ baryons (10% from each of the two modes above). Kiselev and Likhoded [4] point out that the SELEX result requires "exotically high production rate in comparison with theoretical expectations," and argue that the lifetime of these states is expected to be 160 fs, much larger than the upper limit of 33 fs observed.

In 2000, the FOCUS collaboration performed a search for doubly charmed baryons without any knowledge of the SELEX analysis. FOCUS looked for signals by combining the 9 Ξ_{cc}^{++} and 12 Ξ_{cc}^{+} modes shown in Table 2. The expected signals listed in this table are based on a relatively simple (naive) "first prin-

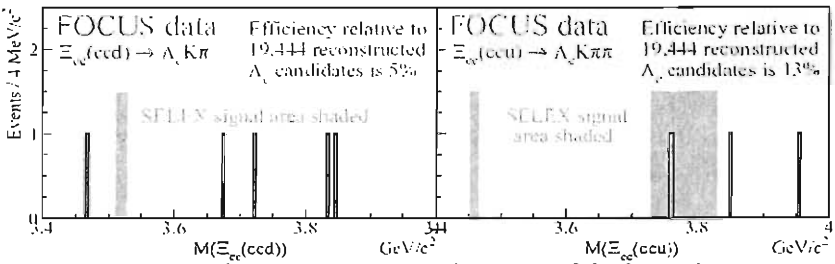

Figure 6: *Combined mass plots from the FOCUS search.*

Table 3: *Comparison of the results of the SELEX and FOCUS searches.*

Decay Mode	$\Xi_{cc}^{+} \to \Lambda_c^{+} K^{-} \pi^{+}$		$\Xi_{cc}^{++} \to \Lambda_c^{+} K^{-} \pi^{+} \pi^{+}$	
Experiment	FOCUS	SELEX	FOCUS	SELEX
Ξ_{cc} Events	< 2.21 @ 90%	15.8	< 2.21 @ 90%	8
Reconstructed Λ_c	$19,444 \pm 262$	1650	$19,444 \pm 262$	1650
Efficiency Relative to Λ_c	5%	10%	13%	5%
Ξ_{cc}/Λ_c^{+}	<0.23% @ 90%	9.6%	<0.09% @ 90%	9.7%
$\frac{\text{SELEX}}{\text{FOCUS}}$ Relative $\frac{\Xi_{cc}}{\Lambda_c}$ Prod	> 42 @ 90%		> 111 @ 90%	

ciples" calculation. Combined mass plots for their search are shown in Fig. 6, with the signal regions for the SELEX candidates highlighted. Despite that fact that FOCUS reconstructs ~12 times more Λ_c^+'s than SELEX, they see no evidence for either of the SELEX states. A comparison of the results of both experiments in given in Table 3. The listed FOCUS efficiencies assume Ξ_{cc}^{+} (Ξ_{cc}^{++}) lifetimes of 0.2 ps (1.0 ps), a mass of 3.6 GeV/c^2, and production characteristics of a 3.6 GeV/c^2 Ξ_c particle in PYTHIA. Given that the production mechanism for the SELEX candidates is very likely exotic, it is not possible for FOCUS to confirm or deny the SELEX results. However, the production ratio of doubly-charmed to singly-charmed baryons must be at least 100 times larger for SELEX than for FOCUS.

4 Summary

Evidence for the wide L=1 charm meson states, long thought to be experimentally unobservable, is being presented by multiple experiments. SELEX has presented candidates for doubly-charmed baryons, but FOCUS does not see these states. If SELEX's observations are real, the production mechanism

would probably have to be exotic.

5 Acknowledgements

I would like to thank the National Science Foundation for their support. I would also like to thank the people who made this conference a well organized and interesting meeting.

References

1. K. Abe *et al*, http://belle.kek.jp/conferences/ICHEP2002/, BELLE-CONF-0235, (2002).

2. K. Hagiwara *et al*, Phys. Rev. **D66**, 010001, (2002).

3. M. Mattson *et al*, Phys. Rev. Lett. **89**, 112001, (2002).

4. V. V. Kiselev and A. K. Likhoded, hep-ph/0208231 (2002).

Frascati Physics Series Vol. XXXI (2003), pp. 89–93
FRONTIERSCIENCE 2002 – Frascati, October 6–11, 2002
Invited Contribution in Plenary Session

SEARCH FOR η_b IN TWO-PHOTON COLLISIONS WITH THE L3 DETECTOR AT LEP

Mikhail Levtchenko *
INFN, Milano

ABSTRACT

A search for the pseudoscalar meson η_b is performed in two-photon interactions at LEP2. The data sample corresponds to a total integrated luminosity of $610pb^{-1}$ collected at the centre-of-mass energies from 189 GeV to 209 GeV. Preliminary results of the analysis in the η_b mass region are presented. Several candidate events are found in different final states.

1 Introduction

Two-photon collisions are well suited for the study of pseudoscalar mesons, for which $J^{PC} = 0^{-+}$. The η_c, $c\bar{c}(1S)$ state, has been studied [1] and a value $\Gamma_{\gamma\gamma} = 6.9 \pm 1.7 \pm 2.1$ keV has been measured. The high energy and luminosity

* On behalf of L3 collaboration

makes LEP a good environment to search also for the η_b, the $b\bar{b}$ state, not yet observed [2]. A first investigation by ALEPH [3] observes a candidate event in the channel $K^0_S K^- \pi^+ \pi^- \pi^+$ with a mass $m = 9.30 \pm 0.02 \pm 0.02$ GeV and upper limits on $\Gamma_{\gamma\gamma}$:

$$\begin{aligned} \Gamma_{\gamma\gamma}(\eta_b) \times \mathrm{BR}(\eta_b \to 4 \text{ charged particles}) &< 48eV \\ \Gamma_{\gamma\gamma}(\eta_b) \times \mathrm{BR}(\eta_b \to 6 \text{ charged particles}) &< 132eV \end{aligned} .$$

Many theoretical estimates [4] exist from potential models and lattice QCD of the mass difference, Δm, between the η_b and the Υ ($m_\Upsilon = 9.46$ GeV). The predictions lie between 30 and 150 MeV. The partial decay width of the η_b into two photons, $\Gamma_{\gamma\gamma}(\eta_b)$ is expected to be $\simeq 500\ eV$.

Here a search is presented which uses the L3 data sample collected at the centre-of-mass energies, $\sqrt{s}$, from 189 GeV to 209 GeV , corresponding to a total integrated luminosity of $610 pb^{-1}$. The formation of the η_b in quasi-real two-photon interactions $e^+e^- \to e^+e^-\eta_b$ is studied through the decay into four and six charged particles only or associated with a π^0. In the last case, because of G-parity conservation, the decay products must include a K^+K^- pair.

2 Data selection

The L3 detector [5] is suitable for the study of two-photon processes since events with few tracks and a low energy deposit in the detector are selected by a track trigger [6].

For quasi-real photon interactions the $e^\pm$ in the final state are mainly scattered at very small polar angles and go undetected. The $e^+e^- \to e^+e^-\eta_b$ events are selected by requiring four or six tracks with charge balance and two isolated electromagnetic clusters in case of a π^0 decay.

No other track or electromagnetic bump must be present in the event.

Events are excluded if a photon conversion is detected, i.e. when, assigning the electron mass to an opposite charge pair, the effective mass of the pair is smaller than 50 MeV .

The $\gamma\gamma \to \tau^+\tau^-$ background is reduced in the four track events by requiring the invariant mass of 3π to be greater than 1.9 GeV. Only 2% of η_b events are eliminated by this cut.

Table 1: *Detector resolution, mass shift due to (K/π) ambiguity and total efficiency for the different channels as obtained from Monte Carlo.*

Channel	Resolution (MeV)	(K/π) Mass shift (MeV)	Total efficiency %
4tr	297 ± 3	110	4.7 ± 1.9
4tr π^0	259 ± 8	95	1.9 ± 0.7
6tr	254 ± 4	310	3.6 ± 0.6
6trπ^0	231 ± 7	265	0.94 ± 0.15

To ensure that no final state particle of the resonance decay has escaped detection, the squared vectorial sum of the transverse momenta of all detected particles, $\sum \vec{p_i}^2$, is required to be smaller than 0.1 GeV^2.

The ionisation loss measurement, dE/dx, has a good π/K separating power only for tracks with a momentum below 0.5 GeV. As the momenta of the decay particles of the η_b extend from 0.15 to 3 GeV the dE/dx has a very weak separating power. The mass of the charged particles is therefore considered to be that of a pion. The uncertainty due to π-K misidentification is studied for each η_b candidate.

2.1 Efficiency, mass resolution and background

In Table 1 the mass resolution and the total efficiencies, including acceptance and selection cuts are given. Trigger inefficiencies are negligeable. The total efficiency depends on the nature of the particles in the channel, the variation due to this effect is given in the table. The mass shift, due to (π/K) misidentification is also indicated.

The mass spectra of the channels under study are well represented by a two-photon cross-section slowly decreasing with $W_{\gamma\gamma}$. By comparing the mass spectra to the data we obtain a good agreement by weighting each MC event with an exponential function $\exp(-cW_{\gamma\gamma})$, with $c \simeq 1\ GeV^{-1}$.

The main background due to $e^+e^- \to e^+e^-\tau^+\tau^-$ events, it is estimated with a MC sample six times larger than the data.

Inclusive channels can also be a source of background, when one or more particles go undetected. We estimate this background by using the exclusive channels with an higher number of particles and by considering the side bands

Table 2: *Mass of the η_b candidates in the channels studied at $189 \leq \sqrt{s} \leq 208 GeV$. The first column gives the minimal value of the mass obtained assuming that all tracks are pions if no π^0 is present and that there is a K^+K^- pair otherwise. The second column gives the average mass of all possible π/K combinations; the error includes detector resolution and misidentification uncertainty. The corresponding cross-section and the 95% confidence level limit for the two-photon width times branching ratio are also listed.*

Channel	Minimum Mass (GeV)	Average Mass (GeV)	Cross section (pb)	$\Gamma_{\gamma\gamma}\times$ BR (keV)
4tr	9.89	10.02 ± 0.32	0.026	<0.3
4tr π^0	—	—	—	<0.5
6tr	9.39	9.70 ± 0.40	0.021	<0.4
6tr π^0	9.99	10.21 ± 0.38	0.120	<1.4

of the π^0, it is found to be smaller than 1%.

3 Results

In Table 2 two possible values of the candidates mass are listed together with the mass resolution, assuming first that all tracks are pions if no π^0 is present and that there is a K^+K^- pair otherwise. The η_b is expected to decay through two gluons, which are flavour blind. We calculate then an average mass, using different π/K hypothesis, by assuming that the production of pions and kaons is equally probable.

The cross section for each channel i is obtained by :

$$\sigma_i = \frac{N_i - B_i}{\mathcal{L}\varepsilon_i}$$

Here N_i is the number of the observed events, B_i the expected background, ε_i the total efficiency and $\mathcal{L} = 610\ pb^{-1}$ the integrated luminosity for the data between $\sqrt{s} = 189$ GeV and $\sqrt{s} = 209$ GeV. Upper limits at 95% confidence level [3] for $\Gamma_{\gamma\gamma}(\eta_b)\times \mathrm{BR}(\eta_b)$ are calculated for each channel. The results are listed in Table 2.

In Fig. 1 the mass spectrum, obtained by adding all channels together is presented. Assuming that the η_b branching ratio for each channel is the same, the combined upper limit for $\Gamma_{\gamma\gamma}(\eta_b)\times$ BR(η_b) is 0.2 keV .

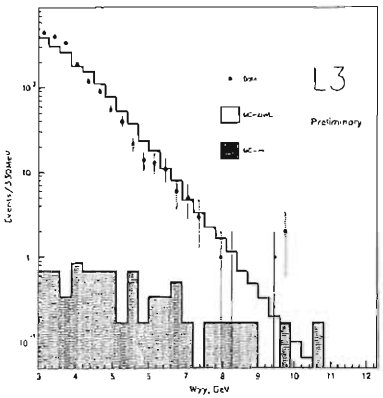

Figure 1: *The mass spectrum of all analysed channels added together. Superimposed to the data is the expected number of events from the exclusive channels. The* $e^+e^- \to e^+e^-\tau^+\tau^-$ *background is shown as a shaded area.*

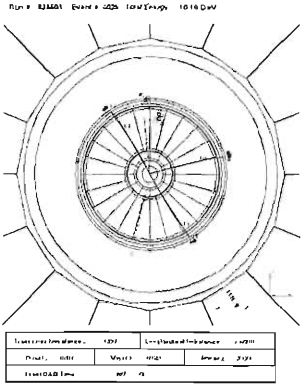

Figure 2: *The scan of a selected event for the 6 tracks channel.* $M = 9.70 \pm 0.34$ *GeV*

References

1. L3 collaboration, Phys.Let. B 461(1999) 155-166.
2. Particle Data Group,
3. ALEPH collaboration, Phys.Lett.**B530** (2002) 56.
4. G.S. Bali, Phys. Rept. **343** (2001) 1;
   L. Marcantonio et al., Nucl. Phys. Proc. Suppl. **94** (2001) 363;
   G.S. Bali, K. Schilling and A. Wachter, Phys. Rev. **D56** (1997) 2566;
   N. Brambilla, Y. Sumino, and A. Vairo, Phys. Lett. **B513** (2001) 381;
   S. Narison, Phys. Lett. **B387** (1996) 162;
   E.J. Eichten and C. Quigg, Phys. Rev. **D49** (1994) 5845.
5. L3 Coll. B. Adeva et al., Nucl. Instr. Meth. A289 35 (1990).
6. P. Bene et al., Nucl. Inst. Meth. A 306 (1991) 150;
   D. Haas et al., Nucl. Inst. Meth. A 420 (1999) 101.

Frascati Physics Series Vol. XXXI (2003), pp. 95–102
FRONTIERSCIENCE 2002 – Frascati, October 6–11, 2002
Invited Review Talk in Plenary Session

CHARM AND BEAUTY LIFETIMES

Olivier Schneider
University of Lausanne, CH–1015 Lausanne, Switzerland

ABSTRACT

The status of the experimental determination of the lifetimes of the weakly-decaying charm and beauty hadrons is reviewed, with emphasis on recent measurements. Averages are given and compared with theoretical expectations.

1 Introduction

Experimental data on the lifetimes of hadrons containing a heavy b or c quark provide a unique opportunity to improve our understanding of a difficult and challenging part of strong interaction theory, namely non-perturbative QCD. In a naive picture, one could assume that a heavy quark undergoes its weak decay independently of the other light quarks present in the hadron, and hence predict that all hadrons containing such a quark have equal lifetimes. However, this "spectator" model fails dramatically, as the D^+ meson is known to live

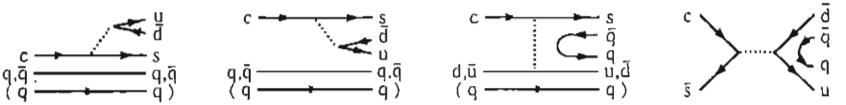

Figure 1: *Cabibbo-allowed diagrams contributing to the hadronic decay width of charm hadrons.*

$\sim$ 2.5 times longer than the D^0 meson. So the accompanying quarks in the hadron do indeed play a significant role in the decay dynamics of heavy hadrons.

Differences amongst charm hadrons are mainly due to their hadronic decay widths and can be explained by considering diagrams that don't contribute equally in all species of hadrons (see examples in Fig. 1). If there are two identical quarks in the final state, the internal and external spectator diagrams may interfere. This Pauli interference is destructive in D^+ mesons and constructive in strange charm baryons. The W-exchange (WE) and weak-annihilation (WA) diagrams are only Cabibbo-allowed for the D^0, Λ_c^+ and Ξ_c^0 hadrons, and for the D_s^+ meson respectively; these processes are helicity-suppressed for the mesons, but WE is not for the baryons where a third quark is present. These considerations usually lead to the following expected hierarchy for the charm hadron lifetimes (and similarly for beauty hadrons):

$$\tau(D^+) > \tau(D^0) \sim \tau(D_s^+) \geq \tau(\Xi_c^+) > \tau(\Lambda_c^+) > \tau(\Xi_c^0) > \tau(\Omega_c^0)\,. \qquad (1)$$

More quantitative predictions can be made in the framework of the Heavy Quark Expansion (HQE) theory, a systematic QCD-based approach for the treatment of inclusive decays. Considering an operator product expansion in powers of $\Lambda_{\rm QCD}/m_Q$, where m_Q is the mass of the heavy quark Q ($= b$ or c), the decay width of a heavy hadron can be written as

$$\Gamma = \frac{G_F^2 m_Q^5}{192\pi^3}\left[A_0 + A_2/m_Q^2 + A_3/m_Q^3 + \mathcal{O}(1/m_Q^4)\right]\,, \qquad (2)$$

where the A_0 term corresponds to the spectator model, the A_2/m_Q^2 correction introduces differences between mesons and baryons, and the A_3/m_Q^3 correction includes the WA, WE and Pauli interference effects [1]. HQE thus predicts that the lifetime differences are smaller amongst beauty hadrons than amongst charm hadrons. This expansion is expected to be reliable for beauty hadrons (since $m_b \gg \Lambda_{\rm QCD}$), but may be questionable for charm hadrons.

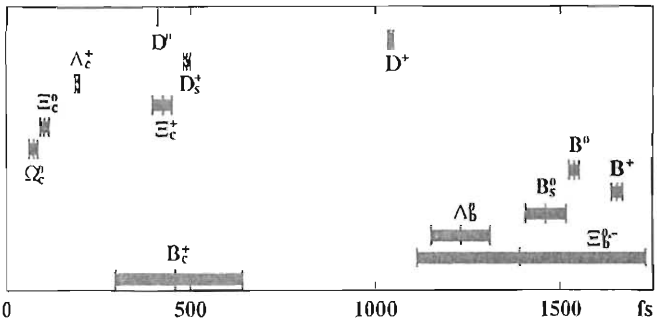

D^0	411.3	±1.3 fs
D^+	1039.4	±6.3 fs
D_s^+	490	± 9 fs
Λ_c^+	200	± 6 fs
Ξ_c^+	442	± 26 fs
Ξ_c^0	109	$^{+\ 13}_{-\ 10}$ fs
Ω_c^0	77	± 12 fs
B^0	1540	± 14 fs
B^+	1656	± 14 fs
B_s^0	1461	± 57 fs
Λ_b^0	1229	± 80 fs
Ξ_b^-	1390	$^{+\ 140}_{-\ 130}$ fs
B_c^+	460	$^{+\ 180}_{-\ 170}$ fs

Figure 2: *Experimental lifetime averages, including preliminary measurements.*

2 Charm lifetime measurements

The current world averages [2, 3] of all charm lifetime measurements are listed in Fig. 2. Recent measurements have been performed by fixed-target experiments at Fermilab, where charm is either hadro-produced (E791, SELEX) or photo-produced (FOCUS), and by experiments at e^+e^- colliders running near the $\Upsilon(4S)$ energy (CLEO, BABAR, Belle). In both cases, charm hadrons are fully reconstructed in exclusive hadronic modes, and their direction is used to determine the production point using other primary tracks (fixed-target case) or the beam-spot constraint in the transverse plane ($\Upsilon(4S)$ case). The momentum p, and hence the boost $\beta\gamma = p/(mc)$ (typically 40–100 and $\simeq 1.7$ respectively), is very well measured. Therefore the resolution on the decay length L determines the proper-time resolution ($20-60$ fs and $150-200$ fs respectively). The background level is low at $\Upsilon(4S)$ machines (non-prompt charm from $B\bar{B}$ events being rejected by requiring $p > 2.5$ GeV/c in the center-of-mass), but much higher in fixed-target experiments where a detachment cut is needed. Such requirement, expressed as $L/\sigma_L > N$, introduces a bias in the distribution of the proper time $t = L/(c\beta\gamma)$; however, this can largely be corrected for by considering instead the reduced proper time $t' = (L - N\sigma_L)/(c\beta\gamma)$, which is expected to have (for the signal) the same exponential distribution as t.

The most precise determinations of the D^+ and D^0 lifetimes are from the FOCUS collaboration [4] (see Fig. 3). These are affected by relatively important systematic uncertainties in the determination of the overall acceptance function (which includes geometrical effects, reconstruction efficiency, hadronic

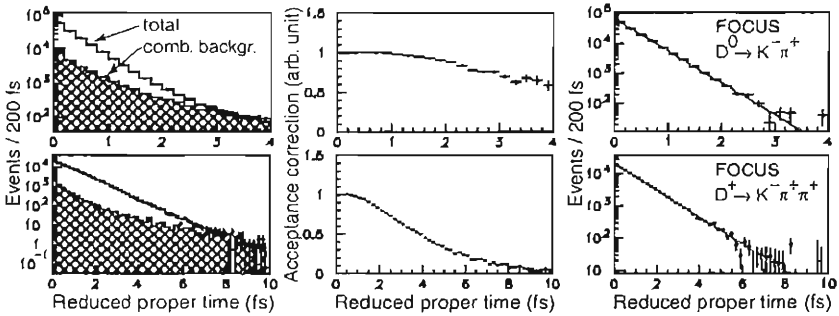

Figure 3: *Reduced proper-time analysis for fully reconstructed* $D^0 \to K^-\pi^+$ *(top row) and* $D^+ \to K^-\pi^+\pi^+$ *(bottom row) candidates in FOCUS* [4]. *Left: raw distributions. Middle: overall acceptance functions from Monte Carlo simulations. Right: background-subtracted and acceptance-corrected distributions, with exponential lifetime fits superimposed.*

absorption and decay of charm secondaries). BABAR and Belle, however, are now collecting large statistics as well and should be able to get similar (and eventually better) precision, but with very different systematics [5]. Combining all available results, the lifetime ratio $\tau(D^+)/\tau(D^0) = 2.527 \pm 0.017$ reaches an impressive relative precision of 0.7%. This can be used together with the measured semileptonic branching ratios [2] to yield a semileptonic decay width ratio consistent with unity, $\Gamma(D^0 \to e^+\nu_e X)/\Gamma(D^+ \to e^+\nu_e X) = 1.01 \pm 0.12$, clearly indicating that the large lifetime difference is driven by hadronic decays. This is largely attributed to a destructive Pauli interference in D^+ decays, although a small effect is expected from WE in D^0 decays. Is it interesting to note that D^0 lifetime measurements performed with decays to CP-even final states ($\pi^+\pi^-$ and K^+K^-) can be compared with the ones performed for a mixture of CP eigenstates ($K^-\pi^+$) to extract information on a possible small decay width difference $\Delta\Gamma$ induced by mixing in the $D^0 - \bar{D}^0$ system. The determinations of $\Delta\Gamma/(2\Gamma)$ with this method are all consistent with zero [2, 6], but the most precise ones (from BABAR and Belle) have recently reached the 1% level, getting close to the largest Standard Model predictions [7].

The ratio $\tau(D_s^+)/\tau(D^0) = 1.191 \pm 0.022$ (using the D_s^+ average of Fig. 2, which does not include a preliminary FOCUS measurement [8] without quoted systematic uncertainty), is significantly different from unity, and is interesting to understand the relative WA/WE contributions in D_s^+ and D^0 mesons. In-

deed, when compared to theoretical predictions [9], such a large ratio indicates that WA/WE effects are significant and perhaps less suppressed than expected.

The lifetime averages of the charm baryons have significantly improved in the last year or so, due to the new precise FOCUS measurements [2, 10]. While the ratio $\tau(\Omega_c^0)/\tau(\Xi_c^0) = 0.71 \pm 0.13$ is consistent with expectations, the ratio $\tau(\Xi_c^+)/\tau(\Lambda_c^+) = 2.21 \pm 0.15$ is at disagreement with the theory, which prefers the range 1.2–1.7 [11]. Again this could perhaps point to an underestimate of the WE contribution, this time in Λ_c^+ decays.

3 Beauty lifetime measurements

The first b lifetime measurements, performed in 1983 at PEP (SLAC), were surprisingly large, and hence the first indication for the small value of the CKM matrix element $|V_{cb}|$. Today, the inclusive b lifetime (averaged over all species of weakly-decaying b hadrons) is known very precisely from measurements at the Z pole, $\langle\tau_b\rangle = 1573 \pm 7$ fs [12], and is still useful for the extraction of $|V_{cb}|$ from the measurements of the $b \to c\ell\nu$ branching ratio at LEP.

Lifetime measurements of specific b hadrons have mostly been performed in the last 10 years at high-energy machines, either at LEP (ALEPH, DELPHI, L3, OPAL) and SLC (SLD), or at the Tevatron (CDF). Full reconstruction of hadronic modes, the cleanest technique in terms of purity and resolution, suffers from low statistics, so partial reconstruction (*e.g.* association of a lepton with a reconstructed charm hadron) is often preferred. More inclusive techniques based on identified leptons or reconstructed secondary vertexes, although more difficult in terms of systematics, have also been applied very successfully (*e.g.* in a recent DELPHI analysis [13], illustrated in Fig. 4-left). In all cases the production vertex is reconstructed using tracks from the fragmentation. Although the mean lifetime is sometimes extracted using the impact parameter method (useful when the decay vertex is not reconstructed), the proper time $t = (m/p)L$ is usually determined for each candidate. The resolution $\sigma_t \sim (m/\langle p\rangle)\sigma_L \oplus (\sigma_p/p)t$ includes a constant term due to σ_L (typically $0.05 - 0.3$ ps) and a term due to the momentum resolution ($10 - 20\%$ for partial reconstruction) which increases with proper time.

Since a couple of years, the B^0 and B^+ lifetimes have also been measured at asymmetric $\Upsilon(4S)$ machines, where produced B^+B^- or $B^0\bar{B}^0$ pairs are boosted along the beam (z) axis. The z positions of the two decay vertexes (one

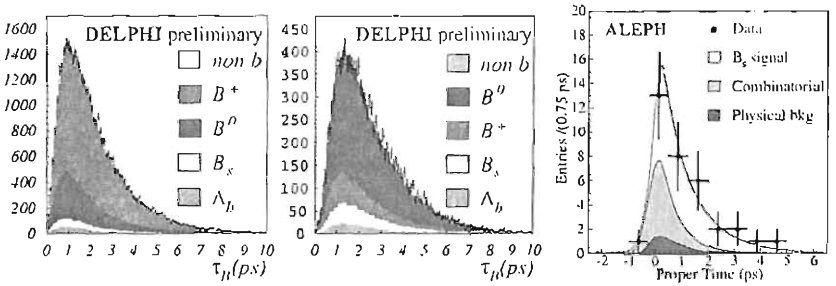

Figure 4: *Proper-time distributions measured at LEP, with lifetime fits superimposed. Left: inclusive samples enriched in B^+ and B^0 candidates from DELPHI* [13]. *Right: $B_s^0 \to \phi\phi X$ candidates from ALEPH* [17].

from a reconstructed B candidate and the other one formed with the remaining tracks) are determined with the help of a beam-spot constraint in the transverse plane. The proper-time difference is approximated as $\Delta t \simeq \Delta z/(c\beta\gamma)$ using the known boost $\beta\gamma$ from the beam energies. The production point does not need to be determined, as $|\Delta t|$ follows an exponential distribution from which the mean lifetime can be directly extracted. The Δt resolution, dominated by that of Δz, is very large due to the small boost ($\beta\gamma \simeq 0.5$, compared to ~ 6 in $Z \to b\bar{b}$ events) and is comparable to the mean lifetimes to be measured. Hence, the modeling of the resolution function in such analyses (of which Fig. 5 shows two examples) is one of the main sources of systematic uncertainties.

The beauty lifetime averages [12] are shown in Fig. 2. Only the B^0 and B^+ averages have changed since 1999; their accuracy is now twice better due to recent analysis improvements at LEP and new B factory results [2, 13, 16]. The ratio $\tau(B^+)/\tau(B^0) = 1.073 \pm 0.014$ is now significantly larger than unity (a 5.2σ effect compared to 2.8σ in 1999), in agreement with predictions. Furthermore, $[\tau(B^+)/\tau(B^0) - 1]/[\tau(D^+)/\tau(D^0) - 1] = 0.05 \pm 0.01$ is consistent with $(f_B/f_D)^2/(m_b/m_c)^2$, as expected from HQE (although the quark masses and decay constants f_B and f_D still have rather large theoretical uncertainties).

The B_s^0 and B^0 lifetimes are found to be consistent (within 1.3σ), however the precision on $\tau(B_s^0)$ is not sufficient yet for an interesting test of the theory, which predicts equality within 1%. Note that the B_s^0 average includes measurements performed on samples with different mixtures of the two B_s^0 mass eigenstates, which are expected to have a relative decay width difference

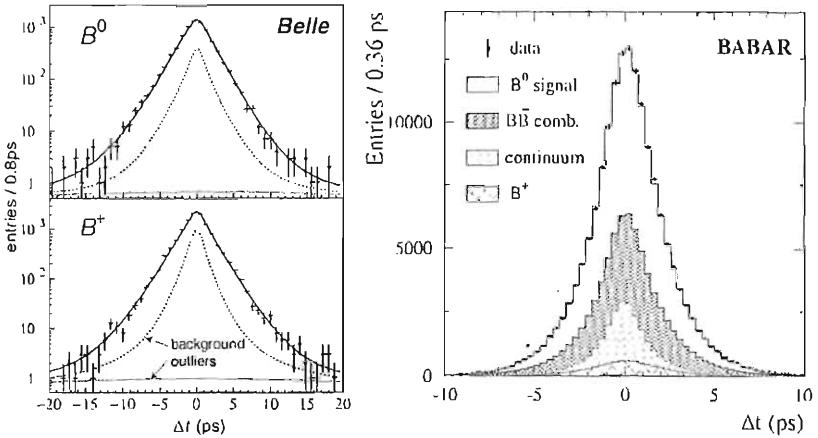

Figure 5: *Δt distributions measured at asymmetric B factories, with lifetime fits superimposed. Left: fully reconstructed B^0 and B^+ candidates in Belle* [14]. *Right: partially reconstructed $B^0 \to D^* \ell\nu$ candidates in BABAR* [15].

$\Delta\Gamma_s/\Gamma_s$ of order 10%. Not included in the average is a low statistics measurement from ALEPH [17] based on the $\phi\phi X$ final state, assumed to be almost pure CP-even and to yield the lifetime of the short-lived mass-eigenstate (see Fig. 4-right). Combining all available experimental information yields a 95% CL limit of $\Delta\Gamma_s/\Gamma_s < 0.52$, or < 0.31 if the constraint $1/\Gamma_s = \tau(B^0)$ is imposed [18]. For the B^0 system, DELPHI obtains $\Delta\Gamma_d/\Gamma_d < 0.18$ at 95% CL [19], while at most 0.01 is expected.

For several years, the low ratio $\tau(\Lambda_b^0)/\tau(B^0) = 0.798 \pm 0.052$ could not be accommodated within the theory. However, recent calculations of next-to-leading order QCD corrections to spectator effects in lifetime ratios, combined with the latest lattice determinations of the relevant hadronic matrix elements, now yield reasonable agreement with all data on beauty lifetimes [20].

4 Summary and outlook

In the last couple of years, impressive improvements have been achieved for all seven singly-charmed hadrons, as well as for the B^0 and B^+ mesons. While theory still fails to explain some lifetime ratios in the charm sector, in particular $\tau(\Xi_c^+)/\tau(\Lambda_c^+)$, HQE predictions seem now in agreement with all available

beauty lifetime data. However, better experimental precision is highly desirable on the more rare b hadrons (B_s^0, B_c^+ and the different b-baryon species). This will certainly be provided by the large statistics aimed for at Run II of the Tevatron, as shown by the first promising results of CDF [21].

References

1. G. Bellini, I.I. Bigi and P.J. Dornan, Phys. Reports **289**, 1 (1997).
2. K. Hagiwara *et al*, Particle Data Group, Phys. Rev. **D 66**, 010001 (2002).
3. A. Stocchi, plenary talk at ICHEP02*.
4. J.M. Link *et al*, FOCUS collab., Phys. Lett. **B 537**, 192 (2002).
5. Belle collab., BELLE-CONF-0131, contrib. to Int. Europhysics Conf. on High Energy Physics, Budapest, July 2001.
6. A. Pompili (for the BABAR collab.), talk at XXXVIIth Rencontres de Moriond, March 2002, hep-ex/0205071, May 2002.
7. A. Petrov, these proceedings.
8. H.W.K. Cheung, talk at 8th Int. Symposium on Heavy Flavour Physics, Southampton, July 1999, hep-ex/9912021, December 1999.
9. I.I. Bigi and N.G. Uraltsev, Z. Phys. **C 62**, 623 (1994); H.-Y. Cheng and K.-C. Yang, Phys. Rev. **D 61**, 014008 (2000).
10. J.M. Link *et al*, FOCUS collab., Phys. Lett. **B 541**, 211 (2002); C. Riccardi (for the FOCUS collab.), talk at ICHEP02*.
11. see for example B. Guberina and B. Melic, Eur. Phys. J. **C 2**, 697 (1998).
12. b-lifetime working group, `http://www.cern.ch/LEPBOSC/lifetimes`
13. DELPHI collab., DELPHI-2002-072 CONF 606, contrib. to ICHEP02*.
14. K. Abe *et al*, Belle collab., Phys. Rev. Lett. **88**, 171801 (2002).
15. B. Aubert *et al*, BABAR collab., Phys. Rev. Lett. **89**, 011802 (2002).
16. BABAR collab., SLAC-PUB-9306, hep-ex/0207071, contrib. to ICHEP02*.
17. R. Barate *et al*, ALEPH collab., Phys. Lett. **B 486**, 286 (2000).
18. $\Delta\Gamma_s$ working group, `http://www.cern.ch/LEPBOSC/deltagamma_s`
19. DELPHI collab., DELPHI 2002-073 CONF 607, contrib. to ICHEP02*.
20. see for example E. Franco, V. Lubicz, F. Mescia and C. Tarantino, Nucl. Phys. **B 623**, 212 (2002).
21. F. Bedeschi (for the CDF collab.), plenary talk at ICHEP02*, FERMILAB-CONF-02-259-E, October 2002.

* 31st Int. Conf. on High Energy Physics, Amsterdam, July 2002.

Frascati Physics Series Vol. XXXI (2003), pp. 103–107
FRONTIERSCIENCE 2002 – Frascati, October 6–11, 2002
Invited Contribution in Plenary Session

Λ_c^+ AND Ξ_c^+ BRANCHING RATIOS IN THE FOCUS EXPERIMENT

Lorenzo Agostino *
University of Colorado at Boulder

ABSTRACT

We report a measurement of branching ratios for the Cabibbo suppressed decay $\Lambda_c^+ \to \Sigma^+ K^{*0}(892)$ and the Cabibbo favored decays $\Lambda_c^+ \to \Sigma^+ K^+ K^-$, $\Lambda_c^+ \to \Sigma^+ \phi$ and $\Lambda_c^+ \to \Xi^{*0}(\Sigma^+ K^-) K^+$ relative to $\Lambda_c^+ \to \Sigma^+ \pi^+ \pi^-$. We also report two 90% confidence level limits for $\Lambda_c^+ \to \Sigma^- K^+ \pi^+$ and $\Lambda_c^+ \to \Sigma^+ K^+ K^-_{NR}$. Recently, we also searched for new Ξ_c^+ decay channels. In particular we measure the branching ratio of the Cabibbo suppressed mode $\Xi_c^+ \to \Sigma^+ K^+ K^-$ relative to $\Xi_c^+ \to \Sigma^+ K^- \pi^+$ and the branching ratios of $\Xi_c^+ \to \Sigma^+ K^- \pi^+$, $\Xi_c^+ \to \Sigma^*(1385)^+ \bar{K}^0$ and $\Xi_c^+ \to \Omega^- K^+ \pi^+$ relative to $\Xi_c^+ \to \Xi^- \pi^+ \pi^+$.

1 Introduction

During the past year FOCUS [1] and BELLE [2] have discovered new decay modes for the baryon Λ_c^+. FOCUS concentrated on decays to three final state

* On behalf of the FOCUS collaboration

particles containing a Σ^+. We also investigated many possible decays for Ξ_c^+. Few decay modes of the Ξ_c^+ have been reported, for example, the only observed Cabibbo suppressed mode [3] was $\Xi_c^+ \to pK^-\pi^+$. FOCUS now has the first evidence for three new decay modes of the Ξ_c^+, one of which is Cabibbo suppressed. In this report we will describe hyperon reconstruction, then we will show the charm baryon signals and finally, we will report the measurements with the conclusions. These measurements might offer a useful tool for investigating different contributions (like exchange diagram) to the total decay width of charm baryon decays. Cabibbo suppressed decays can also serve as input parameters for lifetime predictions in the charm sector.

2 Hyperon reconstruction [4]

The Σ decays into a charged particle (proton or pion) and a neutral particle (neutron or pion). Since the direction of the neutral particle is not detected, FOCUS reconstructs both the decay modes by imposing kinematic constraints on the decay. This technique creates a two-fold ambiguity on the Σ^+ momentum (80% of the time for the (p, π^0) mode and 20 % of the time for the (n, π^+) mode where calorimeter information serves to break the ambiguity). The two solutions in the Σ^+ momentum for some of the decays change the shape of the invariant mass of the final state particles. For this reason we implement a double-Gaussian to fit the signal region over a linear background. In order to minimize any possible bias due to this feature we normalize each branching ratio to the high statistics modes $\Lambda_c^+ \to \Sigma^+\pi^+\pi^-$ (Fig. 1a) and $\Xi_c^+ \to \Sigma^+K^-\pi^+$ (Fig. 2a) which contain a Σ^+ particle in the final state. For Ξ_c^+ modes without Σ^+ in the final state we normalize to the decay $\Xi_c^+ \to \Xi^-\pi^+\pi^+$ (Fig. 2b). The hyperons, Ξ^- and Ω^-, are reconstructed in the (Λ^0, π^-) and (Λ^0, K^-) modes where the Λ^0 decays in the (p, π^-) mode. For this analysis we only selected events which had SSD information for the hyperon, Ξ^-/Ω^-, tracks ie. events in which the hyperon decays after the SSD system.

3 Λ_c^+ and Ξ_c^+ signals

We investigated two Cabibbo suppressed Λ_c^+ decays into $\Sigma^+K^+\pi^-$ and $\Sigma^-K^+\pi^+$ final states and the Cabibbo favored decay to $\Sigma^+K^+K^-$. For the Cabibbo suppressed modes $\Sigma^+K^+\pi^-$ we find that most if not all of the decay proceeds via

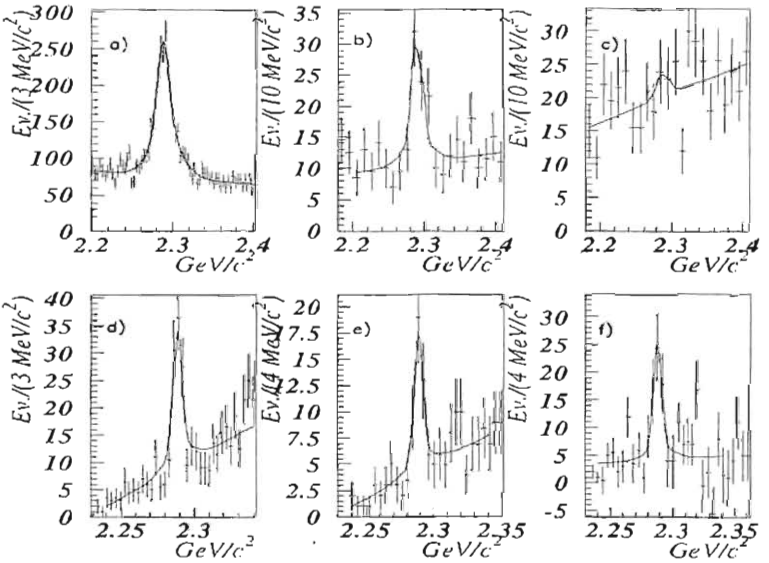

Figure 1: *a)* $\Sigma^+\pi^+\pi^-$, *b)* $\Sigma^+K^*(892)^0$, *c)* $\Sigma^-K^+\pi^+$, *d) Full sample* $\Sigma^+K^+K^-$, *e)* $\Xi^*(1385)^0K^+$, *f)* $\Sigma^+\phi$.

the resonant mode $\Sigma^+K^*(892)^0$ (Fig. 1b). Suppression of a three body non-resonant decay has also been observed also in the $\Sigma^-K^+\pi^+$ mode where the K^* resonance is not possible and where we find no evidence of signal(Fig. 1c). In the $\Sigma^+K^+K^-$ case (Fig. 1d) we find that the decay is dominated by two resonant contributions, namely $\Xi^*(1690)^0K^+$ (Fig. 1e) where the $\Xi^*(1690)^0$ decays in (Σ^+, K^-) and $\Sigma^+\phi$ (Fig. 1f). The non-resonant contribution has been evaluated by excluding the resonances signal regions and by correcting for phase-space.

We report three new observations of Ξ_c^+ decays: the Cabibbo suppressed decay $\Xi_c^+ \to \Sigma^+K^+K^-$ and the Cabibbo favored decays $\Xi_c^+ \to \Omega^-K^+\pi^+$ and $\Xi_c^+ \to \Sigma^*(1385)^+\bar{K}^0$ where the $\Sigma^*(1385)^+$ is reconstructed in (Λ^0, π^+). For the modes $\Sigma^+K^+K^-$ and $\Omega^-K^+\pi^+$ we find no significant evidence for resonant contributions and the signals are presented in Fig. 2 c-e.

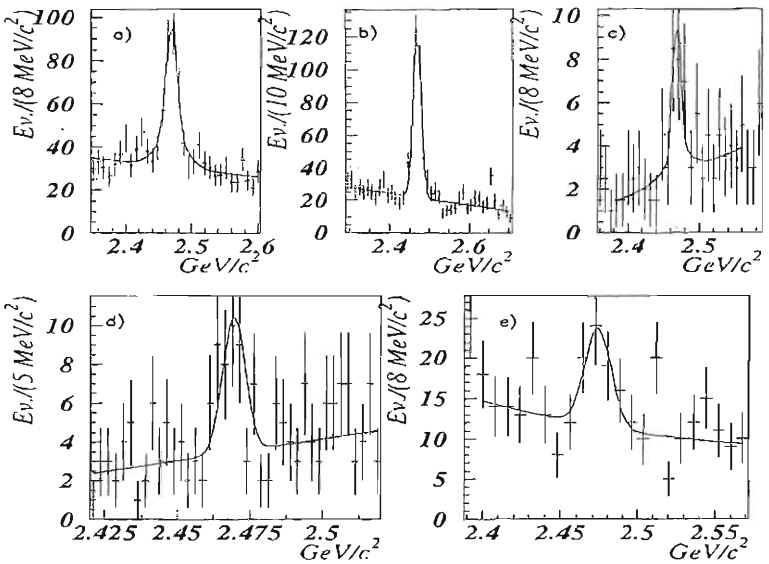

Figure 2: *a)* $\Sigma^+K^-\pi^+$, *b)* $\Xi^-\pi^+\pi^+$, *c)* $\Sigma^+K^+K^-$, *d)* $\Omega^-K^+\pi^+$, *e)* $\Sigma^*(1385)^+\bar{K}^0$.

4 Results

We measured several branching ratios for hadronic decays of Λ_c^+ and Ξ_c^+. The results are shown in Table 1.

The FOCUS experiment has measured for the first time the relative branching ratio of the Cabibbo suppressed decay $\Lambda_c^+ \to \Sigma^+K^*(892)^0$ and has placed a limit on the similar mode $\Lambda_c^+ \to \Sigma^-K^+\pi^+$. Further, we measured the relative branching ratio for the Λ_c^+ decay to the final state $\Sigma^+K^+K^-$ and our results agree with BELLE [2] and CLEO [5] measurements. We find that these Λ_c^+ decays exhibit a highly favored two-body resonant component. We searched for new Ξ_c^+ decays and we observe for the first time three modes $\Xi_c^+ \to \Sigma^+K^+K^-$ (Cabibbo suppressed), $\Xi_c^+ \to \Sigma^*(1385)^+\bar{K}^0$ and $\Xi_c^+ \to \Omega^-K^+\pi^+$. Finally, we improved the existing measurement of the branching ratio for $\Xi_c^+ \to \Sigma^+K^-\pi^+$ relative to $\Xi_c^+ \to \Xi^-\pi^+\pi^+$. Contrary to the suppression of

Table 1: Λ_c^+ *and* Ξ_c^+ *branching ratios from FOCUS*

	Yield	Branching Ratio
Λ_c^+		
$\Sigma^+K^*(892)^0/\Sigma^+\pi^+\pi^-$	49 ± 10 (1706 ± 88)	$(7.8 \pm 1.8 \pm 1.3)\%$
$\Sigma^-K^+\pi^+/\Sigma^+K^*(892)^0$	10 ± 11	$< 35\%$ @ 90% CL
$\Sigma^+K^+K^-/\Sigma^+\pi^+\pi^-$	103 ± 15	$(7.1 \pm 1.1 \pm 1.1)\%$
$\Sigma^+\phi/\Sigma^+\pi^+\pi^-$	57 ± 10	$(8.7 \pm 1.6 \pm 0.6)\%$
$\Xi^*(\Sigma^+K^-)^0K^+/\Sigma^+\pi^+\pi^-$	34 ± 8	$(2.2 \pm 0.6 \pm 0.6)\%$
$\Sigma^+K^-K^+)_{NR}/\Sigma^+\pi^+\pi^-$	8 ± 8	$< 2.8\%$ @ 90% CL
Ξ_c^+		
$\Sigma^+K^+K^-/\Sigma^+K^-\pi^+$	17 ± 6	$(18.1 \pm 6.8 \pm 0.5)\%$
$\Sigma^*(1385)^+\bar{K}^0/\Xi^-\pi^+\pi^+$	31 ± 10 (269 ± 21)	$(3.4 \pm 1.2 \pm 0.4)$
$\Omega^-K^+\pi^+/\Xi^-\pi^+\pi^+$	25 ± 8	$(5.4 \pm 1.8 \pm 1.3)\%$
$\Sigma^+K^-\pi^+/\Xi^-\pi^+\pi^+$	234 ± 23	$1.05 \pm 0.13 \pm 0.07$

the Λ_c^+ three-body non resonant behavior, the Ξ_c^+ do not exhibit such a strong suppression. The low statistics warrant a verification by another experiment.

5 Acknowledgments

I would like thank my FOCUS collaborators and in particular, the people that directly contributed to these analyses, Ilaria Segoni, Eduardo Ramirez and Cristina Riccardi.

References

1. J.M. Link *et al*, Phys. Lett. **B 540**, 25 (2002).

2. K. Abe *et al*, Phys. Lett. **B 524**, 33 (2002).

3. J.M. Link *et al*, Phys. Lett. **B 512**, 277 (2001).

4. J.M. Link *et al*, Nucl. Instrum. Meth. **A 484**, 174 (2002).

5. P. Avery *et al*, Phys. Rev. Lett. **17**, 2391 (1993).

Heavy Flavour QCD – Session III

Chairpersons: S. Ratti, C. Guaraldo

Frascati Physics Series Vol. XXXI (2003), pp. 111-119
FRONTIERSCIENCE 2002 – Frascati, October 6–11, 2002
Invited Review Talk in Plenary Session

LIGHT QUARK SPECTROSCOPY AND CHARM DECAYS

Alberto Reis
Centro Brasileiro de Pesquisas Físicas
Rua Dr. Xavier Sigaud, 150 - Rio de Janeiro - Brazil

ABSTRACT

The connection between light quark spectroscopy and hadronic decays of D mesons is discussed, with emphasis on the physics of the light scalar mesons. Recent results from charm decays are presented.

1 Introduction

Forty years have passed since the birth of the Constituent Quark Model (CQM). This model provided a very successful description of almost all the hadronic spectrum. The nonets of pseudo-scalar, vector and tensor mesons are now well identified. There is, however, one remaining and crucial problem: the identification of the scalar meson nonet(s). The solution of this enigma is of vital importance for understanding QCD at the low energy limit.

On the other side, there has been tremendous progress in charm physics in the past decade. High quality data allowed the basic properties of charm mesons to be well measured. Recently hadronic decays of charm mesons started being used to study properties of scalar mesons, abundant products of these decays.

Charm decays have unique features, making them a very interesting tool for light quark spectroscopy: large couplings to scalar mesons and very small (less than 10%) non-resonant components; an initial state which is always well defined: the spin-0 D meson; and a spectrum that is not constrained by isospin and parity conservation.

There are, however, some conceptual issues related to the formalism commonly used in the analysis of resonant substructure of hadronic decays: the correct representation of overlapping broad states, which is closely connected to the issue of formulating the unitarity constraint in three and four-body problems. Moreover, there is the question of how to relate the observations from charm to those from scattering.

In what follows I will briefly state the problem of the scalar mesons. Then I will discuss how we can use charm decays for new insights on the scalars. Finally, I will discuss the picture so far offered by hadronic decays of charm.

2 The puzzling light scalars

The light scalars are, in some sense, victims of their own simplicity. Due to their broad widths and the lack of a distinctive angular distribution, the distinction between scalar mesons and the non-resonant background is rather difficult. Moreover, there are many overlapping states within a limited range of the mass spectrum (up to 1.8 GeV). An additional difficulty is the fact that non-$q\bar{q}$ states, like the lightest scalar glueball or multiquark states, all sharing the same quantum numbers ($J^P = 0^+$), are expected to populate the same region of the spectrum. We can say that the identification of the scalar mesons will always be a difficult subject. Comprehensive reviews on scalar mesons can be found in [1] and references therein.

The main candidates, according to their isospin, are: $f_0(600)$ or $\sigma(500)$, $f_0(980)$, $f_0(1370)$, $f_0(1500)$ and $f_0(1710)$ ($I = 0$); $\kappa(800)$ and $K_0^*(1430)$ ($I = 1/2$); $a_0(980)$ and $a_0(1450)$ ($I = 1$).

If all these states are confirmed, we have 19 states! Too many candidates

to fit even in two nonets. While the actual existence of some of these states - the $\sigma(500)$ and $\kappa(800)$ - is controversial, other states just have poorly known parameters - $f_0(980)$, $a_0(980)$, $f_0(1370)$. The interpretation of most of the scalar candidates is also controversial. Are they genuine $q\bar{q}$ mesons or more complex objects? Take the case of the $a_0(980)$, for instance. Its expected width is 500 MeV, according to the CQM, whereas the measured width is in the range 50-100 MeV. This fact leads to the interpretation of this state as a $qq\bar{q}\bar{q}$.

The most problematic states are the isoscalars. In addition to the controverse about the $\sigma(500)$, the nature of the $f_0(980)$, there is the issue of the f_0 family above 1 GeV and a possible mixing with the scalar glueball [5]. The remaining of this note is devoted to isoscalars and to what can we learn about them from charm decays. The $I = 1/2$ states states including the $\kappa(800)$, will be addressed in the talk by Carla Göbel, to appear in these proceedings.

3 Charm decays and light scalars

Hadronic decays of charm mesons are a natural place to look for scalars, with unique features that provide new and complementary insights on this problem.

Scalars are copiously produced in charm decays. In 3 and 4-body hadronic decays of D mesons, one always has a $\pi\pi$, a $K\pi$ or a KK pair, important decay modes of scalar mesons. The quantum interference between broad scalars and the usually large non-resonant background, which is a plague in scattering experiments, does not affect charm decays because the non-resonant component is always very small.

But the most appealing features of D decays, when compared to scattering experiments, are related to the difference in the constraints that build the $\pi\pi$, $K\pi$ and KK spectra. In scattering experiments, only the strong interaction is involved. The observed spectrum is determined by the conservation of isospin and parity. Parity and isospin are violated in D meson decays, where the observed spectrum is determined by the quark content of the initial state, after the weak decay of the c quark.

It is illustrative to compare, for instance, in the $\pi^+\pi^-\pi^+$ final state, the Dalitz plots from D^+, D_s^+ decays [2, 3] (see fig1) and from $p\bar{n}$ annihilation [4], which is most similar to D decays. The differences due to production dynamics are apparent at a glance. Comparing the D^+ and D_s^+ Dalitz plots we see clearly the effects of the different quark content of the initial state.

There is a related aspect which is also crucial: the bulk of the hadronic decay widths can be explained by a model in which resonances couple directly to the D meson. There is no need to add couplings to other states, like glueballs: $q\bar{q}$ states alone seem to be enough to account for the observed rates. Take the decay $D_s^+ \to K^-K^+\pi^+$ as a typical case. The main amplitudes are the external and internal W-radiation (see fig2). The decay modes corresponding to these amplitudes are $D_s^+ \to \phi\pi^+$ and $D_s^+ \to K^*K^-$. These modes account for almost 100% of the $D_s^+ \to K^-K^+\pi^+$ decay rate. The same argument could be made using many other final states. Hadronic D decays are an extremely complex process, and these types of quark diagrams are only an aproximation. This descripton, however, seems to work fairly well.

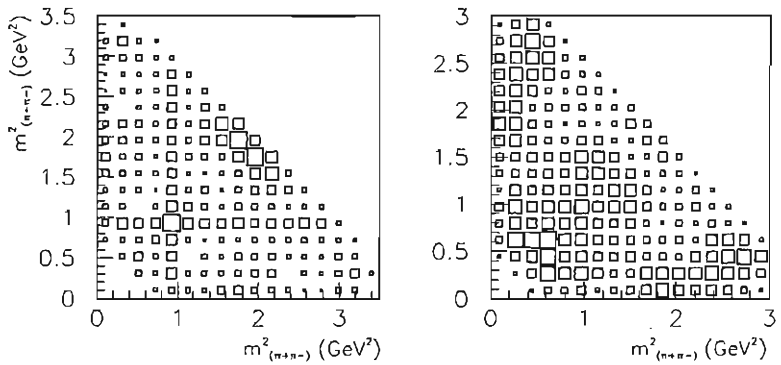

Figure 1: *Dalitz plots from* $D_s^+ \to \pi^+\pi^-\pi^+$ *(left) and* $D^+ \to \pi^+\pi^-\pi^+$ *(right) decays from Fermilab E791.*

It is generally accepted that a resonance, being a real particle, must have the same parameters in whichever process it appears. The question one may ask is whether the states produced in different processes are really the same. Consider, for instance, the $f_0(1370)$, $f_0(1500)$ and $f_0(1710)$ *imbroglio*. All three states have been observed by many experiments, with fairly well measaured parameters (except for the $f_0(1370)$). But according to the CQM, only two $q\bar{q}$ states are expected: one being mostly $s\bar{s}$ and another being mostly $u\bar{u} + d\bar{d}$. So, the three f_0's could not belong to the same $q\bar{q}$ multiplet.

Glueballs are expected to be produced in "gluon-rich" reactions, like central production, in addition to the genuine $q\bar{q}$ mesons. Mixing between the

scalar glueball and the $q\bar{q}$ states is expected [5]. If this is really the case, then the observed states would be mixtures of $q\bar{q}$ and gg, rather than pure states.

On the other hand, in a "gluon-poor" reaction, like D decays, glueballs are not expected to be produced. In D decays one would access directly the $q\bar{q}$ states with no mixing. In this case masses and widths measured in charm decays would be different than those obtained in central production. Also, the number of states present in D decays would be smaller.

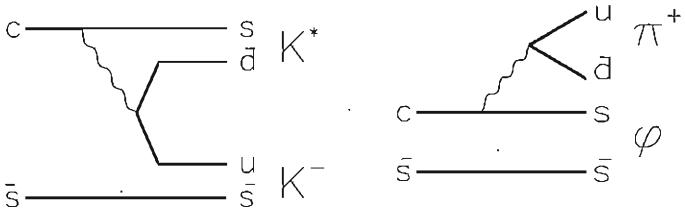

Figure 2: *Dominant amplitudes for* $D_s^+ \to K^-K^+\pi^+$ *decay.*

One last aspect deserves some attention: the role of final state interactions in charm decays. The Dalitz plots of charm decays can only be describe by models allowing interference between amplitudes in which the resonance and the bachelor pseudo-scalar are in different states of relative orbital angular momentum. The role the bachelor pseudo-scalar plays is decisive, which seems not to be the case in $N\bar{N}$ annihilations. In this sense Dalitz plot and partial wave analysis are not quite the same. The case of the $D^+ \to K^-\pi^+\pi^+$ [8] is typical. We see in the Dalitz plot that the upper lobe of the $K^*(892)$ band is shifted with respect to the lower one. This effect is caused by the interference between the l=1 $D^+ \to K^*(892)\pi^+$ and the l=0 amplitudes, like $D^+ \to K_0^*(1430)\pi^+$.

We conclude this section by noting that relating results from scattering and charm decays is not so simple. The $D \to \pi\pi\pi$, for instance, cannot be explained on the basis of pure elastic $\pi\pi$ scattering. The energy dependent s-wave phase from $D \to \pi\pi\pi$ (or $K\pi\pi$) may not be the same as the $\pi\pi$ (or $K\pi$) phase shifts from peripheral hadron-hadron reactions.

4 What have we learned so far from charm decays?

There are only a few experimental results on light scalars from charm decays. I will concentrate on the isoscalars: the σ and the f_0 family.

4.1 $\sigma(500)$ or $f_0(600)$

This is certainly the most controversial state. In charm decays it appears as an excess of signal events at low $\pi^+\pi^-$ mass. This effect is observed in the Dalitz plots of $D^+ \to \pi^+\pi^-\pi^+$, from E791 [3] and FOCUS, and of $D^0 \to \bar{K}^0\pi^+\pi^-$, from CLEO [6]. The same structure was also observed in $J/\psi \to \omega\pi^+\pi^-$ decay, from BES [7]. No such effect is observed in $\pi^+\pi^-$ scattering, where the σ is interpreted not as a real particle, but as a dynamical threshold effect.

The best description of charm decay data requires the presence of a broad, scalar (in E791 analysis different spin assignments were also tested), complex amplitude at low $\pi^+\pi^-$ mass. A crucial aspect is that good fits can only be obtained allowing the phase of this complex amplitude to vary across the Dalitz plot. The above experiments have fitted their data assuming a Breit-Wigner function for this state, although it is known that for states like the σ a Breit-Wigner is only an approximation. Different functional forms may yield different values of mass and width. The very concept of mass and width is model dependent in this case. The CLEO Collaboration [6] do not claim evidence for the σ meson due to the uncertainty in the best parameterization of this amplitude. Anyway, good fits were obtained in all cases, and the values for the mass and width (see table 1) are in good agreement - $M \sim 480$ MeV, $\Gamma_0 \sim 320$ MeV.

It would be interesting, definitely, to show the phase variation across the Dalitz plot without assuming any functional form for the σ amplitude. This is, unfortunately, very difficult because it involves a very large number of free parameters. In any case, it remains to be explained why in charm decays the σ seems to be a real particle, but not in low energy elastic $\pi^+\pi^-$ scattering.

4.2 $f_0(980)$

The width of this state is poorly known. The reason is that the $f_0(980)$ seems to behave differently depending on the reaction in which it is produced. While in scattering it looks broader and with a large coupling to the $K\bar{K}$ channel, in

charm decays it looks just like a narrow regular $q\bar{q}$ resonance decaying mostly into pions. In the decay $D_s^+ \to \pi^+\pi^-\pi^+$ the $f_0(980)\pi^+$ component correspond to over 50% of the decay rate.

E791 used a coupled channel Breit-Wigner (the Flatté formula) in its fit [2]. The coupling to $K\bar{K}$ channel was found to be consistent with zero. An equally good fit was obtained using a regular Breit-Wigner, yielding $\Gamma_0 = (44\pm3)$ MeV. This is in agreement with preliminary results from FOCUS ($\Gamma_0 \sim 55$ MeV, from $D_s^+ \to \pi^+\pi^-\pi^+$) and BES ($\Gamma_0 \sim 45$ MeV, from $J/\psi \to \phi\pi^+\pi^-$).

The large rate in $D_s^+ \to \pi^+\pi^-\pi^+$ suggests a strong affinity of the $f_0(980)$ with $s\bar{s}$, if we take the W-radiation amplitude to be the dominant decay mechanism. In spite of a large $s\bar{s}$ in its wave function, the lack of a significant coupling to $K\bar{K}$ is due essentially to the narrow $f_0(980)$ width.

The above situation reinforces the interpretation of this state as a 4-quark state surrounded by a $K\bar{K}$ molecular cloud. At short distances, as in D decays, we would access the $qq\bar{q}\bar{q}$ component, whereas in peripheral processes the molecular component would manifest itself.

4.3 $f_0(1370)/f_0(1500)$

The situation here is still rather confusing. The third state of the f_0 family above 1 GeV, $f_0(1710)$, which would be mostly $s\bar{s}$, is difficult to access, since it lies near the edge of the D_s^+ decay phase space.

Charm decays are useful not only to measure the $f_0(1370)$ and $f_0(1500)$ masses and widths, but also to infer the quark content of these two states. If both are $q\bar{q}$ resonances, both should appear in charm decays. If, in addition, there is a significant $s\bar{s}$ component in their wave function, these states should appear in the $D_s^+ \to K^+K^-\pi^+$ decay.

Both E791 and FOCUS/E687, when analysing the $D_s^+ \to \pi^+\pi^-\pi^+$ decay, have found that only one state is necessary to describe the Dalitz plot, although they do not agree on the measured parameters for this state. While E687 [10] found a state with mass near 1475 MeV and a width of about 100 MeV (very similar to FOCUS preliminary numbers, and very close to the well measured $f_0(1500)$ parameters), E791 [2] found a somewhat wider state with a lower mass: $M_0 = (1434\pm20)$ MeV, $\Gamma_0 = (172\pm32)$ MeV.

BaBar [9] have found no evidence of neither one of the f_0 states in the $D^0 \to \bar{K}^0K^+K^-$ decay. FOCUS (see L. Edera's talk in these proceedings)

have found a small component of $f_0(1370)\pi^+$ in the $D_s^+ \to K^+K^-\pi$ decay, but the sum of all decay fractions is over 160%. This is due to a large destructive interference, which is likely to be unphysical.

A large $D \to \pi^+\pi^-\pi^+$ (and also $D \to \pi^+\pi^0\pi^0$) sample are necessary to disentangle the $f_0(1370)/f_0(1500)$ contribution. Apparently only one of the two f_0 would be a $q\bar{q}$ state (mostly $n\bar{n}$), reinforcing the interpretation of the other one as the ground-state scalar glueball.

5 Conclusions

The picture offered so far by charm decays points to the existence of two scalar meson nonets, one having states with mass below 1 GeV and the other with masses above 1 GeV.

In the low mass states we have the large rates of the $\sigma\pi$ in $D^+ \to \pi^+\pi^-\pi^+$ and of the $f_0(980)\pi$ in $D_s^+ \to \pi^+\pi^-\pi^+$ decay as an indication that both are $q\bar{q}$, or, perhaps $qq\bar{q}\bar{q}$ states. The evidence for the neutral $\kappa(800)$ would be endorsed if evidence for the charged κ is also found. In the cases of both σ and κ, a demonstration of the phase variation would be very welcome. It is also important to measure the $a_0(980)$ width in either $D_s \to K^+K^-\pi$ or $D_s \to \bar{K}^0K^+K^-$ decays.

In the region above 1 GeV more data is necessary to show which of the f_0's are genuine $q\bar{q}$ states. Perhaps the answer is none of those observed in scattering experiments, since the mixing between the bare $q\bar{q}$ resonances and the scalar glueball would not occur in charm decays. Apparently only one state appears in charm decays, although it is not clear yet which state this is. In any case, this state has no significant coupling to $K\bar{K}$.

There are important conceptual issues to be addressed. The most important is to formulate the unitarity constraint in multi-body decays. The assumption of two-body elastic scattering as the basic process is not trivial and may not be justified. Even in the case of two-body elastic scattering, the introduction of a relative phase can restore unitarity, which would be violated in models in which the amplitude is written as a sum of Breit-Wigners [11].

Decays of charm mesons, with their unique features, offer a new way to look at the light scalar mesons.

Table 1: *Mass and width of the σ assuming a Breit-Wigner model.*

experiment	mass (MeV)	width (MeV)
E791	478 ± 29	324 ± 46
CLEO	390 ± 60	282 ± 77
BES	513 ± 32	335 ± 67

References

1. F.Close and N. Törnqvist, hep-ph/0204205; S.Godfrey and J. Napolitano, Rev. Mod. Phys.**71**, 1411 (1999).
2. E.M. Aitala *et al*, Phys. Rev. Lett. **86**, 765 (2001).
3. E.M. Aitala *et al*, Phys. Rev. Lett. **86**, 770 (2001).
4. A. Bertin *et al*, Phys. Rev. **D57**, 55 (1998).
5. C.Amsler and F.E.Close, Phys. Lett. B**353**, 385 (1995).
6. H.Muramatsu *et al*, hep-ex/0207067.
7. N.Wu *et al*, hep-ex/0104050.
8. E.M. Aitala *et al*, Phys. Rev. Lett. **89**, 121801 (2002).
9. B.Aubert *et al*, hep-ex/0207089.
10. P.L.Frabetti *et al*, Phys. Lett. **B407**, 79 (1997).
11. M.Svec, Phys. Rev. **D64**:096003 (2001).

Frascati Physics Series Vol. XXXI (2003), pp. 121–124
FRONTIERSCIENCE 2002 – Frascati, October 6–11, 2002
Invited Contribution in Plenary Session

DALITZ PLOT ANALYSIS OF THE DECAY $D^+ \to K^-\pi^+\pi^+$ AND NEW INFORMATION ON THE SCALAR $K\pi$ AMPLITUDES FROM E791

Carla Göbel *
Universidad de la República, Montevideo, Uruguay

ABSTRACT

A Dalitz plot analysis of the decay $D^+ \to K^-\pi^+\pi^+$ is performed from the Fermilab E791 data sample. A model constructed from a coherent sum of known $K\pi$ resonant amplitudes plus a constant non-resonant term does not give an acceptable fit. A good fit is obtained by the inclusion of an extra light and broad $K\pi$ scalar state.

1 The $D^+ \to K^-\pi^+\pi^+$ Dalitz-plot Analysis

The decays of charm mesons can be viewed as a new source of information for the study of light meson spectroscopy, complementary to that from scattering experiments, and can be particularly relevant to the understanding of the scalar sector.

* On behalf of the Fermilab E791 Collaboration

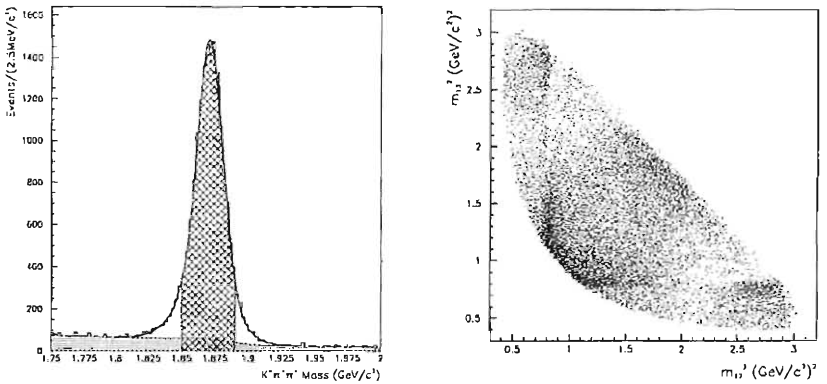

(a) (b)

Figure 1: *(a) The $K\pi\pi$ invariant mass spectrum. The filled area is background; (b) Dalitz plot corresponding to the events in the dashed area of (a).*

Here we present results for the Dalitz-plot analysis of the decay $D^+ \to K^-\pi^+\pi^+$ (see details in [1]) using data from Fermilab E791 [2]. From the original 2×10^{10} events collected, and after reconstruction and selection criteria, we obtained the $D^+ \to K^-\pi^+\pi^+$ sample shown in Figure 1(a). The filled area represents the level of background. The crosshatched region contains the 15090 events selected for the Dalitz-plot analysis, as shown in Figure 1(b), where the two axes are the squared invariant-mass combinations for $K\pi$ (symmetrized for the two identical pions). An unbinned maximun-likelihood fit is performed with probability distribution funtions (PDF's) for both signal and background. The signal PDF is written as the square of the total physical amplitude $\mathcal{A}$ and it is weighted for the acceptance across the Dalitz plot and by the level of signal to background for each event, as given by Figure 1(a).

Our first approach to fit the data includes the known $K\pi$ resonant amplitudes ($\mathcal{A}_n$, $n \geq 1$), plus a constant non-resonant (NR) contribution. We call this Model A. The signal amplitude is constructed as a coherent sum of the various sub-channels, $\mathcal{A} = a_0 e^{i\delta_0}\mathcal{A}_0 + \sum_{n=1}^{N} a_n e^{i\delta_n}\mathcal{A}_n$. Each resonant amplitude is written as $\mathcal{A}_n = BW_n\, F_D^{(J)}\, F_n^{(J)}\, \mathcal{M}_n^{(J)}$ where BW_n is the relativistic Breit-Wigner propagator, $BW_n = \left[m_0^2 - m^2 - im_0\Gamma(m)\right]^{-1}$. The quantities F_D and F_R are the Blatt-Weisskopf damping factors respectively for the D and the $K\pi$ resonances, they depend on the radii of the decaying meson and are set to $r_D = 3.0$ GeV^{-1} and $r_R = 1.5$ GeV^{-1} in Model A. $\mathcal{M}_n^{(J)}$ describes

the angular function according to the spin J of the resonance. See [1]. Each amplitude is Bose symmetrized $\mathcal{A}_n = \mathcal{A}_n[(\mathbf{12})\mathbf{3}] + \mathcal{A}_n[(\mathbf{13})\mathbf{2}]$.

For Model A, we find contributions from the channels: NR, with a decay fraction over 90%, followed by $\bar{K}_0^*(1430)\pi^+$, $\bar{K}^*(892)\pi^+$, $\bar{K}^*(1680)\pi^+$ and $\bar{K}_2^*(1430)\pi^+$. The decay fractions and relative phases are shown in Table 1. These values are in accordance with previous results from E691 [3] and E687 [4]. There is an important interference pattern, since all fractions add up to 140%. We find important disagreements between the fit to Model A and data, with $\chi^2/\nu = 2.7$ (ν being the number of degrees of freedom) in the Dalitz Plot. The discrepancies are found mainly at low $K\pi$ mass squared (below 0.8 $(\mathrm{GeV/c^2})^2$) and near 2.5 $(\mathrm{GeV/c^2})^2$. We thus conclude that a model with the known $K\pi$ resonances, plus a constant NR amplitude, is not able to describe the $D^+ \to K^-\pi^+\pi^+$ Dalitz plot satisfactorily.

A second model (Model B) allows the mass and width of the scalar $K_0^*(1430)$ to float. Gaussian-type form-factors [5] are introduced for this scalar state. Two extra floating parameters are the meson radii r_D and r_R introduced above. We find fractions and phases similar to those of Model A (within errors) and the mass and width of $K_0^*(1439)$ are found to be 1416 ± 27 MeV/c^2 and 250 ± 21 MeV/c^2, respectively, consistent with PDG values [6]. The fit improves but it is still unsatisfactory.

A third fit model, Model C, is constructed by the inclusion of an extra scalar state, with unconstrained mass and width. We maintain the mass and width of the $K_0^*(1430)$ as free parameters, and use the Gaussian form-factors as in Model B. Using this model, we obtain the values of $797 \pm 19 \pm 43$ MeV/c^2 for the mass and $410 \pm 43 \pm 87$ MeV/c^2 for the width of the new scalar state (first error statistical, second error systematic), referred to here as the κ. The values of mass and width obtained for the $K_0^*(1430)$ are respectively $1459 \pm 7 \pm 12$ MeV/c^2 and $175 \pm 12 \pm 12$ MeV/c^2, appearing heavier and narrower than presented by the PDG. The decay fractions and relative phases for Model C are given in Table 1. Compared to the results of Model A (without κ), the NR mode drops from over 90% to 13%. The $\kappa\pi^+$ state is now dominant with about 50%. Moreover, the fit quality of Model C is substantially superior to that of Model A; the χ^2/ν is now 0.73. The meson radii r_D and r_R are found to be respectively 5.0 ± 0.5 GeV^{-1} and 1.6 ± 1.3 GeV^{-1}.

Various studies are done to check these results. For example, we replace

Table 1: *Results without κ (Model A) and with κ (Model C).*

Decay Mode	Model A: No κ		Model C: With κ	
	Fraction (%)	Phase	Fraction (%)	Phase
NR	90.9 ± 2.6	$0°$ (fixed)	$13.0 \pm 5.8 \pm 4.4$	$(-11 \pm 14 \pm 8)°$
$\kappa\pi^+$	-	-	$47.8 \pm 12.1 \pm 5.3$	$(187 \pm 8 \pm 18)°$
$\bar{K}^*(892)\pi^+$	13.8 ± 0.5	$(54 \pm 2)°$	$12.3 \pm 1.0 \pm 0.9$	$0°$ (fixed)
$\bar{K}_0^*(1430)\pi^+$	30.6 ± 1.6	$(54 \pm 2)°$	$12.5 \pm 1.4 \pm 0.5$	$(48 \pm 7 \pm 10)°$
$\bar{K}_2^*(1430)\pi^+$	0.4 ± 0.1	$(33 \pm 8)°$	$0.5 \pm 0.1 \pm 0.2$	$(-54 \pm 8 \pm 7)°$
$\bar{K}^*(1680)\pi^+$	3.2 ± 0.3	$(66 \pm 3)°$	$2.5 \pm 0.7 \pm 0.3$	$(28 \pm 13 \pm 15)°$

the complex κ Breit-Wigner by a real Breit-Wigner, with no phase variation. In this case, we get similar mass and width for this extra state, but with unphysical fractions for this state and the NR, and a worse fit quality. We also replace the κ by hypothetical vector and tensor states, and the fit clearly prefers the scalar state. Other models with the κ are also tried, like modifications to the scalar Breit-Wigner amplitude and to the form-factors. Other studies for the parameterization of the NR amplitude are tried with and without the κ. None of these models without the κ is able to describe our data satisfactorily. All variations of models with κ give similar results for the κ mass and width (within errors) although the fractions for $\kappa\pi$ and NR show correlations.

From our results we find a good indication that a light and broad scalar $K\pi$ resonance gives an important contribution to $D^+ \to K^-\pi^+\pi^+$ decay.

References

1. E791 Collaboration, E.M. Aitala *et al.*, Phys. Rev. Lett **89**, 121801 (2002).
2. E791 Collaboration, E.M. Aitala et al., hep-ex/9809029; Phys. Rev. Lett. 86, 765 (2001); 770; S. Amato *et al.*, hep-ex/0001003; S. Bracker *et al.*, hep-ex/9511009.
3. E691 Collaboration, J.C. Anjos *et al.*, Phys. Rev. D **48**, 56 (1993).
4. E687 Collaboration, P.L. Frabetti *et al.*, Phys. Lett. B **331**, 217 (1994).
5. N.A. Törnqvist, Z. Phys. C **68**, 647 (1995).
6. D.E. Groom *et al.*, Eur. Phys. Jour. C **15**, 1 (2000).

Frascati Physics Series Vol. XXXI (2003), pp. 125–128
FRONTIERSCIENCE 2002 – Frascati, October 6–11, 2002
Invited Contribution in Plenary Session

DALITZ PLOT ANALYSIS IN FOCUS

Laura Edera *
Università degli Studi di Milano

ABSTRACT

Some Focus results about the Dalitz analysis of D-meson decays into three pseudoscalars are presented. The advantages of the K-matrix approach to formalize the S-wave states are briefly outlined.

1 Introduction

In the last years the Dalitz plot analysis has emerged as a proper and powerful tool to understand the main features of the charm hadronic decays, that is to investigate the resonant substructures, the role of the final state interaction (FSI) and of non-spectator diagrams. It is only in more recent years that this analysis has been used even to better investigate the light quark spectroscopy

* On behalf of the FOCUS collaboration

in the scalar sector. In this report I will present some results of the amplitude analysis of the $D^+ \to K^+K^-\pi^+$, $K^+\pi^-\pi^+$, $\pi^+\pi^-\pi^+$ and $D_s^+ \to K^+\pi^-\pi^+$, $\pi^+\pi^-\pi^+$, obtained with the so-called isobar model (see for example [1]). The advantages of the K-matrix approach applyed to the charm sector will be discussed.

2 Dalitz plot analysis results

The Dalitz plot analysis of three-body decays provides the full set of observables of the decay: coefficients and relative phases of the different amplitudes contributing to the same final state. Multibody decays can occur via various strong resonances which can interfere with each other. Measurements of the phase shifts between different resonant components allow us to gauge the role of FSI and thus to shed some light onto the underlying weak decay dynamics. Infact, at tree level, the weak amplitudes are real; relatively immaginary phase shifts in the decay are due to FSI.

A very instructive example for probing the role of FSI is the decay of $D^+ \to K^+K^-\pi^+$. The Dalitz plot (fig.1(a)) is very highly dominated by the $\phi\pi^+$ and $\overline{K}^{*0}K^+$ channels, with an additional contribution corresponding at high $K\pi$ mass region. The asymmetry between the two lobes of $\overline{K}^{*0}$ can be interpreted as an interference between this resonance and a broad scalar. When a complete Dalitz analysis is performed, the fit returns contributions of $\overline{K}^{*0}(892)$ (with a fit fraction of about 20%) and $\overline{K}^{*0}(1430)$ ($\sim$ 67%), that is a broad and large scalar, in a relatively imaginary phase configuration, pointing at relevant FSI effects.

The high statistics and the very good quality of the data collected by Focus allow for investigation of suppressed and heavly suppressed decays, such as the Singly Cabibbo Suppressed Decay $D_s^+ \to K^+\pi^-\pi^+$ (fig. 1(b)), for which Focus is performing the first Dalitz analysis, and the Doubly Cabibbo Suppressed Decay $D^+ \to K^+\pi^-\pi^+$ (fig. 1(c)). Both Dalitz plot analyses indicate a rich resonant structure, dominated by $\rho(770)$ and $K^{*0}(892)$, in a relative real phase configuration, pointing, in these decays, at a non-relevant role of FSI.

A channel that is particular interesting is the $D_s^+ \to \pi^+\pi^-\pi^+$, since it is the best candidate to evaluate annihilation contributions. The amplitude analysis indicates that the f_0, clearly visible over the Dalitz plot (fig. 1(d)), is the dominant contribution ($\sim$ 94%); a band for $S_0(1475)$ is also visible and accounts for

$\sim 17\%$. Finally the tensor $f_2(1270)$ ($\sim 10\%$) and the $\rho(1450)$ ($\sim 5\%$) populate the Dalitz plot corner. A non-resonant contribution is necessary to obtain a good fit quality. Unfortunatelly the experimental scenario is still too poor to draw final conclusion about the annihilation diagram.
The decay $D^+ \to \pi^+\pi^-\pi^+$ (fig. 1(e)) is dominated by $\rho(770)$ ($\sim 30\%$). The preliminary results of the fit show that, if the $\sigma(400)$ (whose existence is still controversial and not widely accepted [2]) is introduced in the fit, it accounts for a fit fraction of $\sim 20\%$.

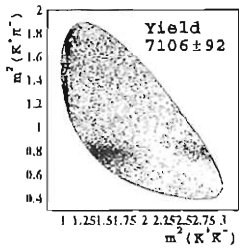

(a) $D \to KK\pi$

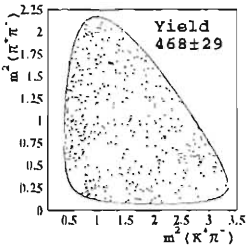

(b) $D_s^+ \to K^+\pi^-\pi^+$

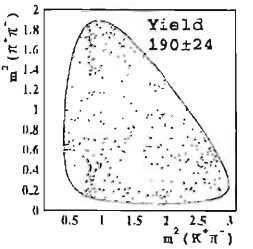

(c) $D^+ \to K^+\pi^-\pi^+$

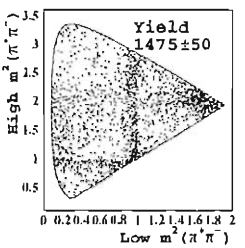

(d) $D_s^+ \to \pi^+\pi^-\pi^+$

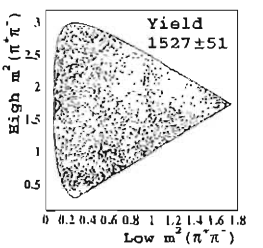

(e) $D^+ \to \pi^+\pi^-\pi^+$

Figure 1: *Dalitz plots from Focus*

3 K-matrix approach

All previous results have been obtained using the isobar model, which should be considered a kind of first order approximation, since it does not respect the unitarity and does not incorporate all the present experimental knowledge in the light meson sector, which is very deep and comprehensive. For sure it is not well suited to analyze charm decays at the high already available statistics of Focus. So the natural next step to investigate charm decay requires a better model to account for strong dynamics. We are rigorously developing the formalism on the basis of the K-matrix approach [3], which naturally embeds unitarity and all the present kwnoledge in light meson scattering and spectroscopy. The K-matrix is a rapresentation of the scattering matrix S, where the resonances are defined as poles of S. This formalism is general and naturally describes, for instance, coupled-channel resonances, such as $f_0(980)$, and nearby resonances, such as $f_0(1370)$ and $f_0(1500)$.
The K-matrix, originally developed in the context of the scattering problems, can be extended to cover the case of more complex resonance formation through the P-vector approach [4]. With this powerful tool the Dalitz plot analysis of charm hadronic decays can provide new useful and independent information on several controversial light-quark resonances.

4 Conclusions

In the last years Dalitz analysis has provided important results to better understand the charm phenomenology. The excellent quality of the available data requires now a better model to formalize the strong dynamics; the K-matrix approach seems to be the proper tool. The preliminary results obtained in Focus are promising.

References

1. P. L. Frabetti *et al.*, Phys. Lett. B **331**, 217 (1994).
2. P. Minkowski and W. Ochs, hep-ph/0209225.
3. S.U. Chung *et al.*, Annalen Phys. **4**, 404 (1995).
4. I.J.R. Aitchison, Nucl. Phys. A **189**, 417 (1972).

Frascati Physics Series Vol. XXXI (2003), pp. 129
FRONTIERSCIENCE 2002 – Frascati, October 6–11, 2002
Invited Review Talk in Plenary Session

HEAVY ION COLLISIONS

Naohito Saito

Kyoto University, Department of Physics, Kitashirakawa-Oiwakecho Sakyo-ku, Kyoto 606-8502, Japan

Written contribution not received

Frascati Physics Series Vol. XXXI (2003), pp. 131–135
FRONTIERSCIENCE 2002 – Frascati, October 6–11, 2002
Invited Contribution in Plenary Session

THE SPIN OF THE NUCLEON AT HERMES

Pasquale Di Nezza
INFN, Laboratori Nazionali di Frascati, via E.Fermi 40, 00044 Frascati - Italy *

ABSTRACT

A short review of HERMES experimental results on the spin structure of the nucleon is presented. Inclusive polarized deep-inelastic scattering (DIS) on a longitudinally polarized targets provided precise and complete informations on the polarized structure function $g_1(x)$. By using both inclusive and semi-inclusive DIS, the polarized quark distributions $\Delta q_f(x)$ for each flavour f has been derived. Measurements of the double-spin asymmetry for the photoproduction of high-p_T hadron pairs has been interpreted as a first evidence for a positive gluon polarization. The beam spin azimuthal asymmetry in the deeply virtual Compton scattering and the target spin azimuthal asymmetry in the pion electroproduction has been measured for the first time. Those two measurements proofed the possibility to access the Generalized Parton Distribution and the still unknown transversity distribution $h_1(x)$, respectively.

* On behalf of the HERMES Collaboration

The understanding of strong interactions including spin as an additional degree of freedom is an intensively discussed question since QCD become the gauge field theory of the strong interaction establishing the intuitive quark model as the valid concept for the nucleon substructure. In this field HERMES, considered a second generation experiment, by using both a polarized target and a polarized beam plays a fundamental role. At leading twist, the structure of the nucleon can be described by three Structure Functions (SF): $F_1(x)$, $g_1(x)$ and $h_1(x)$, all as a function of the Bjorken variable. The unpolarized SF $F_1(x)$ is now well determined over a broad kinematical range. The polarized SF $g_1(x)$ contains information on the helicity-dependent quark contributions to the deep-inelastic scattering cross section. By integrating $g_1(x)$ over x, the total contribution $\Delta\Sigma_q$ of the quark spin to the nucleon spin can be determined. The first result reported by the HERMES collaboration [1], which was largely based on measurements on a longitudinally polarized proton target, provided $\Delta\Sigma_q = 0.30 \pm 0.04 \pm 0.09$ (at Q^2=2.5 GeV^2). Since precise data on the proton are now available [2, 3], the emphasis of the most recent HERMES measurements was on the structure function $g_1^d(x)$ on the deuteron. The preliminary results are plotted together with those obtained on polarized proton and ^{3}He targets [4, 5] in the left panel of fig.1. This figure can be considered the consistent and almost conclusive picture of about one decade on investigations on $g_1(x)$.

Performing measurements of semi-inclusive deep-inelastic scattering, HERMES was able to determine the polarized quark distribution $\Delta q_f(x)$ for each flavour f. Double spin-asymmetries $A_1^h(x)$ were determined for different hadron types h like pions, kaons and protons. The asymmetries $A_1^h(x)$, for each hadron, are related to the quark distributions $\Delta q_f(x)$, for each quark flavour, and the values obtained for $\Delta q_u(x)$, $\Delta q_d(x)$ $\Delta q_{\bar{u}}(x)$, $\Delta q_{\bar{d}}(x)$ and $\Delta q_s(x)$ are shown in the right panel of fig.1. From this figure it is concluded that the u-quarks are strongly polarized in a direction parallel to the proton one, while the d-quarks are less strongly polarized in the opposite direction. The sea quarks overall contribution to the proton spin is small and compatible with zero.

Several NLO-QCD analyses of the Q^2-dependence of the measured $g_1(x, Q^2)$ have been performed to extract the contribution of the gluon polarization. Unfortunately the limited accuracy and the kinematical range of the data did not allow to extract precise information of this observable and even the sign is not completely determined. The first direct study of $\Delta G/G$ has been carried

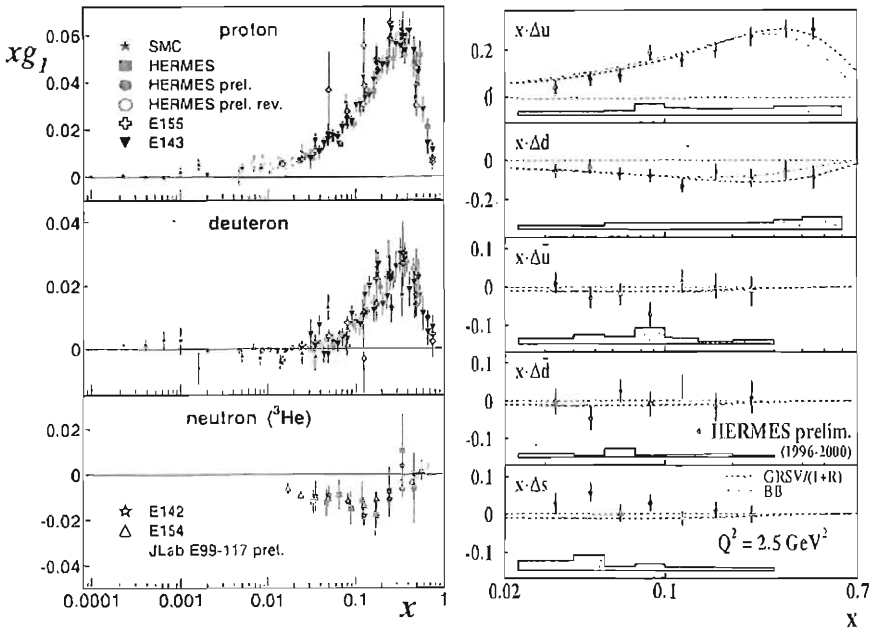

Figure 1: *Left: the longitudinal spin-dependent structure function $xg_1(x)$ as measured on longitudinally polarized hydrogen (top panel), deuterium (middle panel) and ^3He (lower panel) targets. Right: the longitudinal quark spin distribution $x\Delta q$ for $u, d, \bar{u}, \bar{d}, s$-quark. The hatched areas represent the systematic uncertainties of the data. The curves are NLO-QCD predictions from fits to g_1*

out by HERMES [6]. By measuring the double-spin asymmetry for the photoproduction of oppositely charged high-p_T hadron pairs on a longitudinally polarized hydrogen target, a value of $\Delta G/G = 0.41 \pm 0.18 \pm 0.03$ was obtained at $< x_G >= 0.17$ and $< Q^2 >= 0.06$ GeV^2 showing positive gluon polarization. The absolute value, however, is model dependent as a Monte Carlo simulation was needed to determine the relative yield of the signal from the photon-gluon fusion and the background from QCD Compton contributions.

A new and important process studied at HERMES is the Deep Virtual Compton Scattering (DVCS) which provides information on the Generalized Parton Distributions (GPDs). In the 1997 Ji [7] has shown that the first moment of certain GPDs can be related to the total angular momentum of the quarks

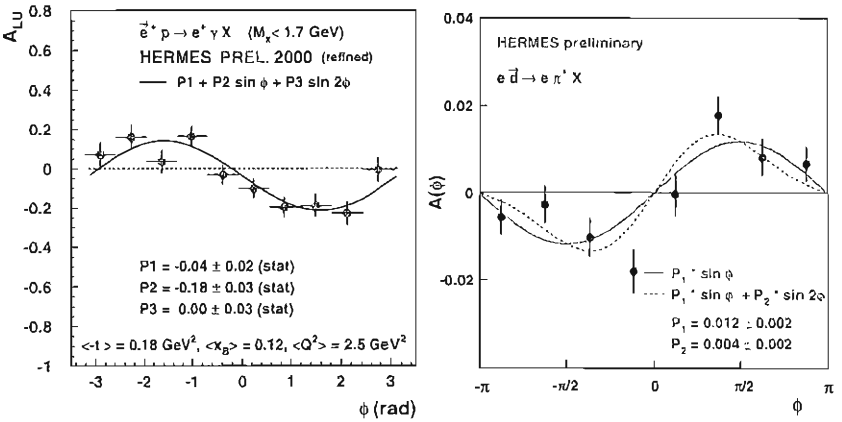

Figure 2: *Left: single beam-spin asymmetry for electroproduction of real photons on an unpolarized hydrogen target as a function of the azimuthal angle ϕ. The curve represents a sin phi-fit to the data. Right: single target-spin asymmetry for the electroproduction of π^+ on a polarized deuterium target as a function of the azimuthal angle ϕ.*

and the gluons in the nucleon. By exploiting the interference between the DVCS and Bethe-Heitler (BH) processes, one obtain access to the DVCS amplitudes. This interference term in the cross section depends on the beam polarization and results in an azimuthal asymmetry of the distribution of the emitted real photons with respect to the virtual one. Such a beam spin asymmetry has been observed at HERMES [8] for interactions $e^+p \to e^+\gamma X$ with a missing mass M_X close to the proton mass as shown in the left panel of fig.2.

Apart from the structure functions $F_1(x)$ and $g_1(x)$, there is a third leading twist but still unknown structure function, $h_1(x)$, known as the transversity distribution. Inclusive DIS cannot be used to measure $h_1(x)$ as it is chirally-odd quantity. In semi-inclusive DIS, informations can be obtained if, the latter, is combined with a fragmentation function chirally-odd too. First evidence of a non-zero transversity distribution has been reported by HERMES [9]. The data show a small asymmetry that can be explained from a combination with $h_1(x)$ and the non-zero corresponding chirally-odd fragmentation function. New preliminary results on deuteron target are shown in the right panel of fig.2. On the basis of the small asymmetries observed on longitudinally polarized targets, it

is expected that sizable asymmetry will be observed if transversely polarized targets are used. At the moment, such measurements are ongoing at HERMES.

As discussed, besides new and precise data on $g_1(x)$, a whole new class of measurements has been performed at HERMES. In this context, the study of gluon polarization in the nucleon, of the flavour decomposition of the quark spin distributions and of the transversity distribution is playing a central role. At the same time new plans have been started to further exploit deeply virtual Compton scattering measurements. Hence, there are good reasons to believe that our understanding of the origin of the nucleon spin will still improve significantly in the next few years.

References

1. K.Ackerstaff *et al* (HERMES Coll.), Phys. Lett. B **464**, 123 (1999).
2. P.L. Anthony *et al* (E155 Coll.), Phys. Lett. B **463**, 339 (1999); and Phys. Lett. B **493**, 19 (1999); B.Adeva *et al* (SMC Coll.), Phys. Rev. D **58**, 112001 (1998); and Phys. Rev. D **60**, 072004 (1999); K.Abe *et al* (E143 Coll.), Phys. Rev. Lett. **76**, 587 (1996); and Phys. Rev. D **58**, 112003 (1998).
3. A.Airapetian *et al* (HERMES Coll.), Phys. Lett. B **442**, 484 (1998).
4. P.L. Anthony *et al* (E142 Coll.), Phys. Rev. Lett. **71**, 959 (1993); and Phys. Rev. D **54**, 6620 (1996); K.Abe *et al* (E154 Coll.), Phys. Rev. Lett. **79**, 26 (1997).
5. K.Ackerstaff *et al* (HERMES Coll.), Phys. Lett. B **404**, 383 (1997).
6. A.Airapetian *et al* (HERMES Coll.), Phys. Rev. Lett. **84**, 2584 (2000).
7. X.Ji, Phys. Rev. D **55**, 7114 (1997).
8. A.Airapetian *et al* (HERMES Coll.), Phys. Rev. Lett. **87**, 182001 (2001).
9. A.Airapetian *et al* (HERMES Coll.), Phys. Rev. Lett. **84**, 4047 (2000); and Phys. Rev. D **64**, 097101 (2001).

Flavour Dynamics and CP Violation – Session I

Chairpersons: M. Piccolo, D. Saxon

N. Uraltsev	Heavy Quark Theory
G. Buchalla	Non Leptonic B Decays and Rare Decays
M. Battaglia	A Review of $\|V_{ub}\|$ and $\|V_{cb}\|$ Determinations
Y. J. Kwon	Semi-leptonic Charm and Beauty Decays
F. Ligabue	Determination of $\|V_{cs}\|$ in the ALEPH Experiment at LEP

Frascati Physics Series Vol. XXXI (2003), pp. 139–146
FRONTIERSCIENCE 2002 – Frascati, October 6–11, 2002
Invited Review Talk in Plenary Session

HEAVY QUARK THEORY

Nikolai Uraltsev
INFN, Sezione di Milano, Milan, Italy

ABSTRACT

The QCD treatment of heavy quarks is illustrated in connection with extracting $|V_{cb}|$ and to an accurate determination of basic heavy quark parameters. Recent data provide at least one precision test of the nonperturbative OPE relation. Experiment points at the proximity to the 'BPS' regime for the heavy quark ground state.

Quantum chromodynamics (QCD) is the well-established theory of the strong interactions. Its practical applications are usually complicated by confinement: QCD is formulated in terms of color quark and gluon fields, while only colorless hadrons are observed in experiment. The transmutation of physical spectrum in QCD has a nonperturbative origin, and its impact must be quantitatively understood in a model-independent way.

Heavy quark (HQ) theory, in particular as applied to b-hadrons, is now a well-developed field occupying a special place in QCD. On one hand, the

b-quark mass often provides a reliable expansion parameter $\Lambda_{\rm QCD}/m_b$ and sets a hard scale where perturbation theory can be sensibly applied. On the other hand, nonperturbative effects are non-negligible and have to be accounted for in precision studies. The application of the dynamical methods of QCD in the context of the HQ expansion has yielded many novel results and insights into the dynamics of heavy flavor hadrons. A recent review of these developments can be found in Ref. [1].

A true measure of our understanding of strong dynamics is how accurately we can extract the underlying quark-level parameters $|V_{cb}|$, $|V_{ub}|$ from the observed decay rates of actual hadrons. The theoretical progress achieved here over the last decade is remarkable. It has become realistic to aim at a percent level in $|V_{cb}|$ – even though our methods do not rely on a fine symmetry *per se*, but rather account for the hadronic effects in a precision way.

A popular method to determine $|V_{cb}|$ uses the decay rate $B \to D^* \ell\nu$ near zero recoil. At this kinematic point the $B \to D^*$ formfactor $F_{D^*}(0)$ is unity when $m_b, m_c \to \infty$. Driven by the charm mass scale, power corrections are still significant: $F_{D^*} \simeq 0.9$ to order $1/m_Q^2$ [2], and the $1/m_c^3$ effects were estimated to be in the 3% range [3]. Relying on an expansion in $1/m_c$ makes it difficult to overcome a 5% level of reliable accuracy here.

These estimates were supported by recent lattice studies which yielded surprisingly close central values, $F_{D^*} \simeq 0.88$ and $F_{D^*} \simeq 0.91$ to order $1/m_Q^2$ and $1/m_Q^3$, respectively [4]. Since the method is based on a $1/m_Q$ expansion for both b and c, an important issue is higher-order as well as exponential in m_c terms. This sophisticated lattice approach will hopefully be refined. Presently a large fraction of the corrections to $F_{D^*}(0) = 1$ is still added theoretically rather than emerges directly in the lattice simulations.

Extrapolating the decay amplitude to zero recoil introduces additional uncertainty. It can be reduced incorporating the model-independent constraints on the IW function stemming from the set of the HQ sum rules [5].

More extensive opportunities are provided by inclusive semileptonic B decays. Nonperturbative effects here are controlled by the QCD theorem [6] which established absence of the leading $\Lambda_{\rm QCD}/m_b$ power corrections to total decay rates. It applies to all sufficiently inclusive decay probabilities, not only semileptonic ones. As pointed out shortly afterwards, the masses and relevant nonperturbative parameters can be determined from the B decay distributions

themselves [7, 8]. Nowadays this strategy is being implemented in a number of experimental studies.

The new generation of data provides accurate measurements of many inclusive characteristics in B decays. Proper theoretical formalism has gradually found its way into their analyses. More recent theoretical findings allow to shrink theoretical uncertainties – among them constraints from the exact HQ sum rules and the consequences of the proximity to the so-called 'BPS' regime signified by the hierarchy $\mu_\pi^2 - \mu_G^2 \ll \mu_\pi^2$ suggested by experiment.

The low-scale running masses $m_b(\mu)$, $m_c(\mu)$, the expectation values $\mu_\pi^2(\mu)$, $\mu_G^2(\mu)$... are completely defined and can be determined from experiment with in principle unlimited accuracy. Violation of local duality potentially limiting theoretical predictability, has been scrutinized and found to be negligibly small in total semileptonic B widths [9]. Present-day perturbative technology allows computing α_s-corrections to the subleading Wilson coefficients. It is also understood how to treat higher-order power corrections.

The ultimate accuracy can be achieved in a comprehensive approach where many observables are measured in B decays to extract necessary 'theoretical' input parameters. Since $b \to c$ widths strongly depend on $m_b - m_c$, previous analyses to some extent relied on expansion in $1/m_c$ employing its relation to $\bar{M}_B - \bar{M}_D$. Reliability of the $1/m_c$ expansion is however questionable. On top of that there are indications that the nonlocal correlators affecting meson masses can be particularly large [10] – a pattern also observed in the 't Hooft model [11]. This expectation is supported by the pilot lattice study [12] suggesting a very large value of $\rho_{\pi\pi}^3 + \rho_S^3$. On the other hand, non-local correlators are not measured in inclusive B decays. A partial cure was suggested recently [10]: The proximity to the 'BPS' limit leads to much smaller power corrections for the mass relation applied to ground-state mass difference $M_B - M_D$ rather than for standard spin-averaged masses.

There is also a way totally free from relying on charm mass expansion [13]. It utilizes the whole potential of the comprehensive approach making full use of a few key facts [8, 7]:

- Total width to order $1/m_b^3$ is affected by a single new Darwin operator (the moments also weakly depend on ρ_{LS}^3).
- No nonlocal correlators ever enter *per se*.
- Deviations from the HQ limit in the expectation values are driven by the

full scale $1/m_b$ and are additionally suppressed by proximity to the BPS limit; they are negligible in practice.

• Exact sum rules and inequalities which hold for properly defined Wilsonian parameters.

Some of the HQ parameters like μ_G^2 are known beforehand. Proper field-theoretic definition allows its accurate determination from the $B^* - B$ mass splitting: $\mu_G^2(1\,\mathrm{GeV}) = 0.35^{+.03}_{-.02}\,\mathrm{GeV}^2$ [10]. A priori less certain is μ_π^2. However, the inequality $\mu_\pi^2 > \mu_G^2$ valid for any definition of kinetic and chromomagnetic operators respecting the commutation relation $[D_j, D_k] = -ig_s G_{jk}$, essentially limits its range: $\mu_\pi^2(1\,\mathrm{GeV}) = 0.45 \pm 0.1\,\mathrm{GeV}^2$.

Running b quark mass was accurately extracted from $\sigma(e^+e^- \to \Upsilon(nS))$ in the end of the 1990s: $m_b(1\,\mathrm{GeV}) = 4.57 \pm 0.06\,\mathrm{GeV}$ for the "kinetic" $m_b(\mu)$. However, considering all available constraints, I think that 4.57 GeV is on the lower side of the m_b range which rather centers around 4.63 GeV.

Often extracted from the data are the "HQET parameters" $(-\lambda_1, \overline{\Lambda})$ – they actually correspond to extrapolating the μ-dependent quantities down to $\mu = 0$. They are ill-defined and meaningful only as intermediate stage entries, however can often be translated into properly defined parameters. Say, in the context of the recent CLEO and BaBar analyses

$$\overline{\Lambda}_{\mathrm{HQET}} \simeq \overline{\Lambda}(1\,\mathrm{GeV}) - 0.255\,\mathrm{GeV}, \qquad -\lambda_1 \simeq \mu_\pi^2(1\,\mathrm{GeV}) - 0.18\,\mathrm{GeV}^2; \quad (1)$$

the recent CLEO's central values [14] thus correspond to $m_b(1\,\mathrm{GeV}) = 4.62\,\mathrm{GeV}$, $\mu_\pi^2(1\,\mathrm{GeV}) = 0.43\,\mathrm{GeV}^2$, surprisingly close to the theoretical expectations!

The utility of hadronic moments $\langle M_X^{2k} \rangle$ follows from the fact [8] that, at least if charm were heavy enough the first, second and third moments would more or less directly yield $\overline{\Lambda}$, μ_π^2 and ρ_D^3, respectively.

Let me give an illustration how such a strategy works. Leptonic moments, for instance, are approximated as

$$\begin{aligned}
\langle E_\ell \rangle &= 1.38\,\mathrm{GeV} + 0.38[(m_b - 4.6\,\mathrm{GeV}) - 0.7(m_c - 1.15\,\mathrm{GeV})] \\
&\quad + 0.03(\mu_\pi^2 - 0.4\,\mathrm{GeV}^2) - 0.09(\tilde{\rho}_D^3 - 0.12\,\mathrm{GeV}^3)\,, \\
\langle (E_\ell - \langle E_\ell \rangle)^2 \rangle &= 0.18\,\mathrm{GeV}^2 + 0.1[(m_b - 4.6\,\mathrm{GeV}) - 0.6(m_c - 1.15\,\mathrm{GeV})] \\
&\quad + 0.045(\mu_\pi^2 - 0.4\,\mathrm{GeV}^2) - 0.06(\tilde{\rho}_D^3 - 0.12\,\mathrm{GeV}^3)\,, \\
\langle (E_\ell - \langle E_\ell \rangle)^3 \rangle &= -0.033\,\mathrm{GeV}^3 - 0.03\,[(m_b - 4.6\,\mathrm{GeV}) - 0.8(m_c - 1.15\,\mathrm{GeV})] \\
&\quad + 0.024(\mu_\pi^2 - 0.4\,\mathrm{GeV}^2) - 0.035(\tilde{\rho}_D^3 - 0.12\,\mathrm{GeV}^3)\,; \qquad (2)
\end{aligned}$$

they depend basically on one and the same combination of masses $m_b - 0.65 m_c$.

The value of $|V_{cb}|$ extracted from $\Gamma_{sl}(B)$ has the following dependence on the HQ parameters [13, 15]:

$$\frac{|V_{cb}|}{0.0421} = 1 - 0.65[(m_b - 4.6\,\mathrm{GeV}) - 0.61(m_c - 1.15\,\mathrm{GeV})] + 0.013\,(\mu_\pi^2 - 0.4\,\mathrm{GeV}^2) + 0.1(\tilde{\rho}_D^3 - 0.12\,\mathrm{GeV}^3) + 0.06(\mu_G^2 - 0.35\,\mathrm{GeV}^2) - 0.01(\rho_{LS}^3 + 0.15\,\mathrm{GeV}^3) = 1 - \frac{0.65}{0.38}\,[\langle E_\ell \rangle - 1.38\,\mathrm{GeV}] - 0.06\,(m_c - 1.15\,\mathrm{GeV}) - 0.07(\mu_\pi^2 - 0.4\,\mathrm{GeV}^2) - 0.05(\tilde{\rho}_D^3 - 0.12\,\mathrm{GeV}^3) - 0.08(\mu_G^2 - 0.35\,\mathrm{GeV}^2) - 0.005\,(\rho_{LS}^3 + 0.15\,\mathrm{GeV}^3); \quad (3)$$

a combination of the parameters has been replaced by $\langle E_\ell \rangle$ in Eq. (2), and sensitivity to μ_G^2 and ρ_{LS}^3 is illustrated. We see that the precise value of charm mass is irrelevant, but reasonable accuracy in μ_π^2 and $\tilde{\rho}_D^3$ is needed.

The first hadronic moment is

$$\langle M_X^2 \rangle = 4.54\,\mathrm{GeV}^2 - 5.0\,[(m_b - 4.6\,\mathrm{GeV}) - 0.62\,(m_c - 1.15\,\mathrm{GeV})] - 0.66\,(\mu_\pi^2 - 0.4\,\mathrm{GeV}^2) + (\tilde{\rho}_D^3 - 0.12\,\mathrm{GeV}^3), \quad (4)$$

i.e., given by nearly the same combination $m_b - 0.7 m_c + 0.1\mu_\pi^2 - 0.2\rho_D^3$ as the lepton moment. Not very constraining, it provides, however a highly nontrivial check of the HQ expansion. This has been recently done [16] with DELPHI data, and resulted in a very convincing agreement. The nonperturbative relation for $M_b - m_b \simeq 650\,\mathrm{MeV}$ has been verified with the uncertainty of only about 50 MeV dominated by the error bar in $\langle E_\ell \rangle$.

The dependence on HQ parameters expectedly changes for higher moments:

$$\langle (M_X^2 - \langle M_X^2 \rangle)^2 \rangle = 1.2\,\mathrm{GeV}^4 - 0.003(m_b - 4.6\,\mathrm{GeV}) - 0.68\,(m_c - 1.15\,\mathrm{GeV}) + 4.5\,(\mu_\pi^2 - 0.4\,\mathrm{GeV}^2) - 5.5\,(\tilde{\rho}_D^3 - 0.12\,\mathrm{GeV}^3)\,,$$

$$\langle (M_X^2 - \langle M_X^2 \rangle)^3 \rangle = 4\,\mathrm{GeV}^6 + (m_b - 4.6\,\mathrm{GeV}) - 3\,(m_c - 1.15\,\mathrm{GeV}) + 5\,(\mu_\pi^2 - 0.4\,\mathrm{GeV}^2) + 13\,(\tilde{\rho}_D^3 - 0.12\,\mathrm{GeV}^3)\,. \quad (5)$$

Ideally, they would measure the kinetic and Darwin expectation values separately. At the moment, however, we have only an approximate evaluation and informative upper bound on $\tilde{\rho}_D^3$. Measuring the second and third hadronic moments is the real step in implementing the comprehensive program of extracting $|V_{cb}|$. It is crucial that this extraction carries no hidden assumptions, and at no point we rely on $1/m_c$ expansion.

There is a caveat in applying the expansion to some experimental data. The true 'hardness' of the moments deteriorates when the cut on E_ℓ is imposed. As a result, say the extraordinary accuracy of CLEO's restricted moments cannot be even nearly utilized by theory, whether or not the expressions we use make this explicit.[1]

For total widths the effective energy scale parameter is generally $\mathcal{Q} = m_b - m_c$. When OPE applies it is typically given by $\mathcal{Q} \lesssim \omega_{\rm max}$, with $\omega_{\rm max}$ the threshold energy at which the decay process disappears once m_b is replaced by $m_b - \omega$. With the $E_\ell > E_{\rm min}$ cut then

$$\mathcal{Q} \simeq m_b - E_{\rm min} - \sqrt{E_{\rm min}^2 + m_c^2} \tag{6}$$

constituting only 1.25 GeV for $E_{\rm min} = 1.5\,{\rm GeV}$. In $b \to s + \gamma$ decays one has $\mathcal{Q} \simeq m_b - 2E_{\rm min}$, once again a rather soft scale 1.2 GeV if the lower cut is set at $E_\gamma = 2\,{\rm GeV}$. For higher moments the hardness deteriorates further. A high premium should be placed for lowering the cuts [17].

Considering alternative kinematic variables will help to improve the theoretical precision for higher hadronic moments [13, 16]. Namely, it is advantageous to trade the traditional hadronic mass M_X^2 for the observable more closely corresponding to the quark virtuality Δ, defined as

$$\mathcal{M}_X^2 = M_X^2 - 2\tilde{\Lambda} E_X\,, \qquad E_X = M_B - q_0 \tag{7}$$

using the B restframe total hadronic energy, and $\tilde{\Lambda}$ a fixed mass parameter. Its preferred values are about $M_B - m_b(1\,{\rm GeV}) \simeq 650\,{\rm MeV}$. The higher moments $\langle(\mathcal{M}_X^2 - \langle\mathcal{M}_X^2\rangle)^2\rangle$, $\langle(\mathcal{M}_X^2 - \langle\mathcal{M}_X^2\rangle)^3\rangle$... should enjoy better theoretical stability.

The kinematic variable $\mathcal{M}_X^2$ is not well constrained inclusively at LEP experiments, however can be used in the B threshold production at CLEO and B factories. This possibility should be carefully explored.

An intriguing theoretical environment opens up if $\mu_\pi^2(1\,{\rm GeV})$ is confirmed to be close enough to $\mu_G^2(1\,{\rm GeV})$. If $\mu_\pi^2 - \mu_G^2 \ll \mu_\pi^2$ it is useful to analyze strong dynamics expanding around the point $\mu_\pi^2 = \mu_G^2$ [10]. This is not just one point of a continuum in the parameter space, but a quite special 'BPS' limit where the ground state satisfies functional relations $\vec{\sigma}\vec{\pi}|B\rangle = 0$, remarkable in many

[1] An instructive example of how naive analysis can miss such effects is given in [17], Sect. 5.

respects. In some instances like the $B \to D$ zero-recoil amplitude it extends the HQ symmetry to higher orders in $1/m_Q$. One practical application has been mentioned – the robust relation for $m_b - m_c$ via $M_B - M_D$. Exclusive $B \to D^*$ decay can also benefit from the proximity to BPS. The exact spin sum rules [5] yield a bound for the IW slope

$$\mu_\pi^2 - \mu_G^2 = 3\bar{\varepsilon}^2(\varrho^2 - \tfrac{3}{4}), \qquad 0.45\,\mathrm{GeV} \lesssim \bar{\varepsilon} \lesssim 1\,\mathrm{GeV} \tag{8}$$

thus leaving only a small room for the slope of the $B \to D^*$ formfactor, excluding values exceeding $1.15 - 1.2$. This would be a very constraining result for a number of experimental studies.

In conclusion: The comprehensive approach will allow to reach a percent level of reliable accuracy in translating $\Gamma_{\rm sl}(B)$ to $|V_{cb}|$. We already observe a nontrivial consistency between quite different measurements, and between experiment and QCD-based theory.

There are obvious lessons to infer. Experiment must strive to weaken the cuts in inclusive measurements used in extracting $|V_{cb}|$. Close attention should be paid to higher moments or their special combinations, as well as exploring complementary kinematic observables. The recent progress in experiment can be complemented by refinement of theory in

- calculating perturbative corrections to subleading operators,
- scrutinizing higher-order power corrections, and
- thoroughly studying alternative kinematic variables, e.g. moments of $\mathcal{N}_X^2$.

To fully realize the physical information in the quest for the ultimate precision, a truly comprehensive analysis must implement all theoretical constraints on HQ parameters; the suitable framework uses well-defined running parameters having physical meaning. Heavy quark sum rules yield strong constraints on the parameter space; it is important to study the question of their saturation. If a low μ_π^2 around $0.45\,\mathrm{GeV}^2$ is confirmed by experiment, the BPS expansion will play an important role in analyzing nonperturbative effects, including higher-order corrections.

Acknowledgments: I am grateful to M. Battaglia, I. Bigi, M. Calvi and P. Roudeau for helpful discussions. It is a pleasure to thank the organizers of the Conference for invitation and for providing creative environment.

References

1. N. Uraltsev, in: Boris Ioffe Festschrift 'At the Frontier of Particle Physics–Handbook of QCD' (Ed. M. Shifman, World Scientific, Singapore, 2001), **3**, 1577; hep-ph/0010328.
2. M. Shifman, N. Uraltsev and A. Vainshtein, Phys. Rev. **D51**, 2217 (1995).
3. N. Uraltsev, Nucl. Instrum. & Methods **A 384**, 17 (1996); I. Bigi, M. Shifman and N. Uraltsev, Ann. Rev. Nucl. Part. Sci. **47**, 591 (1997).
4. S. Hashimoto *et al*, Phys. Rev. **D66**, 014503 (2002).
5. N. Uraltsev, Phys. Lett. **B501**, 86 (2001).
6. I. Bigi, N.G. Uraltsev and A. Vainshtein, Phys. Lett. **B293**, 430 (1992); B. Blok and M. Shifman, Nucl. Phys. **B399**, 441 and 459 (1993).
7. I.I. Bigi *et al*, Int. Journ. Mod. Phys. **A9**, 2467 (1994).
8. I.I. Bigi *et al*, Phys. Rev. **D52**, 196 (1995).
9. I. Bigi and N. Uraltsev, Int. J. Mod. Phys. **A16**, 5201 (2001).
10. N. Uraltsev, Phys. Lett. **B545**, 337 (2002).
11. R. Lebed and N. Uraltsev, Phys. Rev. **D62**, 094011 (2000).
12. A. S. Kronfeld and J. N. Simone, Phys. Lett. **B490**, 228 (2000) [Erratum-ibid. **B495**, 441 (2000)].
13. N. Uraltsev, hep-ph/0210044; to appear in the Proc. of ICHEP 2002.
14. R.A. Briere *et al*, CLEO Collaboration, hep-ex/0209024.
15. N. Uraltsev, hep-ph/0210413; Mod. Phys. Lett. **A**, to appear.
16. M. Battaglia *et al*, hep-ph/0210319.
17. I. Bigi and N. Uraltsev, hep-ph/0202175; Int. Journ. Mod. Phys. **A** (2002), to appear.

Frascati Physics Series Vol. XXXI (2003), pp. 147–156
FRONTIERSCIENCE 2002 – Frascati, October 6–11, 2002
Invited Review Talk in Plenary Session

NONLEPTONIC B DECAYS AND RARE DECAYS

Gerhard Buchalla
Ludwig-Maximilians-Universität München, Sektion Physik,
Theresienstraße 37, D-80333 München, Germany

ABSTRACT

We review selected topics in the field of nonleptonic and rare B meson decays. We concentrate in particular on exclusive channels, discussing recent developments based on the concepts of factorization in QCD and the heavy-quark limit.

1 Introduction

The major goal of B physics is to provide us with novel and decisive tests of the quark flavour sector. The most interesting B decay channels typically have small branching fractions below 10^{-4} and are being studied by the current generation of B physics facilities. Important examples of such decays are nonleptonic modes as $B \to \pi\pi$ or $B \to \pi K$, and the radiative rare decays $B \to K^*\gamma$, $\rho\gamma$, $K^*l^+l^-$, $l\nu\gamma$. They consitute a rich source of information,

in particular on CKM angles and flavour-changing neutral currents (FCNC). Many new results are becoming available from the B factories. Both inclusive and exclusive decays can be exploited. Loosely speaking, the exclusive channels are easier for experiment while they are harder for theory. The challenge for theory is to control the effects of QCD. To achieve this it is necessary to devise a systematic factorization of short-distance and long-distance contributions, which usually results in a considerable simplification of the problem. For B decay matrix elements this factorization relies on the hierarchy $m_b \gg \Lambda_{QCD}$. This allows us to perform an expansion around the heavy-quark limit and to factorize perturbative contributions (scales of order m_b) from nonperturbative dynamics (Λ_{QCD}). Since the general concept of factorization in QCD has recently found new applications in the important domain of *exclusive* B decays, we shall focus the following presentation on this area.

2 Exclusive hadronic B decays in QCD

The calculation of B-decay amplitudes, such as $B \to D\pi$, $B \to \pi\pi$ or $B \to \pi K$, starts from an effective Hamiltonian, which has, schematically, the form

$$\mathcal{H}_{eff} = \frac{G_F}{\sqrt{2}} \lambda_{CKM}\, C_i Q_i \tag{1}$$

Here C_i are the Wilson coefficients at a scale $\mu \sim m_b$, Q_i are local, dimension-6 operators and λ_{CKM} represents the appropriate CKM matrix elements. The main theoretical problem is to evaluate the matrix elements of the operators $\langle Q_i \rangle$ between the initial and final hadronic states. A typical matrix element reads $\langle \pi\pi | (\bar{u}b)_{V-A} (\bar{d}u)_{V-A} | B \rangle$.

These matrix elements simplify in the heavy-quark limit, where they can in general be written as the sum of two terms, each of which is factorized into hard scattering functions T^I and T^{II}, respectively, and the nonperturbative, but simpler, form factors F_j and meson light-cone distribution amplitudes Φ_M (Fig. 1). Important elements of this approach are: i) The expansion in $\Lambda_{QCD}/m_b \ll 1$, consistent power counting, and the identification of the leading power contribution, for which the factorized picture can be expected to hold. ii) Light-cone dynamics, which determines for instance the properties of the fast light mesons. The latter are described by light-cone distribution amplitudes

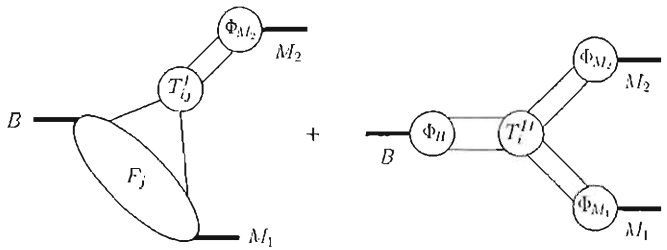

Figure 1: *Graphical representation of the factorization formula.*

Φ_π of their valence quarks defined as

$$\langle \pi(p)|u(0)\bar{d}(z)|0\rangle = \frac{if_\pi}{4}\,\gamma_5\,\not{p}\int_0^1 dx\; e^{ixpz}\,\Phi_\pi(x) \tag{2}$$

with z on the light cone, $z^2 = 0$. iii) The collinear quark-antiquark pair dominating the interactions of the highly energetic pion decouples from soft gluons (colour transparency). This is the intuitive reason behind factorization. iv) The factorized amplitude consists of hard, short- distance components, and soft, as well as collinear, long-distance contributions.

More details on the factorization formalism can be found elsewhere [1]. Here we would like to emphasize an important phenomenological application. Consider the time-dependent, mixing-induced CP asymmetry in $B \to \pi^+\pi^-$

$$\begin{aligned} \mathcal{A}_{CP}(t) &= \frac{\Gamma(B(t) \to \pi^+\pi^-) - \Gamma(\bar{B}(t) \to \pi^+\pi^-)}{\Gamma(B(t) \to \pi^+\pi^-) + \Gamma(\bar{B}(t) \to \pi^+\pi^-)} && (3) \\ &= -S\sin(\Delta M_d t) + C\cos(\Delta M_d t) && (4) \end{aligned}$$

Using CKM-matrix unitarity, the decay amplitude consists of two components with different CKM factors and different hadronic parts, schematically

$$A(B \to \pi^+\pi^-) = V^*_{ub}V_{ud}(\text{up} - \text{top}) + V^*_{cb}V_{cd}(\text{charm} - \text{top}) \tag{5}$$

If the penguin contribution $\sim V^*_{cb}V_{cd}$ could be neglected, one would have $C = 0$ and $S = \sin 2\alpha$, hence a direct relation of $\mathcal{A}_{CP}$ to the CKM angle α. In reality the penguin contribution is not negligible compared to the dominant tree contribution $\sim V^*_{ub}V_{ud}$. The ratio of penguin and tree amplitude, which

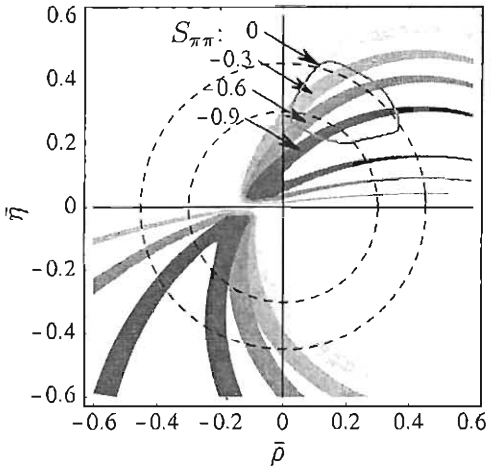

Figure 2: *Constraints in the $\bar{\rho}$, $\bar{\eta}$ plane from CP violation observable S in $B \to \pi^+\pi^-$. The constraints from $|V_{ub}/V_{cb}|$ (dashed circles) and from the standard analysis of the unitarity triangle (irregular shaded area) are also shown.*

enters the CP asymmetry, depends on hadronic physics. This complicates the relation of observables S and C to CKM parameters. QCD factorization of B-decay matrix elements allows us to compute the required hadronic input and to determine the constraint in the $(\bar{\rho}, \bar{\eta})$ plane implied by measurements of the CP asymmetry. This is illustrated for S in Fig. 2. The widths of the bands indicate the theoretical uncertainty [2]. Note that the constraints from S are relatively insensitive to theoretical or experimental uncertainties. The analysis of direct CP violation measured by C is more complicated due to the importance of strong phases. The current experimental results are

$$\begin{array}{llll} C = -0.94^{+0.31}_{-0.25} \pm 0.09 & \text{(Belle)} & -0.30 \pm 0.25 \pm 0.04 & \text{(Babar)} \\ S = -1.21^{+0.38+0.16}_{-0.27-0.13} & \text{(Belle)} & +0.02 \pm 0.34 \pm 0.05 & \text{(Babar)} \end{array} \qquad (6)$$

QCD factorization to leading power in Λ/m_b has been demonstrated at $\mathcal{O}(\alpha_s)$ for the important class of decays $B \to \pi\pi$, πK. For $B \to D\pi$ (class I), where hard spectator interactions are absent, a proof has been given explicitly at two loops [1] and to all orders in the framework of soft-collinear effective theory (SCET) [3]. Complete matrix elements are available at $\mathcal{O}(\alpha_s)$ (NLO) for

$B \to \pi\pi$, πK, including electroweak penguins. Power corrections are presently not calculable in general. Their impact has to be estimated and included into the error analysis. Critical issues here are annihilation contributions and certain corrections proportional to $m_\pi^2/((m_u + m_d)m_b)$, which is numerically sizable, even if it is power suppressed. However, the large variety of channels available will provide us with important cross checks and arguments based on SU(2) or SU(3) flavour symmetries can also be of use in further controling uncertainties.

3 Radiative decays $B \to V\gamma$

Factorization in the sense of QCD can also be applied to the exclusive radiative decays $B \to V\gamma$ ($V = K^*$, ρ). The factorization formula for the operators in the effective weak Hamiltonian can be written as [4, 5]

$$\langle V\gamma(\epsilon)|Q_i|\bar{B}\rangle = \left[F^{B\to V}(0)\, T_i^I + \int_0^1 d\xi\, dv\, T_i^{II}(\xi, v)\, \Phi_B(\xi)\, \Phi_V(v)\right] \cdot \epsilon \qquad (7)$$

where ϵ is the photon polarization 4-vector. Here $F^{B\to V}$ is a $B \to V$ transition form factor, and Φ_B, Φ_V are leading twist light-cone distribution amplitudes (LCDA) of the B meson and the vector meson V, respectively. These quantities describe the long-distance dynamics of the matrix elements, which is factorized from the perturbative, short-distance interactions expressed in the hard-scattering kernels T_i^I and T_i^{II}. The QCD factorization formula (7) holds up to corrections of relative order Λ_{QCD}/m_b. Annihilation topologies are power-suppressed, but still calculable in some cases. The framework of QCD factorization is necessary to compute exclusive $B \to V\gamma$ decays systematically beyond the leading logarithmic approximation. Results to next-to-leading order in QCD, based on the heavy quark limit $m_b \gg \Lambda_{QCD}$ have been computed [4, 5] (see also [6]).

The method defines a systematic, model-independent framework for $B \to V\gamma$. An important conceptual aspect of this analysis is the interpretation of loop contributions with charm and up quarks, which come from leading operators in the effective weak Hamiltonian. These effects are calculable in terms of perturbative hard-scattering functions and universal meson light-cone distribution amplitudes. They are $\mathcal{O}(\alpha_s)$ corrections, but are leading power contributions in the framework of QCD factorization. This picture is in contrast to the common notion that considers charm and up-quark loop effects as generic,

uncalculable long-distance contributions. Non-factorizable long-distance corrections may still exist, but they are power-suppressed. The improved theoretical understanding of $B \to V\gamma$ decays strengthens the motivation for still more detailed experimental investigations, which will contribute significantly to our knowledge of the flavour sector.

The uncertainty of the branching fractions is currently dominated by the form factors F_{K^*}, F_ρ. A NLO analysis [5] yields (in comparison with the experimental results in brackets) $B(\bar{B} \to \bar{K}^{*0}\gamma)/10^{-5} = 7.1 \pm 2.5$ (4.21 ± 0.29 [7]) and $B(B^- \to \rho^-\gamma)/10^{-6} = 1.6 \pm 0.6$ (< 2.3 [8]). Taking the sizable uncertainties into account, the results for $B \to K^*\gamma$ are compatible with the experimental measurements, even though the central theoretical values appear to be somewhat high. $B(B \to \rho\gamma)$ is a sensitive measure of CKM quantities such as the angle γ.

4 Forward-backward asymmetry zero in $B \to K^* l^+ l^-$

Substantial progress has taken place over the last few years in understanding the QCD dynamics of exclusive B decays. The example of the forward-backward asymmetry in $B \to K^* l^+ l^-$ nicely illustrates some aspects of these developments.

The forward-backward asymmetry A_{FB} is the rate difference between forward ($0 < \theta < \pi/2$) and backward ($\pi/2 < \theta < \pi$) going l^+, normalized by the sum, where θ is the angle between the l^+ and B momenta in the centre-of-mass frame of the dilepton pair. A_{FB} is usually considered as a function of the dilepton mass q^2. In the standard model the spectrum dA_{FB}/dq^2 (Fig. 3) has a characteristic zero at

$$\frac{q_0^2}{m_B^2} = -\alpha_+ \frac{m_b C_7}{m_B C_9^{eff}} \tag{8}$$

depending on short-distance physics contained in the coefficients C_7 and C_9^{eff}. The factor α_+, on the other hand, is a hadronic quantity containing ratios of form factors.

It was first stressed in [9] that α_+ is not very much affected by hadronic uncertainties and very similar in different models for form factors with $\alpha_+ \approx 2$. After relations were found between different heavy-light form factors ($B \to P$, V) in the heavy-quark limit and at large recoil [10], it was pointed out in [11]

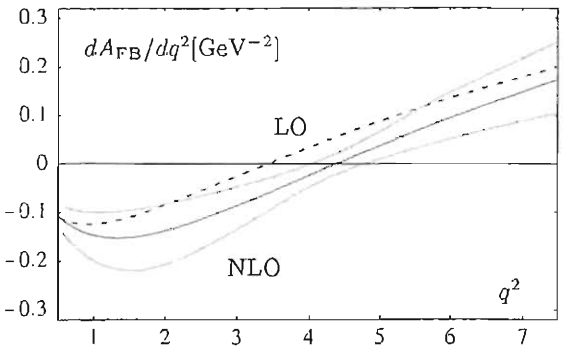

Figure 3: *A_{FB} spectrum for $\bar{B} \to K^* l^+ l^-$ at leading and next-to-leading order in QCD (from* [4]*).*

that as a consequence $\alpha_+ = 2$ holds exactly in this limit. Subsequently, the results of [10] were demonstrated to be valid beyond tree level [4, 12]. The use of the A_{FB}-zero as a *clean* test of standard model flavour physics was thus put on a firm basis and NLO corrections to (8) could be computed [4]. More recently also the problem of power corrections to heavy-light form factors at large recoil in the heavy-quark limit has been studied [13]. Besides the value of q_0^2, also the sign of the slope of $dA_{FB}(\bar{B})/dq^2$ can be used as a probe of new physics. For a $\bar{B}$ meson, this slope is predicted to be positive in the standard model [14].

5 Radiative leptonic decay $B \to l\nu\gamma$

The tree-level process $B \to l\nu\gamma$ is not so much of direct interest for flavour physics, but it provides us with an important laboratory for studying QCD dynamics in exclusive B decays, which is crucial for many other applications. The leading-power contribution comes from the diagram in Fig. 4 (b), which contains a light-quark propagator that is off-shell by an amount $(q-k)^2 \sim q_- k_+$ Here q is the hard, light-like momentum of the photon with components scaling as m_b (this restricts the region of phase-space where the present discussion applies), and k is the soft momentum of the spectator quark. The decay is thus

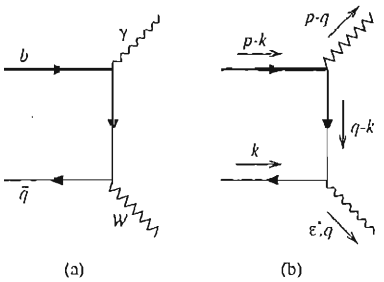

Figure 4: *Tree-level diagrams for $B \to l\nu\gamma$. Only diagram (b) contributes at leading power (see* [16]*).*

determined by a hard-scattering process, but also depends on the structure of the B meson in a non-trivial way [15]. Recently, in [16] it has been proposed, and shown to one loop in QCD, that the form factors F for this decay factorize as

$$F = \int d\bar{k}_+ \Phi_B(\bar{k}_+)\, T(\bar{k}_+) \tag{9}$$

where T is the hard-scattering kernel and Φ_B the light-cone distribution amplitude of the B meson defined as

$$\Phi_B(\bar{k}_+) = \int dz_- e^{i\bar{k}_+ z_-} \langle 0|b(0)\bar{u}(z)|B\rangle|_{z_+=z_\perp=0} \tag{10}$$

The hard process is characterized by a scale $\mu_F \sim \sqrt{m_b\Lambda}$. At lowest order the form factors are proportional to $\int d\bar{k}_+ \, \Phi_B(\bar{k}_+)/\bar{k}_+ \equiv 1/\lambda_B$, a parameter that enters hard-spectator processes in many other applications. The analysis at NLO requires resummation of large logarithms $\ln(m_b/\bar{k}_+)$. An extension of the proof of factorization to all orders was subsequently given by [17] within the SCET.

6 Conclusions

Factorization formulas in the heavy-quark limit have been proposed for a large variety of exclusive B decays. They justify in many cases the phenomenological factorization ansatz that has been employed in many applications. In addition they enable consistent and systematic calculations of corrections in powers of α_s. Non-factorizable long-distance effects are not calculable in general but

they are suppressed by powers of Λ_{QCD}/m_b. So far, $B \to D^+\pi^-$ decays are probably understood best. Decays with only light hadrons in the final state such as $B \to \pi\pi$, $K^*\gamma$, $\rho\gamma$, or $K^*l^+l^-$ include hard spectator interactions at leading power and are therefore more complicated. An important new tool that has been developed is the soft-collinear effective theory (SCET), which is of use for proofs of factorization and for the theory of heavy-to-light form factors at large recoil. Recent studies of the prototype process $B \to l\nu\gamma$ have also led to a better understanding of QCD dynamics in exclusive hadronic B decays. All these are promising steps towards achieving a good theoretical control over QCD dynamics in rare hadronic B decays, which is necessary for probing CP violation, flavour physics and new phenomena at short distances.

Acknowledgements

I thank the organizers of the Frontier Science Workshop in Frascati for the invitation to a very interesting and pleasant meeting.

References

1. M. Beneke *et al.*, Phys. Rev. Lett. **83** (1999) 1914; Nucl. Phys. B **591** (2000) 313.
2. M. Beneke et al., Nucl. Phys. B **606** (2001) 245.
3. C. W. Bauer et al., Phys. Rev. Lett. **87** (2001) 201806.
4. M. Beneke, T. Feldmann and D. Seidel, Nucl. Phys. B **612** (2001) 25.
5. S. Bosch and G. Buchalla, Nucl. Phys. B **621** (2002) 459.
6. A. Ali and A. Y. Parkhomenko, Eur. Phys. J. C **23** (2002) 89.
7. T. E. Coan *et al.*, Phys. Rev. Lett. **84** (2000) 5283; B. Aubert *et al.*, Phys. Rev. Lett. **88** (2002) 101805; A. Ishikawa, hep-ex/0205051.
8. B. Aubert *et al.*, hep-ex/0207073.
9. G. Burdman, Phys. Rev. D **57** (1998) 4254.
10. J. Charles et al., Phys. Rev. D **60** (1999) 014001.

11. A. Ali et al., Phys. Rev. D **61** (2000) 074024.

12. C. W. Bauer et al., Phys. Rev. D **63** (2001) 114020; hep-ph/0211069.

13. M. Beneke et al., Nucl. Phys. B **643** (2002) 431.

14. G. Buchalla, G. Hiller and G. Isidori, Phys. Rev. D **63** (2001) 014015;

15. G. P. Korchemsky, D. Pirjol and T. M. Yan, Phys. Rev. D **61** (2000) 114510.

16. S. Descotes-Genon and C. T. Sachrajda, hep-ph/0209216.

17. E. Lunghi, D. Pirjol and D. Wyler, Nucl. Phys. B **649** (2003) 349.

Frascati Physics Series Vol. XXXI (2003), pp. 157–165
FRONTIERSCIENCE 2002 – Frascati, October 6–11, 2002
Invited Review Talk in Plenary Session

A REVIEW OF $|V_{ub}|$ AND $|V_{cb}|$ DETERMINATIONS

Marco Battaglia
CERN, Geneva, Switzerland

ABSTRACT

This paper reviews the status of experimental determinations of the $|V_{ub}|$ and $|V_{cb}|$ elements in the Cabibbo-Kobayashi-Maskawa (CKM) mixing matrix.

1 Introduction

Measurements of the $|V_{ub}|$ and $|V_{cb}|$ elements in the Cabibbo-Kobayashi-Maskawa (CKM) mixing matrix, with small and well understood uncertainties, represent a key goal for the present heavy flavour physics program.

Because $|V_{ub}|$, the smallest quark mixing element, provides a bound on the upper vertex of one of the triangles representing the unitarity property of the CKM matrix and $|V_{cb}|$ gives the overall normalisation, these studies play a crucial role in examining these unitarity constraints and the fundamental

questions which relate to them. Comparing the direct determinations of the CP violating phases with the values predicted by the Standard Model (SM), from the size of these and other CKM elements, may reveal sources of CP violation arising from New Physics beyond the SM.

Theories, phenomenological models and experimental techniques are making constant progresses to address these requirements. Within the present and foreseen experimental accuracies, theory uncertainties dominate the error budget, making the test of their underlying assumptions an absolute priority.

The extraction of the CKM elements from inclusive s.l. decay is based on Heavy Quark Theory implemented through an Operator Product Expansion (OPE). This provides a consistent theory framework for computing inclusive rates and partially integrated spectra. The main input parameters are the heavy quark masses m_b, m_c [or $\tilde{\Lambda}$], the kinetic energy of the b-quark inside the heavy hadron μ_π^2 [or λ_1] and the coefficients governing the $1/m_b^3$ corrections. Recently, their extraction directly from measurements of the moments of spectral distributions in $b \to X_c \ell \bar{\nu}$ and $b \to X_s \gamma$ decays has become possible. Also the shape function, which encodes the non-perturbative effects relating the parton level dynamics to the physical distributions, could be constrained using the photon energy spectrum in $b \to X_s \gamma$ radiative decays.

It is important to observe at this point that the OPE predictions rely on an implicit assumption of quark-hadron duality. While this is expected to hold best for s.l. decays, at the levels of accuracies achieved, experimental tests are required. Performing several determinations with different methods and verifying their consistency will add trust.

Different kinematics and detector configurations available at symmetric $\Upsilon(4S)$ colliders, asymmetric B-factories and at colliders operating at the Z^0 peak and the large recorded data sets have brought an healthy competition of complementary approaches to this program.

2 $|V_{cb}|$ DETERMINATIONS

2.1 Inclusive Determinations

The $|V_{cb}|$ value can be obtained from the measured b-quark s.l. decay partial width, by measuring the inclusive s.l. branching fraction of B hadrons and their lifetime(s). These are presently known to a few percent and a fraction

of percent respectively. This brings the experimental uncertainty on $|V_{cb}|$ to about 1%. New results from BABAR and BELLE have added further accuracy, while confirming the central value determined at LEP and CESR. Issues on the model uncertainties of the LEP results are also better understood. After averaging the $\Upsilon(4S)$ and Z^0 results and correcting for the $b \to u$ contribution, the B s.l. decay width is $\Gamma(b \to X_c \ell \nu) = 0.434 \times (1 \pm 0.018) \times 10^{-10}$ MeV.

Theoretical expressions for the s.l. decay width depend on several parameters and include perturbative and non-perturbative QCD corrections. The uncertainty on the heavy quark masses, has been a major source of uncertainties, due to the m_b^5 dependence of the partial width. There has been a significant progress in evaluating the b quark mass and the mass definition itself has been refined by moving from pole masses to short-distance masses, which are free from renormalon ambiguities. Several determinations have been reported and $\bar{m}_b(m_b)$=(4.21±0.08) GeV, or m_b(1 GeV)=(4.57±0.09) GeV, represents a generally accepted estimate. Extracting $|V_{cb}|$ in this way has a ±3% relative uncertainty from m_b and μ_{π}^2. More recently the analysis of spectral moments in $b \to s\gamma$ and $b \to X_c \ell \nu$ has offered the means to extract these parameters directly from the data. This turns the uncertainties from theory parameters, whose ranges and statistical meaning have a degree of arbitrariness, into experimental uncertainties. A recent analysis based on moments determined by DELPHI and the average s.l. width gives $|V_{cb}| = 0.0419 \times (1 \pm 0.016(\text{stat}) \pm 0.015(\text{moments}) \pm 0.010(\text{pert}))$ [2].

2.2 Exclusive Determinations

Determining $|V_{cb}|$ using exclusive s.l. $B \to D^{(*)} \ell \bar{\nu}$ decays takes advantage of Heavy Quark Effective Theory (HQET), which relates the differential decay rate $d\Gamma/dw$ to $|V_{cb}|$ by means of a form factor $\mathcal{F}(w)$ for which the normalisation $\mathcal{F}(\infty) = 1$ at zero recoil is known for $m_Q \to \infty$. The $D^{*+} \to D^0 \pi^+$ decay is reconstructed either through the exclusive $D^0 \to K\pi$, $K\pi\pi^0$, $K\pi\pi\pi$ modes or inclusively. The first method gives higher signal purities and better w resolution, while the inclusive reconstruction provides with higher statistics. One advantage found in performing this measurement at the Z^0 peak is the flat acceptance vs. w, since the slow π^+ momentum is enhanced by the large B boost. At the $\Upsilon(4S)$, the reduced charged pion acceptance is compensated in part by adding the $D^{*+} \to D^+ \pi^0$ mode. An important source of corre-

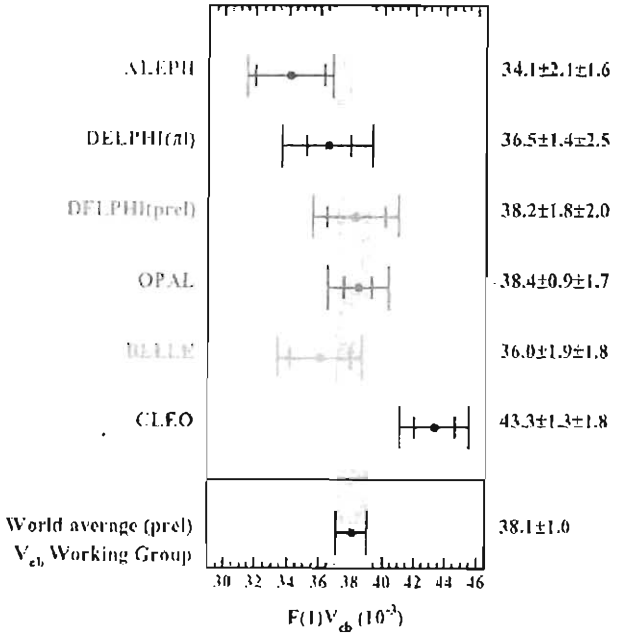

Figure 1: *Summary of exclusive determinations of* $|V_{cb}|$

lated systematics is represented by the $b \to D^{**}\ell\nu$ background, which is still quite poorly known. Recent analyses fit the $D^*X\ell\nu$ fraction directly on data by using angular distributions or track topology. A recent DELPHI study [3] finds $\mathrm{BR}(b \to D^{*+}X\ell\bar{\nu}) = (0.64\pm0.08\pm0.09)\%$. The functional dependence of $d\Gamma/dw$ towards $w = 1$ is not known, but costraints are provided by dispersion relations [1]. An expansion around $w = 1$ in terms of the form factor slope ρ is adopted for the extraopolation at zero recoil. The results for the measured product of $\mathcal{F}(1) \times |V_{cb}|$ are summarised in Figure 1.

In order to extract $|V_{cb}|$, the $\mathcal{F}(1)$ corrections due to finite b-quark mass need to be estimated. Computations have been performed using quark models, sum rules and lattice QCD. Results agree. Quark models, which rely on a quark-hadron duality assumption are not used and the adopted average [9] is $\mathcal{F}(1)$=0.91±0.04. This gives $|V_{cb}|$=(41.9±1.1±1.9)×10^{-3}. There has been a thorough review of the error budget for the lattice result and an effort to define the result in terms of a full probability density function [10], useful as input into fits of the unitarity triangle.

3 $|V_{ub}|$ DETERMINATIONS

Contrary to the case of $|V_{cb}|$, where the backgrounds are benign and the main questions are related to the experimental resolution and the theory inputs, the central issue in the determination of $|V_{ub}|$ is the extraction of the $b \to X_u \ell \bar{\nu}$ signal in presence of a $\simeq 75$ times larger $b \to X_c \ell \bar{\nu}$ backgrounds. This requires to know and control differential rates in regions of phase space where the $b \to X_c$ transitions are suppressed. The first determination of $|V_{ub}|$ was in fact obtained by measuring the yield of leptons produced above the kinematical limit for $b \to X_c \ell \bar{\nu}$ decays. However, the accuracy was limited by the model dependence. A recent review can be found in [11].

New paths, capable of leading to significant improvements in the control of these model uncertainties, have been undertaken. The first is the study of inclusive s.l. B decays, where the signal is isolated by selections based on the lepton energy, hadronic mass, $\ell\nu$ mass or a combination of them. The second is the determination of the branching fractions of exclusive decays, such as $B \to \pi,\ \rho \ell \bar{\nu}$, which is now reached a good statistical accuracy. Owing to the divergent directions taken by these developments, the present picture has been enriched by new data of good experimental accuracy, affected by largely uncorrelated systematic uncertainties.

3.1 Inclusive Determinations

There are three main regions, available in the s.l. b decay decay phase space. to enhance signal $b \to X_u \ell \bar{\nu}$: i) the lepton energy end-point region: $E_\ell > \frac{M_B^2 - M_D^2}{2M_B}$, ii) the low hadronic mass region: $M_X < M_D$ and iii) the high q^2 region: $M_{\ell\nu}^2 = q^2 > (M_B - M_D)^2$. They select $\simeq$15%, 70% and 20% of the inclusive charmless s.l. rate, respectively.

The lepton endpoint region has originally been affected by large systematics due to the uncertainties in extrapolating from a small fraction of selected events, at the edge of the phase space, to the full rate. However, it has been known since some time that, at leading twist, the same shape function corrects the parton level $b \to X_s \gamma$ photon spectrum and the $b \to X_u \ell \bar{\nu}$ lepton spectrum. CLEO first determined the shape function parameters from the photon spectrum. using different ansatz for its functional form [14]. This allowed to derive the fraction of $b \to u$ s.l. transitions yielding a lepton with energy

2.2 GeV< E_ℓ <2.6 GeV. A new preliminary analysis has now been presented by BABAR [12], which uses the same CLEO shape function result, but restricts the acceptance to 2.3 GeV< E_ℓ <2.6 GeV. The near future will provide with more accurate determinations of the E_γ spectrum, allowing even better determinations. However, it will be important to understand the effects of subleading corrections which, although suppressed by Λ_{QCD}/m_b factors, have recently been recognised to be numerically enhanced [13].

The use of an upper cut on the reconstructed hadronic mass, M_X, recoiling against the lepton, was first attempted by DELPHI, exploiting the favourable kinematics of LEP. This method has an advantage in the larger fraction of decay rate accepted but has to deal with a rather limited signal-to-background ratio. The shape function sensitivity is smaller compared to the end-point method, as it has been verified using the range of parameters determined by CLEO. At LEP, inclusive analyses have been performedby ALEPH and OPAL, using a Neural Network (NN) discriminant, based on a selection of kinematic variables providing separation of the $b \to X_u \ell \bar{\nu}$ signal.

A recent development has been the introduction of a combined $M_X - q^2$ analysis to reduce the theory uncertainties, while restricting to a part of the phase space where the $b \to c$ background is suppressed. CLEO has presented the first experimental attempt to implement this method [15]. The analysis is based on a full fit to $q^2/(E_\ell + E_\nu)^2$, M_X and $\cos\theta_{W\ell}$. Models are needed to extract the sample composition and to relate the regions of higher sensitivity and theoretically safer to the inclusive charmless s.l. branching fraction.

With the severe selections needed to extract the signal, the effects of experimental cuts trimming inclusive distributions must be understood. An important question to assess is to which degree the inclusive analyses are evenly probing the selected phase space. The NN analyses are biased towards the region of large E_ℓ and low M_X where the signal-to-background ratio is more favourable. While the resulting uncertainty is accounted by the range of models tested, for example in the ALEPH analysis, it is desirable to test more unbiased methods. DELPHI has shown that the M_X analysis has a reasonably uniform sensitivity on the M_X-E_ℓ plane. The recent CLEO analysis has been repeated for different sets of M_X-q^2 selections, finding compatible $|V_{ub}|$ results.

3.2 Exclusive Determinations

The exclusive reconstruction of charmless s.l. decays offers the comfortable signal-to-background ratios that the inclusive analyses lack. However, since here there is no equivalent to the HQET predictions for the form factors at zero recoil which make the $B \rightarrow D^* \ell \bar{\nu}$ channel so attractive, the form factors represent the main limitation in the accuracy of the exclusive V_{ub} determinations. These uncertainties stem from three sources: i) the signal efficiency, ii) the subtraction of the cross-feed background and iii) the rate normalisation. Form factors have been computed with a variety of techniques. Typically, Light-Cone Sum Rules give 15-20% accuracy and are subject to quark-hadron duality uncertainties. Quenced Lattice calculations give a comparable precision, but their applicability is mostly confined to the high q^2 region. Progresses with Lattice calculations is expected to reduce these uncertainties significantly in the coming years.

Larger statistics will also allow to reduce model systematics. CLEO has reported the preliminary results of a $B^0 \rightarrow \pi^- \ell^+ \nu$ analysis where the signal rates are extracted in three regions of q^2 independently [16]. This reduces the form factor sensitivity from the first two sources. The statistical accuracy of the data is also becoming sensitive to the details of the q^2 dependence of the signal yield predicted by different form factor computations. Results have been presented by both CLEO and BELLE for the $\pi \ell \nu$ channel. This makes possible to discriminate between models and the CLEO fit shows that the ISGW II model, with a χ^2 probability of less than 1%, is not a reliable reference for this channel.

The $\pi \ell \nu$ mode, which involves a single form factor, is free from non-resonant backgrounds and has reduced feed-down uncertainties. It will most probably enjoy the role of golden channel for performing the exclusive determination of $|V_{ub}|$. The ρ, ω, $\eta \ell \nu$ channels will also play an important role in adding confidence, if they will result in compatible measurements.

An overall summary of the results presently available is given in Figure 2. At present no attept is made to average these measurements. As the understanding of the model dependence improves and parameter ranges can be consistently defined for different analyses, averages for the inclusive and exclusive determinations will become possible. While there is a remarkable agreement between the measurements obtained with a variety of different techniques, it

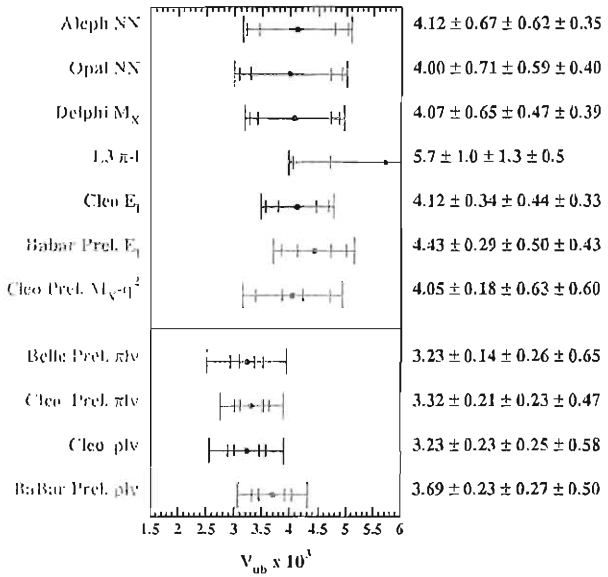

Figure 2: *Summary of inclusive and exclusive determinations of* $|V_{ub}|$

will be interesting to monitor possible systematic shifts between the inclusive and exclusive measurements.

Other paths may also become available to the large data sets of the B factories. An inclusive techniques, which uses a direct ratio of $b \to s\gamma$ and $b \to u\ell\nu$ spectra has been recently proposed [18].

4 CONCLUSIONS

A large set of determinations of $|V_{ub}|$ and $|V_{cb}|$ exploiting different techniques and affected by different assumptions and sources of uncertainties has become available. The determination of $|V_{cb}|$ is reaching a precision better than 1%. New approaches start allowing a determination of most of the input parameters directly from the data. Tests of OPE through moment analyses are also becoming available. The increasing ingenuity of experimentalists and phenomenologists in devising methods to measure $|V_{ub}|$ has brought individual accuracies to approach 15%.

The overall consistency is encouraging for the perspectives of bringing $|V_{ub}|$ and $|V_{cb}|$ towards the domain of precision physics. Averaging inclusive

and exclusive results can improve numerical accuracy due to partly uncorrelated uncertainties. A deeper understanding of the sources of systematic uncertainties and thorough checks of consistency to the level of the anticipated total accuracy will be required to validate the new frontier of accuracy

References

1. C.G. Bloyd, B. Grinstein and R. Lebed, Phys. Lett **B353** (1995) 306.
2. M. Battaglia *et al.*, Phys. Lett. **B556** (2003), 41.
3. A. Oyanguren *et al* (DELPHI Coll.), DELPHI 2002-074 CONF608.
4. D. Buskulic *et al.* (ALEPH Coll.), Phys. Lett. **B395** (1997) 373.
5. K. Abe *et al.* (BELLE Coll.), Phys. Lett. **B526** (2002) 247.
6. R. A. Briere *et al.* (CLEO Coll.), Phys. Rev. Lett. **89** (2002) 081803.
7. P. Abreu *et al.* (DELPHI Coll.), Phys. Lett. B510 (2001) 55.
8. G. Abbiendi *et al.* (OPAL Coll.), Phys. Lett. B482 (2000) 15.
9. M. Artuso and E. Barberio, in K. Hagiwara *et al.* Phys. Rev. D66 (2002) 010001.
10. A. S. Kronfeld, *et al.*, arXiv:hep-ph/0207122.
11. M. Battaglia and L. Gibbons, in K. Hagiwara *cit.*
12. B. Aubert *et al.* (BABAR Coll.), SLAC-PUB-9282, arXiv:hep-ex/0207081.
13. A. K. Leibovich, Z. Ligeti and M. B. Wise, Phys. Lett. B539 (2002) 242.
14. D. Cronin-Hennessy *et al.* (CLEO Coll.), Phys. Rev. Lett. 87 (2001) 251808.
15. A. Bornheim *et al.* (CLEO Coll.), CLEO CONF 02-08.
16. N.E. Adam *et al.*, (CLEO Coll.), CLEO-CONF 02-09.
17. B. Aubert *et al.* (BABAR Coll.), SLAC-PUB-9305, arXiv:hep-ex/0207080.
18. U. Aglietti, M. Ciuchini and P. Gambino, Nucl. Phys. B637 (2002) 427.

Frascati Physics Series Vol. XXXI (2003), pp. 167–172
FRONTIERSCIENCE 2002 – Frascati, October 6–11, 2002
Invited Review Talk in Plenary Session

SEMI-LEPTONIC CHARM AND BEAUTY DECAYS

Youngjoon Kwon
IPAP, Yonsei University

ABSTRACT

Leptonic and semileptonic decays of B and D mesons have been actively investigated both experimental and theoretical sides to understand the electroweak decays of quarks and mesons and the

effects of strong interactions therein. In this paper, recent experimental results on leptonic and semileptonic B and D meson decays are summarized.

1 Introduction

Semileptonic decays of charm and bottom mesons are important in studying weak decays of quarks and mesons and understanding the effects of strong interactions therein. For this reason, semileptonic B and D decays have been actively studied in both experiment and theory over the last decade and many advances have been made. In this paper, I will make a very brief review on the

recent experimental results. Some topics will not be mentioned in this talk as they are covered by other people in this conference.

This paper is organized as follows. In the next section, we start with a purely leptonic B decays. Recent Belle results on $B^+ \to \ell^+\nu_\ell$ and BaBar results on $B \to \ell^+\ell^-$ are described. In section 3, recent experimental efforts on semileptonic B decays will be listed. In section 4, we will review recent results on the semileptonic decay $D \to K\pi\ell\nu$ and the observation of interference phenomena from FOCUS. In section 5, recent results on the neutrinoless B semileptonic decays from CLEO, BaBar and Belle will be presented.

2 Search for purely leptonic B decays

In the Standard Model (SM), purely leptonic decays $B^0 \to \ell^+\ell^-$ and $B^+ \to \ell^+\nu_\ell$ occur via highly-suppressed vertical penguin, W-box (for $B^0 \to \ell^+\ell^-$) or W-annihilation diagram (for $B^+ \to \ell^+\nu_\ell$). Because of high suppression of these modes, they can be used for sensitive tests of the Standard Model (SM). For example, such particles from beyond the SM as leptoquarks or charged Higgs, etc. may interfere with the SM processes and enhance the decay rate to the level of experimental sensitivity.

2.1 Search for $B^0 \to \ell^+\ell^-$ from BaBar

The BaBar collaboration has searched for purely leptonic decays $B^0 \to e^+e^-$, $B^0 \to \ell^+\ell^-$, and $B^0 \to e^\pm\mu^\mp$, using 54.4fb^{-1} sample of $B\bar{B}$ events. The signal candidates are reconstructed by locating the B decay vertex from two oppositely-charged high-p leptons and using the kinematic variables $\Delta E = \sum_i \sqrt{m_i^2 + (p_i^*)^2} - E^*_{\rm beam}$ and $m_{ES} = \sqrt{(E^*_{\rm beam})^2 - (\sum_i \vec{p}_i^*)^2}$. Electron candidates are selected with $> 90\%$ efficiency and $\sim 0.1\%$ fake rate, while muon candidates are selected with approximately 70% efficiency and $\sim 2.5\%$ fake rate.

Background events from continuum are suppressed using the cosine angle between the thrust axes of the signal tracks and the rest of the event, and the thrust value itself of the rest of the event. For each mode, the number of events in the signal region is either zero or consistent with the background level estimated with the side-band data. The following upper limits are obtained with 90% confidence level (CL): $B^0 \to e^+e^- < 3.3 \times 10^{-7}$, $B^0 \to \mu^+\mu^- < 2.0 \times 10^{-7}$, and $B^0 \to e^\pm\mu^\mp < 2.1 \times 10^{-7}$.

2.2 Search for $B^+ \to \ell^+\nu_\ell$ from Belle

A striking signature of $B^+ \to \ell^+\nu_\ell$ ($\ell = e$ and μ) events is a nearly monochromatic lepton in the B rest frame. To exploit this feature, the momentum spectrum of charged leptons for $p_\ell^* > 2.2$ GeV/c, where p_ℓ^* is measured in the B rest frame, is analyzed. The 4-momenta of the signal B and opposite B are determined by measuring the 4-momenta of all charged and neutral particles in an event except for the signal lepton. To suppress background, we use the beam-constrained mass and energy difference of the opposite B. The continuum background events are suppressed using event-shape variables.

The signal yield in each mode is obtained by fitting the p_ℓ^* distributions. The signal and background components are determined with MC event samples. Analyzing 60fb^{-1} $B\bar{B}$ events, there was no evidence for signals in either $B^+ \to e^+\nu_e$ or $B^+ \to \mu^+\nu_\mu$ and the following upper limits are obtained with 90% CL: $\mathcal{B}(B^+ \to e^+\nu_e) < 5.4 \times 10^{-6}$ and $\mathcal{B}(B^+ \to \mu^+\nu_\mu) < 6.8 \times 10^{-6}$.

3 Semileptonic B decays

Semileptonic B decays $B \to X\ell^+\nu_\ell$ are very good places to measure CKM matrix elements V_{cb} and V_{ub} because strong interaction effects are much simplified due to the appearance of two leptons in the final state. In particular, $B \to X_u\ell^+\nu_\ell$ decays are used to measure V_{ub} which is a crucial element to test the KM mechanism of CP violations in B and K decays [1].

In recent years, there are so many new experimental results on semileptonic B decays that it is virtually impossible for me to cover them all in this limited space. Moreover, much of the experimental results related with V_{cb} and V_{ub} determinations are already covered by another talk in this workshop [2]. Therefore, I will only list the subjects that were covered in the workshop and will not give detailed description of each result.

- Analysis of hadronic and leptonic moments in B semileptonic decays by CLEO, DELPHI, and BaBar.
- Exclusive $B \to D^{**}\ell^+\nu$ by DELPHI.
- Inclusive $B \to X_c\ell^+\nu$ by ALEPH.
- Inclusive $B \to X_u\ell^+\nu$ by LEP experiments, especially the 2001 analysis by OPAL.

- V_{ub} measurement by CLEO using the lepton end-point analysis combined with photon energy spectrum of $B \to X_s\gamma$.
- V_{ub} measurement by CLEO using combined inclusive variables q^2, M_{X^2} and $\cos\theta_{W\ell}$ to determine $\mathcal{B}(B \to X_u\ell^+\nu)$.
- Exclusive $B \to X_u\ell^+\nu$ analyses by CLEO, Belle and BaBar. In particular, the q^2 distribution of $B \to \pi\ell\nu$ decay is studied by Belle and CLEO.

4 Semileptonic D decays: interference in $D^+ \to (K^-\pi^+)\ell\nu$

Two subjects on semileptonic D decays were discussed in the talk: (i) evidence of interference in $D^+ \to (K^-\pi^+)\ell\nu$ from FOCUS, and (ii) new branching fraction measurements of $D_s \to \phi\ell\nu$ and $D \to K^*\ell\nu$ from FOCUS and CLEO. In this paper, only (i) will be mentioned.

In the process of studying $D^+ \to K^-\pi^+\mu^+\nu$ decay distribution, FOCUS found significant discrepancies in the angular distributions between data and expectations for pure $D^+ \to \bar{K}^{*0}\mu^+\nu$. In particular, they observed a significant forward-backward asymmetry in θ_V ($A_{FB}(\theta_V)$), the angle between π and D in the $K^-\pi^+$ rest frame. The data are explained by adding a coherent $K^-\pi^+$ s-wave contribution to $D^+ \to K^-\pi^+\mu^+\nu$, which is modeled as a constant amplitude of the approximate value $0.36\exp(i\pi/4)$ $(\mathrm{GeV})^{-1}$. This new interference creates a $\approx 15\%$ $A_{FB}(\theta_V)$ with $m_{K\pi}$ below the K^* pole, which is consistent with data. The data can also be described by K^{*0} interference with broad spin 0 resonance.

5 Neutrinoless semileptonic B decays: electroweak penguins and beyond

5.1 Electroweak penguin decays $B \to X_s\ell^+\ell^-$ from BaBar and Belle

While most of the semileptonic B decays occur via charged-current processes mediated by W, flavor-changing neutral current decays (FCNC) are also possible through electroweak penguin processes. Since FCNC decays are highly suppressed in the SM, they provide very sensitive search for new physics. Recently, Belle and BaBar made observations of such decays.

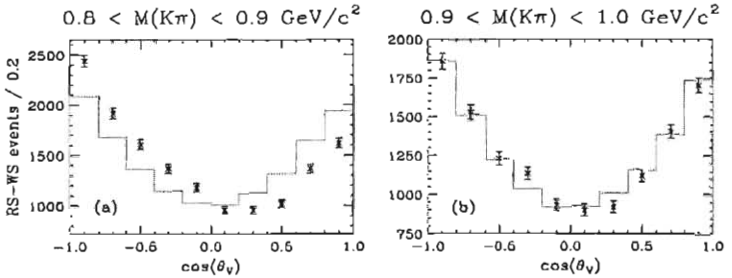

Figure 1: *The $\cos\theta_V$ distributions, separately for $M(K\pi)$ below and above 0.9 GeV/c^2. The points with error bar are FOCUS data and the solid histogram is a MC simulation, including all known backgrounds.*

Searches for exclusive FCNC modes $B \to K\ell^+\ell^-$ and $K^*\ell^+\ell^-$ are straightforward with dominant backgrounds coming from $\psi^{(\prime)}$ and continuum events. The $B \to K^{(*)}\psi^{(\prime)}$ events are suppressed by $m(\ell^+\ell^-)$: BaBar used $m(\ell^+\ell^-)$ cuts that are correlated with ΔE, while Belle used simple cuts in $m(\ell^+\ell^-)$. With 60fb^{-1} data, Belle observed $B \to K\ell^+\ell^-$ decays with 5.4σ significance: the measured branching fraction is $\mathcal{B}(B \to K\ell^+\ell^-) = (5.8^{+1.7}_{-1.5}\pm 0.6)\times 10^{-7}$. Using 78fb^{-1}, BaBar also obtained an evidence for $B \to K\ell^+\ell^-$ with 4.4σ significance: their measured branching fraction is $\mathcal{B}(B \to K\ell^+\ell^-) = (7.8^{+2.4+1.1}_{-2.0-1.8}) \times 10^{-7}$. Neither experiments observed significant excess for $B \to K^*\ell^+\ell^-$ and the following upper limits are obtained with 90% CL: $\mathcal{B}(B \to K^*\ell^+\ell^-) < 1.4\times 10^{-6}$ (Belle) and $< 3.0 \times 10^{-6}$ (BaBar). In case of BaBar, the significance of $B \to K^*\ell^+\ell^-$ is 2.8σ.

Belle also measured the inclusive $B \to X_s\ell^+\ell^-$ decays. The decays are *pseudo-reconstructed* by matching up to 4 pions to a K^+ or K^0_S for the hadronic X_s system: for each event, a best candidate is selected based on ΔE and $\cos\theta_B$ where θ_B is the angle between the flight of B and the beam axis. Then, M_{bc} (which is equivalent to m_{ES} explained in Sec. 2.1) is calculated to assess the signal yield. Figure 2 shows the M_{bc} distribution for $X_s e^+e^-$, $X_s\mu^+\mu^-$ and combined. Also shown in Fig. 2 is $B \to X_s e^\pm\mu^\mp$ where we don't expect any signal. Combining e^+e^- and $\mu^+\mu^-$ modes, the significance of the signal excess is 5.4σ and the branching fraction is measured: $\mathcal{B}(B \to X_s\ell^+\ell^-) = (6.1 \pm 1.4^{1.3}_{1.1}) \times 10^{-6}$.

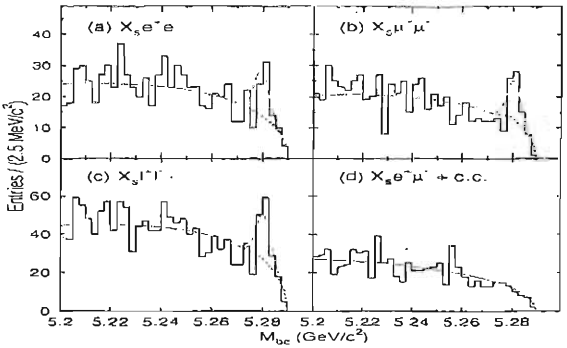

Figure 2: *The M_{bc} distributions from pseudo-reconstruction of the $B \to X_s \ell^+ \ell^-$ decays.*

5.2 Leptono-flavor violating $B \to h\ell\ell$ from CLEO

Recently, CLEO searched for different kinds of B decays to two charged leptons: $B \to K^{(*)} e^{\pm} \mu^{\mp}$ which is not allowed in SM except via neutrino flavor mixing, and $B \to h\ell^{\pm}\ell^{\pm}$ the observation of which could provide a strong evidence for majorana neutrino. A total of 16 exclusive modes are searched for. The signal yield for each mode is determined using a likelihood function based on kinematic variables of B decays, event shape information combined with Fisher discriminant [3], and missing energy. Analyzing 9.2fb^{-1} of $B\bar{B}$ event sample, no signal is observed in any mode and upper limits are obtained in the range $(1.0 \sim 8.3) \times 10^{-6}$.

References

1. M. Kobayashi and T. Maskawa, Prog. Theor. Phys. **49** 652 (1973).

2. "Update on CKM parameters", a plenary talk in this workshop presented by M. Battaglia.

3. R. A. Fisher, Annals of Eugenics **7**, 179 (1936).

Frascati Physics Series Vol. XXXI (2003), pp. 173–176
FRONTIERSCIENCE 2002 – Frascati, October 6–11, 2002
Invited Contribution in Plenary Session

DETERMINATION OF $|V_{cs}|$ IN THE ALEPH EXPERIMENT AT LEP

Franco Ligabue
Scuola Normale Superiore, Pisa

ABSTRACT

Pair production of W bosons at LEP has allowed the indirect determination of the CKM matrix element $|V_{cs}|$ through the measurement of the W hadronic branching fraction. A more direct determinatio, based on the measurement of the charm content in hadronic W decays provides a largely uncorrelated though less precise value for $|V_{cs}|$. The preliminary ALEPH result from the data collected at LEPII is $|V_{cs}| = 0.967 \pm 0.018_{stat} \pm 0.014_{syst}$.

1 Introduction

Prior to LEPII, V_{cs} was the least well-known of the CKM matrix elements, at least as far as absolute uncertainty is concerned. The 1998 PDG value [1] $|V_{cs}| = 1.01 \pm 0.17$ was determined from the study of D meson decays. At LEP2, the measurement of the W hadronic branching ratio can provide an

indirect determination of $|V_{cs}|$. In the Standard Model, this is related to the sum of the squared CKM matrix elements involved in the W decay:

$$\frac{B_h}{1-B_h} \simeq (1+\alpha_s(m_W^2)/\pi)\left(|V_{ud}|^2 + |V_{us}|^2 + |V_{ub}|^2 + |V_{cd}|^2 + |V_{cs}|^2 + |V_{cb}|^2\right) \quad (1)$$

where $B_h \equiv B(W \rightarrow \text{had})$.

An alternative, more direct determination comes from the measurement of the inclusive charm production in hadronic W decays. In the Standard Model the branching fraction $R_c^W \equiv \Gamma(W \rightarrow cX)/\Gamma(W \rightarrow \text{had})$ is given by

$$R_c^W = \frac{|V_{cd}|^2 + |V_{cs}|^2 + |V_{cb}|^2}{|V_{ud}|^2 + |V_{us}|^2 + |V_{ub}|^2 + |V_{cd}|^2 + |V_{cs}|^2 + |V_{cb}|^2} \quad (2)$$

and is equal to 0.5 due to unitarity of the CKM matrix, which also predicts the sum of the six squared matrix elements, appearing in Eq. 1 and Eq. 2, to be equal to 2.0. The unitarity constraint can be dropped to allow indirect determinations of V_{cs} from the measurement of R_c^W and the knowledge of the remaining five matrix elements.

2 Measurement of B(W → had)

The hadronic branching ratio of the W is determined from the measurement of the W pair production cross-section. Based on the three possible combinations of decay channels for the two bosons, W pairs are selected as fully hadronic, semileptonic and fully leptonic, and classified according to the lepton species (electron, muon, tau) for the leptonic channels. The selection algorithms for the leptonic channels are based on topological properties and lepton identification techniques. Neural networks combining the information of several discriminating variables are used for the semileptonic and fully hadronic selections.

The production cross-sections for all the considered decay channels are measured at each centre-of-mass energy. The results are then combined in a global fit which extracts the total cross-section values at all the energy points and a single value for the W hadronic branching fraction, assuming lepton universality. The result presented here is the ALEPH preliminary value obtained from the data collected in the years 1987-2000 at eight e^+e^- centre-of-mass energy points ranging from 183 to 207 GeV [3]. The total integrated luminosity

is roughly 680 pb^{-1}. The fitted value of the hadronic branching fraction is

$$B(W \to had) = (66.97 \pm 0.65_{stat} \pm 0.32_{syst})\%,$$

where the main contribution to the systematic error comes from uncertainties in the simulation of the QCD two-fermion background for the fully hadronic selection.

Using $\alpha_s(m_W^2) = 0.121 \pm 0.002$ and the measured values [1] of the five remaining CKM elements in Eq. 1 , the following result is obtained:

$$|V_{cs}| = 0.967 \pm 0.018_{stat} \pm 0.014_{syst}.$$

3 Determination of R_c^W

An independent analysis [4], based on an integrated luminosity of 67.7 pb^{-1} collected by ALEPH in 1996 and 1997, obtained a measurement of R_c^W from the properties of W pair events selected in the fully hadronic and semileptonic channels. A charm-jet tag algorithm based on a Neural Network was developed, which allowed to discriminate, on a statistical basis, $W \to cX$ from $W \to uX$ decays. The Neural Network was built out of twelve jet variables, related to topological and kinematic properties expected for charmed jets. The jet with the highest NN output was taken as charm-jet candidate within a given jet pair. The resulting charm tag distribution for jet pairs in semileptonic and fully hadronic events is shown in fig. 1.

The analysis led to the result

$$R_c^W = 0.51 \pm 0.05_{stat} \pm 0.03_{syst}$$

where the main contribution to the systematics came from uncertainties in the hadronization modelling. Making use of Eq. 2 and of the known values of the remaining CKM elements, this was turned into

$$|V_{cs}| = 1.00 \pm 0.11_{stat} \pm 0.06_{syst}.$$

Although intrinsically less precise, this V_{cs} determination is largely uncorrelated with the one from the hadronic branching fraction. The two results can in principle be combined, as was done in reference 4, at a time when the two statistical errors were still comparable in size.

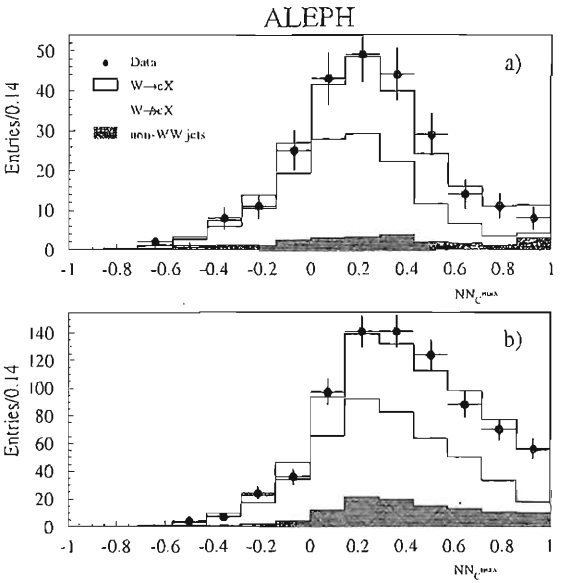

Figure 1: *Distribution of the charm-tag variable for jet pairs in a) semileptonic and b) fully hadronic candidate W decays. Data and Monte Carlo are normalized to the same number of entries.*

References

1. C. Caso et al. (Particle Data Group), Review of Particle Physics, Eur. Phys. J **C3**, 1 (1998).

2. The ALEPH collaboration, Phys. Lett. **B 484**, 205 (2000).

3. The ALEPH collaboration, *Measurement of W pair production and W branching ratios in* e^+e^- *collisions up to 208 GeV*, contribution to 2001 Winter Conferences, ALEPH 2001-013, CONF 2001-010.

4. The ALEPH collaboration, Phys. Lett. **B 465**, 349 (1999).

Flavour Dynamics and CP Violation – Session II

Chairpersons: G. Capon, K. Seth

J.P. Alexander	Rare Decays of Bottom, Charm, and Strange Quarks
A. Maier	Recent Results form NA48 on Rare Decays of Neural Kaons
T. Spadaro	KLOE Results and Prospects for Semileptonic K_S Decay Studies
M.H. Schune	Review on B_d^0 and B_S^0 Mixing Measurements
R. Ray	CP Violation in Systems other than Heavy Flavours

Frascati Physics Series Vol. XXXI (2003), pp. 179–185
FRONTIERSCIENCE 2002 – Frascati, October 6–11, 2002
Invited Review Talk in Plenary Session

RARE DECAYS OF BOTTOM, CHARM, AND STRANGE QUARKS

J. P. Alexander
Cornell University, Ithaca, New York. USA

ABSTRACT

A brief and selective survey of the main issues, the present status, and the future prospects for studies of rare decays of bottom, strange, and charm quarks.

1 Introduction

Rare decays of bottom, strange, and charm quarks are interesting principally for two reasons. First, Standard Model (SM) contributions are small and the possibility of observing new physics is correspondingly improved; and second, rare decays in many cases provide a means to measure or explore SM parameters and processes which are interesting in their own right and not necessarily under adequate control at the present time. Depending on the decays under study, sensitivity to new physics may include supersymmetric extensions of

the SM and any of the large number of parametrically determined varieties of such, or may probe the validity of fundamental symmetries. SM parameters of interest that may be uniquely or distinctively probed by rare decay studies include CKM elements – both magnitudes and phases – and issues related to hadronization, including form factors, strong interaction phases, the range of validity of factorization assumptions, the role of final state interaction and other so-called long-distance effects.

In this talk we begin with a brief summary of the main features of flavor-changing neutral currents (FCNC) in the SM. [1] The decay of a down-type quark into another down-type quark, or an up-type quark into another up-type quark is an example of FCNC, which in the SM must proceed through higher-order processes involving internal loops. Of course not all rare decays of interest involve FCNC, but the natural suppression of FCNC in the SM provides one means to open the window on new physics.

The decay diagrams relevant to FCNC are the penguin and box diagrams. For b and s quarks the internal quark lines are u, c, and t, with top dominating because of the $\sim m_q^{1.9}$ dependence of the corresponding Inami-Lim function in the region of the top quark mass. This dominance implies that the decays $b \to s$ and $s \to d$ are mainly sensitive to the CKM elements $|V_{tb}^* V_{ts}|$ and $|V_{ts}^* V_{td}|$. In the case of FCNC decays of charm quarks, the internal loop quarks must be d, s, and b, and absent strong domination of one quark species such diagrams are heavily GIM suppressed. This distinctive feature makes rare charm decays particularly rare in the Standard Model; correspondingly, it makes the window for new physics in such decays particularly clean. We note that in general the presence of loops means that non-SM particles can contribute to the total decay amplitude, possibly with the introduction of new phases. The indication of new physics may thus be a discrepancy between an observed rate and the SM-calculated rate, or a discrepancy between an observed distribution (such as an angular distribution) and the SM prediction, or may be the presence of a CP or other asymmetry that differs from the SM prediction. In all cases, the advantage of having small SM contributions is obvious.

Computation of FCNC decay rates can be complicated by competing long-distance processes which may have significant contributions, but which do not involve the interesting short-distance physics. The complications affect rare kaon decays most significantly, followed by rare charm decays, and are least

important for rare b decays. Strongly CKM suppressed modes, however, such as $b \to d$ modes can also suffer long distance contributions.

The remainder of this article is organized by decay type, proceeding roughly from the (conceptually) simplest decays to the more complex. Note that experimental simplicity typically has little (or negative) correlation with theoretical simplicity.

2 Lepton-Neutrino Modes

Decays of the form $M^- \to \ell^- \bar{\nu}$ proceed through an annihilation diagram. The decay rate is helicity suppressed, favoring the heaviest charged lepton (usually $\tau\bar{\nu}_\tau$) and is proportional the the square of the decay constant and the square of the CKM element at the annihilation vertex. Interest in such decays stems primarily from the experimental access to decay constants which can be used to check LQCD calculations, but may also be used to measure CKM elements if the decay constant can be normalized out by ratio with a suitable alternate process. $\mathcal{B}(B \to \tau\bar{\nu})/\Delta m_d$ is a possible route to determine $|V_{ub}|/|V_{td}|$. [2] Minimal extensions of the SM can include charged Higgs particles which may mediate these decays. The scalar Higgs does not inflict helicity suppression as the vector W does, but its mass-dependent coupling to the final state leptons results in essentially identical dependence on lepton mass.

Experimentally the search for $B \to \tau\bar{\nu}$ has reached a sensitivity which is still a factor 10 above the SM prediction. The most recent results from CLEO [3] have not changed this situation. About 500M $\Upsilon(4S)$ decays will be needed for observation, assuming the analysis of choice requires full reconstruction of the companion B meson. Because of the weak signature it is unlikely that any non-$\Upsilon(4S)$ will be able to measure these decays.

In the charm sector the situation is much better. Measurements of $D_s \to \mu\bar{\nu}$ are available [4], as is a single observation of $D \to \mu\nu$ from BES [5]. With the advent of CLEO-c [6] precision measurements of both will become available within the next couple of years.

3 Lepton-Lepton

Decays of the form $M \to \ell^+\ell^-$ proceed via penguin and box diagrams and are exceedingly suppressed in the SM. Theoretical calculations for $\mathcal{B}(B_{s,d} \to$

$\ell^+\ell^-) \sim f^2_{B_{d,s}}|V_{tq}|^2$ and are reliable but predict tiny branching ratios that will delay observation of useful yields at least to the end of the decade. Long distance physics are expected to be prominent in charm to dilepton modes, and the precise measurement of $K_L \to \mu^+\mu^-$ is almost entirely a measurement of long distance physics.

4 Neutrino-Neutrino

No calculations or serious attempts to look for totally invisible mesonic decays are known to the author. The decay mechanisms should be similar to those of the lepton-lepton modes, minus the photonic penguin contribution. In principle experimental searches for such modes should not be significantly different from searches for $M \to \ell\bar{\nu}$.

5 Lepton-Lepton-Meson

The constraints imposed by a purely leptonic final state are substantially lifted by admitting a hadron into the picture, and decays of the kind $M \to m\ell^+\ell^-$ play an important role in rare bottom, charm, and strange decay studies. The presence of the meson also introduces hadronic uncertainties for predictions of exclusive channels. In addition to branching ratio measurements there will eventually be dilepton mass distributions and forward-backward asymmetries. In principle even polarization asymmetries can be measured in $\tau^+\tau^-$ final states.

Recent results from Babar and Belle [7] show statistically significant signals in the $B \to K\ell^+\ell^-$ mode, with branching ratios averaged over muon and electron final states just below $\sim \times 10^{-6}$. The $K^*\ell^+\ell^-$ mode is not yet statistically significant at this writing. Belle also reports signal in $B \to X_s\ell^+\ell^-$ at a rate about ten times higher than the exclusive mode. Future datasets could yield $K^*\ell^+\ell^-$ signals in the range of $\sim 10^2$ events each for Babar, Belle, CDF, and D0, and $\sim 10^3$ events for LHCb and BTeV. (At this writing the fate of the BTeV proposal is still being debated.)

In the charm sector, $D \to \pi\ell^+\ell^-$, $D \to K\ell^+\ell^-$, and related modes still fall below experimental sensitivity [8] but theoretical calculations [9] indicate that at least the Standard Model long distance contribution to such modes could be just around the corner.

In the strange sector, KTeV has set a limit of 5×10^{-10} on the direct CP violating mode $K_L \to \pi\ell^+\ell^-$, still substantially above expected rate of $\sim 4\times10^{-12}$.

6 Neutrino-Neutrino-Meson

Modes of the form $B \to K\nu\bar{\nu}$ and $K \to \pi\nu\bar{\nu}$ are theoretically clean probes of CKM matrix elements, but pose serious experimental challenges due to the low branching ratios and unseen neutrinos in the final state. Limits on $B \to K\nu\bar{\nu}$ are at the $\sim \times10^{-4}$ level [10] while theoretical predictions are closer to $\sim \times10^{-6}$. In the strange sector two events have been observed in $K^+ \to \pi^+\nu\bar{\nu}$ in BNL E787 [11], but the yet more difficult mode $K_L \to \pi^0\nu\bar{\nu}$ remains in the future.

7 Hadronic

Rare hadronic B decay modes are being pursued agressively at Babar [12] and Belle [13], and CLEO [14] has released what are probably its last results on this topic. Direct CP violation is one of the important targets of these measurements, and determination of the phase of V_{ub} is another target.. In the latter case, there is a wealth of theoretical literature [15] to support treatment of experimental data. The possibility to constrain the unitarity triangle independently of the conventional constructions based on B mixing, $\sin 2\beta$, and kaon physics is an intriguing option that may be opened by these rare charmless hadronic B decay modes [16].

8 Conclusions

In the search for Physics Beyond the Standard Model, the pursuit of rare decay modes of bottom, charm, and strange quarks offers a useful experimental approach.

References

1. hep-ph/9806471 Andrzej J. Buras "Weak Hamiltonian, CP Violation and Rare Decays", to appear in "Probing the Standard Model of Particle Interactions", F. David and R. Gupta, eds, Elsevier Science B.V.; Report-no: TUM-HEP-316/98

2. P.F. Harrison, Jonathan L. Rosner. EFI-92-05. J.Phys.G18:1673-1677,1992

3. T. Browder, *et al, (CLEO Collaboration),Phys.Rev.Lett.86:2950-2954,2001*

4. *M. Chadha et al, (CLEO Collaboration) CLNS-97-1526, CLEO-97-28. Phys.Rev.D58:032002,1998*

5. *J.Z. Bai et al, (BES Collaboration). SLAC-REPRINT-1998-077, 1998. Phys.Lett.B429:188-194,1998*

6. *R.A. Briere et al, "CLEO-c and CESR-c: A New Frontier of Weak and Strong Interactions", CLNS 01/1742*

7. *B. Aubert et al, (Babar Collaboration) hep-ex/0207082; K. Abe, et al, (Belle Collaboration) Phys.Rev.Lett. 88 (2002) 021801*

8. *Will E. Johns (FOCUS Collaboration) hep-ex/0207015*

9. *Gustavo Burdman, Eugene Golowich, JoAnne Hewett, Sandip Pakvasa. SLAC-PUB-9057, Phys.Rev.D66:014009,2002*

10. *T. Browder, et al, (CLEO Collaboration),Phys.Rev.Lett.86:2950-2954,2001 B. Aubert et al, (Babar Collaboration), hep-ex/0207069;*

11. *Shaomin Chen "Measurement of Rare Kaon Decay $K^+ \to \pi^+ \nu\bar{\nu}$" Contributed to the XXXVIIth Rencontres de Moriond session for Electroweak Interactions And Unified Theories, hep-ex/0205031; M.V. Diwan Talk given at Les Rencontres de Physique, La Thuile, Aosta Valley (Italy), March 3-9, 2002; hep-ex/0205089; Laurence Littenberg "Rare K decay: results and prospects" , submitted to the Proc. 9th Intl. Symp. on Heavy Flavor Physics AIP Conf.Proc. 618 (2002) 89-102; hep-ex/0201026; Gerhard Buchalla, "Rare Kaon Decays - Overview", Invited Talk at KAON 2001, Pisa; CERN-TH/2001-292; hep-ph/0110313; Gino Isidori "Rare decays: theory vs. experiments", invited talk at 20th International Symposium on Lepton and Photon Interactions at High Energies, Rome, August 2001; Int.J.Mod.Phys. A17 (2002) 3078-3098*

12. *B. Aubert, et al, BABAR Collaboration, ArXiv:hep-ex/0207055; B. Aubert, et al, BABAR Collaboration, ArXiv:hep-ex/0207063; B. Aubert, et al, BABAR Collaboration, ArXiv:hep-ex/0207065; B. Aubert, et al, BABAR Collaboration, ArXiv:hep-ex/0206053;*

13. *B.C.K. Casey, et al, Belle Collaboration, Phys. Rev. D* **66**, *092002 (2002); K. Abe, et al, Belle Collaboration, Phys. Rev. D* **66**, *092002 (2002)*

14. *A. Bornheim et al, (CLEO Collaboration), hep-ex/0302026*

15. *Y.-Y. Keum, H.-N. Li, and A.I. Sanda, arXiv:hep-ph/0201103; M. Neubert, JHEP* **9902** *(1999) 014; M. Neubert and J.L. Rosner, Phys. Rev. Lett.* **81**, *5076 (1998); M. Neubert and J.L. Rosner, Phys. Lett. B* **441**, *403 (1998); M. Neubert, Phys. Lett. B* **424**, *2752 (1998); R. Fleischer and T. Mannel, Phys. Rev. D* **57**, *2752 (1998)*

16. *M. Neubert, ArXiv:hep-ph/0207327, CLNS-02/1794; M. Beneke, G. Buchalla, M. Neubert, and C.T. Sachrajda, Nucl. Phys. B* **606**, *245 (2001); M. Beneke, G. Buchalla, M. Neubert, and C.T. Sachrajda, Phys. Rev. Lett.* **83**, *1914 (1999);*

Frascati Physics Series Vol. XXXI (2003), pp. 187–192
FRONTIERSCIENCE 2002 – Frascati, October 6–11, 2002
Invited Contribution in Plenary Session

RECENT RESULTS FROM NA48 ON RARE DECAYS OF NEUTRAL KAONS

Andrew Maier*
University of Siegen, Fachbereich Physik,
Walter-Flex Straße 3, D-57068 Siegen, Germany

ABSTRACT

New and recent measurements of the branching ratios of rare decays of neutral K_S and K_L mesons are presented. The results have been extracted from data collected during the NA48 ϵ'/ϵ runs as well as in a special high intensity K_S and hyperon run. In particular the presentation focuses on the decay of $K_L \to \pi^0\gamma\gamma$, $K_S \to \pi^0 e^+ e^-$ and $K_S \to \gamma\gamma$.

1 Introduction

The NA48 experiment has been designed to measure the direct CP-violation parameter ϵ'/ϵ [1, 2, 3] to a precision of 2×10^{-4} using simultaneous almost

* on behalf of the NA48 collaboration: Cagliari, Cambridge, CERN, Dubna, Edinburgh, Ferrara, Firenze, Mainz, Orsay, Perugia, Pisa, Saclay, Siegen, Torino, Vienna, Warsaw.

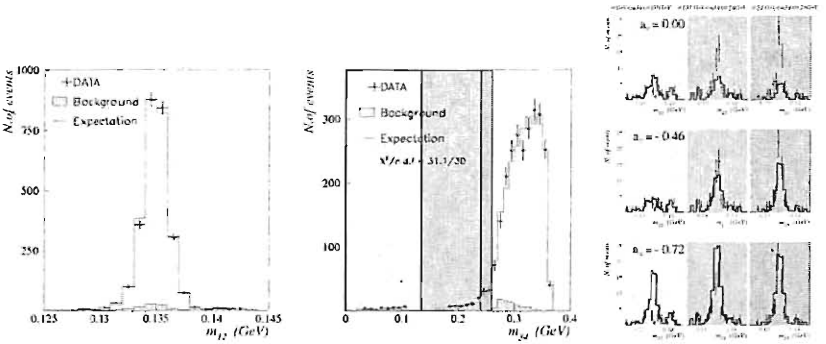

Figure 1: *Invariant mass distribution of the photons resulting from π^0 and $\gamma\gamma$. The photons associated with the π^0 are labeled 1 and 2, while the $\gamma\gamma$ pair is labeled 3 and 4, respectively. The rightmost figure displays the distribution of the low mass tail for the $\gamma\gamma$ system for both data and Monte Carlo.*

collinear K_S and K_L beams [4]. The design of the experiment, its good understanding of the systematics necessary for the measurement of ϵ'/ϵ and the high kaon flux make NA48 an excellent tool for the investigation of rare neutral kaon decays.

This paper will review some results obtained from data taken from the ϵ'/ϵ run in 98/99, from a two day high intensity K_S run in 1999 as well as from data taken in 2000 when no spectrometer was present.

2 $K_L \to \pi^0\gamma\gamma$

The decay of $K_L \to \pi^0\gamma\gamma$ has two interesting aspects. First it can be used to measure the CP conserving component of $K_L \to \pi^0 e^+ e^-$, which has also a direct CP-violating component. In addition it is a good test of chiral perturbation theory (χPT) One loop calculations of this decay rate are finite, yet O(4) calculations predict only 1/2 to 1/3 of the measured rate. Calculations of O(6) including Vector Meson Dominance (VMD) contributions can accommodate for the measured rare by the choice of a parameter a_v which has to be determined from experiment. VMD also predicts a mass tail at low $\gamma\gamma$ mass.

The data for this analysis were taken from the 98/99 ϵ'/ϵ run, using a

large $K_L \to 2\pi^0$ data set with the same topology as $K_L \to \pi^0\gamma\gamma$. $K_L \to 2\pi^0$ was also used as a normalization channel, hence trigger efficiencies cancel.

The main background to this channel comes from $K_L \to 2\pi^0$ and $K_L \to 3\pi^0$ decays. The $2\pi^0$ background is removed using a mass constraint and by constructing a χ^2 like variable with a π^0 mass hypothesis in order to reject $2\pi^0$ events.

Background from $3\pi^0$ decays originates mainly from missing or overlapping showers in the liquid krypton electromagnetic calorimeter (LKr). These backgrounds are removed using combinatorial cuts and mass constraints, which, under a $3\pi^0$ hypothesis, result in the vertex of the decay to be in an unphysical region for signal events, but not for background. Additional cuts on the shower width remove background from hadronic showers.

Figure 1 shows the mass distribution of the remaining signal for the 2 photons associated with the π^0 as well as the remaining 2 γ. A low mass tail is evident in two γ distribution indicating a value of a_v different from 0.

Depending on the value of a_v, different numbers of events are expected in the various mass regions of $m_{\gamma\gamma}$. This is illustrated in the rightmost picture of Figure 1. Comparing data with Monte Carlo simulations a value of $a_v = -0.46 \pm 0.03_{stat} \pm 0.03_{syst} \pm 0.02_{theo}$ can be extracted, which indicates a negligible contribution of indirect CP violation in $K_L \to \pi^0 e^+ e^-$. Applying this value of a_v, a branching ratio of $BR(K_L \to \pi^0\gamma\gamma) = (1.36 \pm 0.03_{stat} \pm 0.03_{syst} \pm 0.03_{norm}) \times 10^{-6}$ is measured. This analysis has now been published [5].

3 $K_S \to \gamma\gamma$

A new measurement of $K_S \to \gamma\gamma$ has been performed using data collected during the 2000 neutral run. This run was divided into a K_L run from the far target and a high intensity K_S run from the near target.

The motivation for this decay arises from the fact that in χPT, the decay is calculable with no counter terms and the branching ratio is therefore predicted with a small error. Contribution from higher orders are not expected to be large. The previous result [6] was statistically and systematically limited and could not test this prediction.

Since both K_L and K_S are produced in the target it is necessary to subtract the number of decays of $K_L \to \gamma\gamma$ from the number of all $K \to \gamma\gamma$

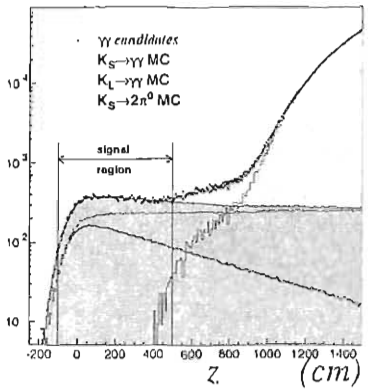

Figure 2: *The vertex distribution for $K_S \to \gamma\gamma$, $K_L \to \gamma\gamma$ and the $\gamma\gamma$ background originating from $K_S \to 2\pi^0$.*

events. Since the branching ratio of $K_L \to \gamma\gamma$ was not known to the required accuracy, NA48 has also measured the branching ratio of $K_L \to \gamma\gamma$ using the data from the far target data. This results in a new result of $\mathrm{BR}(K_L \to \gamma\gamma)/\mathrm{BR}(K_L \to 3\pi^0) = (2.81 \pm 0.01_{stat} \pm 0.02_{syst}) \times 10^{-3}$

Events were selected to have at least two clusters in the LKr. The highest invariant mass $m_{\gamma\gamma}$ that can originate from pairing two photons from $K_L \to 2\pi^0$ is 548 MeV, which translates into a vertex shift of 9 m, if analyzed under a $K \to \gamma\gamma$ hypothesis. The choice of a short decay region therefore allows to distinguish signal from background of $K_L \to 2\pi^0$ with 2 missing photons. Monte Carlo studies show that by including cuts on the shower-width of the clusters a background free region of 5 m fron the target exists.

The vertex distribution for signal and background, both for data and Monte Carlo, is shown in Figure 2. The contribution from $K_L \to \gamma\gamma$ is removed, and, using $K_S \to 2\pi^0$ as a normalization channel, a branching ratio of $BR(K_S \to \gamma\gamma) = (2.78 \pm 0.06_{stat} \pm 0.10_{sys}) \times 10^{-6}$ is measured [7]. This result is the first measurement of $\mathrm{BR}(K_S \to \gamma\gamma)$ to show significant differences from the $O(p^4)$ calculations of χPT.

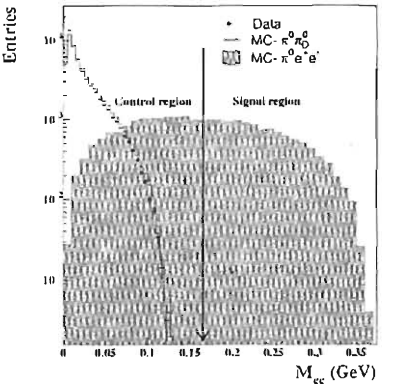

Figure 3: $K_S \to \pi^0\pi^0_D$ and $K_S \to \pi^0 e^+e^-$ for data and Monte Carlo.

4 $K_S \to \pi^0 e^+e^-$

The decays of K_L into $\pi^0 l^+l^-$ are of considerable interest due to their sensitivity to direct CP violation [8]. However, in $\pi^0 e^+e^-$ decay, both CP conserving and indirect CP violating amplitudes contribute. The CP conserving component can be measured from the decay $K_L \to \pi^0\gamma\gamma$, while the indirect CP violating part can be measured from the decay $K_S \to \pi^0 e^+e^-$. The K_S decay is expected to be of the order of $BR(K_S \to \pi^0 e^+e^-) = 5.2a_s^2 \times 10^{-9}$, where a_s is expected to be of O(1) but is not well bounded theoretically. The decay has so far not been observed.

The data for this analysis was taken in a two day high intensity test run after the end of the 1999 ϵ'/ϵ data taking period. Events were selected to have at least 4 clusters in the electro-magnetic calorimeter and two tracks identified as electrons with an $0.9 < E/p < 1.1$, using the calorimeter and the spectrometer. The invariant mass of the event had to be compatible with the K^0 mass and the invariant mass of the two photons resulting from clusters not associated to tracks had to be compatible with the π^0-mass.

Background from the Dalitz decays $\pi^0\pi^0_D$ and $\pi^0_D\pi^0_D$ is removed by requiring that the mass of the $e\gamma$ system be at least 30 MeV larger or smaller than

the π^0 mass. In addition, the mass of the ee system is required to be larger than 165 MeV/c^2. While this cut safely removes all background expected from the simulation, it also removes about 50% of the expected signal (see Figure 3).

After this selection, no events remain in the signal region. Using $K_S \to \pi^0\pi^0_D$ as normalization channel, a new upper limit for the branching ratio can be given to be: $BR(K_S \to \pi^0 e^+ e^-) < 1.4 \times 10^{-7}$ at the 90% confidence level [10]. This result includes a 7% systematic error, and it improves the current best measurement by a factor of 8 [9].

Data taken during this year's 2002 run was to a good extent motivated to improve this limit. During a 78 day run more than 40 times the data compared to 1999 were taken. The analysis of this data is in progress, and results will be reported as soon as possible.

References

1. V. Fanti *et al.*, Physics Letters B **465**,335–348 (1999).
2. NA48 Collaboration, Eur. Phys. J. C, **22**,231–254 (2001)
3. J. R. Barely *et. al*,Phys. Lett. B **544**,97–112 (2002)
4. C. Biino *et al.*in *Proceedings of the 6th European Particle Accelerator Conference* (S. Myers, L. Lijeby, C. Petit-Jean-Genaz, *et. al.*, eds.), 1998.
5. A. Lai *et al.*, Phys. Lett. B **536**, 229–240 (2002)
6. A. Lai *et al.*, Phys. Lett. B **493**, 19–25 (2000)
7. A. Lai *et al.*, Phys. Lett. B **551**,7–15 (2003)
8. G. D'Ambrosio and G. Isidori, Int. J. Mod. Phys. A **A13**,1 (1998)
9. G. Barr *et. al.*, Phys. Lett. B **304** 381 (1993)
10. A. Lai *et. al.*, Phys. Lett. B **514**,253–262 (2001)

Frascati Physics Series Vol. XXXI (2003), pp. 193–197
FRONTIERSCIENCE 2002 – Frascati, October 6–11, 2002
Invited Contribution in Plenary Session

KLOE RESULTS AND PROSPECTS FOR SEMILEPTONIC K_S DECAY STUDIES

Tommaso Spadaro*
Laboratori Nazionali di Frascati dell'INFN

ABSTRACT

The KLOE experiment at the Frascati ϕ-factory DAΦNE is uniquely suited to the study of K_S decays. Neutral kaons at DAΦNE are produced in collinear pairs with momenta of about 110 MeV/c in a pure C-odd quantum state $(K_S K_L - K_L K_S)$. Hence, at KLOE one can tag a pure K_S beam with high efficiency by detecting K_L interactions in the calorimeter or by reconstructing K_L decays in the drift chamber. This has allowed us to perform the best measurement of the branching fraction for the channel $K_S \to \pi^{\pm} e^{\mp} \overline{\nu}(\nu)$ to date. The study of the above decay is particularly interesting as a test of the $\Delta S = \Delta Q$ rule as well as the validity of CPT invariance in the neutral kaon system via measurement of the leptonic charge asymmetry.

---

* On behalf of the KLOE Collaboration:
http://www.lnf.infn.it/kloe/kloe_authors.ps

1 Physics motivations

The branching ratio of the decay $K_S \to \pi e \nu$ is a very well calculable quantity if CPT symmetry and the $\Delta S = \Delta Q$ rule are assumed. From the equality $\Gamma(K_S \to \pi e \nu) = \Gamma(K_L \to \pi e \nu)$ and using the measured values of $\mathrm{BR}(K_L \to \pi e \nu)$ and τ_S/τ_L [1], $\mathrm{BR}(K_S \to \pi e \nu) = (6.70 \pm 0.07) \cdot 10^{-4}$ is obtained.

In the Standard Model no $\Delta S \neq \Delta Q$ transition exists at tree level. At higher order, $\Delta S \neq \Delta Q$ transitions are suppressed by a factor of about $10^{-6} - 10^{-7}$ relative to those with $\Delta S = \Delta Q$ [2]. At present, the best experimental limit on the real part of the amplitude ratio $A(\Delta S \neq \Delta Q)/A(\Delta S = \Delta Q)$ is as low as $6 \cdot 10^{-3}$, obtained from the study of the decay time distribution of tagged K^0 and $\overline{K}^0$ beams [3]. This limit can be improved by measuring the $K_S \to \pi e \nu$ branching ratio with a precision better than 2%.

One can also test CPT conservation by measuring K_S and K_L charge asymmetries in semileptonic decays, defined as:

$$\delta_{L,S} = \frac{\Gamma^+_{L,S} - \Gamma^-_{L,S}}{\Gamma^+_{L,S} + \Gamma^-_{L,S}} \tag{1}$$

where $\Gamma^{+(-)}_{L,S}$ are the decay widths for $K_{L,S}$ decays to a positively (negatively) charged lepton. It can be shown that the quantity $\delta_S - \delta_L$ measures the amount of CPT violation either in the decay or in the kaon mixing matrix [4]. At present, while δ_L is known with an absolute error of about 70 parts per million [5], δ_S has never been measured.

2 DAΦNE and KLOE

DAΦNE, the Frascati ϕ-factory [6], is an e^+e^- collider operating at a center of mass energy of ~1020 MeV, the ϕ-meson mass. The ϕ meson decays ~34% of the time into a $K_S K_L$ pair, which is nearly collinear at DAΦNE. In each event, the identification of the K_L allows the tagging of a K_S of given momentum. DAΦNE is therefore an exceptional source of nearly monochromatic, tagged K_S particles, allowing for detailed studies of their more rare decays.

The KLOE detector [7, 8] consists of a cylindrical drift chamber 4 m in diameter and 3.3 m in length, surrounded by a lead-scintillating fiber electromagnetic calorimeter. A superconducting coil provides a 5.2 KG magnetic

field. The momentum resolution for large-angle tracks is $\sigma_p/p \leq 0.4\%$. Vertices are reconstructed with spatial resolutions $\sigma_{xy} \approx 150\,\mu$m and $\sigma_z \approx 2$ mm. The calorimeter provides a solid angle coverage of 98%, an energy resolution of $\sigma_E/E = 5.7\%/\sqrt{E(\,\mathrm{GeV})}$, and a timing resolution of $\sigma_t = 54\,\mathrm{ps}/\sqrt{E(\,\mathrm{GeV})} \oplus 50\,\mathrm{ps}$.

3 $K_S \to \pi^\pm e^\mp \overline{\nu}(\nu)$ event selection

In KLOE more than one half of the K_L's reach the calorimeter before they decay. An efficient K_S tag is therefore provided by the identification of the K_L interaction in the calorimeter. The signature for such events is the presence of a cluster with relatively large energy deposit and timing compatible with that of a slowly moving ($\beta \approx 0.22$) neutral particle ('KCRASH' events).

In order to search for $K_S \to \pi e \nu$ decay candidates, events with a KCRASH and two oppositely charged tracks from the interaction region are initially selected. Events are then rejected if the two tracks' invariant mass (in the pion hypothesis) and the resulting K_S momentum in the ϕ rest frame are compatible with those expected for a $K_S \to \pi^+\pi^-$ decay.

In order to perform time of flight identification of the charged particles, both tracks are required to be associated with a EmC cluster. For each particle, the time of flight measured by the calorimeter is compared with that expected for an electron (pion) of the same momentum; events in which an electron-pion pair cannot be identified are rejected.

Each selected event is finally kinematically closed. The K_S momentum is estimated making use of the measured direction of the K_L and the 4-momentum of the ϕ. The missing energy and momentum of the K_S-$\pi^\pm e^\mp$ system, which should correspond to those carried away by the neutrino, are then computed. Their difference is distributed as in figure 1; it must be equal to zero for the signal. The data are fit using Monte Carlo spectra for both signal and the residual background (due mostly to $K_S \to \pi^+\pi^-$ events with an early decay of one of the two pions) to obtain the number of $K_S \to \pi e \nu$ decays in the selected sample.

To determine the efficiency for all of the above cuts, several different data control samples are used: (1) $K_L \to \pi e \nu$ events in which the K_L decays near the interaction region and K_S decays into charged pions; (2) $\phi \to \pi^+\pi^-\pi^0$ decays; (3) events with $\phi \to K^0\overline{K}^0$ and $K_S \to \pi^+\pi^-$. Monte Carlo simulation

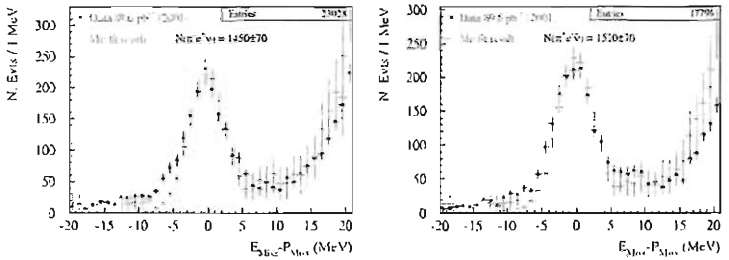

Figure 1: Distribution of the difference between missing energy and missing momentum for $K_S \to \pi e \nu$ candidates (left $\pi^- e^+ \nu$, right $\pi^+ e^- \overline{\nu}$). The peak at zero is the signal. The distribution is fit to a linear combination of Monte Carlo signal and background spectra in the range -40 MeV + 40 MeV.

is used only to determine geometrical acceptance [9].

The above procedure for signal extraction and efficiency determination can be applied separately for the two charged states, taking into account the differences in π^+ and π^- interaction in the calorimeter, thus allowing for the measurement of the charge asymmetry, δ_S of Eq. 1.

4 Results and conclusions

The measurement [10] of the branching ratio irrespective of the lepton charge is given here for the final analysis of the data taken in year 2000, corresponding to an integrated luminosity of $\sim 17\,\mathrm{pb}^{-1}$. The measured yield is of 627 ± 30 events, for a total efficiency of $(21.8 \pm 0.3)\%$. The total number of events is then normalized to the number of observed $K_S \to \pi^+\pi^-$ events, giving $\mathrm{BR}(K_S \to \pi e \nu) = (6.79 \pm 0.33_{\mathrm{stat}} \pm 0.20_{\mathrm{syst}}) \cdot 10^{-4}$ in agreement with the expectation from the $\Delta S = \Delta Q$ rule. In the ratio, the tagging efficiency, which is the largest cause of systematic uncertainty, cancels out identically. The relative uncertainty on the KLOE measurement is less than a third of that on the only previous measurement [11].

The analysis of the data taken in 2001 and 2002 is under way. The analysis of the first $89\,\mathrm{pb}^{-1}$ gives a preliminary value of $\mathrm{BR}(K_S \to \pi e \nu)$ in agreement with the previous result. On this data sample, the charge asymmetry has been measured to be compatible with zero, at the 3% level. The uncertainty is

expected to be lowered to 1% when the entire data set is analyzed.

At the beginning of 2003, major upgrades of the KLOE interaction region are planned, which should allow an increase in the luminosity of the machine. The hope is to reach soon the design luminosity of $5 \cdot 10^{32} \mathrm{cm}^{-2}\mathrm{s}^{-1}$. With this luminosity, the statistical accuracy on the semileptonic charge asymmetry can be lowered to 0.2%, thus allowing a test of CPT symmetry at the level of $5 \cdot 10^{-4}$.

References

1. K. Hagiwara *et al.*, Phys. Rev. **D66**, 010001 (2002).
2. C. O. Dib, B. Guberina, Phys. Lett. **B255**, 113 (1991). M. Luke, Phys. Lett. **B256**, 265 (1991).
3. A. Angelopoulos *et al.*, Phys. Lett. **B444**, 38 (1998). A. Angelopulos *et al.*, Phys. Lett. **B444**, 43 (1998).
4. L. Maiani, CP and CPT violation in neutral kaon decays, in: L. Maiani, G. Pancheri, N. Paver (Eds.), The Second DAΦNE Physics Handbook, Vol. 1, 1995, p. 3.
5. A. Alavi-Harati *et al.*, Phys. Rev. Lett. **88**, 52 (2002).
6. S. Guiducci, Status of DAΦNE, in: P. Lucas, S. Webber (Eds.), Proc. of the 2001 PAC - Chicago, IL U.S.A., 2001, p. 353.
7. M. Adinolfi, *et al.* (the KLOE collaboration), KLOE: A general purpose detector for DAΦNE, LNF-92/019 (IR). M. Adinolfi, *et al.* (the KLOE collaboration), The KLOE detector, technical proposal, LNF-93/002 (IR).
8. M. Adinolfi, *et al.* (the KLOE collaboration), Nucl. Inst. Meth. **A482**, 364 (2002), Nucl. Inst. Meth. **A488**, 51 (2002), Nucl. Inst. Meth. **A492/1-2**, 134 (2002).
9. C. Gatti, T. Spadaro, Measurement of BR($K_S \to \pi e \nu$), KLOE note 176 (2002). URL `http://www.lnf.infn.it/kloe/pub/knote/kn176.ps.gz`
10. M. Adinolfi, *et al.* (the KLOE collaboration), Phys. Lett. **B535**, 37 (2002).
11. R. Akhmetshin, *et al.*, Phys. Lett. **B456**, 90 (1999).

Frascati Physics Series Vol. XXXI (2003), pp. 199–211
FRONTIERSCIENCE 2002 – Frascati, October 6–11, 2002
Invited Review Talk in Plenary Session

REVIEW ON B_d^0 AND B_s^0 MIXING MEASUREMENTS

Marie-Hélène Schune
Laboratoire de l'Accélérateur Linéaire, BP 34,F-91898 Orsay Cedex, France

ABSTRACT

The $B^0\bar{B}^0$ oscillation phenomenon is now well established and measured in the case of the B_d^0 meson. The average value for its frequency oscillation is $\Delta m_d = .503 \pm .006$ ps^{-1}. Within the Standard Model the B_s^0 meson oscillation frequency is expected to be about 20 time larger than the B_d^0 meson frequency. Despite the fact that elaborate analyses have been developed, no measurement of Δm_s have been obtained but a lower limit of $\Delta m_s > 14.4$ ps^{-1} at 95 % CL has been reached.

1 Oscillation analyses overview

1.1 Formalism

The neutral B meson mass eigenstates can be expressed as linear combinations of the weak eigenstates. Solving the Schrödinger equation allows to calculate

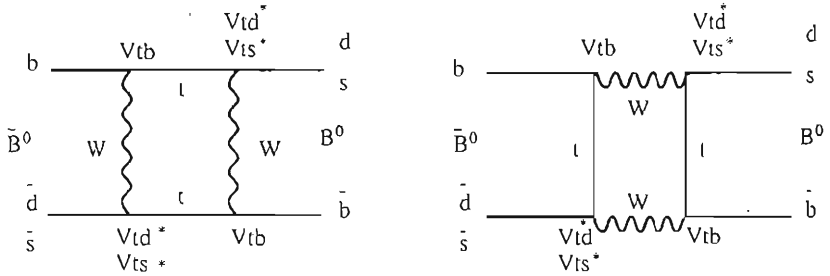

Figure 1: *The two box diagrams, which, in the Standard Model are the source of* $B^0\bar{B}^0$ *oscillations. The three up-type quarks enter in the loop but the top quark dominate the process and is only shown here.*

the probability that a purely B^0 state produced at time $t = 0$ will decay as a B^0 ($\bar{B}^0$)[1] at time t :

$$\mathcal{P} = \frac{1}{\tau_q}\, e^{-t/\tau_q}\, \frac{1 \pm \cos(\Delta m_q t)}{2}, \tag{1}$$

The frequency Δm_q is the mass difference between the two mass eigenstates and τ_q is the average B_q^0 lifetime. It has been assumed that $\Delta\tau_q = 0$ and CP violation has been neglected.

Within the Standard Model $B^0\bar{B}^0$ oscillations are due to box diagrams (Figure 1) in which a top quark exchange dominates.

The frequency Δm_q can be computed:

$$\Delta m_q = \frac{G_F^2}{6\pi^2}|V_{tb}|^2|V_{tq}|^2 M_W^2\, M_{B_q^0} f_{B_q^0}^2 B_{B_q^0} \eta_{B_q^0} S\left(\frac{M_t^2}{M_W^2}\right) \tag{2}$$

with $q = d$ or s. M_W is the W mass , $M_{B_q^0}$ the B_d^0 or B_s^0 mass [1)], $f_{B_q^0}$ the pseudo scalar decay constant of the B_q^0 meson, $B_{B_q^0}$ the so called "Bag factor"

[1]They lead respectively to two types of events : the so-called unmixed and mixed events)

and $f_{B_d^0}\sqrt{B_{B_d^0}}$ is estimated to be of the order of 230 ± 40 MeV. Finally $\eta_{B_q^0}$ is a perturbative QCD correction factor and is of the order of 0.55. The function $S\left(\frac{M_t^2}{M_W^2}\right)$ is known and computable to a high precision given the present knowledge of the top mass. The impact of the large theoretical uncertainty on $f_{B_d^0}\sqrt{B_{B_d^0}}$ can be reduced by the use of the ratio given in Eq 3.

$$\frac{\Delta m_d}{\Delta m_s} = \frac{|V_{td}|^2}{|V_{ts}|^2} \frac{M_{B_d^0}}{M_{B_s^0}} \frac{f_{B_d^0}^2 B_{B_d^0}}{f_{B_s^0}^2 B_{B_s^0}} \tag{3}$$

with $\frac{f_{B_s^0}^2 B_{B_s^0}}{f_{B_d^0}^2 B_{B_d^0}} = \xi_s^2$. This factor reflects the SU(3) flavour symmetry breaking and is theoretically better known : $\xi_s^2 = 1.16 \pm 0.06$ [8].

1.2 Various experimental contexts

The study of the $B^0\bar{B}^0$ oscillation phenomenon is now performed in various places in the world. It is namely done at LEP (ALEPH, DELPHI, L3 and OPAL) where the Z^0 decay produces both B_d^0 and B_s^0 mesons (about 15 % Z^0 decay in a $b\bar{b}$ pair). The neutral B mesons are produced with a large boost and fly about 3 mm before decaying. There is thus a clear separation of the two hemispheres allowing to perform both inclusive and exclusive analyses. The amount of statistics is of the order of 4 10^6 Z^0 per experiment. The first experimental evidence for time dependent oscillations for the B_d^0 was seen at LEP. All the detectors are equipped with high resolution silicon detectors to precisely reconstruct the decay vertex of the B hadrons. At SLD (SLC collider) the experimental situation is similar to LEP except for a smaller beam spot and a more precise vertex determination. In addition there is the possibility to perform the production state tagging with the beam polarisation. The SLD collaboration has registered about $\sim$ 0.4 10^6 Z^0 events. At CDF (Tevatron collider) due to the very large cross section there is a huge production of B_d^0 and B_s^0 . But the difficult experimental environment leads to a large reduction of the number of events (the inclusive $b\bar{b}$ cross section is about 1000 times smaller than the inelastic one). Finally at B factories which are running at the $\Upsilon(4S)$ BaBar and BELLE can only study B_d^0 mixing. They are characterised by very large samples ($\sim$ 90 10^6 B_d^0) but also by a small boost : on average the B_d^0 will fly only 250 μm before decaying.

1.3 Principle of the measurement

The three main ingredients needed for a mixing analysis are the decay time reconstruction, the final state tagging and the initial state tagging. Their influence on the analysis is summarised in the quality factor Q defined in Eq. 4

$$Q = \sqrt{N_{rec}} f_{signal} \sqrt{\varepsilon_{tag}} (1 - 2\eta) e^{-\frac{1}{2}(\Delta m_q \sigma_t)^2} \quad (4)$$

Where N_{rec} (the reconstructed number of B^0) and f_{signal} (the signal fraction in the sample) are determined by the final state reconstruction. The two factors reflecting the tagging performances show clearly that it is relatively more important to tag the event correctly (low mistag fraction η) than to efficiently tag it (ε_{tag}). The exponential term which modelizes the dumping of the signal for large decay time resolution contains the B^0 mixing frequency. From this term it can be seen that the decay time resolution will not be crucial for Δm_d measurements whereas at high Δm_s frequencies it will be the limiting factor.

In order to perform a time dependent oscillation analysis one needs to reconstruct the decay time of the B^0 meson. This reconstruction implies the estimates of the decay length as well as of the momentum. In the B factories context the B^0 momentum reconstruction is not needed since it is produced with a known boost due to the $\Upsilon(4S)$ decay. For the analyses performed at the LEP, SLC or Tevatron colliders the reconstruction of the momentum has to be performed.

In order to decide if the event is mixed or unmixed it is necessary to know the production state of the meson (B^0 or $\bar{B}^0$) as well as the decay state. The decay state is usually determined from the charge of one of the reconstructed decay products : for example from the energetic lepton (a ℓ^+ signs the decay of a B^0 meson). The determination of the production state is more complicated and the information from both hemispheres can be used (at B factories only the other B information is available). In all cases it relies on the fact that a correlated $b\bar{b}$ pair is produced.

- In the hemisphere opposite to the B^0 an energetic lepton with a large transverse momentum with respect to the jet axis can be searched for or the jet charge of the hemisphere can be computed. Their sign indicates if a b or a $\bar{b}$ quark was produced in this hemisphere. Using the fact that a $b\bar{b}$ pair is produced, the production state of the B^0 can therefore be

deduced. The same information can also be obtained from the charge of a kaon produced in $b \to c \to s$ transitions.

- In the B^0 hemisphere the tagging of the production state can be performed using information from the fragmentation tracks. Indeed the charge of the highest order fragmentation tracks is correlated to the production state of the B^0 meson. The same kind of information is also present in the sign of the jet charge of this hemisphere. The B^{**} decay can also be used : $B^{**} \to B^0\pi^+$.

This initial state tagging is not perfect due to experimental problems (misidentification, incorrect linking of the tracks to the primary vertex ...) but also due to physics. For example at colliders other than B factories the opposite hemisphere lepton can in fact come from the decay of a beauty hadron which has undergone oscillation.

2 Δm_d results

The B_d^0 oscillation frequency is small ($\simeq .50$ ps^{-1}) and thus the time resolution is not crucial. However one aims at a precise measurements so there is a clear need for high statistics and a good control of the systematics. Up to now 35 analyses are available. The combination has been performed by the LEP Oscillation Working Group [2], taking into account correlated uncertainties. The overall result is an impressive 1.2 % precision measurement : $\Delta m_d = 0.503 \pm .006$ ps^{-1}. It should emphasised that the average is now fully dominated by the B factories results as can be seen from Figure 2. In the following sections two example analyses are described.

2.1. An example : $D^{(*)}\ell\nu$ with Same Side Tagging from CDF

In this analysis [3] the final state reconstruction consists in $D^{*\pm}\ell^{\mp}\nu$, $D^{\pm}\ell^{\mp}\nu$ and $D^0\ell^{\mp}\nu$. The first two channels are mainly due to B_d^0 decay whereas the last one comes from charged B decay (used as cross checks). The initial state tagging is obtained from the same side information both from fragmentation pions and B^{**} decays. The two cases are not explicitly separated in the analysis and the tagging pion is searched for among tracks compatible within $\pm 3\sigma$ with the primary vertex and close in transverse momentum with the reconstructed B. The time measurement is performed using the distance between the primary

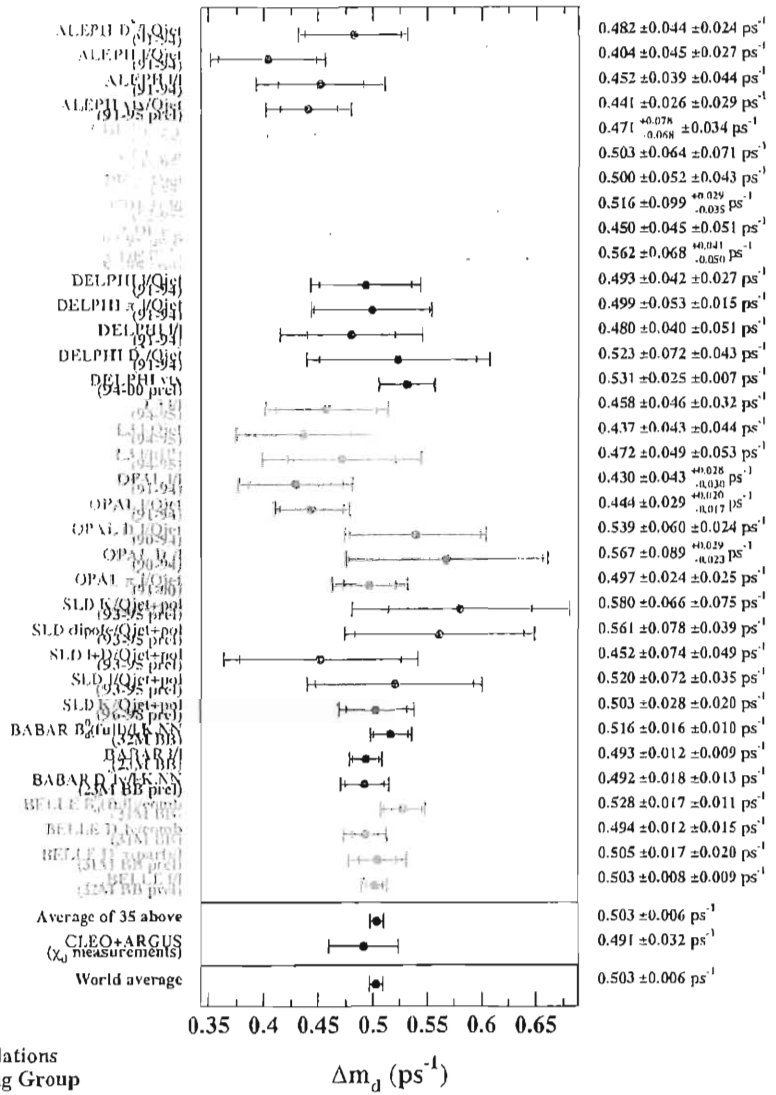

Figure 2: *Summary of all the Δm_d analyses. The results at the bottom of the plot are those obtained at B factories and clearly dominate the average.*

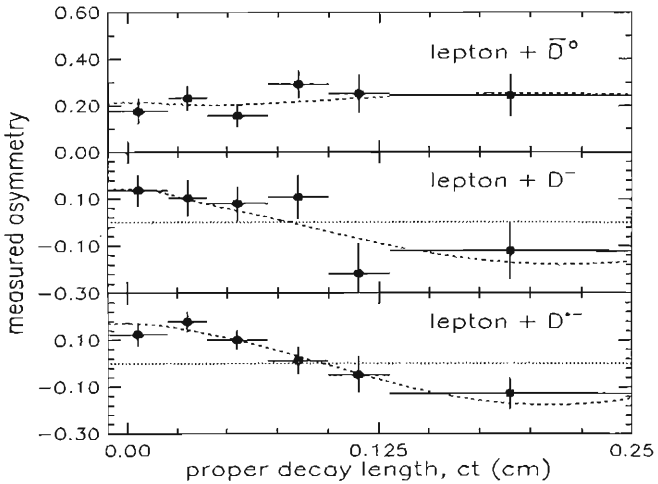

Figure 3: *Mixing asymmetries* $\propto \cos(\Delta m_d t)$ *for the 3* $D\ell$ *combinations. The upper one consists mainly of charged B events and as expected no oscillation is visible. The two lower ones are mostly due to neutral B and the cosine term appears clearly. The points are the data, the line is the result of the unbinned maximum likelihood fit.*

and the B vertices and the B momentum approximated by the $D\ell$ system. A Monte-Carlo correction is applied to correct for the missing neutrino.

The measured time asymmetries are shown together with the fit in Figure 3. The B_d^0 mixing frequency is measured : $\Delta m_d = 0.471\ ^{+0.078}_{0.068}$ (stat) $\pm$ 0.034 (syst) ps^{-1}. The systematical uncertainty is dominated by the knowledge of the sample composition (D^{**} background); however the result is still clearly statistically dominated.

2.2 An example : the BaBar analysis using exclusive reconstruction

This analysis [4] relies on the very large B_d^0 mesons sample accumulated by the BaBar experiment. The B_d^0 is fully reconstructed using the modes : $B_d^0 \to D^{(*)-}\pi^+/\rho^+/a_1^+$ and $B_d^0 \to J/\Psi K^{*0}$. The signal sample contains about 7300 candidates which a very high purity (86 %). The initial state tagging is sequential : a high momentum lepton is searched for among the remaining tracks in the event, in the case where no lepton is found, charged kaons are identified. If no charged kaons are identified a neural network is used to tag the event taking the information from soft pions from $D^{*\pm}$ decays, and fast pions

from the W decay. The time difference is obtained from the distance between the two B vertices. Both the tagging performances and the time resolution function parameters are directly extracted on the data by the fit itself. The time distributions for mixed and unmixed events are shown on Figure 4 as well as the fit which is superimposed. The B_d^0 mixing frequency is measured : $\Delta m_d = 0.516 \pm 0.016$ stat ± 0.010 syst ps^{-1}. The systematical uncertainty is dominated by the knowledge of the alignment and of the resolution function parameters which are parameters of the fit. This systematical uncertainty has thus clearly a part which is of statistical nature and which will decrease in the future.

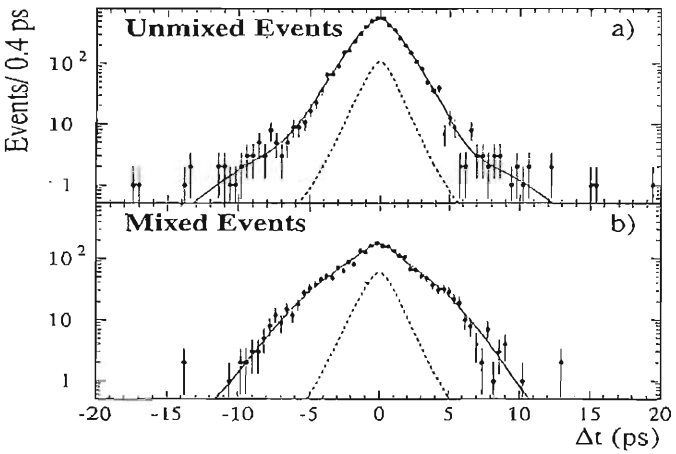

Figure 4: *Time distributions for the unmixed (a) and mixed (b) events. The points are the data, the line is the result of the unbinned maximum likelihood fit over the full sample.*

3 Δm_s results

3.1 Overall result

In this case the frequency which is studied is expected to be about 20 times larger than the B_d^0 mixing frequency. The time resolution is now crucial and in all the analyses emphasis has been put on this point. As no measurement has yet been performed, one has to face various problems such as limit setting,

handling of the systematics and combination of several limits. These problems have been overcome by the use of the amplitude method which consists in adding an amplitude factor in front of the oscillating term [5] (see Eq. 5).

$$\frac{1}{\tau}\, e^{-t/\tau}\, \frac{1 \pm \cos(\Delta m_s t)}{2} \rightarrow \frac{1}{\tau}\, e^{-t/\tau}\, \frac{1 \pm \mathcal{A} \cos(\Delta m_s t)}{2} \qquad (5)$$

For various frequencies one is left with the task of *measuring* this amplitude. To get the average limit $\Delta m_s > 14.4\ ps^{-1}$ at 95% CL 13 analyses have been combined and the limit is set at the Δm_s value for which $\mathcal{A} + 1.645\sigma_{\mathcal{A}} = 1$ which is the standard definition of a one-sided 95 % CL limit. The relative weights of the various analyses vary for different Δm_s values. The overall amplitude plot is shown on Figure 5. Several points should be emphasised : the result is fully dominated by the statistical uncertainty, the limit set is below the sensitivity ($19.2\ ps^{-1}$) and the uncertainties from a point to another are extremely correlated due to the fact that the same data is used.

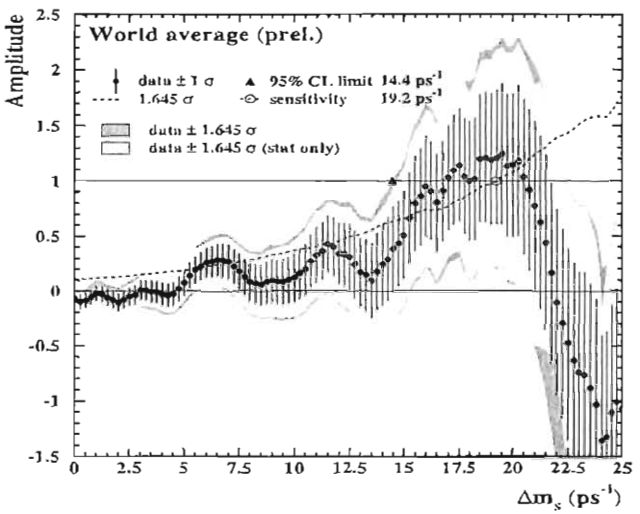

Figure 5: *Amplitude distribution obtained from the average of the 13 available analyses.*

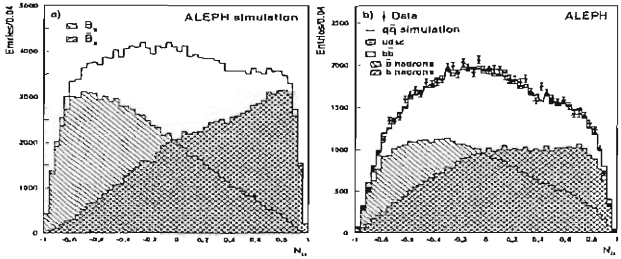

Figure 6: *Initial state tagging variable : for simulated events (a) and for all selected events (b). Neural network outputs for data (points) and MC (histogram) the two shaded distributions show the NN outputs for b and $\bar{b}$ quarks as seen on Monte Carlo.*

3.2 An example : the ALEPH analysis

This analysis [6] incorporates different final state reconstructions. The exclusive reconstruction is characterised by an excellent time resolution which compensates for the very low statistics. With reduced purity the $D_s\ell$ reconstruction has still a good time reconstruction. The last analysis is a fully inclusive reconstruction in which the very large statistics compensates for poorer time reconstruction and for the imperfect final state tagging.

The initial state tagging is performed using a sophisticated algorithm which includes the outputs of various subnets in a final neural network. The dedicated subnets are used for Same Side Tagging (a fragmentation kaon is identified via its momentum, its dE/dx and its proximity with the B_s^0 candidate), as well as for Opposite Side Tagging (the charges of the secondary and primary vertices and of the leptons and kaons if any are used). Figure 6 shows that the NN outputs for data and MC are in very good agreement. The limit is set at $\Delta m_s > 10.9$ ps^{-1} at 95% CL.

3.3 An example : the SLD analysis

Its main characteristics [7] are a very good decay length reconstruction due to the very precise vertex detector and to the small beam spot and a powerful initial state tagging which makes use of the polarised forward-backward asymmetry : polarised electrons tag b quarks in the forward hemisphere. Adding the

information of the jet, vertices as well as of leptons and kaons a mistag fraction as low as 23 % is obtained for a 100% efficient tagging. The final state reconstruction is performed using two different techniques The first one reconstructs a $D\ell$ pair in which the D is only identified topologically. A Neural Network is used to suppress the $b \to c \to \ell$ contribution. The other technique is more inclusive since it consists of reconstructing topologically both the secondary and the tertiary vertices. The final state tagging is done using the so-called charge dipole which is built from the difference of the charges of the secondary (B) and the tertiary (D) vertices multiplied by the distance between these two vertices. The limit is set at $\Delta m_s > 7.6$ ps^{-1} at 95% CL. The amplitude plot is shown on Figure 7. It is worthwhile noting that the sensitivity of this analysis is relatively high : 13.0 ps^{-1}, due to the very good decay length reconstruction and that this result has been obtained with 400000 Z^0 only.

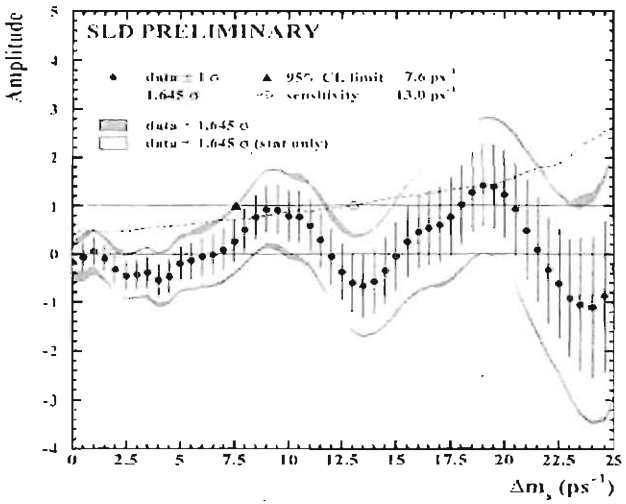

Figure 7: *Amplitude distribution obtained by the SLD experiment.*

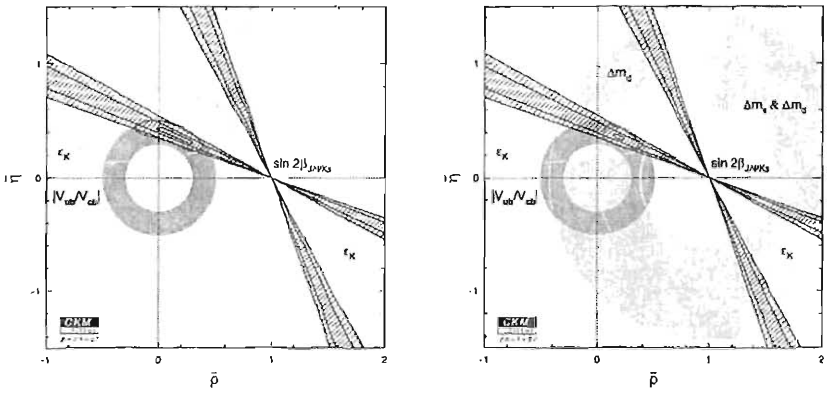

Figure 8: *The preferred region in the $(\bar{\rho}, \bar{\eta})$ is shown together with the various constraints used in the fit (V_{ub}/V_{cb}, ε_K, $\sin 2\beta$). For the left plot, the informations from the B_d^0 and B_s^0 mixing are not used whereas for the right plot they are included. In that last case, the preferred region is reduced by a factor two.*

4 Influence on the Unitarity Triangle

Using the Wolfenstein parametrisation, the CKM matrix can be expressed in the following way :

$$V_{CKM} = \begin{pmatrix} 1-\frac{\lambda^2}{2} & \lambda & A\lambda^3(\rho - i\eta) \\ -\lambda & 1-\frac{\lambda^2}{2} & A\lambda^2 \\ A\lambda^3(1-\rho-i\eta) & -A\lambda^2 & 1 \end{pmatrix} + \mathcal{O}(\lambda^4) \qquad (6)$$

Using the ratio of Eq 3, it follows immediately that the constraint due to the B^0 mixing frequencies appears as a circle in the (ρ, η) plane. Using the results of [8] and omitting the constraints from Δm_d and Δm_s one gets the preferred region shown on the left plot of Figure 8. Including the constraints due to the mixing analyses one gets the results shown on the right plot of Figure 8, the area of the preferred region is reduced by a factor of the order of two.

5 Summary

Since the first evidence of $B_d^0\bar{B}_d^0$ oscillation obtained by ARGUS in 1987, an important number of analyses have been developed and are now combined to get an impressive 1.2% precise measurement : $\Delta m_d = 0.503 \pm 0.006$ ps^{-1}. This

average is now fully dominated by the B factories analyses.

In the case of the B_s^0 mixing frequency measurement a first limit was set by ALEPH in 1994 : $\Delta m_s > 1.9$ ps^{-1} at 95% CL. However, eight years later, despite a lot of improvements in the analyses, the B_s^0 mixing frequency has not yet been measured and only a limit is set : $\Delta m_s > 14.4$ ps^{-1} at 95% CL with an overall sensitivity of 19.2 ps^{-1}. One can reasonably hope that it will be measured at the Tevatron next year by the D0 and CDF collaborations ... or may be one should better wish that it is so high (> 40 to 50 ps^{-1}) that it can't be measured at the Tevatron, this would clearly be a sign of new physics !

6 Acknowledgements

My first thanks go to the First International Workshop on Frontier Science organising committee for this nice conference and to the BaBar Collaboration for offering me the opportunity to give this talk. I also want to thank Sandrine Laplace who has kindly agreed to run the CKM-fitter [8] without and with the $B^0\bar{B}^0$ constraints. All the averages are kindly provided by the LEP B-Oscillations Working Group which I thank. Finally, I thank Anne-Marie Lutz for the careful reading of this proceeding.

References

1. K. Hagiwara *et al*, Phys Rev D 66, 010001 (2002).
2. LEP B Oscillation WG, results for summer 2002 conferences
3. CDF Collaboration, Phys. Rev. Lett. **80**, 2057 (1998).
4. BABAR Collaboration, Phys. Rev. Lett. **88**, 221802 (2002).
5. H-G Moser and A. Roussarie, Nucl.Instrum.Meth. **A384**, 491-505 (1997).
6. ALEPH Collaboration, CERN-EP-2002-016, Feb 2002 submitted to Eur. Phys. J. C.
7. SLD Collaboration, SLAC-PUB-8568, contributed paper to ICHEP2000 (Osaka).
8. A. Höcker *et al*, Eur.Phys.J. **C21**, 225-259 (2001) and references therein.

Frascati Physics Series Vol. XXXI (2003), pp. 213
FRONTIERSCIENCE 2002 – Frascati, October 6–11, 2002
Invited Review Talk in Plenary Session

CP VIOLATION IN SYSTEMS OTHER THAN HEAVY FLAVOURS

R. Ray

Fermi National Accelerator Laboratory, Batavia, Illinois, USA

Written contribution not received

Flavour Dynamics and CP Violation – Session III

Chairpersons: P. Franzini, R. Baldini

G. Ross	Theories of Flavour Mixing and CP Violation
M. Martini	Status on ε'/ε Measurement
S. Denisov	Search for CP Violation in Charged Kaon Decays
M. Sokoloff	CP Violation in Charm and Beauty
B. Melić	Nonfactorizable Effects in the $B \to J/\psi K$
U. Egede	Mixing in the D^0–$\bar{D}^0$ System at BABAR
A.A. Petrov	Mixing and CP Violation in Charmed Mesons

Frascati Physics Series Vol. XXXI (2003), pp. 217
FRONTIERSCIENCE 2002 – Frascati, October 6–11, 2002
Invited Review Talk in Plenary Session

THEORIES OF FLAVOUR MIXING AND CP VIOLATION

G. Ross

Oxford University, UK

Written contribution not received

Frascati Physics Series Vol. XXXI (2003), pp. 219–228
FRONTIERSCIENCE 2002 – Frascati, October 6–11, 2002
Invited Review Talk in Plenary Session

STATUS ON ϵ'/ϵ MEASUREMENT

Mara Martini*
Ferrara University and INFN

ABSTRACT

Kaons have strongly influenced the construction of the Standard Model. During the last ten years the measurement of the direct CP violation in the $K^0 - \overline{K^0}$ system has been vigorously carried out by the experiments NA48 at CERN and KTeV at Fermilab. We review recent results on the direct CP violation search and the experimental techniques used. The final result from NA48 is $Re(\epsilon'/\epsilon) = (14.7 \pm 2.2) \times 10^{-4}$ establishes the existence of direct CP violation.

1 CP violation in the neutral Kaon system

CP Violation has been discovered in the neutral Kaon system in 1964 [1].
In strong interactions K_0 and $\bar{K}_0$ are produced differing only by their strangeness

* On behalf of NA48 collaboration

value. Their linear combinations K_1 and K_2 are CP eigenstates. However the physical mass-states, K_S and K_L deviate, from pure CP $= \pm 1$ eigenstates: the long-lived K_L is made 99.8% of K_1, which decays in three bodies, but it also contains 0.2% of K_2 which allows the decay into 2 bodies. This kind of CP Violation is the main component of the effect and it is called *Indirect* as it comes from the mixing and it is described by the parameter ε.
Moreover another type of CP Violation can occur in Kaon decays to two pions as the K_L can also decay to 2 bodies via its K_2 component, through the so-called penguin diagrams allowing the interference of amplitudes in different isospins. This effect is called *Direct* CP Violation and is described by the parameter ε'.
In the Standard Model both indirect and direct CP Violation appears naturally because the existence of more than two quark families implies an irreducible complex phase in the CKM matrix [2].
The quantity which can be measured experimentally is the double ratio R of the decay widths:

$$R = \frac{\Gamma\left(K_L \to \pi^0\pi^0\right)/\Gamma\left(K_S \to \pi^0\pi^0\right)}{\Gamma\left(K_L \to \pi^+\pi^-\right)/\Gamma\left(K_S \to \pi^+\pi^-\right)} \approx 1 - 6 \times Re(\varepsilon'/\varepsilon) \qquad (1)$$

On the theoretical side, the short distance contributions to ε'/ε are under control [3] but the presence of considerable long distance hadronic uncertainty precludes a precise value of ε'/ε in the Standard Model. Consequently while theorists were able to predict the sign and the order of magnitude of the effect, the range is still pretty wide: $(\varepsilon'/\varepsilon)_{th} = (5 \text{ to } 30) \times 10^{-4}$

2 $\mathbf{Re}(\varepsilon'/\varepsilon)$ measurements

In the experimental reality the double ratio R of equation (1) is measured by detecting the four decay modes in the detector acceptance. Later the true $Re(\varepsilon'/\varepsilon)$ value is deduced correcting for fluxes, acceptances, detector efficiencies and effects from accidental induced event losses.
At first order corrections on R cancel if data are collected simultaneously in the four decay modes. Only second order differential effects have to be quantified. As $Re(\varepsilon'/\varepsilon)$ is expected to be small a significant result can be achieved if an high experimental accuracy ($\approx 10^{-4}$) is reached. This means that more than 3×10^6 $K_L \to \pi^0\pi^0$ decays, which is the statistical limiting mode, must be

collected.

2.1 The first generation of experiments

The first generation of experiments have been designed to achieve a statistical error of the order of $\approx 10^{-3}$. They published their final result on $Re(\epsilon'/\epsilon)$ in 1993:

$$\begin{array}{ll} \text{NA31 at CERN } [4] & (23.0 \pm 6.5) \times 10^{-4} \\ \text{E731 at Fermilab } [5] & (7.4 \pm 5.9) \times 10^{-4} \end{array}$$

They were both fixed target experiments exploring different method to build the K_S beam. E731 measured one single final mode at the time with simultaneous beams using the regenerator technique. Some data were also taken with the four modes. NA31 recorded both final modes in a single beam. The K_S target had 41 different positions in order to simulate the K_L decay vertex distribution. The two experiments had different systematics, their results were inconclusive: NA31 claimed the existence of Direct CP Violation with 3.5 standard deviations significance while E731 found a result compatible with zero.

2.2 The second generation of experiments

The new experiments have been conceived in order to achieve precisions on $Re(\epsilon'/\epsilon)$ of $\approx 1 - 2 \times 10^{-4}$ and to collect simultaneously the four decay modes: NA48 [6] at CERN, KTeV [7] at Fermilab and KLOE [8] at Frascati.
This paper is an attempt to drawn a comparative presentation of KTeV and NA48 as they have recently published results.

3 Beams and Detectors

NA48 and KTeV are fixed target experiments. NA48 uses the 450 GeV/c SPS protons [1] and two targets, while KTeV profits of the 800 GeV/c protons from the Tevatron and of the regeneration technique for K_S production.

[1] in 2001 the machine duty cycle was improved and 400 GeV/c protons were extracted from the SPS

3.1 KTeV implementation

In the KTeV experiment two parallel K_L beams from the same beryllium target are produced cleaned and collimated and let fly for 120 m. One beam is going through an active regenerator made of plastic scintillator blocks ($2\lambda_I$) and because of the K_0 and $\bar{K}_0$ different nuclear cross section a component ρ of regenerated K_S take places (regenerated beam).
The charge decays modes are reconstructed by a magnetic spectrometer while the neutral decays modes by the an electro-magnetic calorimeter made of 3100 pure CsI crystals. The CsI calorimeter [9] performs very well in terms of energy resolution ($\sigma_E/E = 2\%/\sqrt{E} \oplus 0.4\%$) and the non-linearity is within 0.5% for all the energy range (2-100 GeV). The detector has two holes to let the neutral beams to go through. The regenerator moves from one hole to the other every minute, in such a way that K_L and K_S decays are equally sensitive to eventual left-right asymmetries of the detectors.

3.2 NA48 implementation

NA48 uses two different production targets, located 126 m and 6 m upstream the decay region, in order to take into account the different mean decay lengths of K_L and K_S. The K_S beam is created close to the detector by deviated protons hitting the second target. The two beams are quasi-collinear and converge at the LKr with an angle of 0.6 mrad. The charge decays modes are reconstructed by a magnetic spectrometer while the neutral decays modes by the an electro magnetic calorimeter made of a 10 m^3 tank of liquid Krypton and 13212 channels. The LKr calorimeter [10] is very stable and offers a good energy resolution ($\sigma_E/E = 3.2\%/\sqrt{E} \oplus 9\%/E \oplus 0.42\%$) and a very little non-linearity ($< 0.1\%$). The detector is traversed by a beam pipe which confines the intense neutral beam.

3.3 Data samples

The following table summarise the NA48 and KTeV data taking periods. Both experiments published first results in 1999.

4 Analysis strategy

Here it follows a list of some of the main analysis items.

Year	KTeV	# of $K_L \to \pi^0\pi^0$	NA48	# of $K_L \to \pi^0\pi^0$
1996	$Re(\epsilon'/\epsilon)$		debugging	
		2.5×10^6		
1997	$Re(\epsilon'/\epsilon)$		$Re(\epsilon'/\epsilon)$	0.5×10^6
1998	Not running		$Re(\epsilon'/\epsilon)$	
				3.3×10^6
1999	$Re(\epsilon'/\epsilon)$	2.5×10^6	$Re(\epsilon'/\epsilon)$	
2000			Checks	
2001			$Re(\epsilon'/\epsilon)$	1.4×10^6

4.1 Kaon identification: KTeV K_S regeneration

The identification of the Kaon type in KTeV is made looking at the center of gravity, in both charged and neutral decay modes. As the left-right position of the regenerator is known and the two parallel beams are 10 cm apart a K_L decay is unambiguous disentangled from a K_S decay. The advantage of using a regenerator is in the fixed ratio of regenerated and vacuum decays. However care must be taken to identify inelastic and diffractive Kaon scattering. In the energy centroids in the calorimeter the shadow of the two beam holes apart 10 cm is visible. One of the two beam projection has an evident halo, which comes from scattered events in the regenerator. The effect is precisely studied in charge mode looking at the ${P_T}^2$ distribution and then introduced into the simulation for evaluate its contribution to the neutral mode. The regenerator scattering is an important background to $\pi^0\pi^0$ events in the regenerator beam (1.13%) while is only 0.25% in the vacuum beam. The regenerator vertex Z distribution for two pion events shows a clear $K_S - K_L$ interference pattern, which implies a K_L contamination of 3×10^{-3} while is down to 10^{-5} in NA48.

4.2 Kaon identification: NA48 proton tagging

In order to distinguish K_L and K_S decays, the protons directed to the K_S target are detected by an array of scintillation counters which comprise the tagging detector. The presence (absence) of a proton in coincidence (within 2 nsec) with the event time as measured by the detector, defines the event as K_S (K_L). The tagging performances is straightforward for $\pi^+\pi^-$ events, where the good charge vertex resolution can be used.
Whenever the time measurement of one of the components of the tagging sys-

tem fails, a K_S can be misinterpreted as a K_L ($\alpha_{SL}{}^{\pm} = (1.12 \pm 0.03) \times 10^{-4}$)[2]. However the effect tend to cancel out between $\pi^+\pi^-$ and $\pi^0\pi^0$ and only the difference requires a correction to R, which turn out to be negligible with an uncertainty of $\pm 3.0 \times 10^{-4}$. Occasionally due to the high rate of protons crossing the tagger, in time coincidence with a genuine K_L one can find a proton, which induces the K_L to be misidentified as s K_S ($\alpha_{LS}{}^{\pm} = (8.115 \pm 0.010)\%$). Again, it is the neutral-charge difference which is relevant and the correction $\Delta R = (6.9 \pm 2.8) \times 10^{-4}$ was derived.

4.3 Charge mode reconstruction

Both experiments use a magnetic spectrometer with four drift (wire for KTeV) chambers and reconstruct the decaying particle's mass, the momentum and the vertex position under the $\pi^+\pi^-$ assumption. The resolution in the reconstructed Kaon mass is $\sigma(\pi^+\pi^-)$=2.5 MeV for NA48 and $\sigma(\pi^+\pi^-)$=1.6 MeV for KTeV which bending power is stronger.
The 3-body background to $K_S \to \pi^+\pi^-$ is negligible while it is important for $K_L \to \pi^+\pi^-$, mainly due to K_{e3} and $K_{\mu 3}$. It is rejected by a $P_T{}^2$ cut and the residual $K_{\mu 3}$ background is tagged by the muon veto detector while the K_{e3} decays are recognised from the ratio $\frac{E}{p}$.
The amount of left-over background is similar for the two experiments: for KTeV is 0.09% for the vacuum beam and 0.003% for the regenerator one, while in NA48 it is 0.14%.

4.4 Neutral mode reconstruction

The $K \to \pi^0\pi^0$ are reconstructed using energies and positions of four photons in the calorimeter. NA48 reconstructs m_{π^0} and the vertex decay position using the M_K constraint, while KTeV reconstructs the M_K and vertex decay position using the m_{π^0} constraint. Both compute a χ^2 to test the event compatibility with the $\pi^0\pi^0$ hypothesis. The $3\pi^0$ background with fused or lost photons is located in the tail of the χ^2 distribution. The final $3\pi^0$ background level is 0.06% in NA48 while is 0.11% in the KTeV vacuum beam and 0.03% in the regenerator one. Furthermore, in KTeV, the regenerator contributes to an

[2]Here we report the result of the analysis of 2001 data taken with slightly different condition from 1998-1999 data period

additional kind of background which becomes especially important in neutral final states (1.23%).

4.5 Definition of the fiducial volume

This is a crucial point as the fiducial volume has to be the same for $\pi^0\pi^0$ and $\pi^+\pi^-$ decays to allow the cancellation of the fluxes of Kaon in the ratio. It is defined by applying cuts on the reconstructed Kaon energy and the decay vertex position. The distance scale is then translated in energy scale definition. The uncertainty introduced on R is small if the beginning of the K_S decay region is defined by the position of a geometrical object by vetoing K_S decays occurring upstream. The uncertainty of 1 cm on the vertex position is induceing an error of 10^{-4} on the energy scale. KTeV uses the regenerator edge, which position is reconstructed and adjusted with the Monte carlo with a precision of $\approx$5 cm. NA48 uses the position of a set of scintillators with a converter (called AKS) which is reconstructed with an uncertainty of $\approx$3 cm.

4.6 Acceptance to four modes

Because of the very different K_L and K_S lifetime the average acceptance for decays in the two beams is different.
The acceptance correction on R in KTeV is based on a detailed Monte carlo simulation, tuned with $K_L \to \pi e\nu$ and $K_L \to \pi^0\pi^0\pi^0$ decays, and it is as large as 5.1%. However this is mostly due to the well-know detector geometry (85%). The remaining effort is to understand detector response and resolution. The errors quoted on this correction to R are derived from data-Monte carlo comparison in $\pi^+\pi^-$ and $\pi^0\pi^0\pi^0$ events.
NA48 weights the K_L events by the reconstructed K_S lifetime in order to minimise $K_L - K_S$ decay spectra differences. The acceptance correction to R in calculated after weighting and it is decreased to the 0.22%, with a precision limited by the knowledge of the beam positions and shapes. The drawback of the weighting method is a 35% increase of the statistical error on R.

5 Fitting R

In NA48 the four final decay distributions, corresponding to $\pi^+\pi^-$ and $\pi^0\pi^0$ decays for K_L and K_S, are corrected for the mistagged fraction of K_L events

and for trigger inefficiencies, weighted and background subtracted. The raw R ratio is corrected for the acceptance in 5 GeV energy bins and the final result is given combining 20 values with an unbiased estimator shown in figure 1. KTeV after background subtraction has four samples corresponding to Vacuum beam (K_L decays) and Regenerator beam (essentially K_S decays) to $\pi^+\pi^-$ and $\pi^0\pi^0$ final modes. They are corrected for acceptances from the very detail Monte carlo that include all other possible effects. Data are fitted in 10 GeV bins, as in figure 2, resulting in $Re(\epsilon'/\epsilon)$ and two regenerator parameters.

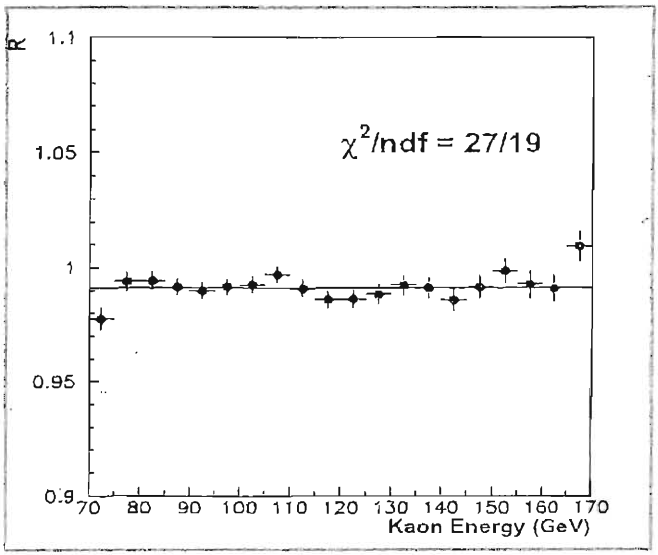

Figure 1: *Final result for the double ratio in 5-GeV energy bins as fitted by NA48.*

5.1 Results

The experimental world average result on $Re(\epsilon'/\epsilon)$ is $(16.7 \pm 2.3) \times 10^{-4}$. The NA48 measurement $(14.7 \pm 2.2) \times 10^{-4}$ is the average of the three results for each data taking period: 1997 $(18.5 \pm 4.5 \pm 5.8) \times 10^{-4}$ [11], 1998-1999 $(15.0 \pm 1.7 \pm 2.1) \times 10^{-4}$ [12] and 2001 $(13.7 \pm 2.5 \pm 2.0) \times 10^{-4}$ [13].

The KTeV measurement $(20.7 \pm 2.8) \times 10^{-4}$ is the average of two different data sets : 1996-1997a (improved analysis) $(23.2 \pm 3.0 \pm 3.9) \times 10^{-4}$ and 1997b $(19.8 \pm 1.7 \pm 2.9) \times 10^{-4}$ [14]. KTeV has still to analyse an equal amount of data.

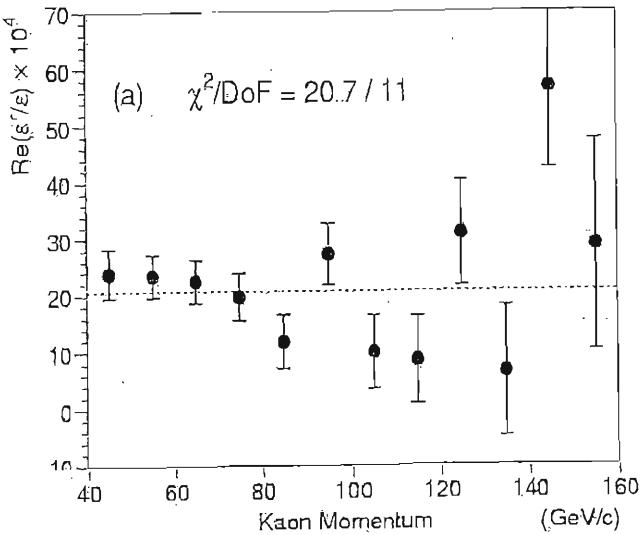

Figure 2: *Data from KTeV in 10-GeV energy bins.*

5.2 Cross checks

Many many check have been made to test the stability of the results against the cut variations or grouping data in periods. KTeV has also introduce a weighted analysis which results differs from the standard one by only $(1.5 \pm 3.9) \times 10^{-4}$.

6 Conclusions

Is almost 40 years that a significant portion of the physics community tried to understand the CP violation phenomenum in the Kaon system. Different techniques have been used by two groups to measure $Re(\epsilon'/\epsilon)$. This showed the importance of several systematics. The value of $Re(\epsilon'/\epsilon) = (16.7 \pm 2.3) \times 10^{-4}$ is

now stabilised and solid: Direct CP Violation exists and it is precisely measured (10σ). However theoretical predictions have still large uncertainties.

References

1. J.H. Christenson *et al*, Phys. Rev. Lett. **13**, 138 (1964).
2. M. Kobayashi and K. Maskawa, Prog. Theor. Phys. **49**, 652 (1973).
3. A.J. Buras, Flavour physics and CP Violation in the SM, in: Proc. KAON 2001, International Cpnference on CP Violation (ed. F. Costantini, G. Isidori, M. Sozzi, Pisa, June 2001), 1, 15 (Frascati Physics Series).
4. G. Barr *et al*, Phys. Lett. B **317**, 233 (1993).
5. L.K. Gibbons *et al*, Phys. Rev. Lett. **70**, 1203 (1993).
6. G.D. Barr *et al*, CERN/SPSC/90-22 SPSC/P253 (1990).
7. K. Arisaka *et al*, FERMILAB-FN-580 (1992).
8. M. Adinolfi, *et al.* (the KLOE collaboration), KLOE: A general purpose detector for Dafne, LNF-92/019 (IR). M. Adinolfi, *et al.* (the KLOE collaboration), The KLOE detector, technical proposal, LNF-93/002 (IR).
9. R.S. Kessler *et al*, Nucl. Inst. Meth. A **368**, 653 (1996).
10. G.D. Barr *et al*, Nucl. Inst. Meth. A **370**, 413 (1996).
11. V. Fanti *et al*, Phys. Lett. B **465**, 335 (1999).
12. A. Lai *et al*, Eur. Phys. J. C **22**, 231 (2001).
13. J.R. Batley *et al*, Phys. Lett. B **544**, 97 (2002).
14. A. Alavi-Harati *et al*, accepted by Phys. Rev. D. (Nov. 8,2002).

Frascati Physics Series Vol. XXXI (2003), pp. 229–232
FRONTIERSCIENCE 2002 – Frascati, October 6–11, 2002
Invited Contribution in Plenary Session

SEARCH FOR CP-VIOLATION IN CHARGED KAON DECAYS

S. Denisov *
Institute for High Energy Physics, Protvino, Russia

ABSTRACT

The first experiment dedicated to the measurement of the charge asymmetry of Dalitz plot parameters for $K^{\pm} \to \pi^{\pm}\pi^0\pi^0$ decays is described. The results on the linear and quadratic coefficients and the charge asymmetry of the slope are presented.

1 Introduction

Recent results [1] on the direct CP-violation obtained with K^0 beams at CERN and Fermilab demonstrate that CP-violation can also be observed for $K^{\pm}$ de-

*coauthors A.Durum, G.Akopdzhanov, V.Anikeev, V.Bezzubov, Yu.Gilitsky, S.Gurzhiev, V.Korablev, V.Koreshev, A.Kozelov, E.Kozlovsky, V.Kurbakov, V.Lipaev, V.Onuchin, A.Rybin, Yu.Sapunov, A.Schukin, M.Soldatov, K.Trushin, A.Usachev, I.Vasilyev, V.Yakimchuk, S.Zvyagintsev, *Institute for High Energy Physic, Protvino, Russia*

cays, in particular for $K^{\pm} \to \pi^{\pm}\pi^0\pi^0$ by measuring the charge asymmetry of the Dalitz plot slope $\Delta g = (g^+ - g^-)/(g^+ + g^-)$. At this moment both theoretical and experimental estimations of Δg are rather uncertain. Theoretical predictions are model dependent and vary from about 10^{-3} to 10^{-6}. The most precise experimental results [2, 3] obtained in the independent experiments and quoted in PDG-2002 [4] give Δg=0.117±0.020. It is very unprobable to expect the CP-violation at this level and one can assume that systematic errors are underestimated in one or both experiments. New data on $g^- = 0.697 \pm 0.007^{stat} \pm 0.019^{syst}$ published in May 2002 [5] somewhat clarify the situation. Using this result and those from [3] one can obtain Δg=0.027±0.011(stat)±0.016(syst).

It is hard to expect that the systematic error of Δg can be less than 10^{-2} if Δg is derived from different experiments. So both g^+ and g^- should be measured simultaneously in the same high statistics experiment to reach the accuracy of the order of 10^{-3} or better. Such an experiment [6] was performed for $K^{\pm} \to \pi^{\pm}\pi^{\pm}\pi^{\mp}$ decays where $\Delta g = -0.0070 \pm 0.0053$ was obtained. The results of the first experiment dedicated to search for the direct CP-violation in $K^{\pm} \to \pi^{\pm}\pi^0\pi^0$ decays are presented in this report.

2 Experimental setup

The experiment was performed at 70 GeV IHEP accelerator. The experimental layout is shown in Fig.1. Unseparated 35 GeV/c positive and negative hadron beams produced by 70 GeV protons in the external 30 cm Al target were used for kaon decay studies. The typical particle flux was 4×10^6 per 1.7 s spill. Scintillation counters S1-S4 and beam hodoscopes BH1-BH4 were used to monitor the beam intensity and to measure particle trajectories and beam profiles. Kaons were selected with three threshold C1-C3 and two differential D1, D2 gas Cherenkov counters. The threshold counters were also used to select 10 GeV/c electrons to calibrate GEPARD calorimeter.

About 20% of kaons decayed in the 58.5 m vacuum pipe. Kaons that pass the decay pipe were detected by the anticoincidence scintillation counter AC.

Particles from kaon decays were detected by the three scintillation hodoscopes H1-H3 [7] and the gamma spectrometer GEPARD consisted of 1968 lead-scintillator cells. GEPARD calibration was made using both 10 GeV/c electron beam scanned over all cells and reconstructed events of $K^{\pm} \to \pi^{\pm}\pi^0$ decays. Both methods gave consistent results. The π^0 mass resolution obtained from the reconstructed decays turned out to be 13 MeV.

Signals from the scintillation and Cherenkov counters were used to form the first level trigger $T1 = S1 \cdot S2 \cdot S3 \cdot S4 \cdot (D1 + D2) \cdot \overline{C1} \cdot \overline{C2} \cdot \overline{C3} \cdot \overline{AC}$.

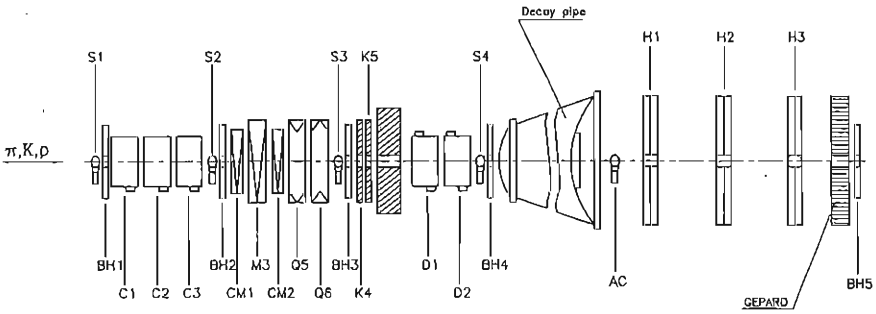

Figure 1: *Experimental setup (M – magnets, Q – quadrupoles, K – collimators, S – beam counters, BH – beam hodoscopes, C – threshold Cherenkov counters, D – differential Cherenkov counters, AC - anticoincidence counter, H – scintillation hodoscopes).*

For the further reduction of the trigger rate down to 10^3 per spill 3 or more clusters with energy above 1 GeV were required to be registered in GEPARD.

Stability of the particle beam and detectors was carefully monitored during the runs. Beam polarity was changed every 1-2 days to minimize systematic uncertainties in measuring charge asymmetry for $K^{\pm}$ decays.

3 Data analysis and results

Two sets of criteria were used for off-line selection of $K^{\pm} \to \pi^{\pm}\pi^0\pi^0$ decays. The first set includes the following main requirements: a) decay vertex is reconstructed with the confidence level of $\geq$0.05 and is inside the decay pipe, b) only one track is reconstructed in the H1 - H3 hodoscopes, c) 4 gammas with energies above 2 GeV are registered in GEPARD. In the second set the two last requirements were more loose: b) one or two tracks are reconstructed in the H1 - H3 hodoscopes, c) 4 gammas with energies above 1 GeV are registered in GEPARD. The selected events were subjected to a kinematic fit to check their consistence with the hypothesis of $K^{\pm} \to \pi^{\pm}\pi^0\pi^0$ decay. Events with confidence level higher than 0.05 were accepted.

Up to now about 50% of the total statistics have been analysed. The numbers of selected events are equal to 59k(K^+), 69k(K^-) and 227k(K^+), 285k(K^-) for the first and second sets of criteria respectively.

Kinematic parameters of the decays obtained in the fit were used to calculate the Dalitz plot variables u and v. The matrix element M of $K \to 3\pi$ decays as a function of u, v can be presented in the form [4]:

$$|M|^2 \propto 1 + g \cdot u + h \cdot u^2 + k \cdot v^2.$$

To estimate the Dalitz plot parameters g, h and k the least square fitting procedure with weighted MC events was used to obtain the best agreement between MC and experimental u, v-distributions of the events selected with the first set of criteria. Obtained parameters for K^+ and K^- decays turned out to be equal within the errors and their average values are:

$$g = 0.688 \pm 0.021, \quad h = 0.050 \pm 0.021, \quad k = -0.010 \pm 0.006.$$

To evaluate Δg the method mentioned above was applied to the difference of normalized u-distributions for K^+ and K^- events selected with the second set of criteria. As a result $\Delta g = -0.0003 \pm 0.0025(stat)$ was obtained. The systematic error was estimated to be less than $1.5 \cdot 10^{-3}$. This is the best experimental estimation of the charge asymmetry of the Dalitz plot slope.

We would like to thank A.Logunov, N.Tyurin, A.Zaitsev for the continuous support of our experiment. This work was supported in part by RFBR grants 00 15 96733 and 02 02 17019.

References

1. A.Glazov et al., Proc.Int.Conference on Kaon Physics, Frascati, 2001, p.115. J.R.Batley et al., Physics Letters B 544(2002) 97-112.
2. V.N.Bolotov et al., Sov.J.Nucl.Phys., 44(1986) 73.
3. V.Y.Batusov et al., Nucl.Phys., B516(1998) 3.
4. K.Hagiware et al., Physical Review D66, 010001 (2002).
5. I.V.Ajinenko et al., Preprint IHEP 2002-16.
6. W.T.Ford et al., Phys.Rev.Lett., 25(1970) 1370.
7. A.V.Vasiliev et al., Prib.Tekh.Eksp., N2(1993) 50.

Frascati Physics Series Vol. XXXI (2003), pp.233
FRONTIERSCIENCE 2002 – Frascati, October 6–11, 2002
Invited Review Talk in Plenary Session

CP VIOLATION IN CHARM AND BEAUTY

M.D. Sokoloff

Cincinnati University, 2624 Clifton Avenue, Cincinnati, Ohio

Written contribution not received

Frascati Physics Series Vol. XXXI (2003), pp. 235–238
FRONTIERSCIENCE 2002 – Frascati, October 6–11, 2002
Invited Contribution in Plenary Session

NONFACTORIZABLE EFFECTS IN $B \to J/\psi K^*$

B. Melić[†]
Institut für Theoretische Physik und Astrophysik,
Universität Würzburg, D-97074 Würzburg, Germany
Institut für Physik, Universität Mainz, D-55000 Mainz, Germany

ABSTRACT

The method of QCD light-cone sum rules is applied in the calculation of soft nonfactorizable contributions to the decay amplitude for $B \to J/\psi K$. The result confirms expectations that in color-suppressed decays nonfactorizable corrections can be sizable.

1 Decay amplitude

Precise measurements of exclusive nonleptonic B decays have initiated theoretical considerations which go beyond *the naive factorization approach* frequently

[*] Work done in collaboration with R. Rückl.

[†] Alexander von Humboldt Fellow. On leave of absence from the Rudjer Bošković Institute, Zagreb, Croatia.

used in the calculation of decay amplitudes. Nonfactorizable contributions have been investigated in several approaches [1, 2, 3] for different classes of two-body nonleptonic B decays. In this talk we focus on nonfactorizable corrections in the decay $B \to J/\psi K$. This channel is particularly interesting because of a substantial discrepancy between the prediction from naive factorization and experiment by more than a factor of three in the branching ratio. Also, this mode belongs to the color-suppressed class-2 decays for which large nonfactorizable contributions are expected.

The weak matrix element can be written in the form

$$\langle J/\psi K|H_W|B\rangle = \sqrt{2}\,G_F\,V_{cb}V_{cs}^*\,\epsilon\cdot q\,m_{J/\psi}f_{J/\psi}F_{BK}^+(m_{J/\psi}^2)\,a_2\,, \qquad (1)$$

where F_{BK}^+ is the $B \to K$ form factor and the parameter a_2 incorporates factorizable and nonfactorizable contributions. A particular useful parametrization is given by

$$a_2 = C_2(\mu) + \frac{C_1(\mu)}{N_c} + 2\,C_1(\mu)\,\frac{\tilde{F}_{BK}^+(\mu)}{F_{BK}^+(m_{J/\psi}^2)}\,, \qquad (2)$$

where $C_{1,2}$ are the short-distance Wilson coefficients. The first two terms in (2) result from the naive factorization, while the term proportional to $\tilde{F}_{BK}^+$ represents nonfactorizable contributions. Since a_2 parametrizes a physical decay amplitude, the scale dependence of the individual terms in a_2 must cancel. Taking $\mu = m_b$, one has, numerically, $C_1(m_b) = 1.802$ and $C_2(m_b) = -0.185$ [4].

2 Nonfactorizable effects

According to the large N_c analysis [5], there could be a cancellation between the last two terms in (2), which are both of order $1/N_c$ relative to the leading term. In case of such a cancellation, $a_2 \sim C_2$ would be negative. While the negative value of a_2 is consistent with experiment on D decays, experimental data on B decays suggest a positive a_2. However, different explicit estimates of nonfactorizable contributions in B decays have predicted different signs of a_2.

In [6], the *QCD light-cone sum rule method* [3] was applied to the calculation of soft nonfactorizable contributions in $B \to J/\psi K$. The relevant operators in the weak Hamiltonian H_W are

$$\mathcal{O}_2 = (\bar{c}\Gamma_\mu c)(\bar{s}\Gamma^\mu b)\,, \qquad \tilde{\mathcal{O}}_2 = (\bar{c}\Gamma_\mu \frac{\lambda^a}{2} c)(\bar{s}\Gamma^\mu \frac{\lambda^a}{2} b)\,. \qquad (3)$$

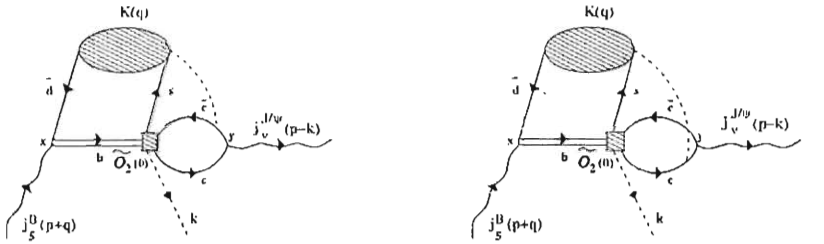

Figure 1: *Leading soft nonfactorizable contributions as estimated by QCD light-cone sum rules. The shaded ellipse denotes the K meson light-cone distribution amplitude. The currents $j_\nu^{J/\psi}$ and j_5^B generate states with J/ψ and B quantum numbers, respectively. The square stands for the $\tilde{O}_2$ four-quark weak operator* [6].

It is the contribution of $\tilde{O}_2$ to the matrix element (1), which is expected to give rise to the leading nonfactorizable effects. The sum rule approach allows to estimate the contribution of soft-gluon exchange between the J/ψ and the $B-K$ system, see Fig. 1. To this end, one has to isolate the ground state contribution in the correlation function [6]

$$F_\nu(p,q,k) = \int d^4x e^{-i(p+q)x} \int d^4y e^{i(p-k)y} \langle K(q)|T\{j_\nu^{J/\psi}(y)\mathcal{O}(0)j_5^B(x)\}|0\rangle \tag{4}$$

represented graphically in Fig.1. Taking to account twist-3 and twist-4 contributions calculated at the appropriate scale $\mu_b \sim m_b/2$, one finds

$$\tilde{F}_{BK}^+(\mu_b) = 0.009 - 0.017\,, \tag{5}$$

and substituting (5) in (2),

$$a_2 = 0.14 \div 0.17\,|_{\mu=\mu_b}\,. \tag{6}$$

Although the nonfactorizable matrix element (5) is rather small, it enhances a_2 by $30 \div 70\%$, due to the large coefficient $2C_1(\mu_b)$.

In addition, one has nonfactorizable contributions from hard-gluon exchange. They have been estimated in *QCD factorization* [1] and amount to another 25% correction [7]. Thus, in total one obtains

$$a_2 = 0.16 \div 0.19\,|_{\mu=\mu_b}\,. \tag{7}$$

One can see, that the theoretical expectation (8) is still too small to explain the experimental value

$$|a_2|^{exp} = 0.29 \pm 0.03\,. \tag{8}$$

However, it is interesting to note, that the theoretical approach described here predicts a positive sign of a_2 in agreement with experiment and in the contradiction with the argument based on $1/N_c$ expansion [5]. Finally, a comparison of the value (8) deduced from the measurement of $B \to J/\psi K$ with $|a_2|^{exp} = 0.4 \div 0.5$ for $\overline{B}^0 \to D^{(*)0}\pi^0$ decays [8] indicates a substantial nonuniversality of a_2 in color-suppressed decays.

Acknowledgments

I wish to thank the organizers of Frontier Science 2002 for the invitation and for their support. I would also like to acknowledge the support by the Alexander von Humboldt Foundation and partial support of the Ministry of Science and Technology of the Republic of Croatia under the contract 0098002.

References

1. M. Beneke, G. Buchalla, M. Neubert, C.T. Sachrajda, Nucl. Phys. B **591**, 313 (2000); Nucl. Phys. B **606**, 245 (2001).

2. Y.-Y. Keum, H.-n. Li, A.I. Sanda, Phys. Lett.B **504**, 6 (2001); Phys. Rev. D **63**, 054008 (2001).

3. A. Khodjamirian, Nucl. Phys. B **605**, 558 (2001).

4. G. Buchalla, A.J. Buras, M.E. Lautenbacher, Rev. Mod. Phys. **68**, 1125 (1996).

5. A.J. Buras, J.M. Gerard, R. Rückl, Nucl. Phys. B **268**, 16 (1986).

6. B. Melić, R. Rückl, Soft nonfactorizable corrections to $B \to J/\psi K$, preprint WUE-ITP-2002-020.

7. H.-Y. Cheng, K.-Ch. Yang, Phys. Rev. D **63**, 074011 (2001).

8. M. Neubert, A.A. Petrov, Phys. Lett. B 519 (2001) 50.

Frascati Physics Series Vol. XXXI (2003), pp. 239–243
FRONTIERSCIENCE 2002 – Frascati, October 6–11, 2002
Invited Contribution in Plenary Session

MIXING IN THE D^0-$\bar{D}^0$ SYSTEM AT *BABAR*

Ulrik Egede*
Imperial College London,
London SW7 2BW,
United Kingdom

ABSTRACT

We report a preliminary result for D^0-$\bar{D}^0$ mixing and the doubly Cabibbo suppressed decay rate R_D based on an analysis of $D^0 \to K^+\pi^-$ decays from 57.1 fb^{-1} of data collected at or just below the $\Upsilon(4S)$ resonance with the *BABAR* detector at the PEP-II collider. We set 95% confidence limits for the mixing parameters x'^2 and y' and find that our result is compatible with no mixing and no CP violation. In the limit of no mixing we find the doubly Cabibbo suppressed decay rate $R_D = (0.357 \pm 0.022\ (\text{stat.}) \pm 0.027\ (\text{syst.}))\%$ and the CP violating asymmetry $A_D = 0.095 \pm 0.061\ (\text{stat.}) \pm 0.083\ (\text{syst.})$.

1 Motivation

Mixing can be characterised by the two parameters $x \equiv \Delta m/\Gamma$ and $y \equiv \Delta\Gamma/2\Gamma$, where Δm ($\Delta\Gamma$) is the difference in mass (width) between the two different mass

* On behalf of the *BABAR* collaboration.

eigenstates and Γ is the average width.

Within the Standard Model the level of D^0-$\overline{D}^0$ mixing and *CP* violation is predicted to be below the sensitivity of current experiments [1]. For this reason it is a good place to look for signals of physics beyond the Standard Model. Other experiments [2, 3] have already tried this with smaller datasets using a technique similar to what is described here. In any attempt to measure mixing one should consider the possibility of *CP* violation also as, with new physics, there is no *a priori* expectation that it is insignificant.

Mixing and *CP* violation can be detected by observation of the wrong-sign decay $D^0 \to K^+\pi^-$ (charge conjugation is implied unless otherwise stated). Production through direct decay is doubly Cabibbo suppressed (DCS) but it is also possible for the D^0 to oscillate into a $\overline{D}^0$ and subsequently decay through the right-sign Cabibbo favoured (CF) decay $\overline{D}^0 \to K^+\pi^-$. The two processes can only be distinguished by an analysis of the time evolution of the decay.

Assuming x', $y' \ll 1$ and that *CP* is conserved, the time-dependent decay rate for the wrong-sign decay $D^0 \to K^+\pi^-$ from DCS decays and mixing is

$$\Gamma(D^0 \to K^+\pi^-)(t) \propto e^{-t/\tau_{D^0}} \left(R_{\rm D} + \sqrt{R_{\rm D}} y' \, t/\tau_{D^0} + \frac{x'^2 + y'^2}{4} (t/\tau_{D^0})^2 \right) \quad (1)$$

where τ_{D^0} is the D^0 lifetime and $R_{\rm D}$ is the ratio of DCS to CF decays[1]. Because x' only appears in the time distribution as a squared value, it is not possible to determine the sign of x' in an analysis based on the $D^0 \to K^+\pi^-$ decay alone.

CP violation can be either direct, in mixing or in the interference between the two. The *CP* violation gives rise to different apparent values for the parameters in eq. 1 so we define $R_{\rm D}^{+(-)}$, $x'^{+(-)}$ and $y'^{+(-)}$ for D mesons produced as a D^0 ($\overline{D}^0$).

2 The *BABAR* detector and data selection

For this analysis, we use 57.1 fb^{-1} of data collected with the the *BABAR* detector which is described in detail elsewhere [4]. Reconstruction of charged particles and particle identification of Kaons and pions are the most essential. Tracking is provided by a five-layer silicon vertex tracker (SVT) and a

[1] $x' = x\cos\delta_{K\pi} + y\sin\delta_{K\pi}$ and $y' = -x\sin\delta_{K\pi} + y\cos\delta_{K\pi}$ where $\delta_{K\pi}$ is an unknown strong phase.

forty-layer drift chamber (DCH), both in a 1.5 T solenoidal magnetic field. A Cherenkov ring imaging detector (DIRC) is placed outside the tracking volume.

Kaons (pions) are identified by calculating a likelihood product of the information from dE/dx measurements in the SVT and DCH and the reconstructed Cherenkov angle and photon statistics from the DIRC, with an efficiency above 75% (80%) and mis-id rate below 8% (7%) for $p < 4$ GeV/c.

We select D^0 candidates from reconstructed $D^{*+} \to D^0\pi^+$ decays. The charge of the pion in the decay identifies the flavour of the D^0 and also serves to create a clean sample of D^0 decays. Both right-sign and wrong-sign D^0 candidates are selected. We select only D^{*+} candidates with $p_{D^{*+}} > 2.6\,\mathrm{GeV}/c$ in the centre-of-mass frame to reject D^{*+} candidates from B decays. Other event selection criteria are employed to ensure that we have high quality tracks and do not have any D^{*+} candidates with multiple overlapping tracks.

3 Results

An unbinned maximum likelihood fit is used to extract the mixing parameters. For each D^{*+} candidate we use the D^0 candidate mass $m_{K\pi}$, the mass difference δm between the D^{*+} and the D^0 candidate and the proper lifetime and error on the lifetime of the D^0 candidate. The D^0 lifetime and the signal resolution model is determined from the large right-sign sample. Sidebands are included in $m_{K\pi}$ and δm such that the level and time evolution of the different background types can be evaluated. In figure 1 we show the time evolution of the wrong-sign sample. In total we observe around 120,000 (440) right-sign (wrong-sign) signal events.

Since the fit allows x'^2 to take unphysical negative values an error estimate from the log-likelihood surface (LLS) would require a Bayesian analysis where the choice of prior is not clear. In addition, an accurate error estimate from the LLS requires a LLS shape that is independent of the outcome of the fit. At the current level of statistics these requirements are not even approximately met, especially for the small mixing values observed.

Instead we use a method where we define a 95% confidence limit contour in x'^2 and y' space using toy Monte Carlo experiments[2]. Contours are constructed

[2]With a toy Monte Carlo experiment we mean a Monte Carlo sample of the same size as the data generated from the PDF of the fit.

such that there is a 95% probability for any point $\vec{\alpha}_c = (x'^2_c, y'_c)$ on the contour that the likelihood ratio

$$\Delta \ln \mathcal{L}(\vec{\alpha}_c) = \ln \mathcal{L}(\vec{\alpha}_c) - \ln \mathcal{L}_{\max} , \qquad (2)$$

will be greater than the corresponding value $\Delta \ln \mathcal{L}_{\rm data}(\vec{\alpha}_c)$ calculated for the data. $\mathcal{L}_{\max}$ is here the maximum likelihood obtained from the fit to either data or a toy Monte Carlo sample. The probability is evaluated by creating multiple toy Monte Carlo samples at the point $\vec{\alpha}_c$ and for each of the samples evaluate $\Delta \ln \mathcal{L}(\vec{\alpha}_c)$ after a fit.

As well as for the general case allowing for *CP* violation we also calculate our results for the special cases where *CP* is conserved and where no mixing is allowed. In the case where we assume no mixing we calculate the direct *CP* violation term $A_D \equiv (R_D^+ - R_D^-)/(R_D^+ + R_D^-)$.

Table 1: *A summary of our results including systematic errors. A central value is reported for both the full fit allowing $x'^2 < 0$, and from a fit with x'^2 fixed at zero. The 95% confidence limits are for the case where x'^2 is free.*

		Fitted Central Value		
Fit type	Parameter	x'^2 free	x'^2 fixed at 0	95% C.L. interval
	R_D^+ [%]	0.32	0.35	$0.18 < R_D^+ < 0.62$
	R_D^- [%]	0.26	0.27	$0.12 < R_D^- < 0.56$
CP violation	x'^{+2}	-0.0008	0	$x'^{+2} < 0.0035$
allowed	x'^{-2}	-0.0002	0	$x'^{-2} < 0.0036$
	y'^+ [%]	1.7	0.7	$-7.5 < y'^+ < 3.4$
	y'^- [%]	1.2	0.9	$-5.7 < y'^- < 3.6$
No *CP*	R_D [%]	0.30	0.31	$0.22 < R_D < 0.46$
violation	x'^2	-0.0003	0	$x'^2 < 0.0021$
	y' [%]	1.3	0.8	$-3.7 < y' < 2.4$
No mixing	$R_D = (0.357 \pm 0.022$ (stat.) ± 0.027 (syst.))%			
	$A_D = 0.095 \pm 0.061$ (stat.) ± 0.083 (syst.)			

The confidence contours for the mixing results including systematic errors are shown in figure 2 and the overall results are summarised in table 1.

For our systematic errors we evaluate the contributions from uncertainties in the parametrisation of the PDF's, detector effects, and effects of our selection criteria. For detector effects like alignment errors or charge asymmetry we measure their effect on the right-sign control sample. For variations in the

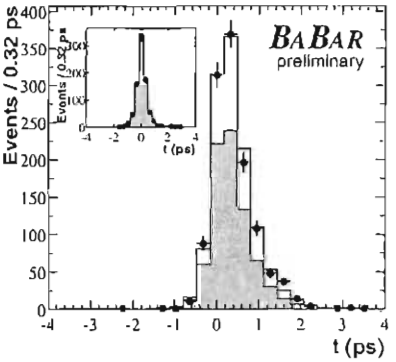

Figure 1: *A projection of the wrong-sign data on the time axis with the main plot showing the signal region and the inset a sideband. The plots show data as points and the resulting projection of the background (shaded) and signal (open) from the fit.*

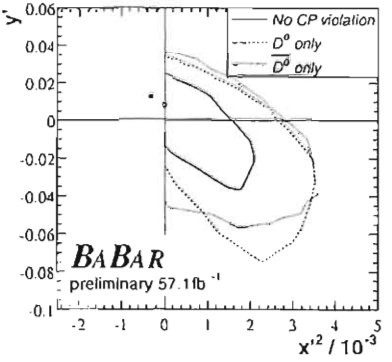

Figure 2: *95% confidence limits for D^0 (dashed) and $\bar{D}^0$ (dotted) separately (allowing for CP violation) and the contour when no CP violation is allowed (full). The solid point represents the most likely fit point in the case of no CP violation and the open circle the same but forcing $x'^2 > 0$.*

event selection we assign for this preliminary result the full variations in the resulting contours as systematic errors.

In summary we have set new and improved limits on mixing and *CP* violation for neutral D mesons. Our results are compatible with no mixing and no *CP* violation, all of which fits well with the predictions from the Standard Model given our current sensitivity.

References

1. A. A. Petrov, hep-pb/0209049 (2002).

2. E791, E. M. Aitala *et al.*, Phys. Rev. **D57**, 13 (1998), hep-ex/9608018.

3. CLEO, R. Godang *et al.*, Phys. Rev. Lett. **84**, 5038 (2000), hep-ex/0001060.

4. BABAR, B. Aubert *et al.*, Nucl. Instrum. Meth. **A479**, 1 (2002), hep-ex/0105044.

Frascati Physics Series Vol. XXXI (2003), pp. 245–250
FRONTIERSCIENCE 2002 – Frascati, October 6–11, 2002
Invited Contribution in Plenary Session

MIXING AND CP-VIOLATION IN CHARMED MESONS

Alexey A. Petrov
Department of Physics and Astronomy
Wayne State University
Detroit, MI 48201, USA

ABSTRACT

The Standard Model contribution to $D^0 - \overline{D}^0$ mixing is dominated by the contributions of light s and d quarks. Neglecting the tiny effects due to b quark, both mass and lifetime differences vanish in the limit of $SU(3)_F$ symmetry. Thus, the main challenge in the Standard Model calculation of the mass and width difference in the $D^0 - \overline{D}^0$ system is to estimate the size of $SU(3)$ breaking effects. We prove that D meson mixing occurs in the Standard Model only at *second* order in $SU(3)$ violation. We find that $y = (\Delta\Gamma)/(2\Gamma)$ of the order of one percent is natural in the Standard Model. We also discuss the sensitivity to new physics in measurements of D meson mixing.

One of the most important motivations for studies of $D^0 - \overline{D}^0$ mixing is the possibility of observing a signal from new physics which can be separated from the one generated by the Standard Model (SM) interactions. The $D^0 - \overline{D}^0$ mixing proceeds extremely slowly, which in the Standard Model is usually

operator that creates a D^0 meson and annihilates a $\overline{D}^0$, the matrix element, whose $SU(3)$ flavor group theory properties we will study, may be written as $\langle 0|\, D\, \mathcal{H}_w \mathcal{H}_w\, D\, |0\rangle$. Since the operator D is of the form $\bar{c}u$, it transforms in the fundamental representation of $SU(3)$, which we will represent with a lower index, D_i. We use a convention in which the correspondence between matrix indices and quark flavors is $(1,2,3) = (u,d,s)$. The only nonzero element of D_i is $D_1 = 1$. The $\Delta C = -1$ part of the weak Hamiltonian has the flavor structure $(\bar{q}_i c)(\bar{q}_j q_k)$, so its matrix representation is written with a fundamental index and two antifundamentals, H_k^{ij}. This operator is a sum of irreps contained in the product $3 \times \overline{3} \times \overline{3} = \overline{15} + 6 + \overline{3} + \overline{3}$. In the limit in which the third generation is neglected, H_k^{ij} is traceless, so only the $\overline{15}$ and 6 representations appear. We introduce $SU(3)$ breaking through the quark mass operator $\mathcal{M}$, whose matrix representation is $M_j^i = \mathrm{diag}(m_u, m_d, m_s)$ as being in the adjoint representation to induce $SU(3)$ violating effects. We set $m_u = m_d = 0$ and let $m_s \neq 0$ be the only $SU(3)$ violating parameter. All nonzero matrix elements built out of D_i, H_k^{ij} and M_j^i must be $SU(3)$ singlets.

We now prove that $D^0 - \overline{D}^0$ mixing arises only at second order in $SU(3)$ violation, by which we mean second order in m_s. First, we note that the pair of D operators is symmetric, and so the product $D_i D_j$ transforms as a 6 under $SU(3)$. Second, the pair of $\mathcal{H}_w$'s is also symmetric, and the product $H_k^{ij} H_n^{lm}$ is in one of the reps which appears in the product $\left[(\overline{15} + 6) \times (\overline{15} + 6)\right]_S$ A direct computation shows that out of many possible representations, only three actually appear in the decomposition of $\mathcal{H}_w \mathcal{H}_w$, the $\overline{60}$, the 42, and the $15'$ (actually twice, but with the same nonzero elements both times). So we have product operators of the form $DD = \mathcal{D}_6$, $\mathcal{H}_w \mathcal{H}_w = \mathcal{O}_{\overline{60}} + \mathcal{O}_{42} + \mathcal{O}_{15'}$, where the subscript denotes the representation of $SU(3)$. Since there is no $\overline{6}$ in the decomposition of $\mathcal{H}_w \mathcal{H}_w$, there is no $SU(3)$ singlet which can be made with $\mathcal{D}_6$, and no $SU(3)$ invariant matrix element $\langle 0|\, D\, \mathcal{H}_w \mathcal{H}_w\, D\, |0\rangle$ can be formed. This is the well known result that $D^0 - \overline{D}^0$ mixing is *prohibited by* $SU(3)$ *symmetry*. Now consider a single insertion of the $SU(3)$ violating spurion $\mathcal{M}$. The combination $\mathcal{D}_6 \mathcal{M}$ transforms as $6 \times 8 = 24 + \overline{15} + 6 + \overline{3}$. There is still no invariant to be made with $\mathcal{H}_w \mathcal{H}_w$, thus $D^0 - \overline{D}^0$ mixing is *not induced at first order in* $SU(3)$ *breaking*. With two insertions of $\mathcal{M}$, it becomes possible to make an $SU(3)$ invariant. The decomposition of $\mathcal{D}\mathcal{M}\mathcal{M}$ is

$$6 \times (8 \times 8)_S = (60 + \overline{42} + 24 + \overline{15} + \overline{15}' + 6) + (24 + \overline{15} + 6 + \overline{3}) + 6\,. \qquad (2)$$

There are three elements of the 6×27 part which can give invariants with $\mathcal{H}_w \mathcal{H}_w$. Each invariant yields a contribution to $D^0 - \overline{D}^0$ mixing proportional to $s_1^2 m_s^2$. Thus, $D^0 - \overline{D}^0$ mixing arises only at *second order* in the $SU(3)$ violating parameter m_s.

Table 1: *Values of $y_{F,R}$ and branching fractions for the corresponding multiplets for some two-, three-, and four-body final states. A contribution of a multiplet to y is given by a product of the third and fourth columns.*

Final state representation		$y_{F,R}/s_1^2$	$y_{F,R}$ (%)	Fraction
PP	8	-0.0038	-0.018	5%
	27	-0.00071	-0.0034	
PV	8_A	0.032	0.15	10%
	8_S	0.031	0.15	
	10	0.020	0.10	
	$\overline{10}$	0.016	0.08	
	27	0.04	0.19	
$(VV)_{s\text{-wave}}$	8	-0.081	-0.39	5%
	27	-0.061	-0.30	
$(VV)_{p\text{-wave}}$	8	-0.10	-0.48	
	27	-0.14	-0.70	
$(VV)_{d\text{-wave}}$	8	0.51	2.5	
	27	0.57	2.8	
$(3P)_{s\text{-wave}}$	8	-0.48	-2.3	5%
	27	-0.11	-0.54	
$(3P)_{p\text{-wave}}$	8	-1.13	-5.5	
	27	-0.07	-0.36	
$(3P)_{\text{form-factor}}$	8	-0.44	-2.1	
	27	-0.13	-0.64	
$4P$	8	3.3	16	10%
	27	2.2	11	
	27′	1.9	9.2	

One can explicitly study the contributions to y from on-shell final states, which result from every common decay product of D^0 and $\overline{D}^0$. In the $SU(3)$ limit, these contributions cancel when one sums over complete $SU(3)$ multiplets in the final state. The cancellations depend on $SU(3)$ symmetry both in the decay matrix elements and in the final state phase space. While there are $SU(3)$ violating corrections to both of these, it is difficult to compute the

$SU(3)$ violation in the matrix elements in a model independent manner. Yet, with some mild assumptions about the momentum dependence of the matrix elements, the $SU(3)$ violation in the phase space depends only on the final particle masses and can be computed. We estimate the contributions $y_{F,R}$ to y from several *complete* $SU(3)$ *multiplets* originating solely from $SU(3)$ violation in the phase space. We find that this source of $SU(3)$ violation can generate y of the order of a few percent [5]. Our results are summarized in Table 1. We observe that there are entries in Table 1, like nonresonant $4P$, which could make contributions to y at the level of a percent or larger. There, the rest masses of the final state particles take up most of the available energy, so phase space differences are very important. One can see that y on the order of a few percent is completely natural, and that anything an order of magnitude smaller would require significant cancellations which do not appear naturally in this framework. Indeed, some degree of cancellation is possible between different multiplets, as would be expected in the $m_c \to \infty$ limit, or between $SU(3)$ breaking in phase space and in matrix elements. It is not known how effective these cancellations are, and the most reasonable assumption in light of our analysis is that they are not significant enough to result in an order of magnitude suppression of y, as they are not enforced by any symmetry arguments. Therefore, any future discovery of a D meson width difference should not by itself be interpreted as an indication of the breakdown of the Standard Model.

References

1. S. Bergmann *et al*, Phys. Lett. B **486**, 418 (2000).
2. A. F. Falk, Y. Nir and A. A. Petrov, JHEP **9912**, 019 (1999).
3. M. Gronau, Y. Grossman and J. L. Rosner, Phys. Lett. B **508**, 37 (2001).
4. D. Atwood and A. A. Petrov, arXiv:hep-ph/0207165.
5. A. Falk *et al*, Phys. Rev. D **65**, 054034 (2002).
6. H. N. Nelson, arXiv:hep-ex/9908021.
7. E. Golowich and A. A. Petrov, Phys. Lett. B **427**, 172 (1998).

Future in Flavour

Chairperson: C. Matteuzzi

K. Yip	Heavy Flavor Physics at Tevatron Run II
K.K. Seth	Future in Flavour Physics at CLEO-c
T. Yamanaka	Kaon Factories
L. Schmitt	Charm Physics with Antiprotons at GSI
W. Kozanechi	e^+e^- B–Factories
D. Christian	BTEV – A Dedicaed B Experiment at the Tevatron
N. Harnew	B Physics at the LHC

Frascati Physics Series Vol. XXXI (2003), pp. 253–258
FRONTIERSCIENCE 2002 – Frascati, October 6–11, 2002
Invited Talk in Plenary Session

HEAVY FLAVOR PHYSICS AT TEVATRON RUN II

Kin Yip *
Brookhaven National Lab., Upton, New York 11973-5000, USA

ABSTRACT

We present the performance of the Tevatron and its experiments CDF and DØ in the current Run II at Fermilab. First measurements in heavy flavor physics are shown and possible measurements in the future are described.

1 Tevatron Run II and Detector Upgrade

Tevatron Run II at Fermilab started more than one year ago. It has been running at 1.96 TeV with 396 ns bunch crossing. The peak instantaneous luminosity at Tevatron by October 2002 was above 3×10^{31} $cm^{-2}s^{-1}$. Though the detector commissioning for the CDF nd DØ experiments is not complete, some of the data taken may already be used for future publication.

* On behalf of the CDF and DØ collaborations.

One advantage of a hadron collider such as Tevatron is that charm and bottom quarks are produced copiously by the strong interaction and then fragment into all kinds of hadron states such as B_s, B_c, Λ_b, which are not are not produced at B factories running at the $\Upsilon(4S)$ resonance. Therefore, Tevatron provides unique capabilities for studying these particles and their interactions.

The $b\bar{b}$ production cross-section at Tevatron is several orders of magnitudes higher than the e^+e^- machines, but the inelastic scattering cross-section is even larger. In order to study b decays which belong to the lower end of the energy and momentum spectra at Tevatron, specialized lepton and di-lepton triggers such as $J/\psi \rightarrow \mu^+\mu^-$ are required. In Run II, both the CDF and DØ experiments have moved the track triggers to Level 1 and have the capabilities of triggering on displaced tracks at Level 2 using the silicon vertex detectors (SVX). This allows triggering and studying purely hadronic B decays such as $B^0 \rightarrow \pi^+\pi^-$ and $B_s^0 \rightarrow D_s^-\pi^+$. Precise secondary vertex reconstruction is necessary for any of these B decay studies to succeed.

Detailed Run II detector upgrade information for CDF and DØ experiments can be found in the reference [1].

CDF has extended their SVX acceptance by a factor of 2 compared to Run I and the innermost "Layer 00" layers are less than 2 cm from the beampipe. CDF has also added a "Time of Flight" (TOF) detector between the (new) Central Outer Tracker and the superconducting solenoid magnet. The timing resolution for an individual particle in TOF is about 100 ps. It provides a $K-\pi$ separation at the level of about 1-2 σ (standard deviation).

As an important part of the Run II upgrade, DØ now has a 2.8 m long superconducting solenoid magnet with a magnetic field strength of 2 Tesla, enclosing the the scintillating fiber tracker (CFT) and the SVX. This allows DØ to measure momentum with a resolution dP_T/P_T^2 about 0.002. With some preliminary alignment, the impact parameter resolution at DØ has achieved the level of 20 μm (Fig. 1).

DØ excels in lepton measurements including excellent coverage, trigger efficiency and identification capability. The addition of central and forward preshowers in the upgrade adds to the strength of electron triggering and identification. There is also a major upgrade in the muon system, especially in its trigger front-end electronics. The momentum threshold of the muon trigger is now as low as 1.5 GeV/c and the pseudo-rapidity $|\eta|$ coverage is extended to 2.

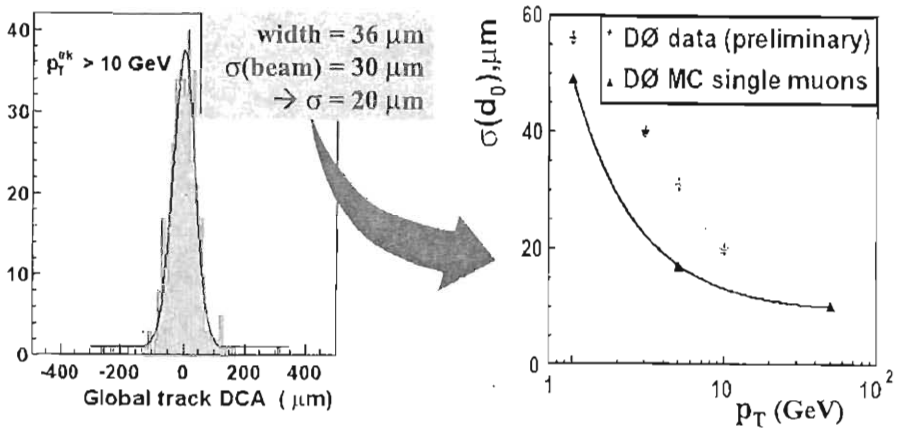

Figure 1: *DØ impact parameter resolution has achieved a resolution about 20 mμ (excluding the beamspot) with preliminary alignment.*

Detector and trigger commissioning came together rather quickly for CDF. By this summer, the CDF trigger rates have been about 6400 Hz, 145 Hz and 25 Hz at Level 1, 2 and 3 respectively. The number of CDF triggers has increased quickly and currently stabilizes at about 140.

For DØ, new detectors such as the SVX and central fiber tracker (CFT) have worked well such that more than 95% of SVX channels and 98% of CFT channels have been successfully read out. The DØ trigger rates have achieved 400 Hz, 150 Hz and 50 Hz at Level 1, 2, and 3 respectively.

2 First results from CDF and DØ

By October 2002, both experiments have collected more than 80 pb^{-1} of data and about 10 pb^{-1} of the high quality data for each experiment have been selected to be used for sophisticated data analyses.

As one of the first Run II measurements by CDF, the inclusive B lifetime is $c\tau = 458 \pm 10(stat) \pm 11(syst)$ μm and for the exclusive $B^+ \to J/\psi K^+$, $c\tau = 446 \pm 43(stat) \pm 13(syst)$ μm. DØ has also made its first inclusive B lifetime measurement $c\tau = 492 \pm 37(stat)$ μm (Fig. 2). In addition, CDF has

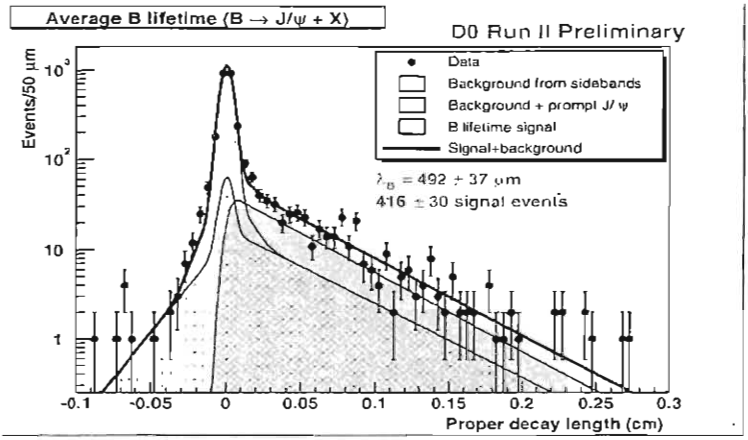

Figure 2: *DØ inclusive B lifetime measurement from fitting the J/ψ proper decay length spectrum. The error here is statistical only.*

measured various B meson and $\psi(2S)$ masses which are all compatible with the results published by the Particle Data Group (PDG) [2].

The purely hadronic B trigger has allowed CDF to collect a large charm sample. Assuming the targeted integrated luminosity of 2 fb^{-1} for Run IIa, CDF expects to reconstruct D decay events in the order of 10 millions, which will be even more than any dedicated charm experiments have done before. Moreover, with the purely hadronic trigger, CDF can now measure the mass difference between $D_s^{\pm}$ and $D^{\pm}$ (Fig 3). The preliminary result is $\Delta m = 99.28 \pm 0.43 \pm 0.27$ MeV, which is compatible with the PDG value 99.2 ± 0.5 MeV.

Another example of the charm physics measurements that CDF is able to do is the measurement of the Cabibbo-suppressed decay rates:

$$\Gamma(D \to KK)/\Gamma(D \to K\pi) = (11.17 \pm 0.48 \pm 0.98)\% \quad (PDG: 10.83 \pm 0.27)$$
$$\Gamma(D \to \pi\pi)/\Gamma(D \to K\pi) = (3.37 \pm 0.20 \pm 0.16)\% \quad (PDG: 3.76 \pm 0.17)$$

The second measurement above has an accuracy which is already comparable to the world average published by the PDG. The large charm sample will allow measurements of rare decays and perhaps even CP violation and mixing in the D sector.

Other measurements include DØ b-quark production and J/ψ cross-sections at the higher center-of-mass energy and extended η region ($|\eta| \leq 2$). Exclusive

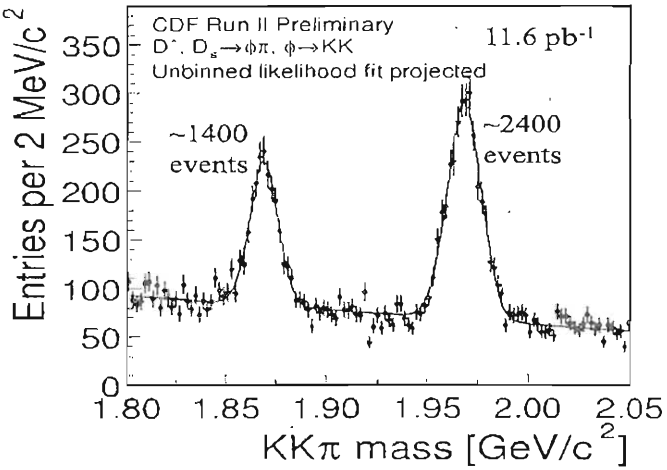

Figure 3: *CDF measurement of* $D_s^{\pm} - D^{\pm}$ *mass difference.*

$B^{\pm} \to J/\psi + K^{\pm}$ channel has also been reconstructed by DØ for the first time.

3 Upcoming measurements

Both experiments have made progress to measure B_s^0 mixing. Hadronic decays have been reconstructed and the next step is to reconstruct $B_s^0 \to D_s^- \pi^+$ as well as $D_s^- \to \phi \pi^-$. Sophisticated flavor tagging algorithms and extended SVX acceptance in both experiments will be exploited. This is one of the measurements that e^+e^- B factories cannot do but Tevatron can. From the B physics Tevatron report [3], CDF and DØ are expected to measure the B_s^0 mixing parameter up to a value about 50-60 and 30 respectively.

DØ is also working towards measuring the Λ_b^0 lifetime. Currently, the ratio $\tau(\Lambda_b^0)/\tau(B^0)$ has been measured to be 0.798 ± 0.052 [4] using semi-leptonic decays. But the theoretical expectation for this ratio is $\simeq 0.9 - 1.0$. It will be very interesting to measure $\tau(\Lambda_b^0)$ at Run II using exclusive and full hadronic decay modes which would not depend on the Monte Carlo K factor (momentum) correction as needed in the semi-leptonic analyses.

CDF was the first to measure a significantly non-zero CP violation parameter $\sin(2\beta)$ using the Run I data [5]. CDF and DØ can measure this parameter

with better precision. According to the B physics Tevatron report [3], with the assumption of an integrated luminosity of 2 fb^{-1}, each experiment is capable of measuring $\sin(2\beta)$ with an error as small as 0.03.

4 Summary

Though the Run II commissioning is yet to be complete, both CDF and DØ experiments have produced the first series of results in heavy flavor physics, each with a selected data sample about 10 pb^{-1} that have passed stringent quality criteria. The prospect for heavy flavor physics studies at Run II is excellent. In particular, collider experiments at Tevatron currently have the unique opportunity to perform accurate studies of the neutral $B_s^0/\overline{B_s^0}$ mesons such as their masses and lifetime differences. Thanks to the new hadronic trigger capabilities, a huge charm sample from Tevatron will allow all sorts of measurements in the D sector including mixing and CP violation.

5 Acknowledgements

The author acknowledges the useful suggestions from the CDF and DØ colleagues such as K. Pitts, V. Jain, B. Abbott and.R. Jesik during the preparation for the presentation in this workshop.

References

1. CDF detector upgrade information may be found at http://www-cdf.fnal.gov/upgrades/ ; and DØ detector upgrade information may be found at http://www-d0.fnal.gov/hardware/upgrade/upgrade.html .

2. K. Hagiwara *et al*, Phys. Rev. **D66**, 010001 (2002).

3. "*B* Physics at the Tevatron: Run II and Beyond", K. Anikeev *et al*, hep-ph/0201071 [FERMILAB-Pub-01/197], http://www-theory.lbl.gov/Brun2/report/.

4. LEP B lifetimes working group: http://lepbosc.web.cern.ch/LEPBOSC/lifetimes/.

5. T. Affolder *et al*, [CDF Collaboration], Phys. Rev. **D61**, 072005 (2000).

Frascati Physics Series Vol. XXXI (2003), pp. 259–269
FRONTIERSCIENCE 2002 – Frascati, October 6–11, 2002
Invited Talk in Plenary Session

FUTURE IN FLAVOUR PHYSICS AT CLEO-c

Kamal K. Seth *
Northwestern University, Evanston, IL 60208, USA

ABSTRACT

The CESR/CLEO facility at the Cornell University is undergoing conversion to CESR-c/CLEO-c, a facility dedicated to precision physics in the energy region of $\sim$ 3-5 GeV. It includes, among others, the physics of open charm, charmonium, QCD exotics, and tau leptons. The facility is expected to be operational in 2003.

1 Introduction

The accelerator CESR and the detector CLEO I became operational at Cornell in 1979. The physics they were dedicated to was that of the $b\bar{b}$ bottomonium system, and heavy quark flavored mesons. There have been since several upgrades of both CESR and CLEO. In 1989 CLEO II, and in 2000 CLEO III,

* On behalf of the CLEO Collaboration

became operational. CESR attained a record luminosity of 1.33×10^{33} cm^{-2}s^{-1} at 10.6 GeV. The new plan is to convert to CESR-c/CLEO-c by 2003, and to operate in the $\sqrt{s} \approx$ 3-5 GeV region with luminosity $\sim (1.5-4.4) \times 10^{32}$ cm^{-2}s^{-1}. It is an ambitious $\sim$3 yr. dedicated program of cutting edge research in the physics of open charm, charmonium, QCD exotics, and tau leptons. Details of the proposed program can be found in Ref. 1. Several smaller reports are available in Ref. 2.

The physics reach of CESR-c/CLEO-c is clear from the various thresholds that open in its energy range. Charmonium physics starts with η_c at 2.98 GeV, and extends at least upto 4.5 GeV. The τ pair production starts at 3.55 GeV. Open charm, or the physics of D mesons, starts at 3.73 GeV, with D, D^* and D_s pairs produced upto 5.2 GeV. Charmed baryon pair production begins with $\Lambda_c^+ \Lambda_c^-$ at 4.56 GeV, and extends upto $\Omega_c \bar{\Omega}_c$ at 5.5 GeV. And then, there are the QCD exotics, the light quark hybrids with masses in the 1.5-2.5 GeV region, the charm quark hybrids with masses in the 4-5 GeV region, and glueballs from 1.5 to 5.0 GeV. These will become accessible as secondary products.

2 The CESR-c/CLEO-c Conversion

CESR has been operating in the $\sqrt{s}$ = 10-11 GeV region, where it has achieved luminosity upto 13.3 $\times 10^{32}$ cm^{-2}s^{-1}! As it goes down to lower energies, it will require reoptimization of its beams. This mainly consists of the installation of 18 meters of wiggler magnets. A prototype is already in the lattice, and seven others are in construction, which is expected to be completed before summer 2003. The luminosity expected at various center of mass energies, and the expected production of various particles of interest is given in Table I. It is worth pointing out that these production rates are orders of magnitude larger than what has been achieved anywhere before. For example, in 4 months running 1.3 billion J/ψ are expected to be produced. For comparison, the cumulative world total of J/ψ produced from discovery in 1974 to present is approximately a factor 20 less.

The CLEO III detector is a well-proven, hermetic detector with state-of-the-art capabilities for charged and neutral particle detection and identification. Two minor changes are being made to adopt it to CLEO-c. The silicon strip tracker (which suffered radiation damage) is being replaced by a stereo drift chamber, and the solenoid magnetic field is being reduced from 1.5 T to 1.0 T.

Table 1: *Expected production of events at CLEO-c (1 yr = 10^7 s.)*

E_{cm} (GeV)	Luminosity (10^{32}cm^{-2}s^{-1})	Integrated $\mathcal{L}$ (fb^{-1})	Events
3.10	1.46	~ 0.5 (4 months)	$1.3 \times 10^9 J/\psi$
3.69	~ 4.1	~ 1.5 (4 months)	$1 \times 10^9 \psi'$
3.77	~ 4.13	~ 3 (9 months)	3×10^7 $D\bar{D}$
4.14	~ 4.4	~ 3 (9 months)	$1.5 \times 10^6 D_s \bar{D}_s$
4.60	~ 4.4	~ 1 (3 months)	$\sim 4 \times 10^5 \Lambda_c \bar{\Lambda}_c$
10.5-10.6	13.3	~ 13.8	$\Upsilon(4S)$, bkg.

Table 2: *A comparison of the CLEO-c and BES-II detectors.*

Detector Element	CLEO-c	BES II
Tracking Resolution		
at 1 GeV/c	0.5%	2.5%
Maximum momentum for π/K separation	1.5 GeV/c	600 MeV/c
dE/dx Resolution	4.9%	9%
Photon Energy Resolution		
at 1 GeV	21.5 MeV	220 MeV
at 100 MeV	3.9 MeV	70 MeV
Minimum Photon Energy	30 MeV	80 MeV
Solid Angle for Tracking	0.93	0.8
Solid Angle for Photons	0.93	0.75

Table II shows a comparison of the CLEO-c detector with BES II (at the Beijing collider, BEPC) which is the current best detector operating in this energy range. Note that the CLEO-c detector is more hermetic, and has factor 5 better charged particle tracking resolution, and more than an order of magnitude better photon energy resolution.

3 Open Charm, D-Physics

Precision studies in D-physics are important in order to validate lattice QCD predictions of non-perturbative strong interaction phenomena, which in turn are needed to interpret measurements in the quark flavour changing sector

of the Standard Model (quark mixing, CP violation, new physics, $\rightarrow$) from BABAR, BELLE, CDF/D0/BTEV, CMS/ATLAS/LHC-b.

CLEO has been making significant contributions to D-physics for many years via D production in B decays. CLEO-c will bring unparalleled precision to D-physics, primarilly due to the advantages of threshold production and high luminosity.

The important advantages of threshold production are:

- Avoiding backgrounds: Background from decays of higher mass particles, e.g., b quarks, are excluded.
- Measuring backgrounds: By going to just below the production thresholds of τ or $D\bar{D}$ etc., all true backgrounds can be actually measured, not estimated by Monte Carlo calculations, as at other machines.
- Tagging: since τ leptons and heavy flavoured objects, e.g., D^0, $D^{\pm}$, $D_s^{\pm}$, $\Lambda_c^{\pm}$, Σ_c, ... are produced in pairs, one of them can be used to tag the other, which can then be studied in any and all of its decay modes.
- Small Lorentz boost: Avoids analysis complications.
- Precision Calibrations: Available because of high yield reactions with J/ψ and ψ' decays.

Tables III and IV list the kind of measurements which we intend to make at CLEO-c and the precision which is expected with the investment of 3 fb^{-1} of luminosity. As can be seen there, in each measurement CLEO-c will make significant improvements over the existing levels of precision, and also above the projected level at BaBar. The particle identification for some of these measurements is illustrated in the four panels of Fig. 1.

4 CP violation

In the Standard Model, indirect CP violation via $D^0\bar{D}^0$ mixing is predicted to be small, with $B(D^0 \rightarrow \bar{D}^0 \rightarrow \bar{f})/B(D^0 \rightarrow f) \approx 10^{-4}$ to 10^{-5}, $f \equiv l^+X^-$, or $K^+\pi^-$. It is difficult for this to be feasible at CLEO-c. For direct CP violation one needs to measure asymmetry $A \equiv [R(D \rightarrow f) - R(\bar{D} \rightarrow f)]/\text{sum}$, with $f = K^+K^-\pi^+$ or $\eta\pi^+$. Asymmetry measurements at the level of $\sim 2 \times 10^{-2}$ per year are possible at CLEO-c. Of course, a single event of the type $\psi''(\text{CP} = +1) \rightarrow D^0\bar{D}^0(\text{C} = -1, \text{L} = 1)$, with $D_0\bar{D}$ decaying to two identical CP eigenstates like K^+K^-, $\pi^+\pi^-$ or $K_L^0\pi^0$ would prove CP violation in the up-quark sector.

Table 3: *Summary of CLEO-c Charm Decay Measurements.*

Decay Constant	Reaction	Current sensitivity	BaBar sensitivity	CLEO-c $\mathcal{L} = 3$ fb^{-1}
f_D	$D^+ \to \mu^+\nu$	UL	$10-20\%$	2.3%
f_{D_s}	$D_s^+ \to \mu^+\nu$	14%	$5-10\%$	1.9%
f_{D_s}	$D_s^+ \to \tau^+\nu$	33%		1.6%
Absolute Values				
$Br(D^0 \to K\pi)$		2.4%	$2-3\%$	0.6%
$Br(D^+ \to K\pi\pi)$		7.2%	$3-5\%$	0.7%
$Br(D_s^+ \to \phi\pi)$		25%	$5-10\%$	1.9%

Table 4: *CKM Matrix Elements.*

	V_{cd}	V_{cs}	V_{cb}	V_{ub}	V_{td}	V_{ts}
Current	7%	16%	5%	25%	36%	39%
After CLEO-c	1.7%†	1.6%†	3%*	5%*	5%*	5%*

† V_{cs} from $D^0 \to Kl^+\nu$, and V_{cd} from $D^0 \to \pi l^+\nu$, both with $\mathcal{L} = 3$ fb^{-1} at CLEO-c

* Estimated with CLEO-c validated lattice QCD contributions, and expected B-factory and Tevatron data.

5 Charmonium Physics

Charmonium was discovered in 1974, and one would think that we have exhausted its spectroscopy by now (see Fig. 2). Unfortunately, nothing could be farther from the truth. The fact is that lots of discovery physics has been done, but little of precision spectroscopy has been done. The easier measurements have been made, the difficult ones remain.

A brief summary of the present shortcomings would include the following. The spin singlet states $h_c(^1P_1)$ and $\eta_c'(2^1S_0)$, and most of the states above the $D\bar{D}$ threshold have not been identified. The data for the charmonium ground state η_c is extremely poor, with only $\sim 26\%$ of hadronic decays having been identified, and with none of the branching ratios measured with less than $\pm 30\%$ error. No more than 10% of the hadronic decays of the $\chi_c(^3P_J)$ states have

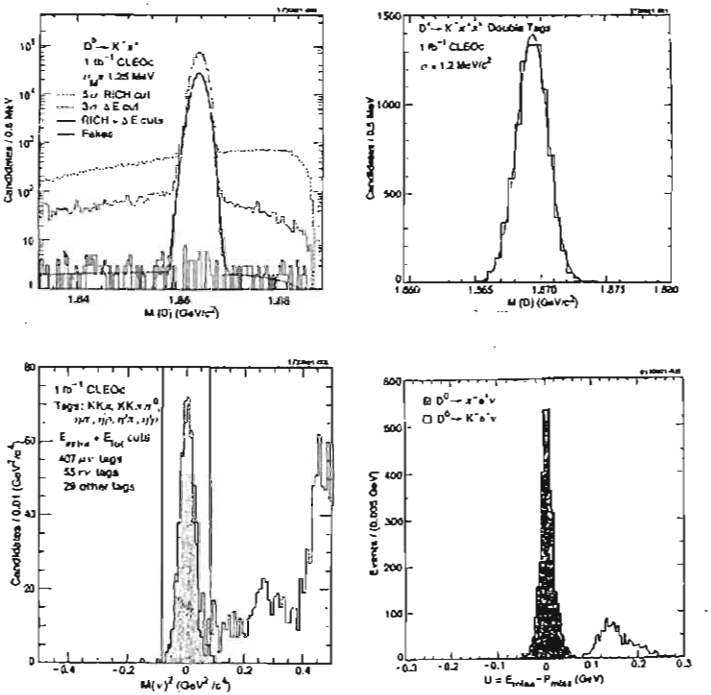

Figure 1: *Illustrations of CLEO-c capabilities in 1 fb^{-1}. (Top left) $M(K\pi)$ in $\psi(3770) \to D^0\bar{D}^0$, $D^0 \to K^-\pi^+$, $\Delta E(= E(D) - E_b)$ and RICH cuts; $S/N = 50/1$. (Top right) $M(K^-\pi^+\pi^+)$, $\psi(3770) \to D\bar{D}, D^+ \to K^-\pi^+\pi^+$, with tag on one D. $\Delta E, dE/dx$ cuts. Absolute $B(D \to K\pi\pi)$ determined. (Bottom left) $M(\nu^2)$ for $\sqrt{s} = 4100\ MeV \to D_s\bar{D}_s, D_s \to \mu^+\nu$ tagged pairs. $D_s \to \mu\nu$ events are shaded. (Bottom right) $M(\nu)$ for $\psi(3770) \to D\bar{D}, D_0 \to \pi^- e^+\nu$ tagged events. $D_0 \to \pi e\nu$ events are shaded. Kaon events are outside RICH.*

ever been measured. The two photon widths of η_c, χ_0, χ_2, and η_c' remain poorly determined, with large discrepancies between results from experiments using different techniques. Different measurements of the all important R parameter, $R \equiv \sigma(\text{hadron})/\sigma(\mu\mu)$ do not agree even qualitatively. I can not go into details of all these here (see Ref. 3), but let me describe a few.

Consider the ground states of quarkonia, $|c\bar{c}>$ charmonium and $|b\bar{b}>$ bottomonium, whose importance cannot be exaggerated. The bottomonium ground state has never been identified. After several false starts, the charmonium ground state, $\eta_c(1^1S_0)$ was identified at SLAC in radiative transitions

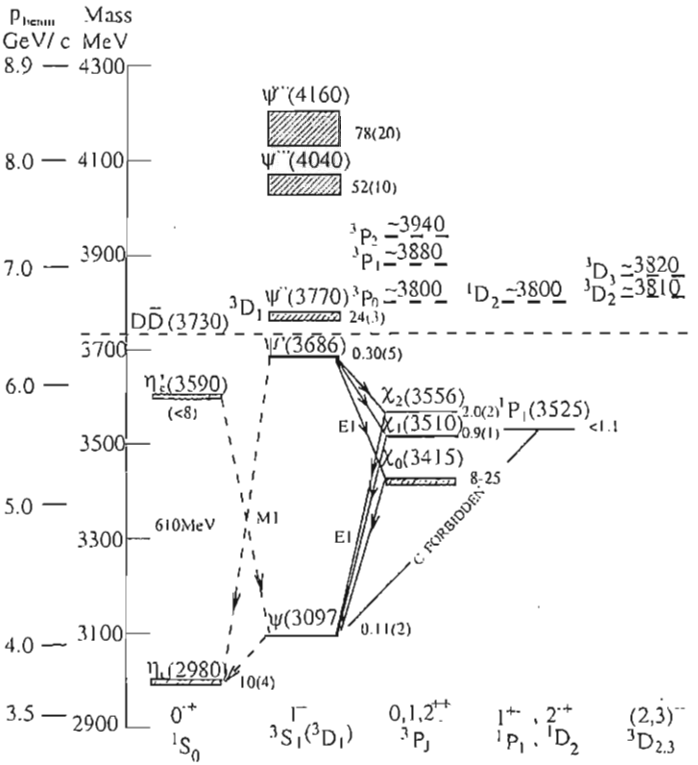

Figure 2: *Charmonium Spectrum. The bound states $h_c(^1P_1), \eta_c'(2^1S_0)$, and states above the $D\bar{D}$ breakup threshold have not yet been identified.*

from $J/\psi(3097)$ and from $\psi'(3686)$. However, since these transitions are M1 allowed, and M1 forbidden respectively, they are extremely weak, the knowledge of η_c parameters is quite poor. The errors are large, and different experiments disagree, often outside their errors. Further, as noted earlier, none of the few hadronic decays of η_c which have been measured have errors less than $\pm 30\%$. This is an apalling state of affairs, and must be improved. As Table I shows, at CLEO-c we expect to produce 1.3 billion J/ψ in 4 months of running. These in turn should lead to $\sim$ 1.6 million η_c despite the weakness of the M1 transition, and make it possible to make precision measurements in essentially all decay channels of the η_c. Just to highlight one important decay: The decay $\eta_c \to p\bar{p}$ has at present a world total of 41 events. This will be increased nearly

a thousand-fold at CLEO-c.

The Fermilab $p\bar{p}$ annihilation experiments E760/E835 have provided precision data on the mass, and importantly on the total, radiative, and two-photon widths of ^3P_J states. However, because of the limitations of their non-magnetic detector, they have not been able to measure hadronic decays. At CLEO-c we will have samples of $\sim$ 100 million each of χ_0, χ_1, and χ_2 from the radiative decays of ψ', and it will be possible to make precision measurements of essentially all decays of these states. The χ_J states sample the confinement region of the $q\bar{q}$ potential, and these measurements should shed important light on this still dark aspect of QCD.

Two measurements which are going to be challenging even for CLEO-c are the identification of the spin-singlets, $h_c(^1P_1)$ and the radial excitation of the ground state, $\eta_c'(2^1S_0)$. Neither the old (e^+e^-) experiments, nor the $(p\bar{p})$ Fermilab experiment have been successful in identifying these states. At CLEO-c, h_c can be searched for in the reaction $\psi' \to h_c(\sim 3525)+\pi^0$, although the available phase space is quite small. Similarly, the search for η_c' will require the very best of CLEO-c's photon detection capability. If the recent claim of BELLE is correct, and the η_c' mass is near 3654 $\pm$ 10 MeV, one needs to identify a photon line of $\sim$ 35 MeV in the radiative decay $\psi' \to \gamma\eta_c'$!

Above the $D\bar{D}$ threshold at 3.73 GeV, very little is known reliably. As shown in Fig. 3, different measurements of $R \equiv \sigma(\text{hadrons})/\sigma(\mu^+\mu^-)$ are in substantial disagreement, and the current knowledge of the charmonium vector states with $M > 4$ GeV, based on the 1979 measurement of R by DASP, does not appear to be confirmed by the latest measurement by BES(2000). At CLEO-c it is proposed to make precision measurments of R in the 3.73 - 5 GeV region to clarify this situation.

6 QCD Exotics

Among the unique predictions of QCD are the exotic structures, the gg glueballs and the $q\bar{q}g$ hybrids. Lattice calculations predict their masses in the range of 1.5 $\rightarrow$ 4.5 GeV, a range accessible to CLEO-c. In fact, CLEO-c will be in an excellent position to make definitive searches for these.

The competing candidates for the 0^{++} scalar glueball are three states; $f_0(1370), f_0(1500)$, and $f_0(1710)$. Unfortunately, none of them exhibit the flavour blind decay which is expected of a pure glueball, mainly because the

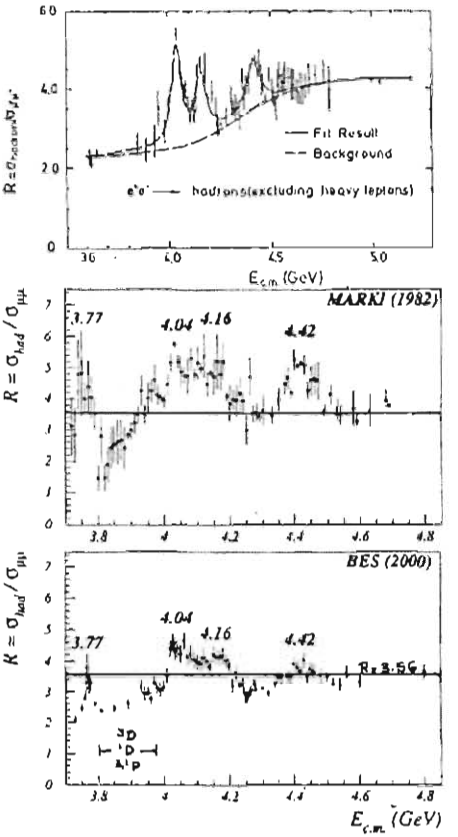

Figure 3: *The R-parameter, $R \equiv \sigma(hadron)/\sigma(\mu\mu)$ as measured by three different detectors. The top panel is from DASP (1979). Note the considerable disparity in the delineation of the higher vector states.*

scalar glueball is mixed with normal scalar $q\bar{q}$ states. Since glue does not couple to photons, it is expected that the dominantly gluball state will have a very small two photon width. The present measurements give upper limits *at keV levels*, and are incapable of distinguishing between the three candidates. At CLEO-c, we expect to make very high statistics measurements of J/ψ radiative decays to these states and to establish two photon decay width upper limits *at eV levels*. This should help ferret out the most glueball like state of the three.

The 2^{++} tensor glueball is predicted to have a mass of $\sim$ 2200 MeV. Indeed, a tensor glueball claim for an exceptionally narrow 2^{++} state with mass $\sim$ 2230 MeV observed in radiative decay of J/ψ was made first by SLAC, and more recently by BEPC. The BEPC claim was based on a 3-4 sigma enhance-

ment in several decay channels, with 25 to 75 counts in each. At CLEO-c, with a billion J/ψ sample, 5,000 to 25,000 counts are expected in each of these channels, which will definitely settle the issue of whether or not the narrow $\xi(2230)$ really exists. (Parenthetically, we note that it is reported that with 58 million J/ψ in the new BES-II run, the resonance is not observed.)

7 Electromagnetic Form Factors of Hadrons

Among the most fundamental and important questions in hadron physics is the partonic structure of hadrons. The electromagnetic structure of the proton and the pion are considered to be ideal testing grounds for the validity of perturbative QCD. Yet, precision experimental data are extremely sparse.

For protons, precision data for spacelike momentum transfers exists, with G_M, the magnetic form factor, well measured upto ~ 35 GeV^2. However, G_E is very poorly known, and very recent measurements have revealed entirely unexpected behavior of G_E even at < 4 GeV^2. The situation is even poorer for timelike momentum transfers. Until recently, data only existed for $Q^2 <\sim 5$ GeV^2. The Fermilab experiment E760/E835 has provided $p\bar{p} \to e^+e^-$ form factor data upto $Q^2 =\sim 13$ GeV^2. These data have revealed more surprises; it is found that the timelike form factor is about twice as large as the spacelike. The reason for this is not at all clear, and it is extremely important to determine if this trend continues at larger Q^2. The Fermilab measurements run out of steam already at ~ 14.5 GeV^2, where only two counts were observed. At CLEO-c, we expect ~ 200 $e^+e^- \to p\bar{p}$ identified events for $Q^2 = 15$ GeV^2 with an investment of ~ 0.5 fb^{-1} of luminosity. In fact, it may be possible to make meaningful measurements upto $Q^2 \approx 20$ GeV^2.

One of the great advantages of CLEO-c is that one can measure the timelike form factors of pions and kaons by identifying $e^+e^- \to \pi^+\pi^-$ and $e^+e^- \to K^-K^-$ events without any additional investment of luminosity. The present knowledge of these form factors is in far worse shape than that of protons. Essentially no data are available for either spacelike or timelike momentum transfers for $Q^2 > 4$ GeV^2, and the data that exist have $\pm 50\%$ to 100% errors. Measurement of timelike form factors for pions and kaons for Q^2 even less than 10 GeV^2 will be a major contribution to settling the contentious debate about the onset of the perturbative regime of QCD.

8 Tau Physics

At CLEO-c, a large yield of $\tau^+\tau^-$ pairs is expected. It ranges from 0.5 million/fb^{-1} at threshold ($\sqrt{s}$ = 3.56 GeV) to 11 million/fb^{-1} at $\sqrt{s}$ = 4.14 GeV. At threshold, one can take full advantage of cleanliness of threshold production, excellent knowledge of backgrounds, and tagging. These can be used to make precision measurements of the tau mass, key branching ratios like $B(\tau^- \rightarrow \pi^-\nu_\tau)$, and $B(\tau^- \rightarrow \pi^-\pi^0\nu_{tau})$, Michel parameters, and even CP violation in τ decay by comparing $\tau^\pm \rightarrow \nu_\tau + a + b$.

9 Summary

CLEO-c offers the particle physics community an unparalleled opportunity for precision physics over a broad spectrum. It promises to provide crucial data for the validation of lattic calculations and for the exploration of new frontiers of QCD.

10 Acknowledgements

The research reported in this paper was partly supported by the U.S. Department of Energy. The support of the Humboldt Foundation is also gratefully acknowledged. The author would like to thank David Joffe for help in the preparation of this report.

References

1. "CLEO-c and CESR-c: A New Frontier of Weak of Strong Interactions", CLNS Report 01/1742, (2001).

2. "Snowmass 2001: E2 Working Group", report by I. Shipsey, and talks by M. Artuso, D. Cassel, S. Dytman, L. Gibbons, Y. Maravin, and I. Shipley.

3. K. K. Seth, Proc. PANIC02, Osaka, in press.

Frascati Physics Series Vol. XXXI (2003), pp. 271–276
FRONTIERSCIENCE 2002 – Frascati, October 6–11, 2002
Invited Talk in Plenary Session

KAON FACTORIES

Taku Yamanaka
Department of Physics, Osaka University
1-1 Machikaneyama, Toyonaka, Osaka 560-0043, Japan

ABSTRACT

High intensity accelerators will serve as kaon factories, and various experiments there will use rare K decays to make precise measurements of the Standard Model parameters and to search for physics beyond the Standard Model.

1 Introduction

Kaons have been the probes to search for forbidden decays such as lepton number violation, to study CP violation, and to study long distance contributions. Now that the existence of direct CP violation has been confirmed by extensive measurements of $Re(\epsilon'/\epsilon)$, kaon physics is entering a new era. For example, instead of lowering the upper limits of branching ratios, rare decays are becoming the tools to make precise measurements of the Standard Model and CP parameters. This becomes possible with the advance of new high intensity

accelerators. Here, we will go through such kaon factories and experiments except for DAFNE which is well covered in other talks.

2 VEPP ϕ Factory

Another ϕ factory in the world is BINP VEPP-2M collider at Novosibirsk [1]. They ran from 1992 till 2000 at the center of mass energy $\sqrt{s} = 0.36 \sim 1.4$GeV. At the ϕ resonance they have accumulated 33 pb^{-1} and collected 41 million ϕ decays in total.

There were two experiments at VEPP-2M; CMD-2 [2] and SND [3]. Together, they have made precise measurements of ϕ meson parameters such as the mass and width of $\phi(1020)$. Using the K_L and K_S pairs from the ϕ decay, CMD-2 have also observed $K_S \to \pi^{\pm} e^{\mp} \nu$ decays for the first time and measured its branching ratio $BR(K_S \to \pi^{\pm} e^{\mp} \nu) = (7.2 \pm 1.4) \times 10^{-4}$ [4]. SND has searched for CP violating $K_S \to 3\pi^0$) decay and set an upper limit: $BR(K_S \to 3\pi^0) < 1.4 \times 10^{-5}$ (CL 90%) [5].

Their next plan is to upgrade the accelerator to increase the center of mass energy up to 2GeV [6]. By using beams with round transverse cross-sections, they plan to achieve 1.0×10^{32}cm^{-2}s^{-1} luminosity.

3 $K_L \to \pi^0 \nu\bar{\nu}$

Before moving on to other kaon facilities and experiments, let us review the golden kaon decay modes, $K \to \pi\nu\bar{\nu}$.

In the standard model, CP violation is described by one imaginary parameter in the CKM quark mixing matrix [7]. In the Wolfenstein's parametrization [8], this imaginary parameter is η, as it appears as $V_{td} = A\lambda^3(1 - \rho - i\eta)$. This η effectively determines the size of CP violation. The unitarity of the CKM matrix can be expressed geometrically in a so called unitarity triangle. The $K \to \pi\nu\bar{\nu}$ decays are golden decay modes to measure the parameters of the triangle, since their decay amplitudes are dominated by a penguin diagram which includes V_{td}.

In case of $K^+ \to \pi^+ \nu\bar{\nu}$ decay, its branching ratio is thus proportional to $|V_{td}|^2$ to the first order. The current branching ratio is $B(K^+ \to \pi^+ \nu\bar{\nu}) = (1.57^{+1.75}_{-0.82}) \times 10^{-10}$ based on 2 observed events [9].

In case of $K_L \to \pi^0 \nu\bar{\nu}$ decay, since $|K_L > \simeq (|K^0> - |\overline{K^0}>)/\sqrt{2}$, the

decay amplitude is proportional to $V_{td} - V_{td}^* \propto Im(V_{td})$, and the branching ratio of $K_L \to \pi^0 \nu\bar{\nu}$ is thus proportional to $|\eta|^2$ with only 2% theoretical uncertainty. Current estimate on the branching ratio based on best known Standard Model parameters is $\sim 3 \times 10^{-11}$, but the experimental limit is $< 5.9 \times 10^{-7}$ (90% CL) [10].

These golden decay modes can determine the unitarity triangle precisely from kaon sector alone, and the comparison between the results from K and B meson sectors is a powerful way to search for physics beyond the Standard Model.

4 Fermilab CKM

The goal of Fermilab CKM experiment is to collect 100 $K^+ \to \pi^+ \nu\bar{\nu}$ events to measure its branching ratio. The current BNL E787 and E949 experiments stop kaons in a target, but the kaon rate is limited by the interaction rate in the target. CKM avoids this problem by using kaons decaying in flight in vacuum. CKM uses high intensity 120 GeV protons from the Main Injector to produce K^+. After selecting 22 GeV/c charged particles, the kaons are separated from pions by two RF stations. The pions and kaons are kicked sideways in the same direction at the first RF station, but they separate longitudinally due to the velocity difference, and kicked in opposite directions at the second RF station located 86m downstream. This RF separator reduces the π/K ratio to 0.3.

The K^+ is identified by a RICH counter located upstream of the decay volume. The π^+ from the decay is identified by the second RICH counter and its momentum is measured by a spectrometer. The decay region is covered by photon veto counters to veto $K^+ \to \pi^+\pi^0$ background.

The experiment has been approved by Fermilab, and is now in R&D stage.

5 BNL KOPIO

The goal KOPIO experiment at BNL is to collect 50 $K_L \to \pi^0 \nu\bar{\nu}$ events in 3 years of running to measure its branching ratio. The concept of this experiment is to measure all the kinematical parameters to reduce background. The average momentum of kaons is tuned to be low (0.7GeV/c), and the beam is squeezed into narrow bunches for the reasons described below. The energies and hit positions of photons from the π^0 are measured with a calorimeter lo-

cated downstream. The decay region is surrounded by photon veto counters to reduce background from $K_L \to \pi^0\pi^0$ decay with two escaping photons. In addition, they measure the direction of photons entering the calorimeter with multiple layers of position sensitive preradiators to reconstruct the decay vertex. Next, they measure the timing difference between the target and the calorimeter, and measure the momentum of the kaon from its TOF. The background from $K_L \to \pi^0\pi^0$ is reduced by requiring the two photons to have π^0 mass and small π^0 energy in the kaon CMS. The estimated S/N ratio is 2.

The experiment has been approved by BNL, and it is waiting for funding from NSF.

6 JHF 50 GeV Proton Synchrotron

In Japan, the construction of a new 50 GeV proton synchrotron at JHF (now called J-PARC) has started. The accelerator can deliver 3×10^{14} protons every 3.4sec, corresponding to 0.75MW. There are many experiments which are being considered to utilize this high intensity accelerator. Here I will describe some of those experiments presented at NP02 workshop held at Kyoto in September 2002 [1].

6.1 $K_L \to \pi^0\nu\bar{\nu}$

The purpose of $K_L \to \pi^0\nu\bar{\nu}$ experiment is to measure its branching ratio by collecting more than several hundred signal events. A pilot experiment for JHF, named E391a, is now being prepared at KEK. The concept of this experiment is to cover the decay region with extensive hermetic veto counter and look for π^0 with large transverse momentum. The K_L energy is tuned higher to increase the average photon energy so that vetoing extra photons from background is easier. The transverse momentum of π^0 is measured with a CsI electromagnetic calorimeter at downstream and a "pencil beam". Requiring large transverse momentum reduces the background from $K_L \to \pi^0\pi^0$ where one photon from each π^0 is missed. The experiment at KEK 12GeV PS will start taking data in February 2003 to reach 3×10^{-10} sensitivity. After the experiment, they plan to move the detector to JHF and upgrade necessary parts to reach the ultimate goal.

[1] http://www-jhf.kek.jp/NP02/

6.2 T-Violation in K_{e3}

The purpose of this experiment to search for T-violation in $K^+ \to \pi^0\mu^+\nu$ and $K^+ \to \mu^+\nu\gamma$ decays. A finite polarization of the muon in the direction perpendicular to the decay plane violates T symmetry, and this can be caused by non-standard models such as a 3-Higgs doublet model, etc.. The current value of the polarization is $P_T = -0.0042 \pm 0.0049 \pm 0.0009$ [11]. The experiment at JHF will stop K^+ in a target, and measure the momentum of π^0 with a calorimeter surrounding the target. The momentum of the μ is measured with a tracking system without magnet and range counters which also serve as an active polarimeter. The expected sensitivity to P_T is 10^{-4}.

6.3 $K^+ \to \pi^+\nu\bar{\nu}$

An experiment to measure the branching ratio of $K^+ \to \pi^+\nu\bar{\nu}$ is also being considered. It will use the stopped K^+ as BNL experiments, but improve its rate capabilities, and stopping efficiency, etc. to collect 50 events in 3 years of running.

6.4 $K_L \to \mu e$

An experiment to search for $K_L \to \mu e$ decay is also being considered. It uses a solenoid magnet to measure the momentum of tracks. Compared to the past $K_L \to \mu e$ experiments at BNL which used dipole magnets, it can increase the acceptance by a factor 10. The new experiment uses bunched K_L beam to measure TOF to make more constraints. The goal of the experiment is to improve the current upper limit on the branching ratio by a factor 50, and achieve 10^{-13}.

7 Conclusion

VEPP-2000, BNL AGS, Fermilab Main Injector, and the new JHF 50GeV PS will serve as Kaon Factories. The new kaon experiments and facilities described above will further push the current limit and sensitivities, and will use rare K decays to make precise measurements of the Standard Model parameters and to search for physics beyond the Standard Model.

References

1. A.N. Skrinsky, in Proceedings of the Workshop on Physics and Detectors for DAΦNE, Frascati, Italy, 1995, p.3.
2. G.A. Aksenov *et al.*, Preprint Budker INP 85-118, Novosibirsk (1985), and E.V. Anashkin, ICFA Instr. Bulletin **5**, 18 (1988).
3. M.N. Achasov *et al.*, Nucl. Inst. Meth. in Phys. Res. A **449** 125 (2000).
4. R.R. Akhmetshin *et al.*, Phys. Lett. B **456**, 90 (1999).
5. M.N. Achasov *et al.*, Phys. Lett. B **459**, 674 (1999).
6. I.A. Koop, in Proceedings of the 2001 e^+e^- Physics at Intermediate Energies Workshop, SLAC, California, April 2001, http://www.slac.stanford.edu/econf/C010430/T08.html.
7. M. Kobayashi and T. Maskawa, Prog. Theo. PHys. **49**, 652 (1973).
8. L. Wolfenstein, Phys. Revl Lett. **51**, 1945 (1983).
9. S. Adler *et al.*, Phys. Rev. Lett. **88**, 041803 (2002).
10. A. Alavi-Harati *et al.*, Phys. Rev. D **61**, 072006 (2000).
11. M. Abe *et al.*, Phys. Rev. Lett. **83**, 4253 (1999).

Frascati Physics Series Vol. XXXI (2003), pp. 277–280
FRONTIERSCIENCE 2002 – Frascati, October 6–11, 2002
Invited Contribution in Plenary Session

CHARM PHYSICS WITH ANTIPROTONS AT GSI

Lars Schmitt
TU München, Physik-Department, E18, D-85747 Garching

ABSTRACT

A new facility for stored antiprotons at high luminosity and energies up to 15 GeV is being planned at GSI, Darmstadt. The physics reach of this facility with a focus on experiments with charm hadrons is presented.

1 The Antiproton Facility HESR at GSI

One part of a new facility planned at GSI, Darmstadt, is a storage ring for antiprotons at energies up to 15 GeV for measurements at high luminosity. Electron cooling provides clean beam parameters and high precision.

The detector proposed for HESR covering almost the full solid angle with good tracking and particle identification is subdivided into a target spectrometer with a solenoid around the interaction region and a forward spectrometer based on a dipole [1].

Pellet or gas jet targets for experiments at the HESR requiring hydrogen as target material will be used. Experiments with D mesons need a very precisely determined primary vertex and will use a thin fiber or wire target.

A 5 layer pixel detector will provide good vertex resolution. Tracking through the solenoid field is done by 15 double layers of crossed straw tubes.

A DIRC Cherenkov detector separates pions and kaons up to 3 GeV/c while in the forward direction an aerogel RICH is used. Electromagnetic calorimetry is provided by lead tungstate crystals read out by avalanche photodiodes (APD). The instrumented return yoke of the solenoid identifies muons. Forward tracking will be done by several sets of mini drift chambers (MDC) with 6 planes each. Behind these are a 3 m^2 lead glass calorimeter, a hadronic calorimeter and again muon detectors.

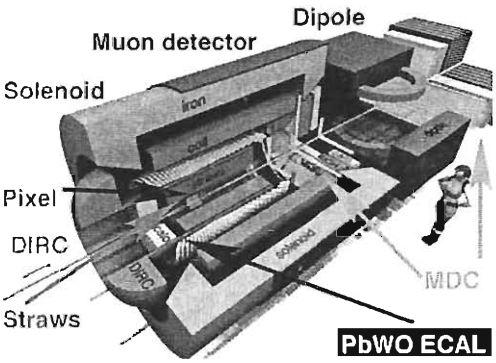

Figure 1: Schematic overview of the detector at HESR.

2 Charm Spectroscopy

2.1 Charmonium states

Experiments E760 and E835 at the FNAL [2] antiproton ring have proved that antiprotons are an excellent tool to scan the spectrum of charm anti-charm states, which is a unique laboratory to study the strong interaction in the domain of bound resonances. In particular $p\bar{p}$-reactions can populate states with various quantum numbers by means of two- and three-gluon exchange graphs in the annihilation whereas e^+e^--machines can only populate $J^{PC} = 1^{--}$ states. Furthermore fine tuning the energy of the antiproton beam is a precise tool to achieve an energy resolution in the order of 100 keV.

HESR will reach a similar energy resolution as the Fermilab ring, but at higher luminosity and with an apparatus sensitive to hadronic as well as electromagnetic final states, thus opening new decay channels at high accuracy.

2.2 Charm hybrids

Exotic states with quantum numbers not reachable by standard $q\bar{q}$- or qqq-states are predicted by QCD and a number of observations have been made in the light quark sector. There however large widths and strong interference with other light states obscure the picture. Predictions show on the other hand that a number of exotic states with charm quarks and gluonic degrees of freedom should be narrow and be undisturbed by other states [3]. This would offer a new, much cleaner view on exotic states and the role of the gluon in hadron spectroscopy.

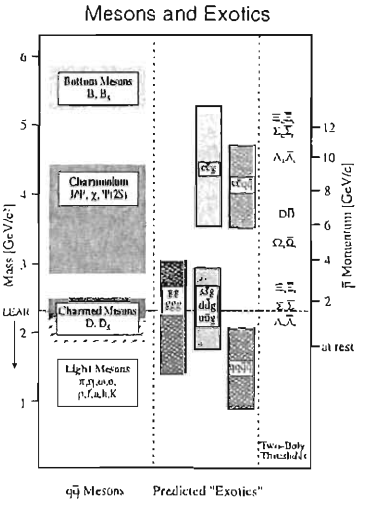

Figure 2: Mass ranges of mesons and exotics.

3 Physics with D-Mesons

Producing charm mesons close to threshold with little phase space for other hadrons will allow a number of measurements under very clean conditions.

3.1 D-Mesons in Nuclear Matter

If one produces Charm mesons close to rest within nuclear matter chiral perturbation theory predicts a lowering of the mass and at the same time a 50 MeV mass splitting for D^+ and D^- [4]. This effect would also open $D\bar{D}$-decay channels to lower lying charmonium states drastically increasing their width and cross section. Figure 3 shows the change of the D-production cross section in the nuclear medium [5] due to the shifted masses.

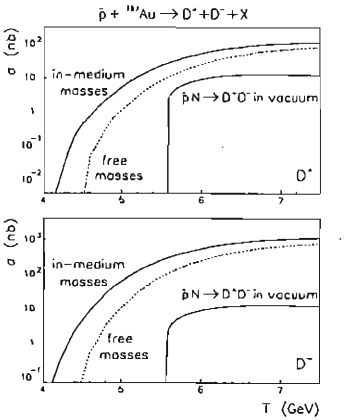

Figure 3: D-meson production on Au with in-medium and free masses [5].

3.2 Search for CP violation

From Standard Model predictions CP violation is expected to be small in the charm sector and proceed only through singly Cabibbo suppressed decays.

What first looks like a disadvantage can however be a great benefit, when small deviations from the Standard Model are looked for, which would point to new physical mechanisms generating CP violation. In addition observing CP violation in Cabibbo favored or doubly Cabibbo suppressed decays would unambiguously indicate new physics.

When HESR will reach its maximum luminosity a dedicated run with a yield of 10^8 reconstructed D-mesons may bring the level of CP violation in charm mesons as given by the Standard Model ($\alpha_{CP} \sim 10^{-3}$) in reach.

4 Conclusion

The new antiproton facility HESR planned at GSI offers rich possibilities in hadron physics at high rates and with high accuracy. A strong emphasis lies in the search for exotic states in the charmonium sector. But also tests of QCD and the electroweak Standard Model by measuring D-mesons are in reach of the projected experiment. Commissioning of the facility and start of data taking is planned for 2009/2010.

References

1. *An International Accelerator Facility for Beams of Ions and Antiprotons*, Conceptual Design Report, GSI, Darmstadt, November 2001

2. M. Ambrogiani *et al.*, Phys. Rev. D62(2000) 52002.

3. C. Michael, Proceedings of Heavy Flavours 8, Southampton, UK, 1999.
   P.R. Page, E.S. Swanson and A.P. Szczepaniak, Phys. Rev. D59 (1999) 034016.

4. F. Klingl, S. Kim, S.H. Lee, P. Morath and W. Weise, Phys. Rev. Lett. 82 (1999) 3396.
   A. Hayashigaki, Phys. Lett. B487 (2000) 96

5. A. Sibirtsev, K. Tsushima and A.W. Thomas, Eur. Phys. J. A6 (1999) 351

Frascati Physics Series Vol. XXXI (2003), pp. 281
FRONTIERSCIENCE 2002 – Frascati, October 6–11, 2002
Invited Review Talk in Plenary Session

e^+e^- B FACTORIES

W. Kozanechi

CEA-Saclay. F-91191 Gif-sur-Yvette CEDEX

Written contribution not received

Frascati Physics Series Vol. XXXI (2003), pp. 283–288
FRONTIERSCIENCE 2002 – Frascati, October 6–11, 2002
Invited Talk in Plenary Session

BTEV - A DEDICATED B EXPERIMENT AT THE TEVATRON

David Christian *
Fermi National Accelerator Laboratory

ABSTRACT

BTeV is a dedicated b-physics experiment that is expected to begin operation at the Fermilab Tevatron in 2008. BTeV is designed to take full advantage of the large production cross section of b particles (including B_S) in high energy hadron collisions. A quick description of the BTeV spectrometer is given in this paper. Two unique aspects of BTeV, the pixel-based trigger and the high quality lead tungstate electromagnetic calorimeter, are described in slightly greater detail.

1 Overview

At the BTeV design luminosity of $2 \times 10^{32} cm^{-2} s^{-1}$, approximately 4×10^{11} b hadrons (including B_S and Λ_B) will be produced every year at the Tevatron

* On behalf of the BTeV collaboration

collider. For comparison, approximately 2×10^8 b's (no B_S or Λ_B) will be produced per year at an e^+e^- factory operating at the $\Upsilon(4s)$ with a luminosity of $10^{34} cm^{-2} s^{-1}$. However, to take full advantage of this supply of B's, one needs a sophisticated trigger, excellent particle identification, excellent photon energy and position measurements, excellent vertex measurement, and excellent momentum measurement for charged particles. A central detector, especially one optimized for high p_T physics, can not satisfy these requirements; a dedicated experiment such as BTeV is required.

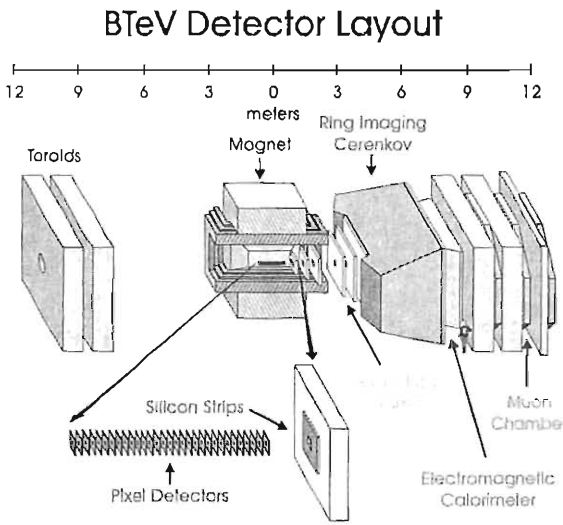

Figure 1: *The BTeV spectrometer.*

As shown in Fig. 1, BTeV is a forward magnetic spectrometer, with a large dipole magnet centered on the $\overline{p}p$ interaction region. A pixel vertex detector is located in the magnet. The long tracking lever arm provides excellent momentum resolution for momenta between ~1 and 100 GeV/c. The open layout allows the use of a ring imaging Cerenkov counter for excellent charged particle identification, and for a toroid muon spectrometer. Finally, the relatively small (compared to the LHC) range of particle momenta means that the charged particle tracking system can be short enough that an electromagnetic calorimeter can be constructed using scintillating crystals and still be affordable.

2 Pixel Vertex Detector and Trigger

The BTeV vertex detector will consist of a number of planar arrays of silicon pixel detectors mounted in the accelerator vacuum, transverse to the beam directions. Two movable carbon fiber half cylinders will support the planes. Silicon pixel detectors have been chosen because they provide excellent radiation tolerance [1] and position resolution better than 9μm at all angles of incidence [2], and most importantly, because they provide superb pattern recognition power.

An R&D program to develop a pixel readout chip optimized for the Tevatron was started at Fermilab in 1997, and is now nearing completion [3]. The BTeV pixel readout chip has been designed using radiation tolerant layout techniques [4] [5] for implementation in either of two commercial processes -. Taiwan Semiconductor Manufacturing Company 0.25 μm CMOS, or the 0.25 μm CMOS process available through CERN. The BTeV pixel size will be 50 μm $\times$ 400 μm. Each pixel chip will read out an array of 22 columns $\times$ 128 rows of pixels.

The most striking feature of BTeV is that the experiment will not use a trigger in the traditional sense of the word. All hit data from all detector elements will be digitized and read out *for every beam crossing*. At the design luminosity, data from the pixel vertex detector will be used to reconstruct tracks and interaction vertices for 15 million events per second (7.5 million crossings per second, with an average of 2 events per crossing). Data from the entire spectrometer will be buffered for up to *0.5 seconds* while the pixel data is reconstructed. The lowest level trigger will identify events containing reconstructable decays of charm and bottom particles [6] using criteria of the type usually applied in offline analyses, while rejecting 99% of the minimum bias events. This is possible only because the extreme granularity and high efficiency of the pixel detector makes pattern recognition exceedingly simple. The first stages of track finding can be parallelized by looking for tracks only where they leave the beam region and where they leave the pixel detector. FPGA-based hardware will perform these operations. Subsequent stages of the trigger are performed by clusters of 2500 DSP's and 2000 conventional processors, each of which operates on data from a single beam crossing.

3 Lead Tungstate Calorimeter

The BTeV electromagnetic calorimeter will be made up of lead tungstate crystals. Lead tungstate, which has been developed for the CMS collaboration, was chosen because it is fast, radiation tolerant, and provides excellent position and energy resolution [7]. BTeV will use photomultiplier tubes to measure the scintillation light produced in the crystals. This is possible since the BTeV calorimeter (unlike the CMS calorimeter) is not located in a magnetic field.

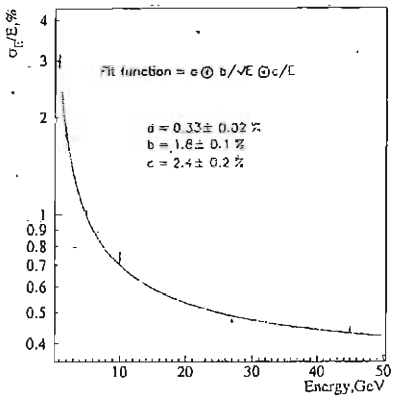

Figure 2: *Energy resolution obtained in beam tests of lead tungstate crystals.*

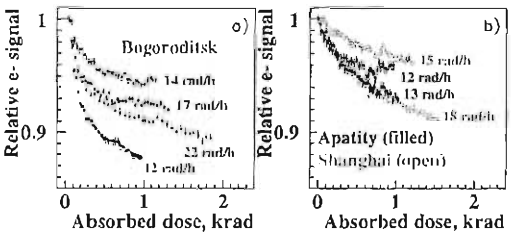

Figure 3: *Signal loss as a function of absorbed dose at different dose rates for lead tungstate crystals manufactured in Bogoroditsk (on the left) and in Apatity and Shanghai (on the right).*

In an ongoing series of beam tests at IHEP, Protvino, BTeV collaborators have verified the expected properties of lead tungstate [8]. Significantly, good

results have been obtained with crystals made by a variety of vendors. Fig. 2 shows the energy resolution obtained. Both the constant term (0.33%) and the stochastic term ($\frac{1.8\%}{\sqrt{E}}$) agree with Monte Carlo simulations. The $\frac{1}{E}$ term in the fitting function reflects the uncertainty in the electron beam energy. Fig. 3 shows the measured loss of signal as a function of absorbed dose for a number of different crystals irradiated at rates between 12 rad/hour and 22 rad/hour. Continuous calibration will be very important for the BTeV calorimeter since the light output is a strong function of dose rate and (as can be seen in the figure) there are large crystal-to-crystal differences.

Table 1: *Summary of Physics Reach of BTeV in* 10^7 *sec*

Decay Mode	BR ($\times 10^{-6}$)	Events	S/B	Parameter	Error (or Value)
$B^0 \to \pi^+\pi^-$	4.5	14,600	3	asymmetry	0.030
$B_s \to D_s K$	300	7500	7	γ	8°
$B^0 \to J/\psi K_s, \psi \to l^+l^-$	445	168,000	10	$\sin(2\beta)$	0.017
$B_s \to D_s\pi^-$	3000	59,000	3	x_s	(75)
$B^- \to D^0(K^+\pi^-)K^-$	0.17	170	1	γ	13°
$B^- \to D^0(K^+K^-)K^-$	1.1	1000	10		
$B^- \to K_s\pi^-$	12.1	4600	1		$< 4^\circ$
$B^- \to K^-\pi^0$	18.8	62000	20	γ	+ theory errors
$B^0 \to \rho^+\pi^-$	28	5400	4		
$B^0 \to \rho^0\pi^0$	5	780	0.3	α	$\sim 4^\circ$
$B_s \to J/\psi\eta$	330	2800	15		
$B_s \to J/\psi\eta'$	670	9800	30	$\sin(2\chi)$	0.024

4 Conclusion

BTeV is designed to make precise measurements of standard model parameters in the b and c quark systems, and to perform an exhaustive search for physics beyond the standard model. Simulations have been done using GEANT3 to determine the sensitivity of BTeV to a large number of b decays. Table 1, which is taken from a recent review of the BTeV physics reach [9], summarizes the expected BTeV sensitivity in a variety of modes important for measuring parameters of the CKM quark mixing matrix. BTeV will also be very sensitive

to a number of rare decays. For example, the annual yield of $B^0 \to K^{*0}\mu^+\mu^-$ is expected to be over 2500 events, when cuts are employed to yield a signal to background ratio of 11/1. Finally, the combination of a very capable spectrometer, including a high quality electromagnetic calorimeter, and a sophisticated vertex trigger, will give BTeV the flexibility to make precise measurements of the full range of b decays, not simply those decays thought to be most important today.

References

1. M.R. Coluccia, et al., "Electrical Characterization of Irradiated Prototype Silicon Pixel Sensors for BTeV", FERMILAB-CONF-02/281-E (2002), to be published in IEEE Trans. Nucl. Sci.

2. J.A. Appel, et al., "Performance of prototype BTeV silicon pixel detectors in a high-energy pion beam", Nucl. Instr. and Meth. **A 485** (2002) 411.

3. D.C. Christian, " The Architecture of the BTeV Pixel Readout Chip", FERMILAB-CONF-02/319-E (2002), presented at Pixel2002, Carmel, CA, September, 2002.

4. D.C. Christian, et al., "FPIX2: a radiation-hard pixel readout chip for BTeV", Nucl. Instr. and Meth. A 473 (2001) 152.

5. G. Chiodini, et al., "Radiation tolerance of prototype BTeV pixel detector readout chips", FERMILAB-CONF-02-147-E (2002), to be published in IEEE Trans. Nucl. Sci. **49**, No.6, 2002.

6. E.E Gottschalk, "BTeV detached vertex trigger", Nucl. Instr. and Meth. **A 473** (2001) 167.

7. J. Yarba, "The BTeV Electromagnetic Calorimeter Requirements for High Quality Reconstruction of Neutral Particles", these proceedings.

8. V.A. Batarin, et al., "Precision Measurement of Energy and Position Resolutions of the BTeV Electromagnetic Calorimeter Prototype", xxx preprint hep-ex/0209055, submitted to Nucl. Instr. and Meth **A**.

9. Penelope Kasper, Fermilab-Conf-02/324-E (2002), to be published in Nucl. Phys. B, Proceedings of the BEACH 2002 conference.

Frascati Physics Series Vol. XXXI (2003), pp. 289–295
FRONTIERSCIENCE 2002 – Frascati, October 6–11, 2002
Invited Talk in Plenary Session

B PHYSICS AT THE LHC

Neville Harnew
University of Oxford, Oxford OX1 3RH, UK

ABSTRACT

The CP-reach of the LHCb, ATLAS and CMS experiments is reviewed. A summary is given of the measurement of the unitarity triangle angle γ in a number of complimentary channels.

1 Introduction

Prior to 2007, BaBar, Belle, CDF and D0, will make first measurements of the parameters of the unitarity triangle. The quantity $\sin(2\beta)$ will be well measured in the "gold plated" $B_d^0 \to J/\psi K_s^0$ channel, perhaps to a world precision exceeding $\sim$0.02. The sides $|V_{td}/V_{ts}|$ and $|V_{ub}/V_{cb}|$ will be known from $B_s^0 - \overline{B}_s^0$ mixing and from $b \to u$ decays, respectively, but limited by theory to between 5–10%. The quantity $\sin(2\alpha)$ will be measured but with poor statis-

Table 1: Comparison of the LHC experiment parameters.

	LHC	
Energy / collision mode	14 TeV pp	
$b\bar{b}$ cross section	$\sim$500 μb	
Inelastic cross section	80 mb	
Ratio $b\bar{b}$ / inelastic	0.6%	
Bunch spacing	25 ns	
	LHCb	ATLAS / CMS
Detector configuration	Single-arm forward	Central detector
Running luminosity	2×10^{32}cm^{-2}s^{-1}	$\leq1\times10^{33}$cm^{-2}s^{-1}
$b\bar{b}$ events per 10^7 sec	$1\times10^{12}\times$ accept.	$\leq5\times10^{12}\times$ accept.
<Interactions/crossings>	0.5 ($\sim$30% single int.)	$\sim$2.3

tical precision, perhaps to $\sim$0.1. There will be no significant measurement of the angle γ.

The LHC will provide an unprecedented source of B hadrons, delivering of the order of 10^{12} $b\bar{b}$ pairs per year (10^7s). Precision measurements can be made of CP violation in many rare decay channels, including the B_s^0 sector. This will enable several redundant measurements of the angle γ to be made. A comparison of the LHC experiment parameters is given in Table 1.

2 The LHC Experiments

2.1 The LHCb Experiment

The LHCb detector [1] is a single-arm dipole spectrometer, which exploits the sharply peaked forward-backward $b\bar{b}$ production cross section. It runs at a tuned LHC luminosity of 2×10^{32}cm^{-2}s^{-1}, which maximizes the number of single interactions per beam-crossing. The detector covers a forward angular aperture between approximately 10 and 250 mrad (300 mrad) in the non-bending (bending) plane. Experimental attributes of LHCb include efficient K/π identification, excellent decay time and mass resolutions, and photon detection.

The detector has recently been reoptimized, resulting in less material and improved performance. The new layout of the LHCb experiment, the so-called "LHCb-Light" geometry, is shown in Fig. 1.

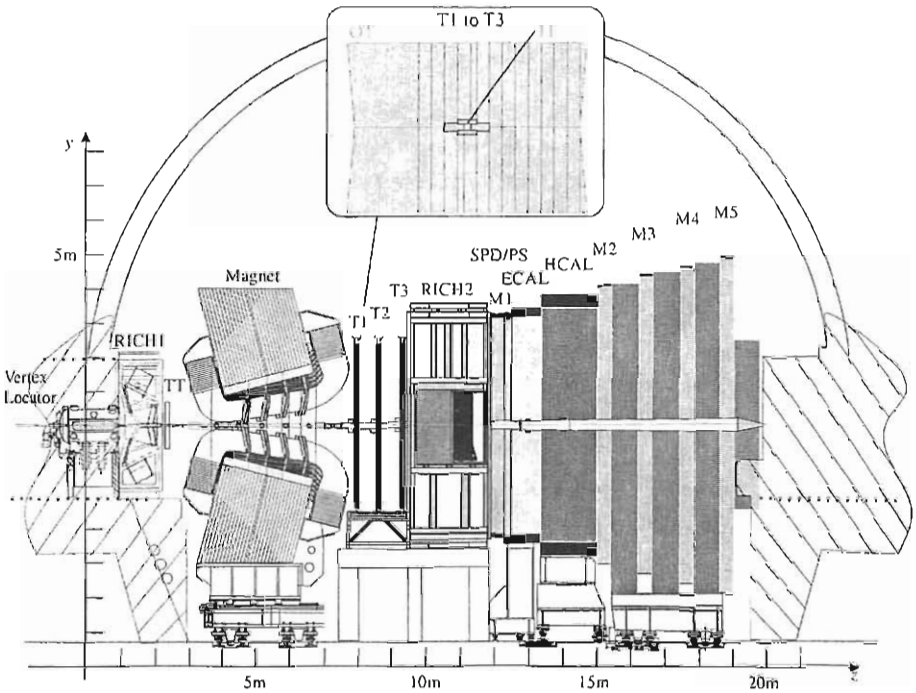

Figure 1: The optimized "LHCb-Light" spectrometer. The layout of the inner and outer regions of the T1 T3 chambers is highlighted.

- The Tracking System has undergone major revision. Nine tracking stations have been reduced to four, resulting in a reduction of the material budget from 0.27 X_0 (0.11 λ_0) to 0.12 X_0.
- The removal of shielding plates in front of the magnet gives ~0.1 T of fringe field in the region of RICH-1, which necessitates a new "vertical" RICH-1 layout with a two-mirror reflective geometry.
- The fringe field in the region between the Vertex Locator (VELO) and the magnet allows a momentum measurement at the Level-1 trigger. This gives a more efficient rejection of fake vertices which result from secondary interactions. At a 40 kHz output rate, the new Level-1 design gives a

preliminary efficiency for $B_d^0 \to \pi^+\pi^-$ events better than 85%.

2.2 The ATLAS/CMS Experiments

The ATLAS [2] and CMS detectors [3] have tracking coverage in the central rapidity region, $|\eta|$ <2.5 and include pixel microvertex layers at a radius of ~5 cm. Specialist B triggers which can operate up to luminosities of typically 1×10^{33} cm^{-2}s^{-1}, appropriate for the first 30 fb^{-1} of running (~3 years). However, there is current uncertainty on whether the data acquisition systems of the experiments will need to be staged and, if so, this would have a detrimental effect on the B physics capabilities.

The detectors have no dedicated hadronic particle identification capabilities. However the ATLAS TRD provides a dE/dx measurement giving limited K/π separation (~0.8σ). An event-by-event maximum likelihood technique can be made to identify B decays using the proper time, reconstructed mass and the K/π separation variable. Nevertheless, complete event analysis of B decay channels which require particle identification will be very challenging.

3 B physics performance

The CP physics reach of the LHC experiments in specific benchmark channels after a year of operation, together with the unitarity triangle parameters which they measure, is summarised in Table 2. The LHCb performance figures are prior to detector optimation, and are currently being re-evaluated for the new LHCb-Light geometry and the improved trigger.

3.1 Measurements of the angle γ with LHCb

A major strength of the LHC is that it provides a copious number of B_s^0 mesons. This allows the angle γ to be measured in a variety of complementary ways. Since particle identification and good mass resolution are essential, rigorous measurements of γ at the LHC are only possible with the LHCb experiment.

- The measurements of four time-dependent decay rates in the channels $B_s^0 \to D_s^{\pm}K^{\mp}$ and the charge conjugate states provide a theoretically clean measurement of the angle $(\gamma - 2\delta\gamma)$ [4]. LHCb will record ~2400 events per one year of running, giving a sensitivity of 3°–16° in $(\gamma - 2\delta\gamma)$.

Table 2: Performance summary of the LHC experiments in a selection of benchmark channels for one year of operation. The quoted numbers are the errors on the parameter in question, unless specified otherwise. A dash for an entry means that no significant measurement can be made.

Measurement	Channel	LHCb	ATLAS	CMS
$\sin(2\beta)$	$B_d^0 \to J/\psi K_s^0$	$0.3° - 0.5°$	$0.6°$	$0.7°$
$\sin(2\alpha)$	$B_d^0 \to \pi^+\pi^-$	$2° - 10°$	$3°$	$5°$
$\sin(2\alpha)$, $\cos(2\alpha)$	$B_d^0 \to \rho\pi$	$5° - 15°$	–	–
$2\beta + \gamma$	$B_d^0 \to D^*\pi$, 3π	down to $7°$	–	–
$\gamma - 2\delta\gamma$	$B_s^0 \to D_s K$	$3° - 16°$	–	–
γ	$B_d^0 \to \overline{D}^0 K^{*0}$	$4° - 18°$	–	–
$\delta\gamma$	$B_s^0 \to J/\psi\phi$	$0.6°$	$0.9°$	
x_s	$B_s^0 \to D_s^- \pi^+$	< 90	< 46	< 48
Rare decay	$B_s^0 \to \mu^+\mu^-$	4.4σ S.M.	4.3σ S.M.	10σ S.M.

- The channels $B_d^0 \to \pi^+\pi^-$ and $B_s^0 \to K^+K^-$ provide a measurement of the angle γ via two time-dependent decay asymmetries [5]. The importance of particle identification and good mass resolution is demonstrated in Fig. 2. Approximately 5000 events are expected per year in each channel. The angle γ can be measured to a precision of 5°–10° after one year of running, limited by theoretical uncertainty.

- The channels $B_d^0 \to D^{*\pm}\pi^{\mp}$ and the charge conjugate states provide a measurement of the angle $(2\beta+\gamma)$ via four time-dependent decay rates [6], with an expectation of ~500 k events per year. The angle γ can be measured to a precision better than 5° after five years of running, assuming β is measured from $B_d^0 \to J/\psi K_s^0$ decays.

- The channel $B_d^0 \to \overline{D}^0 K^{*0}$ and the charge conjugate states provide a determination of the angle γ via a measurement of six time-integrated decay rates [7]. Since visible branching ratios are very small (10^{-8} – 10^{-7}), an annual yield of only 1700 events in all six channels is expected.

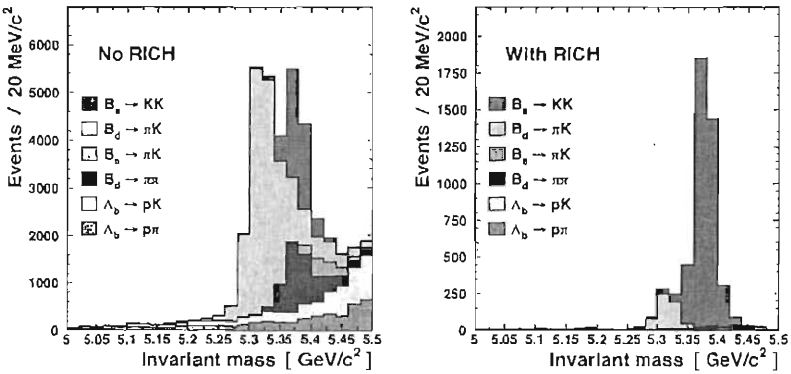

Figure 2: The B_s^0 mass peak from $B_s^0 \to K^+K^-$ combinations before and after particle identification criteria have been applied.

A measurement of the angle γ is possible to a precision of $\sim 10°$ after one year of running.

3.2 The $B_s^0 \to \mu^+\mu^-$ rare decay

The $B_s^0 \to \mu^+\mu^-$ channel is an example of a Standard Model rare decay process, with an expected branching ratio of $\sim 3.5 \times 10^{-9}$ [8]. Here the high p_T di-muon triggers running at high luminosity (1×10^{34} cm^{-2}s^{-1}) give the general-purpose detectors a distinct advantage over the forward detector. With its excellent muon detection capability, CMS can observe an estimated 26 signal events with 6.4 events background for 100 fb^{-1} of running.

4 Summary

The LHC experiments will perform a study of CP violation with unprecedented precision in many different and complimentary channels. The LHCb detector provides good particle identification, vertexing, and has an efficient and flexible trigger. K/π particle identification will be essential for the measurement of B final states involving hadrons. ATLAS/CMS measure leptonic channels very well, but are not so competitive in hadronic modes. Construction of the

detectors is progressing well and the LHC will be ready for data-taking in 2007.

Acknowledgments

I am very grateful to the following people who provided material for this review : Paula Eerola and Nick Ellis (ATLAS), Fabrizio Palla and Samim Erhan (CMS), and Tatsuya Nakada and Guy Wilkinson (LHCb). I also extend my thanks to the Symposium organizers, in particular to Franco Fabbri and Paolo Valente.

References

1. LHCb Technical Proposal, **CERN/LHCC/98-04** (Feb. 1998).
2. ATLAS Technical Proposal. **CERN/LHCC/94-43** (Dec. 1994).
3. CMS Technical Proposal **CERN/LHCC/94-38** (Dec. 1994).
4. See for example R. Aleksan, I. Dunietz and B. Kayser, Z. Phys. **C54** 653 (1992).
5. R. Fleischer, **CERN-TH/2000-101**.
6. I. Dunietz, Beauty'97, *Nucl. Instr. Meth.* **A408** 14 (1998).
7. M. Gronau & D. Wyler, Phys. Lett. **B265** 172 (1991).
8. A. Ali, Beauty'96, *Nucl. Instr. Meth.* **A384** 8 (1996).

Round Table

Chairpersons: M. Artuso, C. Matteuzzi

Frascati Physics Series Vol. XXXI (2003), pp. 299–304
FRONTIERSCIENCE 2002 – Frascati, October 6–11, 2002
Round Table

FLAVOR PHYSICS

A round table discussion at Frontier Science 2002

Marina Artuso
Syracuse University, Syracuse, NY 13244, USA
Clara Matteuzzi
I.N.F.N. Milano and Universita' di Milano-Bicocca, Milano, Italy

1 Introduction: the flavor puzzle

The main achievement of the experimental particle physics program reflects the tremendous success of the Standard Model of electro-weak and strong interactions in describing the complex phenomenology explored in a variety of experiments of increasing precision and complexity. The evidence for neutrino oscillations is perhaps the only observation that points to new physics. However this coherent picture leaves us yearning for a more complete picture. There are many questions that the Standard Model does not answer satisfactorily. One of the most compelling is the origin of flavor. In the Standard Model there are 3 families of quarks and leptons. The family replication and the very different mass scale of the different flavors are empirical facts so far without any satisfactory underlying explanation. This flavor puzzle is one of our strongest

motivation to seek for a new and more complete theory. We believe that the multifaceted aspects of flavor physics can be organized around four key questions:

1. Why does flavor exist?
2. Are there high mass scales whose physics influences the properties of quarks and leptons?
3. What physics is responsible of the baryon asymmetry of the universe?
4. What is the physics underlying the hierarchy of masses and mixings in the quark and lepton sectors?

Progress can be made only through the synergy of experimental inquiry and new theoretical ideas. We have identified a few key physics points that may provides significant milestones in this physics program.

2 Flavor physics: a multifaceted approach

The pattern of masses and interactions of quarks is well-described, but its origin is almost a complete mystery. Progress is being made in mapping out the corresponding pattern for leptons, with many experiments pointing to neutrino mass differences in the sub-eV range and near-maximal mixings. Information on the degree to which lepton number and baryon number is conserved has grown substantially in the past two decades, but many theories predict that experiments with improved sensitivities will begin to detect violations. Any more fundamental theory that we are seeking will have to address the flavor ultimate challenge. The very nature of flavor physics demands diverse approaches, through the study of charm, and B hadrons, decays of τ leptons and K,CP violation in leptonic and hadronic processes, neutrino oscillations and direct mass measurements, neutrinoless double-beta decay,flavor-changing leptonic and hadronic transitions, nucleon decay, and magnetic and electric dipole moments.

2.1 Heavy flavor decays

The study of CP violation asymmetries in charm and beauty decays, as well as the study of rare K, D, B decays will lead to decisive tests of the Standard

Model. An important feature of the fundamental interactions explored in flavor physics is CP violation. After several decades when the only experimental evidence for CP violation was provided by studies of neutral K decays, this year direct evidence for CP violation in B decays has been obtained by the two e^+e^- b-factory experiments, BaBar at PEP-II and Belle at KEK-B. CP violation is crucial to our understanding of the history of the universe. In particular, it is a necessary ingredient of our understanding of the origin of the matter dominated universe [1]. A CP violating phase is naturally incorporated in the Standard Model within the Cabibbo- Kobayashi-Maskawa matrix. Thus several models attempt to explain the baryon asymmetry of the universe as due to a CP violating process occurring at the scale of the electro-weak symmetry breaking. A rough order of magnitude estimate of the expected effect of the CKM induced CP violation on the baryon asymmetry can be obtained by constructing a variable d_{CP} that incorporates all the features of the expected CKM phase: it vanishes when any pair of quarks is degenerate in mass and when any CKM angle vanishes because of the so called "GIM" (Glashow, Iliopoulos, Maiani) cancellation. d_{CP} is defined as:

$$\begin{aligned} d_{CP} = \quad & \sin\theta_{12}\sin\theta_{23}\sin\theta_{13}\sin\delta_{CP} \\ & (m_t^2 - m_c^2)(m_t^2 - m_u^2)(m_c^2 - m_u^2) \\ & (m_b^2 - m_s^2)(m_b^2 - m_d^2)(m_s^2 - m_d^2), \end{aligned} \tag{1}$$

where θ_{ij} are three real "Euler-like" angles defining the CKM matrix together with the imaginary phase δ_{CP}. The d_{CP} parameter that we have just defined is a dimensional quantity, it is conceivable [2] that the natural normalization parameter to transform it into a pure number is the temperature at which the electroweak symmetry breaking occurred. Thus the figure of merit of the strength of the CKM induced CP violating effect is given by:

$$d_{CP}^T = d_{CP}/kT_{ew}^{12} \approx 10^{-18}, \tag{2}$$

where T_{ew} represents the temperature at the time the electro-weak symmetry breaking occurred and k is the Boltzmann constant. This suggests that CKM CP violation is an effect too small to account for the known baryon asymmetry of the universe,

$$\left|\frac{N_B - N_{\overline{B}}}{N_B + N_{\overline{B}}}\right|_{t\approx 10^{-6}s} \approx \left|\frac{N_B}{N_\gamma}\right| \tag{3}$$

This discrepancy is very qualitative in nature and may have a number of explanations. However a very tantalizing hypothesis is the presence of additional CP

Table 1: *Predictions of different SUSY models*

Model	$\frac{d_N}{10^{-25}\ e\ \mathrm{cm}}$	θ_M	θ_D	$a_{D\to K\pi}$	$a_{K\to\pi\nu\bar{\nu}}$
Standard Model	$\lesssim 10^{-6}$	0	0	0	$\mathcal{O}(1)$
Exact Universality	$\lesssim 10^{-6}$	0	0	0	=SM
Approx. Universality	$\gtrsim 10^{-2}$	$\mathcal{O}(0.2)$	$\mathcal{O}(1)$	0	$\approx$SM
Alignment	$\gtrsim 10^{-3}$	$\mathcal{O}(0.2)$	$\mathcal{O}(1)$	$\mathcal{O}(1)$	$\approx$SM
Heavy Squarks	$\sim 10^{-1}$	$\mathcal{O}(1)$	$\mathcal{O}(1)$	$\mathcal{O}(10^{-2})$	$\approx$SM
Approximate CP	$\sim 10^{-1}$	$-\beta$	0	$\mathcal{O}(10^{-3})$	$\mathcal{O}(10^{-5})$

violating phases produced by mechanisms beyond the Standard Model. Thus, the experimental exploration of CP violation observables has a good chance to uncover evidence for new physics. A variety of new CP violation scenarios can be envisaged depending upon the assumed pattern of new physics implementation. In broad terms, we can assume that new physics may introduce a new phase in $B^0\bar{B}^0$ mixing (θ_M), a new phase in the decay amplitude θ_D. Moreover, CP violation in charm decays, probing the u-quark sector physics, can be enhanced with respect to the very small Standard Model expectation through the appearance of a novel phase $\phi_{K\pi}$. It is interesting to note that different "Beyond the Standard Model" scenarios involve quite different expectations for the magnitude of these parameters. For example, Table 1 [3] shows a comparison between the predictions from different SUSY implementations. For completeness the predictions of these models for other exotic processes such as the neutron electric dipole moment have been included. This illustrates how heavy flavor physics and small scale precision measurements can be a powerful tool to identify a path towards a more complete effective theory of the fundamental interactions. Heavy flavor physics has been pursued vigorously at e^+e^- colliders and in hadron colliders for several decades. The experimental tools to acquire a precise knowledge of CP violation and rare decays in the heavy flavor sector have been developed and are planned to be implemented in two ambitious hadron collider experiments, BTeV and LHC-b. Their physics program will be central to our goal to explore this rich landscape of discovery opportunities [4]. In parallel, the study of rare K decays will provide complementary and very valuable constraints [5].

2.2 The lepton sector frontier

The study of neutrino masses and mixing parameters will provide us an ever-enlarging window on physics beyond the Standard Model, and is an alternative path that nature may have taken to implement the CP asymmetry responsible for the baryon asymmetry of the universe. The experimental study of solar neutrinos and atmospheric neutrinos has already provided tantalizing hints of physics beyond the Standard Model. There is no doubt that the emergence of a neutrino mixing matrix analogous to the quark mixing matrix is playing a key role in shaping our thinking in the path towards a new physics and unification [6]. Several ideas have emerged on how to pin down the absolute neutrino mass scale and how to uncover possible CP violation in the lepton sector. The experimental tools to pursue this exciting physics are now being developed and will ultimately uncover very important scientific information. Lepton and baryon number non-conservation, and the study of magnetic and electric dipole moments, can severely constrain theories beyond the Standard Model or provide guidance as to their nature. The search for lepton or baryon number violation is a saga spanning several decades. Early predictions of some unified theories such as SU(5) prompted the first generation of nucleon decay experiments. These experiments ruled out the first and simplest implementation of Grand Unified Theories (GUTs), and, incidentally, were the starting point of the exciting developments in ν physics that we witnessed in recent years. The next generation experiments may very well have sufficient sensitivity for exciting discoveries and provide landmark clues towards the path to unification.

3 Conclusions

The experimental landscape of flavor physics is extremely varied. Experiments planned or proposed range from table top experiments, to complex experiments exploiting well known technologies to novel ideas just in the initial R&D phase. The pursuit of this complex physics program is a necessary complement to the search for new massive exotic particles at the energy frontier. It provides unique contributions to our ultimate goal of achieving a more complete theoretical framework of the fundamental particles and their interactions.

4 Acknowledgements

It is a pleasure to thank the round table participants, G. Martinelli (Universita di Roma La Sapienza), H.Orth (GSI), D. Pedrini (I.N.F.N. Milano and Universita' di Milano), G. Ross (Oxford University), for their interesting contributions. We would like also to thank J. Ellis that, although not able to participate to the roundtable discussion for conflicting engagements, shared his incisive thoughts on the themes discussed in his summary talk. M.A. work was supported by the U.S. National Science Foundation.

References

1. A.D. Sakharov *Sov.Phys.Usp.* **34**417 1991.
2. G. Farrar *Nucl. Phys. Proc. Suppl.* **43** 312 (1995).
3. Y. Nir, *Lectures given in the XXVII SLAC Summer Institute on Particle Physics*, July 7 - 16, 1999.
4. Z. Zhao *et al.*, eConf C010630, E2001 (2001);hep-ex/0201047 (2002).
5. A. Belyaev *et al.*, Cern Preprint CERN-TH/2001-175 (2001); hep-ph/0107046.
6. D. Chang, A. Masiero and H. Murayama, *Nucl.Phys.* **B634** (2002) 105.

Next Frontiers

Chairpersons: P. Sheldon, G Buchalla

R. Petronzio	Perspectives in Lattice Gauge Theories
F. Feruglio	SUSY and Extra-Dimensions
G. Montagna	The Quark and the NASDAQ Non-Linearity and Complexity From Particle Physics to the Real World
J. Garcia Bellido	Particle Physics and Cosmology

Frascati Physics Series Vol. XXXI (2003), pp. 307–310
FRONTIERSCIENCE 2002 – Frascati, October 6–11, 2002
Invited Review Talk in Plenary Session

PERSPECTIVES IN LATTICE GAUGE THEORIES

R. Petronzio
Dipartimento di Fisica, Università di Roma "Tor Vergata", V. R. Scientifica 1, I-00133 Rome, Italy
and
INFN Roma 2, V. R. Scientifica 1, I-00133 Rome, Italy

ABSTRACT

General perspectives in lattice gauge theories simulations are enumerated and a specific one concerning heavy flavour calculations is reviewed.
The main goals of lattice calculations are:

- calculate QCD in the non perturbative regime, i.e. the spectroscopy, weak interaction matrix elements, structure functions, ...
- fix the fundamental parameters of QCD: Λ and the quark masses
- investigate the properties of new states of matter: the quark gluon plasma

Before entering a specific subject, some basic facts must be recalled. The lattice is a 4–dimensional crystal with hypercubic symmetry and a finite lattice spacing, a. The standard QCD action is only recovered in the continuum limit (a going to zero). The lattice spacing acts as an UV cutoff and the continuum limit does exists only for the renormalised theory where the cutoff is traded

against physical units by a physical input. The bare coupling regulates the value of the lattice spacing and must tend to zero in the continuum limit. Gauge field configurations are generated by Monte Carlo algorithms where the choice of a new value of the field at a given lattice point depends upon neighbouring values only (local updates). Fermions are classic fields and their propagation is calculated by expensive inversion algorithms of sparse matrices.

Finite computing resources imply some limitations. In particular one has a finite number of points and a compromise between the total physical extent (that should be large in order to avoid finite volume effects in chiral extrapolations) and the lattice resolution (that should be high in order to avoid lattice artifacts and have safe continuum extrapolations). The possibility of simple local updating algorithms is spoiled by the inclusion of dynamical quark loops (the calculation of the fermion determinant increases the cost of an update by roughly a factor 100 with respect to the so called quenched calculations where they are removed). The present frontiers of the field include:

- the unquenching: restoring the effects of dynamical quark loops
- the chiral limit in theories with an exact chiral invariance at finite lattice spacing
- the *perfect actions* where the continuum limit can be taken at *finite lattice resolution* along a renormalized trajectory
- the *two scales problems*, requiring a huge number of lattice points to match the hierarchy between the two scales.

In the rest of the talk, I will discuss some recent advances in typical two scale problems, i.e. the calculation of the B–meson decay constant f_B. The problem needs to meet two constraints:

- $a \ll 1/m_b$, i.e a lattice resolution high enough to resolve a propagating b–quark
- $Na = L \gg 1/m_{light}$, in order to avoid finite size effects, which imply $N \gg m_b/m_{light}$.

These two requirements imply a number of lattice points

$$N \gg \frac{m_b}{m_{light}} \tag{1}$$

well beyond 60, to match the hierarchy between the two mass scales.

The step scaling method relies on the following hypothesis: volume effects are mainly related to the light quark mass and rather insensitive to the heavy quark mass. The consequence is that volume effects can be safely extrapolated in the heavy quark mass. The following recipe exploits the previous idea:

- calculate f_B on a finite volume and with the appropriate resolution
- calculate the correction factors relating the small volume to the physical one and extrapolate them to the heavy quark mass value
- correct f_B on a finite volume and get the physical value on a sufficiently large volume.

Volume effects are calculated non–perturbatively by estimating with numerical simulations the step scaling function:

$$\sigma = \frac{f_B(2L)}{f_B(L)} \tag{2}$$

that is in general a function of the light and of the heavy quark mass. However,

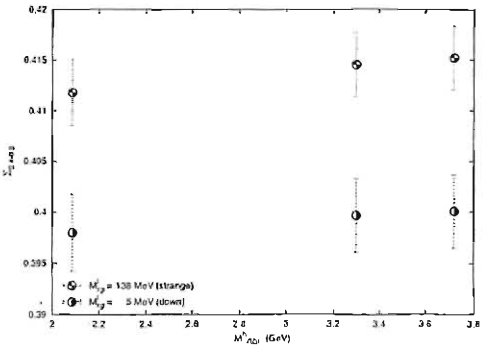

Figure 1: Step scaling function $\Sigma_{0.4-0.8}$ for the evolution of f_{hl} from 0.4 fm to 0.8 fm at $\beta = 6.737$.

as it can be seen in figure 1, the sensitivity to the heavy quark mass decreases for quark masses larger than about the charm mass and make a simple extrapolation in the inverse of the heavy mass, inspired by the heavy quark effective theory, a safe procedure. A small volume calculation can then be promoted to a large volume by multiplying it by the step scaling functions, an appropriate number of times, safely extrapolated to the heavy quark mass region. The numbers are [2]:

$$\begin{aligned} f_B &= 170(11)(5)(22) MeV \\ f_D &= 204(9)(6)(23) MeV \,. \end{aligned} \tag{3}$$

The main advantage of the method is the possibility of taking the continuum limit, an impossible goal for effective theories, as well of making the unquenching affordable. The perspective is to apply the method to other two scale problems, like form factors.

Global perspectives for lattice computations include (see [1)] for recent reviews):

- Exact chiral symmetry and exact supersymmetry on the lattice
- unquenched calculations by default
- B–physics unquenched
- the $\Delta I = 1/2$ puzzle under control
- quark gluon plasma phase diagram explored
- the advent of multi–teraflop machines (APEnext, Columbia, New-Tsukuba).

References

1. M. . Muller-Preussker *et al.*, *Prepared for 19th International Symposium on Lattice Field Theory (Lattice 2001), Berlin, Germany, 19-24 Aug 2001*
2. M. Guagnelli, F. Palombi, R. Petronzio and N. Tantalo, Phys. Lett. B **546** (2002) 237 [arXiv:hep-lat/0206023].

Frascati Physics Series Vol. XXXI (2003), pp. 311
FRONTIERSCIENCE 2002 – Frascati, October 6–11, 2002
Invited Review Talk in Plenary Session

SUSY AND EXTRA-DIMENSIONS

F. Feruglio

Padova University, Via Marzolo 8, 35131 Padova - Italy

Written contribution not received

Frascati Physics Series Vol. XXXI (2003), p. 313–320
FRONTIERSCIENCE 2002 – Frascati, October 6–11, 2002
Invited Review Talk in Plenary Session

THE QUARK AND THE NASDAQ NON-LINEARITY AND COMPLEXITY FROM PARTICLE PHYSICS TO THE REAL WORLD

Guido Montagna*
Dipartimento di Fisica Nucleare e Teorica, Università di Pavia, and Istituto Nazionale di Fisica Nucleare, Sezione di Pavia, Via A. Bassi 6, I-27100, Pavia, Italy.

ABSTRACT

The next workshop on FRONTIER SCIENCE will be dedicated to the physics of complexity and its interdisciplinary applications. To present the event, a personal review of the study of complex systems as an emerging, cross-disciplinary science is given.

1 Introduction and motivations

The series of the international workshops on FRONTIER SCIENCE consists of three events held in alternate years in Frascati (2002), Pavia (2003) and Roma (2004). One of the aims of the workshops is to address different subjects which are somehow correlated and can benefit from mutual knowledge. While the

* On behalf of the organizing committee of FRONTIER SCIENCE 2003.

first workshop was dedicated to a particularly lively topic in nuclear and subnuclear physics, *i.e.* to the physics of heavy quarks and CP violation, the third workshop will be devoted to space physics and astrophysics. In between the microscopic scale of quarks and the cosmic scale of galaxies and the universe, there is the scale of our world, the real world, where many non-linear phenomena, which are studied in disciplines such as geology, meteorology, biology, medicine, economics, computer science, sociology and others, take place. This is the reason why it was decided to dedicate the second event of FRONTIER SCIENCE to the science of complexity and its interdisciplinary applications. The title assigned to the workshop is "A non-linear world: the real world", because the methods of non-linear physics are generally used to study the non-linear phenomena occuring in the real world.

Why to organize a conference on complex systems? To answer this question, I quote M. Gell-Mann, one of the founders of the Santa Fe Institute for the study of complex systems, from the book The Quark and the Jaguar [1]. Gell-Mann writes: *"One of the great challenges of contemporary science is to trace the mix of simplicity and complexity, regularity and randomness, order and disorder up the ladder from the particle physics and cosmology to the realm of complex adaptive systems"*. To this end, Gell-Mann emphasizes that *"...we need to overcome the idea, so prevalent in both academic and bureaucratic circles, that the only work worth taking seriously is highly detailed research in a specialty. We need to celebrate the equally vital contribution of those who dare to take what I call a crude look at the whole"*. Further motivations can be found in a recent review on complex systems by G. Parisi [2]. Parisi writes: *"There have been three revolutions in physics which...have changed the meaning of the word prediction. They are:*

1. *the introduction of statistical mechanics and of the first probabilistic reasoning by Maxwell, Boltzmann and Gibbs in the second half of the last century;*
2. *the discovery of quantum mechanics at the beginning of this century;*
3. *the study of complex systems and the related techniques that have been developed in these last years.*

As remarked by G. Parisi, *"the positive consequence of this process is that the scope of physics becomes much larger and the constructions of physics find many more applications"*.

Even if a precise definition of complex system is unavailable, the editors of Science, in a special section on complex systems [3], suggest that a working definition of complex system is *"...one whose properties are not fully explained by an understanding of its component parts"*. Therefore, according to this

definition, examples of complex systems are a turbulent fluid, the climate, the earthquakes, the DNA, the mechanism of protein folding, the nervous system, an ecosystem, the traffic flow, a financial market, the hadronic jets in high-energy physics, just to cite a few.

Appropriate theoretical methods are available to analyze the complicated dynamics of complex systems. They are the theory of stochastic processes, the theory of chaos and non-linear dynamics and the geometry of fractals and multi-fractals. Generally speaking, these methods point out that a typical property of a complex system is a "scale-free" behaviour, *i.e.* the absence of a characteristic spatial or time scale, which implies the emergence of power laws. Noticeably, also novel computational and dynamical tools have been developed to understand numerically the behaviour of complex systems and, remarkably, some of them, such as neural networks, genetic algorithms and cellular automata, are constructed in analogy with the dynamics of certain complex systems existing in nature.

2 Aspects of complexity in high-energy physics

Before giving a brief (and personal) account of recent achievements in the field of complex systems, it is important to emphasize that ideas and methods of complexity have been successfully applied in high-energy physics in recent years.

A first example concerns the charged particle multiplicity distribution in hadronic Z boson decays [4, 5]. From the studies performed at high-energy electron-positron (e^+e^-) accelerators, it comes out that the Log-Normal Distribution (LND) gives a good parameterization of the data on multiplicity, in different rapidity windows [4]. Since the LND can be derived from the general assumption that multiparticle production proceeds via a scale-invariant stochastic branching process [5], this result emphasizes the role in particle physics of stochastic processes, which is concept widespread in the study of complex systems.

More quantitatively, hadronic Z decays can be used to measure the scaling properties of normalized factorial moments, to investigate dynamical fluctuations in hadron production [6, 7]. In Fig. 1, the factorial moments in three dimensions F_q, as measured by L3 Collaboration at LEP, are compared with a power-law scaling of the form

$$F_q(M) \propto M^{\phi_q} \tag{1}$$

where M is the number of bins in which momentum space is partitioned and ϕ_q is an empirical parameter known as intermittency index. As can be seen in

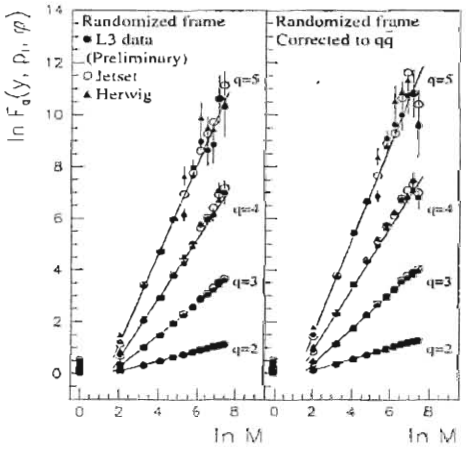

Figure 1: *The factorial moments F_q, as a function of the number of bins M, compared with a power-law fit as in eq. (1) and the results of JETSET and HERWIG Monte Carlo's, for two different reference frames. From* [7].

Fig. 1, the power-law scaling gives a good fit of the data, indicating that the corresponding hadronic system has a self-similar, fractal structure. This phenomenon is known in particle physics as intermittency [6] and is observed in all type of high-energy collisions. It is in analogy with turbulence in hydrodynamics, which is a typical complex system where a similar power-law behaviour is known.

Another interesting and recent application of the methods of complexity to subnuclear physics is the neural network parameterization of deep-inelastic structure functions [8]. Neural networks, which are so widely used in the simulation of complex systems, can provide, after a training on a Monte Carlo sample of pseudo-data, an unbiased and smooth interpolation of existing data of deep-inelastic scattering, because of their capability of approximating non-linear relations. This may be useful for future applications to the precision phenomenology of deep-inelastic scattering.

3 Interdisciplinary applications

Complex systems, non-linear phenomena and self-similar structures are present in different disciplines, such as geophysics, meteorology, biology, ecology, me-

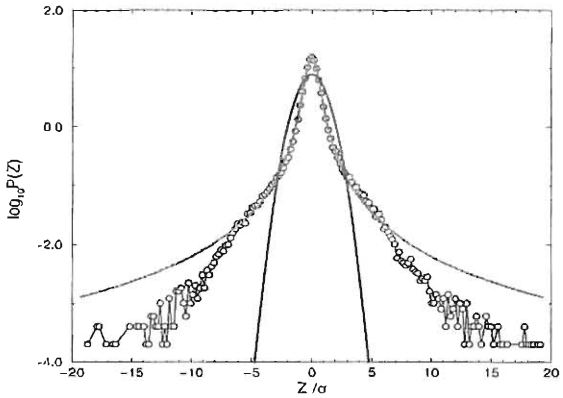

Figure 2: *Probability distribution $P(Z)$ of the S&P 500 index variations $Z(t)$ for $\Delta t = 1$ minute, compared with a gaussian distribution (blue line) and a Lévy non-gaussian profile (red line). From* [13]. *Courtesy of R.N. Mantegna.*

dicine, finance, computer science, linguistics and others. During the last two decades, interesting results have been obtained in such disciplines by physicists, often in collaboration with experts of other fields [9].

A first example concerns seismology and, more precisely, the time interval distribution of earthquakes [10]. The analysis of the statistical properties of seismic time series data in Southern California reveals that the cumulative distribution of time calm intervals, which are the time intervals between successive significant earthquakes above a fixed threshold of magnitude, obeys a scaling law of Zipf-Mandelbrot type [11]. The discovery of this new empirical law indicates a scale-free nature of earthquakes and can be a guideline for one of the extreme goals of seismology, *i.e.* the prediction of a next main shock after an important earthquake.

An example of interest for life sciences is the study of the correlation properties of human heartbeat time series [12]. In particular, it is interesting to compare the fluctuations in the time series of sequential intervals between a beat n and a beat $n+1$, as a function of the beat number, in the two cases of a healthy subject and of a subject with a severe cardiac disease. It is found that, while for a healthy subject long-range correlations are important, indicating an adaptive behaviour of the healthy hearth, a subject with a diseased hearth reveals a pattern close to an uncorrelated random walk noise.

For the modeling of the financial market, it is important to know the probability distribution of the variations of an economic index. Mantegna and Stanley [13], analyzing the data of the Standard & Poor's 500 of the New

York Stock Exchange over a six-year period, observed that the probability distribution associated to the short-term dynamics of that economic index is not gaussian, but corresponds to a non-gaussian Lévy process, especially in the central part of the distribution, as shown in Fig. 2. Since the presence of "fat tails" is observed in many financial markets, this kind of analysis is useful as a framework for the development of better economic models, which generally assume a gaussian distribution of stock prices. For example, a precise knowledge of the dynamics of index variations is necessary to develop models to price financial products known as derivatives [14]. The realization of efficient theoretical and computational algorithms to price financial derivatives is of upmost importance for the activity of financial practitioners operating in the fields of option pricing and risk management, and represents a good example of spin-off of fundamental theoretical physics.

The physics of complexity can provide results of interest also for the study of many social and communication systems which can be modeled as complex networks. A recent example is the analysis of epidemic spreading in networks, and, in particular, of the spreading of computer virus infections in the Internet [15]. An investigation of real data reveals that the survival probability of different computer viruses has a clean exponential tail, with different life-times according to the their infection mechanism, and that an epidemic threshold is absent in scale-free networks. These studies are considered very promising not only for computer science, but also for the fields of epidemiology and pollution control.

Recent progress based on methods of non-linear and statistical physics occured in particle physics and astrophysics too.

A recent progress is related to the thermodynamical approach [16] to hadron production in e^+e^- annihilation [17]. As shown in Fig. 3, the transverse momentum distribution of hadrons with respect to the jet axis deviates from the exponential expectation of Boltzmann-Gibbs (BG) statistics and can be fitted by using anomalous distributions derived from Tsallis non-extensive statistics [18], which is a generalized statistics containing BG as a particular case and able to describe systems that present long-range interactions.

It is remarkable that non-extensive statistics is also able to explain the observed energy dependence of fluxes of cosmic rays [19]. Actually, this energy dependence is not exponential but it can be fitted by an anomalous distribution derived from Tsallis statistics, a result which can be related to a mechanism of fractal generation and transport of cosmic rays.

The concept of self-similarity is also present in astrophysics [20]. An extensive study of all the available red-shift catalogs shows that the conditional average density of galaxies follows a power-law, indicating a fractal distribution

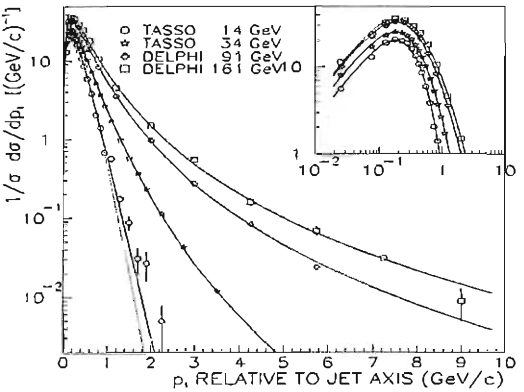

Figure 3: *The distribution of the transverse momentum p_t of charged hadrons with respect to the jet axis, for four different e^+e^- experiments, compared with the Boltzmann-Gibbs exponential behaviour (dotted line) and the best fits using non-extensive statistics (solid lines). From* [17].

of galaxies in the scale range $1\ h^{-1}\mathrm{Mpc} < r < 100\ h^{-1}\mathrm{Mpc}$.

4 Conclusions

The study of complex systems is an emerging, cross-disciplinary science. The next workshop of FRONTIER SCIENCE will be dedicated to complexity and will be held in Pavia, from 8 to 12 September 2003. Presentations on complexity by keynote speakers and young researchers are foreseen, ranging from particle physics and astrophysics, to atmosphere and climate, hydrosphere and solid earth, life sciences and ecology, econophysics. Further information on the topics covered in the conference can be found in [9] and references therein.

5 Acknowledgements

I wish to thank the organizers for the kind invitation, and, in particular, S. Ratti and F.L. Fabbri for giving me this opportunity. I am very grateful to S. Abe, B. Bertotti, G. Bormetti, A. Johansen, R.N. Mantegna, M. Morelli, O. Nicrosini, L. Pietronero, S. Ratti, H.E. Stanley, C. Tsallis and A. Vespignani for discussions, encouragement and advice before and while preparing this talk.

References

1. M. Gell-Mann, The Quark and the Jaguar (Freeman, New York, 1994).

2. G. Parisi, Complex Systems: a Physicist's Viewpoint, cond-mat/0205297.

3. Science, Complex Systems, vol. **284**, 79 (2 April 1999).

4. D. Buskulic *et al.*, ALEPH Coll., Z. Phys. **C69**, 15 (1995).

5. I.M. Dremin and J.W. Gary, Phys. Rep. **349**, 301 (2001).

6. E.A. De Wolf, I.M. Dremin and W. Kittel, Phys. Rep. **270**, 1 (1996).

7. Gang Chen *et al.*, hep-ph/0112092.

8. S. Forte *et al.*, JHEP **0205**, 062 (2002).

9. See, for example, J. Feder, Fractals (Plenum Press, New York, 1988); W. Paul and J. Baschnagel, Stochastic Processes: from Physics to Finance (Springer-Verlag, Berlin Heidelberg, 1999); H.E. Stanley, Physica **A285**, 1 (2000).

10. S. Abe and N. Suzuki, cond-mat/0208344.

11. G.K. Zipf, Human Behaviour and the Principle of Least Effort (Addison-Wesley, 1949); B. Mandelbrot, The Fractal Geometry of Nature (Freeman, New York, 1983).

12. C.K. Peng *et al.*, Phys. Rev. Lett. **70**, 1343 (1993).

13. R.N. Mantegna and H.E. Stanley, Nature **376**, 46 (1995).

14. G. Montagna, O. Nicrosini and N. Moreni, Physica **A310**, 450 (2002); L. Borland, Phys. Rev. Lett. **89**, 098701 (2002).

15. R. Pastor-Satorras and A. Vespignani, Phys. Rev. Lett. **86**, 3200 (2001).

16. R. Hagedorn, Suppl. Nuovo Cimento **3**, 147 (1965); F. Becattini, Z. Phys. **C69**, 485 (1996).

17. I. Bediaga, E.M.F. Curado, J.M. de Miranda, Physica **A286**, 156 (2000).

18. C. Tsallis, J. Stat. Phys. **52**, 479 (1988).

19. C. Tsallis, J.C. Anjos and J.P. Borges, astro-ph/0203258.

20. F. Sylos Labini, M. Montuori and L. Pietronero, Phys. Rep. **293**, 61 (1998).

Frascati Physics Series Vol. XXXI (2003), pp. 321–332
FRONTIERSCIENCE 2002 – Frascati, October 6–11, 2002
Invited Review Talk in Plenary Session

PARTICLE PHYSICS AND COSMOLOGY

Juan García-Bellido
Departamento de Física Teórica C-XI,
Universidad Autónoma de Madrid, Cantoblanco 28049 Madrid, Spain

ABSTRACT

In this talk I will review the present status of inflationary cosmology and its emergence as the basic paradigm behind the Standard Cosmological Model, with parameters determined today at better than 10% level from CMB and LSS observations.

1 Introduction

In this short review I will outline the reasons why the inflationary paradigm [1, 2] has become the backbone of the present Standard Cosmological Model. It gives a framework in which to pose all the basic cosmological questions: what is the shape and size of the universe, what is the matter and energy content of the universe, where did all this matter come from, what is the fate of the universe, etc. I will describe the basic predictions that inflation makes, most of which

have been confirmed only recently, while some are imminent, and then explore the recent theoretical developments on the theory of reheating after inflation and cosmological particle production, which might allow us to answer some of the above questions in the future.

Although the simplest slow-roll inflation model is consistent with the host of high precision cosmological observations of the last few years, we still do not know what the true nature of the inflaton is: although there are many possible realizations, there is no unique particle physics model of inflation. Furthermore, we even ignore the energy scale at which this extraordinary phenomenon occurred in the early universe; it could be associated with a GUT theory or even with the EW theory, at much lower energies.

2 Basic Predictions

Inflation is an extremely simple idea based on the early universe dominance of a vacuum energy density associated with a hypothetical scalar field called the inflaton. Its nature is not known: whether it is a fundamental scalar field or a composite one, or something else altogether. However, one can always use an effective description in terms of a scalar field with an effective potential driving the quasi-exponential expansion of the universe. This basic scenario gives several detailed fundamental predictions: a flat universe with nearly scale-invariant adiabatic density perturbations with Gaussian initial conditions.

2.1 A flat and homogeneous background

Inflation explains why our local patch of the universe is spatially flat, i.e. Euclidean. Inflation does, provides an approximately constant energy density that induces a tremendous expansion of the universe. Thus, an initially curved three-space will quickly become locally indistinguishable from a "flat" hypersurface. Moreover, this same mechanism explains why we see no ripples, i.e. no large inhomogeneities, in the space-time fabric, e.g. as large anisotropies in the temperature field of the cosmic microwave background when we look in different directions. The expansion during inflation erases any prior inhomogeneities. These two are very robust predictions of inflation, and have been confirmed to high precision by the detailed observations of the CMB, first by COBE (1992) for the large scale homogeneity, to one part in 10^5, and recently

by BOOMERanG [3] and MAXIMA [4], for the spatial flatness, to better than 10%.

2.2 Cosmological perturbations

Inflation also predicts that on top of this homogeneous and flat space-time background, there should be a whole spectrum of cosmological perturbations, both scalar (density perturbations) and tensor (gravitational waves). These arise as quantum fluctuations of the metric and the scalar field during inflation, and are responsible for a scale invariant spectrum of temperature and polarization fluctuations in the CMB, as well as for a stochastic background of gravitational waves. The temperature fluctuations were first discovered by COBE and later confirmed by a host of ground and balloon-borne experiments, while the polarization anisotropies have only recently been discovered by the CMB experiment DASI [5]. Both observations seem to agree with a nearly scale invariant spectrum of perturbations. It is expected that the stochastic background of gravitational waves produced during inflation could be detected with the next generation of gravitational waves interferometers (e.g. LISA), or indirectly by measuring the power spectra of polarization anisotropies in the CMB by the future Planck satellite [6].

Inflation makes very specific predictions as to the nature of the scalar perturbations. In the case of a single field evolving during inflation, the perturbations are predicted to be adiabatic, i.e. all components of the matter and radiation fluid should have equal density contrasts, due to their common origin. As the plasma (mainly baryons) falls in the potential wells of the metric fluctuations, it starts a series of acoustic compressions and rarefactions due to the opposing forces of gravitational collapse and radiation pressure. Adiabatic fluctuations give a very concrete prediction for the position and height of the acoustic peaks induced in the angular power spectrum of temperature and polarization anisotropies. This has been confirmed to better than 1% by the recent observations, and constitutes one of the most important signatures in favor of inflation, ruling out a hypothetically large contribution from active perturbations like those produced by cosmic strings or other topological defects.

Furthermore, the quantum origin of metric fluctuations generated during inflation allows one to make a strong prediction on the statistics of those per-

turbations: inflation stretches the vacuum state fluctuations to cosmological scales, and gives rise to a Gaussian random field, and thus metric fluctuations are in principle characterized solely by their two-point correlation function. Deviations from Gaussianty would indicate a different origin of fluctuations, e.g. from cosmic defects. Recent observations by BOOMERanG in the CMB and by gravitational lensing of LSS indicate that the non-Gaussian component of the temperature fluctuations and the matter distribution on large scales is strongly constrained, and consistent with foregrounds (in the case of CMB) and with non-linear gravitational collapse (in the case of LSS).

Of course, in order to really confirm the idea of inflation one needs to find cosmological observables that will allow us to correlate the scalar and the tensor metric fluctuations with one another, since they both arise from the same inflaton field fluctuations. This is a daunting task, given that we ignore the absolute scale of inflation, and thus the amplitude of tensor fluctuations (only sensitive to the total energy density). The smoking gun could be the observation of a stochastic background of gravitational waves by the future gravitational wave interferometers and the subsequent confirmation by detection of the curl component of the polarization anisotropies of the CMB. Although the gradient component has recently been detected by DASI, we may have to wait for Planck for the detection of the curl component.

3 Recent Cosmological Observations

Cosmology has become in the last few years a phenomenological science, where the basic theory (based on the hot Big Bang model after inflation) is being confronted with a host of cosmological observations, from the microwave background to the large scale distribution of matter, from the determination of light element abundances to the detection of distant supernovae that reflect the acceleration of the universe, etc. I will briefly review here the recent observations that have been used to define a consistent cosmological standard model.

3.1 Cosmic Microwave Background

The most important cosmological phenomenon from which one can extract essentially all cosmological parameters is the microwave background and, in particular, the last scattering surface temperature and polarization anisotropies.

Since they were discovered by COBE in 1992, the temperature anisotropies have lived to their promise. They allow us to determine a whole set of both background (0-th order) and perturbation (1st-order) parameters – the geometry, topology and evolution of space-time, its matter and energy content, as well as the amplitude and tilt of the scalar and tensor fluctuation power spectra – in some cases to better than 10% accuracy.

At present, the forerunners of CMB experiments are BOOMERanG and MAXIMA (balloons), and DASI, VSA and CBI (ground based interferometers). Together they have allowed cosmologists to determine the angular power spectrum of temperature fluctuations down to multipoles 1000 and 3000, respectively, and therefore provided a measurement of the positions and heigths of at least 3 to 7 acoustic peaks. A combined analysis of the different CMB experiments yields convincing evidence that the universe is flat, with $|\Omega_K| = |1 - \Omega_{tot}| < 0.05$ at 95% c.l.; full of dark energy, $\Omega_\Lambda = 0.66 \pm 0.06$, and dark matter, $\Omega_m = 0.33 \pm 0.07$. with about 5% of baryons, $\Omega_b = 0.05 \pm 0.01$; and expanding at a rate $H_0 = 68 \pm 7$ km/s/Mpc, all values given with 1σ errors, see Table 1. The spectrum of primordial perturbations that gave rise to the observed CMB anisotropies is nearly scale-invariant, $n_s = 1.02 \pm 0.06$, adiabatic and Gaussian distributed. This set of parameters already constitutes the basis for a truly Standard Model of Cosmology, based on the Big Bang theory and the inflationary paradigm. Note that both the baryon content and the rate of expansion determinations with CMB data alone are in excellent agreement with direct determinations from BBN light element abundances [13] and HST Cepheids [14], respectively.

In the near future, a new satellite experiment, the Microwave Anisotropy Probe (MAP) [15], will provide a full-sky map of temperature (and possibly also polarization) anisotropies and determine the first 2000 multipoles with unprecedented accuracy. When combined with LSS and SN measurements, it promises to allow the determination of most cosmological parameters with errors down to the few% level.

Moreover, with the recent detection of microwave background polarization anisotropies by DASI [5], confirming the basic paradigm behind the Cosmological Standard Model, a new window opens which will allow yet a better determination of cosmological parameters, thanks to the very sensitive (0.1μK) and high resolution (4 arcmin) future satellite experiment Planck [6]. In prin-

Table 1: *Estimates of the cosmological parameters that characterize a minimal adiabatic inflation-based model. From Ref.* [12].

Priors	CMB	CMB+LSS	CMB+LSS+SN	CMB+LSS+SN+HST
$\Omega_{\rm tot}$	$1.05^{+0.05}_{-0.05}$	$1.03^{+0.03}_{-0.04}$	$1.00^{+0.03}_{-0.02}$	$1.00^{+0.02}_{-0.02}$
n_s	$1.02^{+0.06}_{-0.07}$	$1.00^{+0.06}_{-0.06}$	$1.03^{+0.06}_{-0.06}$	$1.04^{+0.05}_{-0.06}$
$\Omega_b\, h^2$	$0.023^{+0.003}_{-0.003}$	$0.023^{+0.003}_{-0.003}$	$0.024^{+0.003}_{-0.003}$	$0.024^{+0.002}_{-0.003}$
$\Omega_{\rm cdm} h^2$	$0.13^{+0.03}_{-0.02}$	$0.12^{+0.02}_{-0.02}$	$0.12^{+0.02}_{-0.02}$	$0.12^{+0.01}_{-0.01}$
Ω_Λ	$0.54^{+0.12}_{-0.13}$	$0.61^{+0.09}_{-0.10}$	$0.69^{+0.04}_{-0.06}$	$0.70^{+0.02}_{-0.03}$
Ω_m	$0.52^{+0.15}_{-0.15}$	$0.42^{+0.12}_{-0.12}$	$0.32^{+0.06}_{-0.06}$	$0.30^{+0.02}_{-0.02}$
Ω_b	$0.080^{+0.023}_{-0.023}$	$0.067^{+0.018}_{-0.018}$	$0.052^{+0.011}_{-0.011}$	$0.049^{+0.004}_{-0.004}$
h	$0.55^{+0.09}_{-0.09}$	$0.60^{+0.09}_{-0.09}$	$0.68^{+0.06}_{-0.06}$	$0.69^{+0.02}_{-0.02}$
Age	$15.0^{+1.1}_{-1.1}$	$14.7^{+1.2}_{-1.2}$	$13.8^{+0.9}_{-0.9}$	$13.6^{+0.2}_{-0.2}$
τ_c	$0.16^{+0.18}_{-0.13}$	$0.09^{+0.12}_{-0.07}$	$0.13^{+0.14}_{-0.10}$	$0.13^{+0.13}_{-0.10}$

The age of the Universe is in Gyr, and the rate of expansion in units of 100 km/s/Mpc. All values quoted with 1σ errors.

ciple, Planck should be able to detect not only the gradient component of the CMB polarization, but also the curl component, if the scale of inflation is high enough. In that case, there might be a chance to really test inflation through cross-checks between the scalar and tensor spectra of fluctuations, which are predicted to arise from the same inflaton potential.

The observed positions of the acoustic peaks of the CMB anisotropies strongly favor purely adiabatic density perturbations, as arise in the simplest single-scalar-field models of inflation. These models also predict a nearly Gaussian spectrum of primordial perturbations. A small degree of non-gaussianity may arise from self-coupling of the inflaton field (although it is expected to be very tiny, given the observed small amplitude of fluctuations), or from two-field models of inflation. Since the CMB temperature fluctuations probe directly primordial density perturbations, non-gaussianity in the density field should lead to a corresponding non-gaussianity in the temperature maps. However, recent searches for non-Gaussian signatures in the CMB have only given stringent upper limits, see Ref. [17].

One of the most interesting aspects of the present progress in cosmolog-

ical observations is that they are beginning to probe the same parameters or the same features at different time scales in the evolution of the universe. We have already mentioned the determination of the baryon content, from BBN (light element abundances) and from the CMB (acoustic peaks), corresponding to totally different physics and yet giving essentially the same value within errors. Another example is the high resolution images of the CMB anisotropies by CBI [12], which constitute the first direct detection of the seeds of clusters of galaxies, the largest gravitationally bound systems in our present universe. In the near future we will be able to identify and put into one-to-one correspondence tiny lumps in the CMB with actual clusters today.

3.2 Large Scale Structure

The last decade has seen a tremendous progress in the determination of the distribution of matter up to very large scales. The present forerunners are the 2dF Galaxy Redshift Survey [18] and the Sloan Digital Sky Survey (SDSS) [19]. These deep surveys aim at 10^6 galaxies and reach redshifts of order 1 for galaxies and order 5 for quasars. They cover a wide fraction of the sky and therefore can be used as excellent statistical probes of large scale structure [16, 20].

The main output of these galaxy surveys is the two-point (and higher) spatial correlation functions of the matter distribution or, equivalently, the power spectrum in momentum space. Given a concrete type of matter, e.g. adiabatic vs. isocurvature, cold vs. hot, etc., the theory of linear (and non-linear) gravitational collapse gives a very definite prediction for the measured power spectrum, which can then be compared with observations. This quantity is very sensitive to various cosmological parameters, mainly the dark matter content and the baryonic ratio to dark matter, as well as the universal rate of expansion; on the other hand, it is mostly insensitive to the cosmological constant since the latter has only recently (after redshift $z \sim 1$) started to become important for the evolution of the universe, while galaxies and clusters had already formed by then. Together, 2dFGRS, plus CMB, weak gravitational lensing and Lyman-α forest data, allow us to determine the power spectrum with better than 10% accuracy for $k > 0.02\ h\ \mathrm{Mpc}^{-1}$, which is well fitted by a flat CDM model with $\Omega_m h = 0.20 \pm 0.03$, and a baryon fraction of $\Omega_b/\Omega_m = 0.15 \pm 0.06$, which together with the HST results give values of the parameters that are compatible with those obtained with the CMB, see

Table 1. It is very reassuring to note that present parameter determination is robust as we progress from weak priors to the full cosmological information available, a situation very different from just a decade ago, where the errors were mostly systematic and parameters could only be determined with an order-of-magnitude error. In the very near future such errors will drop again to the 1% level, making Cosmology a mature science, with many independent observations confirming and further constraining previous measurements of the basic parameters.

An example of such progress appears in the analysis of non-Gaussian signatures in the primordial spectrum of density perturbations. The tremendous increase in data due to 2dFGRS and SDSS has allowed cosmologists to probe the statistics of the matter distribution on very large scales and infer from it that of the primordial spectrum. Recently, both groups have reported non-Gaussian signatures (in particular the first two higher moments, skewness and kurtosis), that are consistent with gravitational collapse of structure that was originally Gaussianly distributed [21, 22]. Moreover, weak gravitational lensing also allows an independent determination of the three-point shear correlation function, and there has recently been a claim of detection of non-Gaussian signatures in the VIRMOS-DESCART lensing survey [23], which is also consistent with theoretical expectations of gravitational collapse of Gaussianly distributed initial perturbations.

The recent precise catalogs of the large scale distribution of matter allows us to determine not only the (collapsing) cold dark matter content, but also put constraints on the (diffusing) hot dark matter, since it would erase all structure below a scale that depends on the free streaming length of the hot dark matter particle. In the case of relic neutrinos we have extra information because we know precisely their present energy density, given that neutrinos decoupled when the universe had a temperature around 0.8 MeV and cooled down ever since. Their number density today is around 100 neutrinos/cm^3. If neutrinos have a significant mass (above 10^{-3} eV, as observations of neutrino oscillations by SuperKamiokande [24] and Sudbury Neutrino Observatory [25] seem to indicate), then the relic background of neutrinos is non-relativistic today and could contribute a large fraction of the critical density, $\Omega_\nu = m_\nu/92\,h^2\,\mathrm{eV} \geq 0.001$, see Ref. [26]. Using observations of the Lyman-α forest in absorption spectra of quasars, due to a distribution of intervening clouds, a limit on the

absolute mass of all species of neutrinos can be obtained [27]. Recently, the 2dFGRS team [28] have derived a bound on the allowed amount of hot dark matter, $\Omega_\nu < 0.13\,\Omega_m < 0.05$ (95% c.l.), which translates into an upper limit on the total neutrino mass, $m_{\nu,\,tot} < 1.8$ eV, for values of Ω_m and the Hubble constant in agreement with CMB and SN observations. This bound improves several orders of magnitude on the direct experimental limit on the muon and tau neutrino masses, and is comparable to present experimental bounds on the electron neutrino mass [29].

3.3 Cosmological constant and rate of expansion

Observations of high redshift supernovae by two independent groups, the Supernova Cosmology Project [30], and the High Redshift Supernova Team [31], give strong evidence that the universe is accelerating, instead of decelerating, today. Although a cosmological constant is the natural suspect for such a "crime", its tiny non-zero value makes theoretical physicists uneasy [32]. A compromise could be found by setting the fundamental cosmological constant to zero, by some yet unknown principle possibly related with quantum gravity, and allow a super-weakly-coupled homogeneous scalar field to evolve down an almost flat potential. Such a field would induce an effective cosmological constant that could in principle account for the present observations. The way to distinguish it from a true cosmological constant would be through its equation of state, since such a type of smooth background is a perfect fluid but does not satisfy $p = -\rho$ exactly, and thus $w = p/\rho$ also changes with time. There is a proposal for a satellite called the Supernova / Acceleration Probe (SNAP) [33] that will be able to measure the light curves of type Ia supernovae up to redshift $z \sim 2$, thus determining both Ω_X and w_X with reasonable accuracy, where X stands for this hypothetical scalar field. For the moment there are only upper bounds, $w_X < -0.6$ (95% c.l.) [34], consistent with a true cosmological constant, but the SNAP project claims it could determine Ω_X and w_X with 5% precision.

Fortunately, the SN measurements of the acceleration of the universe give a linear combination of cosmological parameters that is almost orthogonal, in the plane (Ω_m, Ω_Λ), to that of the curvature of the universe ($1-\Omega_K = \Omega_m+\Omega_\Lambda$) by CMB measurements and the matter content by LSS data. Therefore, by combining the information from SNe with that of the CMB and LSS, one can significantly reduce the errors in both Ω_m and Ω_Λ, see Table 1. It also allows

an independent determination of the rate of expansion of the universe that is perfectly compatible with the HST data [14]. This is reflected on the fact that adding the latter as prior does not affect significantly the mean value of most cosmological parameters, only the error bars, and can be taken as an indication that we are indeed on the right track: the Standard Cosmological Model is essentially correct, we just have to improve the measurements and reduce the error bars.

4 Conclusions

Inflation is nowadays a robust paradigm with a host of cosmological observations confirming many of its basic predictions: large scale spatial flatness and homogeneity, as well as an approximately scale-invariant Gaussian spectrum of adiabatic density perturbations.

It is possible that in the near future the next generation of CMB satellites (MAP and Planck) may detect the tensor or gravitational wave component of the polarization power spectrum, raising the possibility of really testing inflation through the comparison of the scalar and tensor components, as well as determining the energy scale of inflation.

References

1. A. H. Guth, Phys. Rev. D **23** (1981) 347; A. D. Linde, Phys. Lett. B **108** (1982) 389; A. Albrecht and P. J. Steinhardt, Phys. Rev. Lett. **48** (1982) 1220.

2. A. D. Linde, Particle Physics and Inflationary Cosmology, Harwood Academic Press (1990); E. W. Kolb and M. S. Turner, The Early Universe, Addison-Wesley (1990); A. R. Liddle and D. H. Lyth, Cosmological Inflation and Large-Scale Structure, Cambridge Univ. Press (2000); J. A. Peacock, Cosmological Physics, Cambridge Univ. Press (1999).

3. P. de Bernardis *et al.* (Boomerang Collaboration), Nature **404** (2000) 955 [astro-ph/0004404].

4. S. Hanany *et al.*, Astrophys. J. **545** (2000) L5 [astro-ph/0005123].

5. J. Kovac *et al.* (DASI Collaboration), "Detection of Polarization in the Cosmic Microwave Background using DASI," astro-ph/0209478.

6. Planck home page: http://astro.estec.esa.nl/Planck/

7. X. m. Wang, M. Tegmark and M. Zaldarriaga, Phys. Rev. D **65** (2002) 123001 [astro-ph/0105091].

8. G. Efstathiou *et al.* (2dFGRS Collaboration), MNRAS **330** (2002) L29.

9. M. Tegmark and M. Zaldarriaga, astro-ph/0207047.

10. BOOMERANG home page: http://oberon.roma1.infn.it/boomerang/

11. MAXIMA home page: http://cosmology.berkeley.edu/group/cmb/

12. J. L. Sievers *et al.* (CBI Collaboration), "Cosmological Parameters from Cosmic Background Imager Observations and Comparisons with BOOMERanG, DASI, and MAXIMA," astro-ph/0205387.

13. J. M. O'Meara, D. Tytler, D. Kirkman, N. Suzuki, J. X. Prochaska, D. Lubin and A. M. Wolfe, Astrophys. J. **552** (2001) 718 [astro-ph/0011179]; D. Tytler, J. M. O'Meara, N. Suzuki and D. Lubin, "Review of Big Bang Nucleosynthesis and Primordial Abundances," astro-ph/0001318.

14. W. L. Freedman *et al.*, Astrophys. J. **553** (2001) 47 [astro-ph/0012376].

15. Microwave Anisotropy Prove home page: http://map.gsfc.nasa.gov/

16. J. A. Peacock, "Studying large-scale structure with the 2dF Galaxy Redshift Survey," astro-ph/0204239.

17. G. Polenta *et al.*, Astrophys. J. **572** (2002) L27 [astro-ph/0201133].

18. 2dF Galaxy Redshift Survey home page: http://www.mso.anu.edu.au/2dFGRS/

19. Sloan Digital Sky Survey home page: http://www.sdss.org/sdss.html

20. W. J. Percival *et al.* (2dFGRS Collaboration), "Parameter constraints for flat cosmologies from CMB and 2dFGRS power spectra," astro-ph/02006256.

21. L. Verde, R. Jimenez, M. Kamionkowski and S. Matarrese, Mon. Not. Roy. Astron. Soc. **325** (2001) 412 [astro-ph/0011180].

22. I. Szapudi *et al.* (SDSS Collaboration), Astrophys. J. **570** (2002) 75 [astro-ph/0111058].

23. F. Bernardeau, Y. Mellier, L. van Waerbeke, Astron. & Astrophys. **389** (2002) L28 [astro-ph/0201032].

24. Y. Fukuda *et al.* (SuperK Collaboration), Phys. Rev. Lett. **82** (1999) 2644 [hep-ex/9812014]; Phys. Rev. Lett. **85** (2000) 3999 [hep-ex/0009001].

25. Q. R. Ahmad *et al.* (SNO Collaboration), Phys. Rev. Lett. **89** (2002) 011301 [nucl-ex/0204008]; Phys. Rev. Lett. **89** (2002) 011302 [nucl-ex/0204009].

26. W. Hu, D. J. Eisenstein and M. Tegmark, Phys. Rev. Lett. **80** (1998) 5255 [astro-ph/9712057].

27. R. A. Croft, W. Hu and R. Dave, Phys. Rev. Lett. **83** (1999) 1092 [astro-ph/9903335].

28. O. Elgaroy *et al.* (2dFGRS Collaboration), Phys. Rev. Lett. **89** (2002) 061301 [astro-ph/0204152].

29. Review of particle properties, Particle Data Group home page: http://pdg.web.cern.ch/pdg/

30. S. Perlmutter *et al.* (Supernova Cosmology Project Collaboration), Astrophys. J. **517** (1999) 565 [astro-ph/9812133].

31. A. G. Riess *et al.* (Supernova Search Team Collaboration), Astron. J. **116** (1998) 1009 [astro-ph/9805201].

32. S. Weinberg, Rev. Mod. Phys. **61** (1989) 1.

33. Supernova / Acceleration Probe home page: http://http://snap.lbl.gov/

34. S. Perlmutter, M. S. Turner and M. J. White, Phys. Rev. Lett. **83** (1999) 670 [astro-ph/9901052].

Hot Trends in Instrumentation

Chairperson: P. Sheldon

Frascati Physics Series Vol. XXXI (2003), pp. 335–347
FRONTIERSCIENCE 2002 – Frascati, October 6–11, 2002
Invited Review Talk in Plenary Session

THE FUTURE OF CALORIMETRY IN HIGH-ENERGY PHYSICS

Antonio Ereditato
INFN Napoli, Italy

ABSTRACT

The title of this paper would be ambitious even for a thorough review on the subject. For this reason, I will proceed by making a largely arbitrary selection of arguments and of examples. I will start by making general considerations about the present status of calorimetry, focusing on the performance, limitations and possible improvements of calorimeters as widely used in high-energy physics experiments. I will then address a few peculiar applications of calorimetry at LHC experiments, at the future electron linear colliders and at B factory experiments. I will finally conclude by reviewing some of the many astroparticle physics experiments employing state-of-the-art calorimetry.

1 Calorimetry in HEP: present status and limitations

One can schematically summarise a few relevant aspects of the present scenario of HEP experiments by stating that: the Tevatron CDF and D0 experiments

are taking data and aim for high luminosity; LHC detectors are being built with some margin of improvement in view of a moderate increase of the machine luminosity. However, a factor 10 increase in luminosity could not be accommodated due to the dramatic increase in the integrated dose; Belle and BaBar are successfully running: also their calorimeters could not stand a major luminosity increase beyond the present limit; electron linear-collider detectors are being designed for high precision measurements with calorimeters playing a key role; running and planned calorimeters for astroparticle experiments show a large variety of approaches.

An important aspect of future accelerator experiments is the high energy frontier. It is clear that in pushing further this frontier the importance of calorimetry will be increasingly high due to the improvement (or at least not worsening) of the energy resolution with the energy. The opposite occurs in the energy (momentum) measurement by magnetic spectrometers for which one has a linear worsening of the momentum resolution with increasing energy. It is also worth noting that whatever new physics will appear at the energy frontier, this will produce in the final state Standard Model particles, the same particles which are measured with today's calorimeters.

Calorimeters will provide means to detect all known final state particles: electrons, photons, muons, tau's, hadrons, jets and also neutrinos through a missing energy measurement. In nowadays and future experiments as well, a suitable combination of electromagnetic (EM) and hadronic calorimetry allows to perform particle ID by exploiting differences in the X_0 and Λ values of the absorbers (e/π separation) or differences in the electromagnetic radiation cross-section (e/μ separation).

Concerning the calorimetric energy resolution one can easily show that jet, dimass and missing energy resolution are determined by the single particle resolution if the energy measurement is the only error [1]. One can prove that it is possible to achieve high-energy resolution with EM sampling calorimeter with high sampling fraction, realistically yielding to stochastic terms as small as 5% [1]. However, the best energy resolution is obtained by exploiting fully active devices such as crystals. In this case one has no sampling fluctuations, but noise, photon statistics, and light collection non-uniformity limit the achievable resolution. As an example, in the case of the PbWO4 crystals in CMS one obtains $dE/E \sim 0.7\%$ at 100 GeV even if the stochastic coefficient is as small

as 2.3% [1].

Different processes limit the performance of hadronic (sampling) calorimeters. In particular, the large event-by-event fluctuations on the EM content of the shower induce consequently large fluctuations in the energy deposition in the active medium, severely limiting the energy resolution. Compensation is considered a possible solution to improve the resolution. It is well known, in fact, that the medium can respond differently to EM and hadronic shower components due to the differences in ionisation, the existence of nuclear binding energy, of neutrons and undetected fragments. A detector with e/h close to unit shows the best energy resolution since it induces a small constant term in the resolution formula. However, the effect of non-compensation reduces at increasingly high energy, where the energy resolution improves with ln(E).

Despite the many efforts in the technology of hadronic calorimeters, other intrinsic limitations remain limiting their performance. The detector transverse size set by the shower extent (Xo and Λ) limits the smallest tower size. The minimal longitudinal depth is set by containment (about 20 Xo and 10 Λ); the largest depth is set by jet leakage. The speed is limited by 25 ns bunch crossings at LHC; no reduction in pileup is expected if signals would be faster. The jet resolution is limited by final state radiation (FSR) and not really by the calorimeter energy resolution [1].

If one looks at the future, namely at the high-energy frontier that could be explored by a hadron collider such as the LHC, one has to notice that both luminosity and CM energy increases are possible in principle. For particle masses of the order of the CM energy the required luminosity (L) rises rapidly, indicating that the energy is the most important issue; for masses much lower than the CM energy, L goes as the square of the mass. However, higher mass states or higher L in hadron colliders will require calorimetry what can withstand more than 10 (2) Mrad for the ECAL (HCAL) calorimeter for pseudorapidity values larger than 3 units. Scintillators would not survive for ECAL regardless the CM energy. Hermiticity will require a coverage to smaller angles as the CM energy increases and the 'plateau' extends. Forward calorimetry will then need to withstand more than 1 Grad. This dose is a real challenge and likely only gaseous or Cerenkov light detectors could be used.

2 Future calorimetry at electron colliders

After the generation of forthcoming experiments at the Tevatron and LHC and the likely discovery of Higgs and Supersymmetry (!) precision studies will have to be performed at an electron machine, following what happened in the recent past after the discovery of the W and Z bosons at the SPS and the precision Standard Model measurements at LEP. Future linear electron colliders will have to face the challenge of very steeply falling cross-sections of the interesting processes: by large factors lower than the ones at LEP. In order to measure masses from 500 to 1000 GeV one will require very large luminosities in the range from 10^{33} to a few 10^{34} $cm^{-2}s^{-1}$. R&D studies on these machines are in progress in Europe (CLIC, TESLA), in Japan (JLC) and in the USA (NLC).

The main tool of the detectors in addressing the relevant physics issues at the future electron machines will be the detection of jets. This feature is complementary to what is going to be performed at the LHC: detectors at linear colliders have to do well what LHC finds difficult (detection of hadronic decays, multijets, etc.). The primary goal will be revealing the nature of the electroweak symmetry breaking (Higgs, supersymmetry, extra dimensions, etc.) through precision studies.

¿From the point of view of calorimetry the environment at electron machines will be rather clean, with low occupancy apart from the presence of low transverse momentum electron pairs. Large B fields will be employed to 'open' the jets and to apply one of the main distinctive experimental methods at these colliders: the energy flow. This concept is based on the assumption that charged particles in a jet are more precisely measured with the tracker than with a calorimeter. In fact, the energy of a typical linear collider multi-jet event belongs for 64% to low momentum (suitable for tracking) charged particles, for 25% to photons and only for 11% to neutral hadrons [2]. The energy flow method consists in using trackers for the energy measurement of charged particles and calorimeters for neutrals. One has to locate and remove charged particle's calorimetric energy by means of dense, highly-granular ECAL and HCAL. ECAL can be considered 'transparent' to hadrons: one detects hadrons in HCAL and photons in ECAL. The main calorimetric figures of merit are a 'large' BR^2/R_m, suitable for cluster detection in the ECAL, as well as a transverse segmentation of the order of R_m with a small X_0/Λ ratio [2]. An alternative approach, as the one adopted by the present JLC detector design,

envisages the use of compensating calorimetry.

Concerning the calorimeter technology at electron linear colliders, for the ECAL one envisages (NLC and TESLA) large scale tungsten/silicon calorimetry with more than 1000 m^2 total Silicon surface and a 20 longitudinal-layer deep detector (Fig.1). Following the prescriptions of the energy flow concept, one can design a finely segmented calorimeter, such as the one already used, although at a much smaller scale, for luminosity monitors at SLC and LEP. The main drawback is the (presently) large or unaffordable (according to pessimistic/optimistic points of view) cost of the Silicon. However, one could hope of a sort of Moore's law for Silicon that should bring by the year 2010 the cost of this material to a reasonable level [3]. As far as the HCAL is concerned people still consider scintillator tiles as a viable option, or the use of the so-called 'digital' hadronic calorimetry characterised by small segmentation (1 cm^2) with only 1-2 bit readout, possibly employing RPCs or similar cheap detectors.

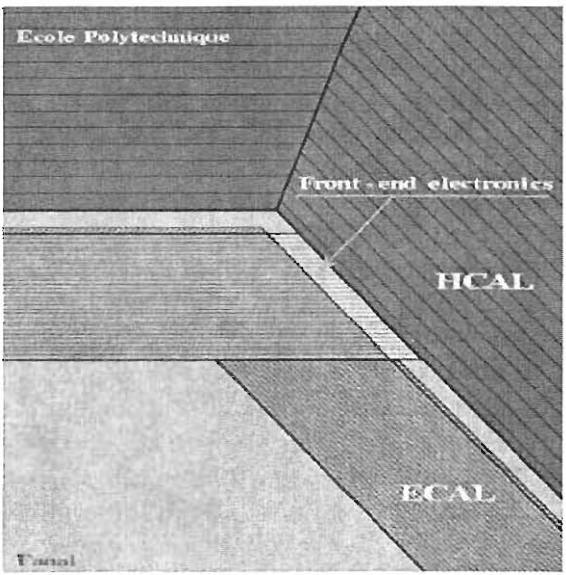

Figure 1: *Possible layout of a W-Si calorimeter for a linear collider (detail).*

3 Calorimetry for future B physics

As far as the next generation B-factories is concerned, one has to notice that the design work for these machines (and of course for the relative detectors and calorimeters) is still rather preliminary. The main reason is that a lot of (good quality) data is being currently provided by the existing B-factories at KEK and SLAC. The principal goal for the next generation will be the realisation of a 10^{36} asymmetric B factory. This machine could lead to new physics on rare B (and D) decay rates and angular distributions, and to studies of deviations from the predictions of CKM parameters in over-constrained tests of the unitarity triangle.

The main requirements to calorimetry can be summarised in the capability of measuring photons from generic and specific B's with high energy and angular resolution, still using the unsurpassed crystal calorimeters. These requirements are, all in all, similar to those of the present detectors, apart from the capability to handle the increase in luminosity. The latter is by far a non-negligible requirement. If one considers, as an example, the BaBar CsI calorimeter, it is evident that a factor 10 increase in luminosity could not be tolerated due to light losses and occupancy increase [4].

As a general consideration the crystal size should correspond to a rather fine segmentation, as required for photon separation (including BG photons) and position resolution. In this spirit the useful crystal transverse size is limited by its properties, namely the R_m (CsI $\sim$ 3.8 cm) and the cost of the readout. The longitudinal dimensions are driven by the energy resolution (up to about 16-17 radiation length may be needed for high-energy electrons and photons). The calorimeter should then cover the maximum solid angle with the minimal interruptions for services, etc. Last but not least the material in front of the calorimeter should be minimised.

Concerning the radiation damage, definitely the major technological challenge, it mainly affects the light yield and light yield uniformity. The design goal is that in 10 years a maximum 20% light yield loss should occur. One has to add the requirement of a sufficiently high quantity of light (needed for the energy resolution) and of signal speed (required to reduce the background). Some crystals are presently considered as good candidates: PbWO4 (already widely used at the LHC), YAP, GSO, LSO, etc.

About the background we note that the calorimeter will be affected by

the creation of fake neutral clusters and by the inclusion of beam background photons during clustering into B decay photon showers [4].

One word on the readout. Due to the presence of high magnetic field one will be forced to use compact photosensors such as photodiodes (for crystals with high light output) or APDs. One can also think to reduce the readout cost by longitudinal segmentation of the crystals achieving better electron ID, higher spatial resolution and background reduction. Radiation hard compact crystal can then be used in front and (cheaper) less radiation hard crystal in the back of the calorimeter [4].

4 Calorimeters in astroparticle physics

The most striking feature of the energy measurement in astroparticle physics experiment is the huge energy interval spanned by the different experiments. One goes from the about 2 K of cosmic relic neutrinos to the more than 10^{20} eV of high energy cosmic ray events. Particles to be detected in this wide energy range are neutrinos, photons and charged-particle cosmic-rays. This subject is clearly extremely broad. Therefore, I will just concentrate on a few issues, such as the direct measurements of particles/photons in space, the use of the atmosphere as a calorimetric medium and the calorimetric detection of cosmic rays and neutrinos (surface/underground/underwater).

Detection of particles in space (balloon or satellite experiments) has a long history and it is nowadays a field in great expansion. The Earth atmosphere tends to hide the information carried out by primary cosmic-ray particles. For this reason high-altitude experiments first and balloon experiments later have been conducted in the past and brought to important discoveries.

Concerning modern satellite experiments, the 'mother' of all space-based calorimeters has been the SOKOL detector on the Kosmos-1543 satellite in the late '70s. The calorimeter was 5 Λ deep for about 2000 kg of weight [5]. If we jump to today's experiments, we note that some of the most advanced calorimetric techniques used in accelerator experiments are also employed in space-based experiments, with the additional challenging requirements of a relatively small weight and volume, low readout power consumption, high component reliability and excellent mechanical properties. Calorimeters play a key role in satellite experiments, which usually combine in a very compact detector high-performance energy measurements of charged and neutral particles, precision

tracking capabilities (magnetic field) and particle ID. We can take as examples the planned PAMELA and GLAST experiments [6].

PAMELA will be soon launched on a satellite elliptic, quasi-polar orbit at 300-600 km altitude. Among the physics goals I mention the study of the primary proton, antiproton, electron and positron spectra from about 50 MeV to several hundreds GeV. The experiment will perform a high sensitivity search for anti-nuclei and the study of energy and time distribution of the solar flare. The detector includes a magnetic spectrometer with silicon-microstrip tracker, TRDs, a TOF detector, an anti-coincidence counter and a performing imaging calorimeter: 16.3 radiation lengths, 0.6 interaction lengths deep. The calorimeter is made of 22 layers of Tungsten plates alternated with Silicon strips (x-y). Its total mass is 110 kg and there are 4416 readout channels for a total power consumption of 48 W. The high energy resolution of the calorimeter of 6% for electrons with energy above 25 GeV is adequate for the physics reach of the experiment.

GLAST aims at the detection of photons in the wide energy range from 5 MeV to 300 GeV. For this reason a state-of-the-art CsI crystal calorimeter is employed. The detector is rather deep (9.5 radiation lengths) and is made of 16 modules each with 8 layers of 12 crystals. The total number of crystals is 1536 for about 1450 kg of weight. A PIN diode/ASIC readout is used for a power budget of 60 W. The energy resolution is excellent: better than 20% up to 100 MeV and better than 6% at the highest energy of 300 GeV.

A completely different detection approach is used by experiments at Earth surface that employ the atmosphere as a calorimetric medium (11 Λ thick) for the showering of primary cosmic rays. In this case one can exploit the detection of particles at ground level, the detection of Cerenkov light from showering particles in the atmosphere and the measurement of the air fluorescence from the shower development.

The first category of experiments features the detection of very high energy particle showers, the coverage of relatively large areas, a large duty cycle, multiple single-point sampling and the possible detection of the shower front through timing measurements. One can mention as examples the MILAGRO (Los Alamos) and the ARGO (Tibet) experiments [6].

The second technique is the detection of the Cerenkov light from relativistic particles in the air shower. In this case we have a 'real' calorimeter

providing information on the shower-inducing particle: its orientations via the direction of the shower axis, the energy through the measurement of the light intensity, and the particle ID via the shower shape analysis.

The third technique is the detection of the air fluorescence light induced by the showering primary-particle. One actually detects the isotropic scintillation light from Nitrogen at about 325 nm wavelength. The excited Nitrogen state (emitting light) is collision quenched. Quenching linearly increases with the atmospheric pressure, but as dE/dx per unit length also linearly increases with the pressure, the two effects nearly compensate. This causes a fast electron to produce about the same amount of light per unit path at all altitudes. Therefore, one obtains that the absolute luminosity of the shower only depends upon the number of electrons at a given depth. The measurement of the longitudinal shower profile can be performed by wide FOV cameras, possibly exploiting stereo event reconstruction. The main drawback of such experiments is the low light yield (only primary particles above 10^{17} eV are detected) and the relatively small duty cycle (since Moon-less nights are required). For these experiments both surface detectors (IRES, AUGER) or orbiting satellites (EUSO) can be used [5, 6].

Finally, I wish to mention the detection of astrophysical neutrinos. Their energy spectrum spans several orders of magnitude: one goes from the MeV energy range of solar of supernovae neutrinos, to the GeV range of atmospheric neutrinos, to the over 1 TeV domain (and more) of astrophysical neutrinos. Therefore, various techniques are exploited by the calorimeters devoted to their detection and energy measurement. High energy neutrinos are excellent carriers of information from galactic and extragalactic sources since, unlike photons and charged particles which cannot travel infinite distances without interacting, they are basically immune to attenuation and intergalactic magnetic fields. The detection of possible cosmic neutrino sources is indeed one of the main goals of the recently born neutrino astronomy.

Many large-mass neutrino detectors exist and more are planned for the next generation, based on the use of multi kton target calorimeters. As an example of future devices one can mention the ICARUS detector [7], a modular large-mass liquid Argon TPC being constructed as a neutrino observatory in the underground Gran Sasso Laboratory. ICARUS provides high-resolution imaging of cosmic events of quality comparable to that of the old bubble cham-

ber detectors. In Fig.2 one can see one event recently collected with a 300 ton detector exposed to cosmic rays at surface.

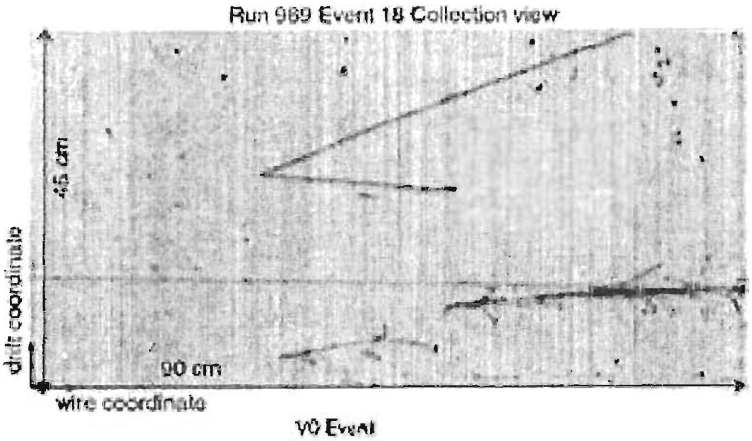

Figure 2: *Cosmic ray event taken with the ICARUS 300 ton detector.*

Much larger masses are to be used to detect neutrinos of very high energy (VHE), say above 1 TeV. The flux of such particles is very low, at the level of one particle per square kilometre per year. This motivates the use of very large active detector masses to be equipped with readout devices able to keep the cost of the detector at a 'reasonable' level. In this case one thinks of water or ice as passive materials with the detection of the Cerenkov light produced by relativistic particles by means of a moderate number of large size PMTs. This approach has been followed by the AMANDA experiment at the south pole (ice) and by the proposed ANTARES (Fig.3), NEMO and NESTOR projects (water) [6]. The main distinctive features of these detectors are the absorption length of the light (20-60 m in water, 100 m in ice), the light scattering length (over 100 m in water and about 100 m in ice) and the angular resolution in measuring the interacting neutrino source (0.5 degrees in water and about 1 degree in ice). We expect that within a few years the commissioning of a 'km cube' observatory will open the road to a high sensitivity search for distant neutrino sources and in general to the systematic study of astrophysical VHE neutrinos.

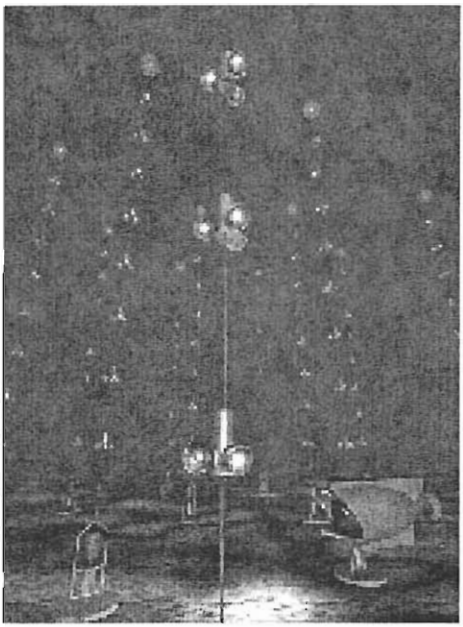

Figure 3: *Artistic view of the ANTARES underwater neutrino detector*

5 Conclusions

The role of calorimetry is becoming increasingly important in high energy physics, since these detectors are well suited to face the challenge of the high energy frontier. After the planned generation of LHC experiments (and calorimeters) we do expect detector improvements and upgrades together with a better understanding of the physics scenario. However, it is also clear that intrinsic and conceptual limitations in the performance of calorimeters will remain. The issue of radiation hardness, in particular, will become fundamental in considering the possible luminosity upgrade of the accelerators as required to access higher-mass states.

Different considerations apply to the next generation electron linear-colliders, expected to be operational after the likely discovery of new physics at the LHC. From the technical point of view linear-collider (highly segmented) calorimeters

could substantially contribute to the precision measurements by employing new methods such as the energy flow. However, both machines and experiments are in a rather early stage of R&D; further prototyping and simulations are needed. The main challenge will be the likely high cost of the detectors.

If we consider the future experiments at B factories the two experimental issues setting requirements to the calorimeters are the increase in luminosity and in background *w.r.t.* the present machines. One has to envisage high-performance crystal calorimeters featuring high granularity and radiation hardness. Also in this case we could benefit from the experience soon being gathered with large size crystal detectors at the LHC.

Finally, there is nowadays a broad variety of calorimetric techniques used for astroparticle physics experiments: crystals for satellite detectors, large surface detector arrays for ground experiments, detection of Cerenkov and fluorescence light for atmospheric showers, large mass active targets for astrophysical neutrinos and liquid/solid water Cerenkov detectors for VHE neutrinos, etc. Once more the experience with state-of-the-art accelerator experiments is (and will be) largely used in the design of the calorimeters, which, aso for these applications, play a crucial role in all experiments.

6 Acknowledgements

I wish to warmly acknowledge F. Fabbri and the other organizers of this conference for the kind invitation. I am also indebted to R. Frey, D. Green, J. Krizmanic, K. Pretzl, S. Swordy, H. Videau and W.J. Wisniewski: their talks at the last CALOR02 Conference in Stanford provided me valuable material in preparing this review.

References

1. D. Green, in Proc. of the X Int. Conf. on Calorimetry in HEP, 25-29 march 2002, World Scientific, 2003.

2. R. Frey, in Proc. of the X Int. Conf. on Calorimetry in HEP, 25-29 march 2002, World Scientific, 2003.

3. H. Videau, in Proc. of the X Int. Conf. on Calorimetry in HEP, 25-29 march 2002, World Scientific, 2003.

4. W.J. Wisniewsky, in Proc. of the X Int. Conf. on Calorimetry in HEP, 25-29 march 2002, World Scientific, 2003.

5. S. Swordy, in Proc. of the X Int. Conf. on Calorimetry in HEP, 25-29 march 2002, World Scientific, 2003.

6. J. Krizmanic, in Proc. of the X Int. Conf. on Calorimetry in HEP, 25-29 march 2002, World Scientific, 2003.

7. ICARUS web page: http://pcnometh4.cern.ch.

Frascati Physics Series Vol. XXXI (2003), pp. 349–356
FRONTIERSCIENCE 2002 – Frascati, October 6–11, 2002
Invited Review Talk in Plenary Session

THE FUTURE OF TRACKING IN HIGH-ENERGY PHYSICS

Manfred Jeitler
Institute of High-Energy Physics of the Austrian Academy of Sciences

ABSTRACT

Higher luminosities and higher beam energies at future accelerators will lead to a significant increase in event numbers and track multiplicities, detectors will be exposed to much higher radiation loads than at present, and improved spatial resolution will be needed for certain physics channels, in particular for B-physics. New developments in detector technology to accept this challenge are described.

1 Introduction

In order to understand the properties of a reaction, the position, charge and momentum of the reaction products are measured by the detector. By using sufficiently light-weight tracking detectors, the position of charged particles can

be measured all along their flight path without strongly influencing their momentum or direction (while calorimeters measure the total energy of a particle by stopping or destroying it). In the special case of muons, a rough measurement of their direction and momentum is made even outside the calorimeters.

The task of "tracking" is complex and comprises a number of different activities. The tracking detectors must be aligned and calibrated and the signals produced by particles must be measured. The reconstruction of tracks usually takes place in two steps. During the stage of *track finding* or *pattern recognition* one determines which detector signals have been caused by one physical particle. During the subsequent stage of *track fitting* one tries to reconstruct the exact track followed by the particle (especially where needed for vertex reconstruction). When the tracker is located in a magnetic field (which is commonly the case) the bending radius of a track also yields information about the particle's charge and momentum. Finally the decay vertex or vertices have to be reconstructed to find out which decay was observed. Normally, vertex reconstruction also takes place in two steps: vertex finding and vertex fitting.

While tracking has been an important part of high-energy physics experiments for a long time, physicists and engineers are presently facing new challenges. Firstly, this is due to the ever increasing luminosity of accelerators. The Large Electron-Positron Collider LEP at CERN achieved a peak luminosity of $3 \times 10^{31}\mathrm{cm}^{-2}\mathrm{s}^{-1}$. The Tevatron at Fermilab is currently running at a similar luminosity but being a hadron machine it produces events of far higher track multiplicity. The asymmetric e^+e^--colliders in Stanford and Japan have already attained luminosities of several times $10^{33}\mathrm{cm}^{-2}\mathrm{s}^{-1}$. The design luminosity for the Large Hadron Collider (LHC) at CERN is $10^{34}\mathrm{cm}^{-2}\mathrm{s}^{-1}$ at a collision energy of 14 TeV, which will result in unprecedented event numbers and track multiplicities (while in e^+e^- colliders production cross sections fall at higher energies, they keep rising in hadron colliders). Thus tracking detectors must be able to handle an ever increasing number of tracks while simultaneously being exposed to very high radiation levels.

Secondly, new physics tasks call for better accuracy in track and vertex reconstruction. For B-tagging, the distance between the primary (production) vertex and the secondary vertex of the decaying B-meson is determined by the short lifetime of B-mesons in the picosecond range. At the asymmetric B-factories, where CP-violation is measured via the decay time asymmetry

between B^0 and $\bar{B}^0$, the B-mesons' boost is relatively small, so that the B^0 decay length is only of the order of 200 μm (during 1 ps light travels 300 μm).

These demands for higher performance, accuracy and radiation hardness have resulted in significant improvements in detector technology, some of which will be described below.

2 Tracking detectors

In a high-energy physics experiment, the layout of the detector and the choice of technology will depend on the type of the accelerator (symmetric or asymmetric e^+e^- collider, hadron collider) and on the specific physics requirements of an experiment (Higgs and SUSY search, B-physics, heavy ions, etc). It is important to satisfy not only the obvious requirements for adequate spatial, momentum and time resolution, but also to guarantee the high level of reliability which is mandatory in a large experiment where interventions for repair may become increasingly difficult and hands-on maintenance may be impossible due to difficulty of access and high irradiation of detector components. In many areas robustness with regard to radiation damage has to be a high priority. Especially in very large detectors the cost of components as well as the material budget may also become decisive factors.

The detector types most frequently used for tracking are on one hand traditional, large-volume gas detectors, with a typical resolution of one hundred to several hundred micrometers, and on the other hand solid-state detectors and micro-pattern gas detectors, with typical resolutions of a few tens of micrometers (varying from the digital resolution of pitch/$\sqrt{12}$ for perpendicular tracks to several times better values where one can make use of charge sharing over several strips).

2.1 Large-volume gas detectors

The original multi-wire proportional chamber (MWPC) has been further developed into a number of different detectors, such as drift chambers, time projection chambers (TPC), straw tube detectors and others. All these detectors have in common that by using a low-density active material (i.e. gas) they may occupy a relatively large volume without leading to prohibitively large scattering of the particles to be detected. Therefore they are especially suited for the outer layers of tracking detectors.

An important factor in the development of new gas detectors (e.g., TPCs) has been the effort to reduce the amount of material and thus the effect of multiple scattering with its adverse influence on the accuracy of the measurement. This extends also to the choice of the gas. The use of low-Z gases is especially important when the particles to be detected have a low energy, either because they are produced at threshold or because the available energy is divided up over a large number of secondary particles. So, the Belle detector where $B/\bar{B}$ pairs are produced at the $\Upsilon 4S$ resonance uses a mixture of 50% He and 50% ethane in its Central Drift Chamber [1]. For the time-projection chamber of the heavy-ion experiment ALICE at LHC the use of 90% Neon and 10% CO_2 is planned [2].

Straw tube detectors have become increasingly popular. One advantage is that if a wire breaks in one tube this will not affect the other channels. Another attractive feature is that by using a suitable gas and placing a radiator material between the straws, the tracker can at the same time be used for particle identification by detecting transition radiation. This is planned for the "Transition Radiation Tracker" of the ATLAS experiment at the LHC [3].

2.2 Solid-state detectors

2.2.1 Silicon detectors

A typical example of a silicon strip detector is shown in Fig. 1a. Highly p doped strips ("$p+$") are created on the surface of a weakly n doped silicon wafer while the opposite surface is highly n doped ($n+$ backplane). Near the junction between $p+$ and n there are no free charge carriers (electron/hole pairs) because free electrons from the n side have united with holes from the $p+$ side. By applying a bias voltage across the wafer, between strips and backplane, all free charge carriers can be removed from it, the detector is "fully depleted". An ionizing particle passing through the detector will again create free charge carriers, giving rise to a current through the wafer and a pulse in the AC-coupled aluminum readout strips. (Without depletion, the detector would contain orders of magnitude more free charge carriers than are produced by one particle, resulting in a prohibitive signal-to-noise ratio).

Many variations of this basic principle have been developed. While the bulk silicon is usually n doped for technological reasons, the doping of strips and backplane may be inverted (creating $n+$ implants and a $p+$ backplane).

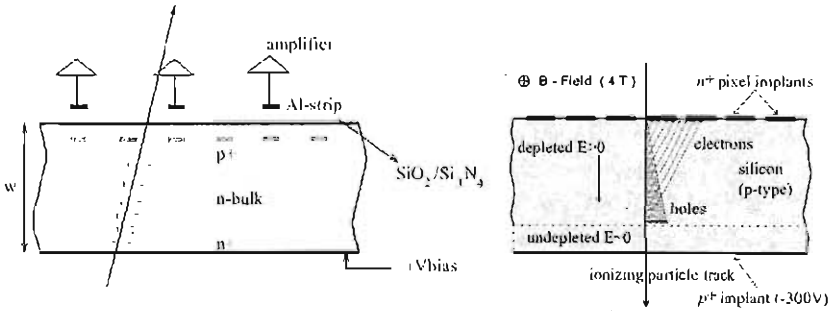

Figure 1: *Typical example of a silicon strip detector (a, left) and of a pixel detector in a magnetic field (b, right).*

The backplane may also be subdivided into strips under an angle to the strips on the top of the wafer, thus allowing to read out two coordinates and obtain information about two dimensions ("double-sided detector"). For example, this approach was used in the silicon vertex detector of the DELPHI experiment at LEP, and is planned for Fermilab experiments and the ALICE detector at LHC. However, such detectors are rather complicated and expensive. Another solution to obtain a measurement of both coordinates with strip detectors is to use two such detectors, glued together under a certain stereo angle (usually a small angle, to optimize the amount of combinatorial background versus measurement precision, as well as for practical reasons). This approach will be used by the ATLAS and CMS experiments at the LHC [3, 4].

The surface may be segmented not into strips but into square or rectangular pixels. This automatically yields information on both coordinates and significantly reduces the occupancy of individual channels at the cost of a much larger overall number of readout channels (Fig. 1b). So, pixel detectors are often used for the innermost detector layers.

Another kind of solid-state detector is the silicon drift detector, where only one coordinate is measured directly while the other is reconstructed from the drift time, much as in a time projection chamber. This system cuts by two the number of readout channels, thus saving on electronics at the cost of a longer readout time. The use of silicon drift detectors is planned for the heavy-ion experiment ALICE at the LHC.

Common features of all solid-state detectors are their potential for good spatial resolution, their high density, and their comparatively higher price. This makes them especially suited for the inner parts of tracking detectors.

A major problem in high-luminosity accelerators, and in particular in hadron machines, will be the large amount of radiation, which may cause problems in all kinds of detectors. The level of ionizing radiation strongly depends on the distance from the interaction region while neutrons, which are a problem in hadron colliders, are more evenly distributed over the whole tracker volume due to backscattering from the calorimeters. Typical values expected over 10 years of operation for the ATLAS pixel detector are 300 kGy of ionizing radiation and over 5×10^{14} neutrons/cm^2 [3].

Radiation damaged silicon detectors need a higher bias voltage for full depletion. However, the voltage that can be applied is limited by the breakdown voltage. So it may happen that strongly damaged silicon detectors cannot be fully depleted, which results in a worse signal-to-noise ratio and thus worse resolution. Another effect is the so-called "type inversion": after absorbing a certain radiation dose, the n bulk silicon starts behaving like p doped material. This is the reason why for detectors in extremely high-radiation environments (often pixels) the somewhat more complicated n-on-n technique is preferred over the p-on-n technique described above. After type inversion (see Fig. 1b), the junction will be next to the readout implants, and even in an underdepleted detector the region near the readout will still be depleted, thus allowing for better spatial resolution. It has been found that cooling improves the long-term behavior of silicon under irradiation, and the silicon detectors of ATLAS and CMS will be operated at a temperature of about $-10°$C [3, 4].

Over the last few years, great progress has been achieved in the radiation hardness of silicon detectors, which therefore might be the best choice for high-radiation environments.

2.2.2 *Other solid-state detectors*

For some time, great hopes concerning radiation hardness were put into *diamond* detectors. Their design is simple: diamond produced by chemical vapor deposition is used as a quasi-insulator, metal electrodes are directly applied on either side, no depletion is needed. However, they yield a much smaller signal than silicon detectors, their radiation hardness is less impressive than originally expected, but above all their exorbitant price has prevented practical use. *Gallium arsenide*, expected to be another radiation-resistant alternative to silicon, has turned out to pose great problems in practice, and R&D efforts

in this direction have been largely abandoned.

2.3 Micropattern gas detectors

Microstrip gas chambers (MSGCs, Fig. 2a) consist of thin metallic strips produced by a photolithographic process on a substrate (a thin glass layer). Electron clouds created by ionizing particles drift towards the anode strips and are multiplied in their vicinity, just as near the anode wires of wire chambers. MSGCs can be produced an order of magnitude smaller than wire chambers, thus creating a high-resolution device, which was originally expected to be simple and much cheaper than silicon. However, they need a complicated gas supply system, there is the danger of sparking, aging properties have remained controversial, and silicon has become cheaper and more radiation-hard than before. Therefore, in some cases where the use of MSGCs had been planned (such as in the outer tracker layers of CMS [4]) they have been replaced by silicon.

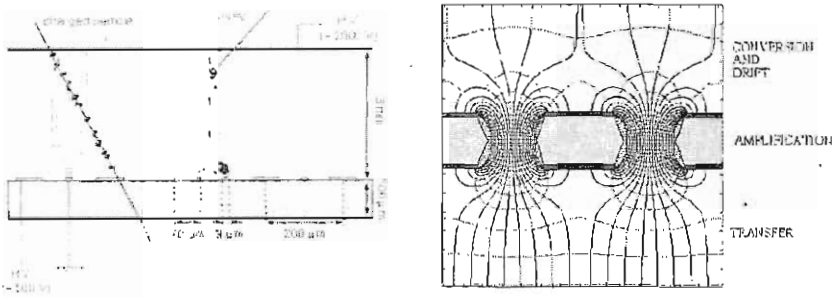

Figure 2: *Operating principle of an MSGC detector (a, left) and field map of a GEM foil (b, right).*

Another micropattern gas detector is the GEM or *"gas electron multiplier"* (Fig. 2b), where gas amplification of the signal takes place in the strong field within microscopic etched holes in thin foils between the gas volume and the readout plane. By using several layers, each foil can be operated at lower voltage, thus reducing the danger of sparking. The readout is accomplished by an MSGC run at lower voltage, or by larger strips without any further gas amplification. GEMs are being successfully used at the COMPASS experiment at CERN.

3 The future of tracking

Only a few years ago it was unclear how detectors would come to grips with the high-radiation environment of future hadron colliders. The recent progress in detector technology, especially in the field of silicon detectors, is ground for optimism. It will be no less important to correctly disentangle the enormous amounts of detector signals. This will be achieved on one hand by hardware measures, using detectors with very fine granularity and therefore low occupancy of individual channels (e.g. pixels), which have to be matched by a corresponding amount of electronics and computing power. On the other hand, new track finding and fitting algorithms will help to correctly interpret detector signals. The Kalman filter, a technique for analyzing developing dynamical stochastic systems, has become more and more popular since it was first used with full performance for tracking at the DELPHI experiment at LEP. It has been further developed into the "deterministic annealing filter" and the "multitrack filter", and these methods have already been implemented and Monte-Carlo tested in the analysis software of the CMS experiment at CERN [5], where they will also play an important role in high-level triggers.

In conclusion, both hardware and software are ready to face the immediate challenges, but more new ideas will be needed in the long run.

References

1. A. Abashian *et al.*, Nucl.Inst.and Meth.in Phys.Res.A, **479**, 1 (2002).

2. ALICE Time Projection Chamber Technical Design Report, CERN/LHCC 2000-001 (2000).

3. ATLAS Inner Detector Technical Design Report, CERN/LHCC 97/17 (1997).

4. CMS Tracker Project Technical Design Report, CERN/LHCC 98-6 (1998), and Addendum, CERN/LHCC 2000-016 (2000).

5. M. Winkler, A Comparative Study of Track Reconstruction Methods; Ph.D. thesis, Vienna, Austria (2002). R. Frühwirth and A. Strandlie, Comp. Phys. Comm. **120**:197 (1999) and **133**:34-42 (2000).

The Next Door

Chairperson: S. Bertolucci

T. Dorigo	Top Studies
B.E. Sauer	Status of EDM Measurement
H. Sobel	Lepton Mixing and Neutrino Oscillations

Frascati Physics Series Vol. XXXI (2003), pp. 359–373
FRONTIERSCIENCE 2002 – Frascati, October 6–11, 2002
Invited Review Talk in Plenary Session

TOP STUDIES

T. Dorigo
Padova University and INFN

ABSTRACT

The top quark, discovered in 1994 at the Tevatron, has proven a very interesting particle. Its characteristics allow both to perform stringent tests of electroweak theory, and to search for new physics through a deviation from standard model predictions for several of its peculiar properties. I will review the status of top physics and briefly describe the potential of experiments of the near future.

1 Introduction: a brief history of top physics

The first hint of the existence of the top quark can be argued to have been the detection of CP violation in the $K^\circ\bar{K}^\circ$ system in 1964: Kobayashi and Maskawa in 1973 demonstrated that three generations of quarks are needed to allow CP violation via a complex phase in the flavour matrix. However, it was

only in 1977, with the discovery of the Υ states, that the top quark became a fixed thought of experimenters and theoreticians worldwide.

On the theoretical side, the renormalizability of the Standard Model (SM) demands a cancellation of triangle anomalies. The existence of a $I_3 = +\frac{1}{2}$ partner of the newborn b quark was thus direly needed for the internal consistency of the model. Moreover, an isosinglet b quark generates copious flavor-changing neutral current decays of strange and bottom hadrons, such as $b \to s l^+ l^-$: none of the resulting B-hadron decays, heavily suppressed in the SM, was observed experimentally.

Additional evidence that the top quark had to complete the third generation soon came from several measurements at e^+e^- machines: first, in 1978 the PLUTO and DASP collaborations measured the leptonic width Γ_{ee} of the $\Upsilon(1s)$ meson [1], determining that the b-quark must have $Q = -\frac{1}{3}$; then in 1983 the JADE experiment measured a large forward-backward asymmetry in $e^+e^- \to b\bar{b}$ reactions [2], when none was predicted in the SM if $I^b_{3,L} = 0$. In 1987 ARGUS results suggested that the top quark mass had to be large, since the mixing parameter X_d was found to be large in the analysis of the $B^0\bar{B}^0$ system [3]. Finally, in 1990 the first precision measurements of electroweak parameters from the LEP experiments at CERN started pouring in; most notably, the precision measurements of $\Gamma(Z \to b\bar{b})$ allowed to establish that $I^b_{3,L} = -\frac{1}{2}$ [4].

These and other determinations of electroweak parameters were used by theorists to produce several standard model predictions and upper limits for the top quark mass.

In the meantime, direct searches were carried out at all available experimental facilities around the world. A jump in $R = \frac{\sigma(e^+e^- \to hadrons)}{\sigma(e^+e^- \to \mu^+\mu^-)}$ and/or changes in event shape were sought, along with direct evidence for T hadrons. None of the experiments found any evidence of top production, and mass limits were set at increasing M_t values, up to $M_Z/2$ (reached first by ALEPH in 1990 [5]).

Hadron colliders soon joined the group and rapidly took over. The first collaboration to produce results was the UA1 experiment at the $Sp\bar{p}S$ ($\sqrt{s} = 630$ GeV), which sought direct evidence of top quark production in the decays of the recently discovered W bosons, $p\bar{p} \to WX \to t\bar{b}X$. In 1984 they obtained 12

$l+jj$ events on a background of 3.5, claiming discovery and quoting $M_t = 40 \pm 10$ GeV/c^2. The new particle, however, refused to show up in added statistics, and the result became $M_t > 44$ GeV/c^2 at 95% CL [6]. In 1990 UA2 improved the limit to $M_t > 69$ GeV/c^2 [7], but by then eyes were already pointed at the Tevatron, where the higher center-of-mass energy promised discovery.

With the 4 pb^{-1} of data collected in 1988-89 the CDF collaboration indeed observed a very clear dilepton event, but was only able to place a 95% confidence level (CL) limit at $M_t > 77$ GeV/c^2, soon improved to $M_t > 91$ GeV/c^2 [8]. The breakthrough came with the increased luminosity of Tevatron Run I in 1992, when the CDF experiment was equipped with a new silicon detector capable of identifying b-quark jets from the reconstruction of b-decay vertices. The seven candidate events identified in 19 pb^{-1} were only enough to claim a 3 σ evidence in 1994, but they allowed to measure $M_t = 174 \pm 16$ GeV/c^2 [9]. Finally, in 1995 conclusive evidence was brought by both CDF and D0 [10]. The quark sector of the Standard Model was now complete. Figure 1 illustrates the convergence of direct and indirect determinations of M_t in the last 15 years.

2 Intrinsic top quark properties

2.1 Top mass and width

The most important property of the top quark is its mass, which is very large when compared to all other SM fermions. The top mass is actually close to the scale of electroweak symmetry breaking: the top quark Yukawa coupling is "natural", because $y_t = \sqrt{2}\frac{M_t}{v} \sim 1$. This coincidence of scales might suggest that the top quark is actively involved in the breaking of electroweak symmetry. It must also be noted that, in the framework of minimal supersymmetric models (MSSM), a large value of M_t was actually *predicted* as far back as in 1982 [11], since without a large value of M_t, radiative corrections to the mass of the lightest neutral scalar M_h would have prevented the spontaneous breaking of SU(2)xU(1) symmetry.

In any case, M_t is a very important parameter for the tests of EW theory. Because of the quadratic dependence of the $\Delta\rho$ parameter on top mass, a precise knowledge of the latter is important for stringent consistency checks

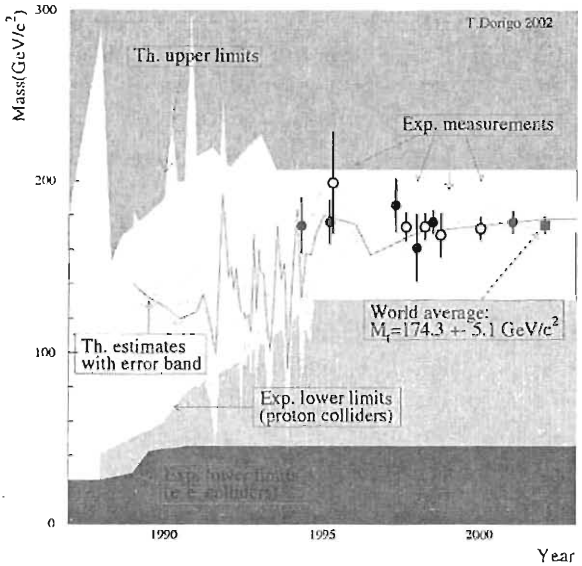

Figure 1: *A compilation of experimental and theoretical results on the top quark search. Experimental lower limits from e^+e^- and $p\bar{p}$ colliders are compared to indirect upper limits and estimates of M_t from SM fits to electroweak observables. The direct measurements by CDF (full points) and D0 (empty points) are also indicated, as well as the current world average (full square).*

of the theory. Also, the large value of the Yukawa coupling y_t would make it advantageous to probe the $t\bar{t}h$ vertex, if the Higgs boson were found. It must finally be stressed that a precise measurement of M_t yields vital information on the mass of the Higgs boson: an uncertainty of 1 GeV/c^2 in the top mass yields the same amount of information on the value of M_h as an uncertainty of 7 MeV/c^2 on the W boson mass [12].

The large value of M_t implies that the decay time is very short: $\Gamma_t \sim M_t^3 \sim 1.5$ GeV/c^2. That value is one order of magnitude larger than the hadronization scale Λ_{QCD}: that implies that top quarks cannot bind to form hadrons, and they decay as free particles. The absence of top hadrons can also be inferred from the non-relativistic quark model: on one side, the mass splitting $M_{B^{**}} - M_B = 450$ MeV/c^2 is independent on the heavy quark mass,

and must hold for T^{**} and T as well; on the other, the splitting between B^* and B depends on $1/M_Q$ and is thus expected to be smaller for top hadrons. Moreover, toponium states cannot exist, since their width ($\Gamma_{t\bar{t}} \sim 2\Gamma_t \sim 3$ GeV/c^2) is larger than the splitting between $1S$ and $2S$ states expected from the perturbative QCD potential. All top resonances therefore merge and act coherently, and what is left in the cross section is only a broad excitation curve.

On the experimental side, several possibilities for testing production and decay properties of top quarks are granted by the large value of Γ_t and have already started to be investigated with Tevatron data. Decay products can provide information about top polarization, because the depolarization time $\tau_d \sim M_t/\Lambda^2_{QCD}$ is much longer than the lifetime. One can also study W helicity and verify the absence of $h_{W^+} = +1$ state, suppressed by the chiral factor $(M_b/M_W)^2$, and the predicted fraction of longitudinal states. It must finally be noted that a measurement of the top quark mass with unmatched precision ($\Delta M_t \sim 100$ MeV/c^2) can in principle be achieved with threshold scans at a high-energy e^+e^- collider, since Γ_t acts as an infrared cut-off in the theoretical computation of the shape of cross section at threshold, removing the influence of non-perturbative contributions.

2.2 Top decay

Since $|V_{tb}| \sim 1$ and $M_t > M_W + M_b$, the decay $t \to W^+b$ dominates. At the Tevatron, $t\bar{t}$ final states are classified according to the decay of the produced W bosons: when these both decay to quark pairs the final state is "all-hadronic" and contains nominally six jets ($B = \frac{4}{9}$); when one of them decays to $e\nu_e$ or $\mu\nu_\mu$ the "single-lepton" final state arises ($B = \frac{8}{27}$), with a $l\nu_l$+ 4 jet topology; when both W bosons decay to electron-neutrino or muon-neutrino pairs one has the "dilepton" final state ($B = \frac{4}{81}$), characterized by a $l\nu_l l'\nu_{l'}$+ 2 jet topology. $W \to \tau\nu_\tau$ decays are excluded from the above classification, since at hadron colliders it is hard to trigger on these decays and to detect τ lepton decays.

Besides the dominant channels, top quarks have been sought in the flavour-changing neutral current decays $t \to Zc(u)$ and $t \to \gamma c(u)$. In addition, in the MSSM a light charged Higgs boson can be produced in the decay $t \to H^+b$. Other supersymmetric decays of the top quark are beyond the purpose of this paper.

3 Topics in top quark physics today

3.1 Measurements of the top quark mass

All direct determinations of the top quark mass to date come from the CDF and D0 collaborations, who have measured it with many different techniques in all available final states. The single most precise determination is based on single lepton events from CDF: it is briefly described below.

Data redution proceeds by selecting events passing high-P_T electron and muon triggers. To select a W sample, charged leptons are required to have E_T (P_T)> 20 GeV($/c^2$), and missing transverse energy $\not\!\!E_T > 20$ GeV. In addition, four hadronic jets are required; three of them must have $E_T > 15$ GeV and rapidity $|\eta| < 2.0$. From the events passing these criteria four disjoint subsets are constructed; in decreasing background content they consist of events with two jets possessing an identified secondary vertex (SVX) tag from b decay, events with one SVX tag, events with one jet containing a soft electron or muon candidate (SLT) from b decay, and events where all four jets have $E_T > 15$ GeV. Background contaminations are mainly due to QCD $Wb\bar{b}$ and $Wc\bar{c}$ production and to fake heavy flavor signals. By keeping the four samples separated the measurement errors on M_t are minimized.

A kinematical fit is applied to each event under the hypothesis of top decay, with the constraints that SVX- or SLT-tagged jets are assigned to b quarks, that the lepton-neutrino and jet-jet masses are compatible with M_W, and that top and antitop masses are equal. The best χ^2 solution is used. A likelihood technique determines the mass for each distribution; the four results are then combined together. The final result is $M_t = 175.9 \pm 4.8$ (stat.) ± 4.9 (syst.) GeV$/c^2$ [13].

All CDF and D0 determinations of the top quark mass have been combined by accounting for correlated systematics. The world average value is $M_t = 174.3 \pm 3.2$(stat.) ± 4.0 (syst.) GeV$/c^2$ [14].

3.2 Top quark production at the Tevatron

At $\sqrt{s} = 1.8$ TeV, the dominant top production process is via strong interaction, 90% of which is due to $q\bar{q}$ annihilation. Fig. 2 summarizes the Tevatron determinations of $\sigma_{t\bar{t}}$ [15]. In total, the averaged CDF and D0 measurements

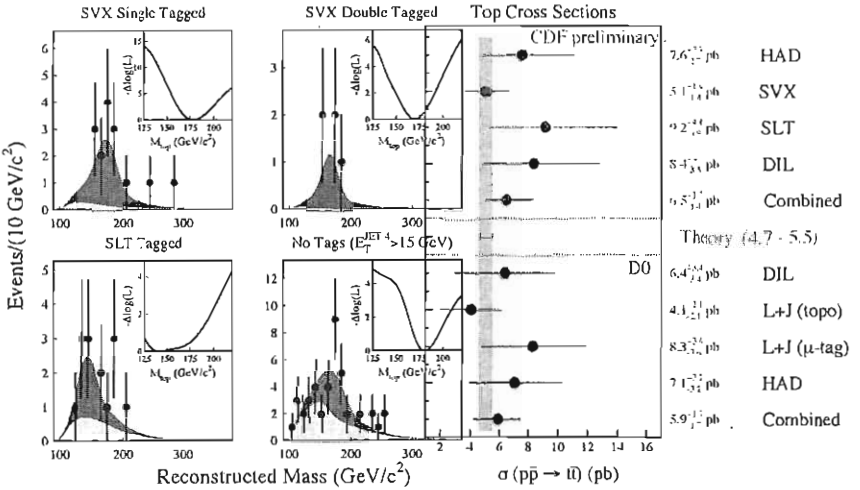

Figure 2: *Left: top mass distributions of the four subsamples of CDF data in the single lepton channel (see text); right: summary of Tevatron determinations of* $\sigma_{t\bar{t}}$.

($\sigma_{t\bar{t}} = 6.5^{+1.7}_{-1.4}$ *pb*, $M_t = 175$ GeV/c^2 (CDF), $\sigma_{t\bar{t}} = 5.7 \pm 1.6$ *pb*, $M_t = 172.1$ GeV/c^2 (D0)) are in good agreement with theoretical predictions [16].

In addition to pair-produced $t\bar{t}$ pairs, single top quarks can be produced by weak interaction via a virtual W (32%) or through Wg fusion; the total is expected to be $\sigma_{tX} = 2.4$ *pb*. Single top production is interesting in its own right: a precise measurement of the cross section would provide a direct determination of $|V_{tb}|$; moreover, the process consistutes a significant background to the most promising signature of a SM Higgs ($p\bar{p} \to W^+HX \to l^+\nu b\bar{b}X$). The identification of single top production is more challenging than $t\bar{t}$ production, since there are fewer jets in the final state, and the topology is less distinctive.

CDF and D0 have both searched for $s-$ and $t-$ channel top production separately; CDF also searched for both processes together [17]. In the combined search, CDF used $W+$ jets data with at least one SVX b-tagged jet, selected with the requirement that $140 < M_{l\nu j_1} < 210$ GeV/c^2. The sum of leptons and jets transverse energy, $H_t = \Sigma_j E_t + P_t^l + \not\!\!E_T$, is very similar in both $s-$ and $t-$

channel top production, and discriminates them from the main backgrounds. A likelihood fit allows to extract the limit $\sigma_{tX} < 14$ *pb* at 95% CL. To find single top events at D0, a neural network is trained to separate the two processes from concurring backgrounds. D0 limits are $\sigma_t^s < 17$ *pb*, $\sigma_t^t < 22$ *pb* (95% CL). CDF searched separately for $s-$channel events in double SVX-tagged $W + 2$ jets data and for $t-$channel events in single SVX-tagged $W + 2$ jets data. The limits extracted are $\sigma_t^s < 18$ *pb*, $\sigma_t^t < 13$ *pb* (95% CL).

3.3 Other measurements with top quarks

3.3.1 Helicity of W bosons in top decay

The SM predicts the polarization of W bosons emitted in t decay. The amplitude for positive helicity W^+ is suppressed by the chiral factor M_b^2/M_W^2. Moreover, at tree level the relative fraction of zero helicity W bosons is $\mathcal{F}_0 = \frac{M_t^2/2M_W^2}{1+M_t^2/2M_W^2} = 0.701 \pm 0.016$.

The V-A coupling at the lepton vertex induces a strong correlation between W helicity and lepton momentum. CDF used both single lepton and dilepton decays to fit the lepton P_T spectrum, obtaining $\mathcal{F}_0 = 0.91 \pm 0.37 \pm 0.13$ and $\mathcal{F}_+ = 0.11 \pm 0.15 \pm 0.06$ [18], in good agreement with SM predictions.

3.3.2 Rare decays and FCNC

Flavour-changing neutral currents in top decay are exceptionally small in the SM: the decays $t \to Zc(u)$, $t \to \gamma c(u)$ are predicted to have branching fractions $B < 10^{-10}$. The CDF collaboration searched these processes by looking for $t\bar{t}$ pairs undergoing mixed decay (one standard and one FCNC) [19]. In the $t \to \gamma q$ search, both leptonic ($\gamma l \not{E}_T jj$) and hadronic signatures ($\gamma \geq 4j$, where a jet is SVX-tagged) were accepted. One $\mu\gamma$ event was observed, with large $E_t^\gamma = 88$ GeV, but not inconsistent with the hypothesis $t\bar{t} \to Wb\bar{W}b\gamma$. The extracted limit is $B < 0.032$ at 95% CL. In the $t \to Zq$ search, leptonic Z decays with four accompanying jets were sought. One event passes the cuts, with an expected background of 0.6 events. The limit obtained is $B < 0.33$ at 95% CL.

Constraints on FCNC couplings of the top quark can be obtained also from the search of single top production at LEP II [20]. Limits on the cross

section for $e^+e^- \to \gamma, Z^* \to t\bar{q}$ can be translated into constraints to the top quark FCNC branching ratios. The ALEPH collaboration found 58 events compatible with the decay in 411 pb^{-1} of data taken at $\sqrt{s} = 189 - 202$ GeV, with an expected background of 50.3, and extracted the limit $B(t \to Zq) < 0.17$ at 95% CL. OPAL found 85 events in 600.1 pb^{-1} of data at energies up to $\sqrt{s} =$ 209 GeV, when 84.1 were expected. The resulting limit was $B(t \to Zq) < 0.137$ at 95% CL.

A search for anomalous top quark production mediated by FCNC via a γut coupling was also performed by both ZEUS and H1 [21]. H1 sought $ep \to etX$ events with both leptonic and hadronic W final states in 115.2 pb^{-1} of data; 5 events were found, with 1.8 expected from SM sources. They set the limit $k_{tu\gamma} < 0.22$ at 95% CL. ZEUS analysed 130 pb^{-1} of data in a similar way. They set a limit of $k_{tu\gamma} < 0.19$ at 95% CL. Fig. 3 compares the HERA, LEP II, and Tevatron limits on these quantities.

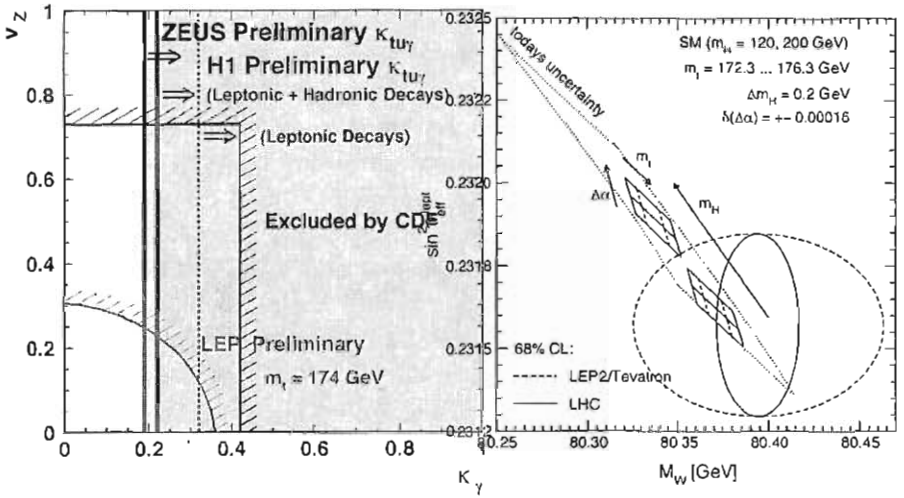

Figure 3: *Left: limits on anomalous FCNC couplings obtained by HERA, LEP II, and CDF. Right: The parametric uncertainties caused by a 2 GeV/c^2 (1 GeV/c^2, dashed) M_t error and by the uncertainty in the hadronic contribution to $\Delta\alpha$ in the theoretical prediction to M_W and $\sin^2\theta^{lept}_{eff}$ are compared to experimental determinations. From Ref.* [12].

3.4 *Using* top quarks

The statistics collected at the Tevatron during Run I allowed D0 and CDF to carry out several additional measurements as well as searches which *use* the top quark as a tag of other processes or as a background. I will briefly mention the most interesting studies in the following.

The top quark samples collected by CDF were used for a direct measurement of $|V_{tb}|$: by fitting the observed yield of events with zero, one, and two SVX b-tags it was possible to determine that $|V_{tb}| = 0.97^{+0.16}_{-0.12}$, or $|V_{tb}| > 0.75$ at 95% CL [22].

Both D0 and CDF [23] searched for $t\bar{t}$ resonances. Models with a dynamically broken EW symmetry (technicolor) predict a top-quark condensate, X, that decays to a $t\bar{t}$ pair. By searching for narrow $t\bar{t}$ resonances, the limit is model-independent. One model [24] predicted a leptophobic $Z' \to t\bar{t}$ with large cross section. The best limit was obtained by the D0 collaboration; for the Z' model, the limit was set at $M_{Z'} > 585$ GeV/c^2 (95% CL).

The studies of the top cross section brought CDF into a deep investigation of their $W+$ heavy flavor data sample. A sample of 13 events with a jet containing both a SVX and SLT b-tag, found to exceed the expectation of 4.4 ± 0.6 events from SM sources, spurred a detailed kinematic analysis. Most of the kinematic characteristics of these events were found to be very different from expectations. A study by some authors claims that the disagreement with a control sample of data with similar biases is at the 10^{-6} level [25]. These anomalies have no explanation in the SM, but are very hard to fit even within exotic models. Run II data will solve this puzzle.

To probe non-standard interactions in the decay of the top quark, spin-spin correlations can be studied: $t\bar{t}$ pairs are not polarized, but their spins should have the same direction in the $t\bar{t}$ rest frame. D0 studied lepton angular correlations in dilepton events, parametrized in terms of k where $\frac{d^2\sigma}{d\cos(\theta_+)d\cos(\theta_-)} = \frac{\sigma(1+k\cos\theta_+\cos\theta_-)}{4}$. The SM predicts $k = 0.88$, and D0 measured $k > -0.2$ at 68% CL [26].

4 The future of top studies

Despite the successes of the conspicuous research program on the top quark carried out at the Tevatron, plus the additional bits from LEP2 and HERA, much more is left to be measured. Fortunately, the Tevatron Run II has already started delivering thousands of $t\bar{t}$ events/year per experiment: these datasets will be used for precision top physics measurements. In a slightly more distant future, the LHC will take over with the huge samples of top quarks it will deliver. But eventually, if a new TeV-scale e^+e^- collider is built, M_t will be determined from threshold scans and our insight in top physics will deepen considerably.

It is impossible to do justice here to the huge amount of work done to anticipate the potential of these experiments in the subject of top physics. I will just highlight some of their most promising aspects in the following.

4.1 The Tevatron upgrade and Run II expectations

The Tevatron collider complex has undergone a massive upgrade during the last five years. The construction of a new main injector with a recycler ring, and the improvements done to the antiproton source and booster ring promise an increase of instantaneous luminosity of an order of magnitude over Run I. The beam energy has also been increased from 900 to 980 GeV, granting up to $30 - 40\%$ increases in the cross section of interesting processes.

Along with the accelerator complex, the CDF and D0 detectors have undergone major improvements. CDF was refurbished with an entirely new tracking system, with seven silicon layers providing precise measurements of track parameters in the region close to the beam line; a revolutionary device provides selection of tracks with significant impact parameter in less than $10\mu s$, enabling triggering capability for hadronic heavy flavor decays. D0 was doted with a $2T$ axial field, and new silicon and fiber trackers; moreover, significant improvements have been made to the calorimeter and muon system.

Run II at the Tevatron promises a great improvement in the measurement of top properties. It is predicted that with 2 fb^{-1} of collected data single top production will be observed and the top mass will be measured with 2 GeV/c^2 accuracy. In order to reach the latter goal, a precise determination of the energy

scale of b-quark jets, which was one of the dominant sources of systematics in the run I measurements, will be granted by the availability of a calibration line from $Z \to b\bar{b}$ decays, whose observability has been proven in Run I [27]. Many other precise measurements of top quark properties are in the agenda.

4.2 LHC top physics at a glance

At $\sqrt{s} = 14$ TeV, top quark pairs are produced mainly (90%) through $gg \to t\bar{t}$, with $\sigma_{t\bar{t}} \sim 840\ pb$. One year of running at low luminosity ($\sim 10\ fb^{-1}$) will thus allow the collection of 2×10^6 single lepton $t\bar{t}$ events per experiment. These samples grant several precision measurements. M_t determinations are systematics-limited; however, the dominant systematics of different methods are different, so important cross-checks can be made. A precision of $\Delta M_t = 2$ GeV/c^2 can be obtained with only one or two years of running. From the study of single top production ($\sigma_{tX} \sim 300\ pb$), $|V_{tb}|$ can be determined to within 10%. Anomalous FCNC couplings can be explored to $10^{-4} \div 10^{-5}$ with $10\ fb^{-1}$; associated $t\bar{t}H$ production can be observed with $30\ fb^{-1}$ if $M_h = 120$ GeV/c^2, when a precision of 16% in the top Yukawa coupling can be obtained.

Measuring M_t with $1 - 2$ GeV/c^2 accuracy will considerably tighten the consistency tests of electroweak theory. Fig. 3 shows the level of accuracy that these measurements will reach.

4.3 Top physics at a high energy linear e^+e^- collider

In a high energy e^+e^- collider ($E_{CM} \sim 500$ GeV, $10^{34}\ cm^{-2}s^{-1}$, $100\ fb^{-1}$/year), the total yield of $t\bar{t}$ pairs is expected to reach $\sim 10^5\ t\bar{t}$ per year of running. The statistical power of these data is smaller than that of LHC, but M_t can be determined with higher accuracy by means of a threshold scan. It is foreseen that the error on M_t could be reduced to $\Delta M_t \sim 100$ MeV/c^2 [28]. Moreover, the width of the top quark may be obtained to within a few percent by the shape of the cross section in the threshold region. Another feature is the study of the γtu coupling via the process $e^+e^- \to t\bar{q}$. Studies dealt with the TESLA design ($\sqrt{s} = 500/800$ GeV) [29]: the use of polarized beams could reduce the $Wq\bar{q}'$ background by up to a factor of 8, while increasing $\sigma_{t\bar{q}'}$ by 20%; limits on γtq, Ztq couplings would improve by a factor 2.5, allowing a $\times 10$ improvement over expected LHC limits.

5 Conclusions

The top quark is a very interesting particle: it is the only quark whose mass can be measured directly, and that can be studied free of QCD effects; moreover, the large impact of M_t on radiative corrections makes it worth measuring it with the utmost precision. A handful of $t\bar{t}$ candidates already provided a wealth of new knowledge at the Tevatron Run I. The new Tevatron Run II, LHC, and a new e^+e^- collider are foreseen to do exquisite precision top physics. Top quarks will be used to corner the SM, and hopefully to open an avenue to new physics.

References

1. C. Berger *et al.*, Phys. Lett. B76, 243 (1978); C. Darden *et al.*, Phys. Lett. B76, 246 (1978).
2. W. Behrends *et al.*, Phys. Lett. B146, 437 (1983).
3. H. Albrecht *et al.*, Phys. Lett. B192, 245 (1987).
4. D. Schaile and P. Zerwas, Phys. Rev. D45, 3262 (1992).
5. D. Decamp *et al.*, Phys. Lett. B236, 511 (1990).
6. G. Arnison *et al.*, Phys. Lett. B147, 493 (1984); C. Albayar *et al.*, Z. Phys. C37, 505 (1988).
7. T. Akesson *et al.*, Z. Phys. C46, 179 (1990).
8. F. Abe *et al.*, Phys. Rev. Lett. 64, 174 (1990), F. Abe *et al.*, Phys. Rev. D45, 3921 (1992).
9. F. Abe *et al.*, Phys. Rev. Lett. 73, 225 (1994).
10. F. Abe *et al.*, Phys. Rev. Lett. 74, 2626 (1995); S. Abachi *et al.*, Phys. Rev. Lett. 74, 2632 (1995).
11. L. Ibanez and G. Ross, Phys. Lett. B110, 215 (1982).
12. M. Beneke *et al.*, *Top quark physics*, Hep-ph/0003033.

13. T. Affolder *et al.*, Phys. Rev. D63, 32003 (2001).

14. L. Demortier *et al.*, *The top averaging group*, FNAL-TM-2084.

15. V. Abazov *et al.*, *Ttbar production cross section in ppbar collisions at* $\sqrt{s} = 1.8$ *TeV*, Hep-ex/0205019; T. Affolder *et al.*, Phys. Rev. D64, 032002 (2001).

16. K. Hagiwara *et al.*, Phys. Rev. D66, 010001 (2002).

17. D. Acosta *et al.*, Phys. Rev. D65, 91102 (2002); V. Abazov *et al.*, Phys. Lett. B517, 282 (2001).

18. T. Affolder *et al.*, Phys. Rev. Lett. 84, 216 (2000).

19. F. Abe *et al.*, Phys. Rev. Lett. 80, 2525 (1998).

20. R. Barate *et al.*, Phys. Lett. B494, 33 (2000); G. Abbiendi *et al.*, Phys. Lett. B521, 181 (2001).

21. N. Malden, *Search for single top production in ep collisions at HERA*, submitted to ICHEP 2002; ZEUS collaboration, *Search for events with isolated* τ *leptons and large missing transverse momentum in ep collisions at HERA*, submitted to ICHEP 2002.

22. T. Affolder *et al.*, Phys. Rev. Lett. 86, 3233 (2001).

23. T. Affolder *et al.*, Phys. Rev. Lett. 85, 2062 (2000).

24. R. Harris, T. Hill, and S. Parke, *Cross section for Topcolor* Z' *decaying to top-antitop*, Hep-ph/9911288.

25. D. Acosta *et al.*, Phys. Rev. D65, 52007 (2002); G. Apollinari *et al.*, Phys. Rev. D65, 032004 (2002).

26. B. Abbott *et al.*, Phys. Rev. Lett. 85, 256 (2000).

27. T. Dorigo, *Observation of Z decays to b quark pairs at the Tevatron collider*, Hep-ex/9806022.

28. T. Abe *et al.*, *Linear collider physics resource book for Snowmass 2001 - part 3*, Hep-ex/0106057.

29. J. Aguilar-Saavedra and T. Riemann, *Probing top flavor-changing neutral couplings at TESLA*, Hep-ph/0102197.

Frascati Physics Series Vol. XXXI (2003), pp. 375
FRONTIERSCIENCE 2002 – Frascati, October 6–11, 2002
Invited Review Talk in Plenary Session

STATUS OF EDM MEASUREMENT

B.E. Sauer

Sussex University , UK

Written contribution not received

Frascati Physics Series Vol. XXXI (2003), pp. 377
FRONTIERSCIENCE 2002 – Frascati, October 6–11, 2002
Invited Review Talk in Plenary Session

LEPTON MIXING AND NEUTRINO OSCILLATIONS

H. Sobel

University of California, Santa Barbara, USA

Written contribution not received

Closing Session

Chairperson: F.L. Fabbri

Frascati Physics Series Vol. XXXI (2003), pp. 381–405
FRONTIERSCIENCE 2002 – Frascati, October 6–11, 2002
Invited Review Talk in Plenary Session

WHAT NEXT IN FLAVOUR PHYSICS AND CP VIOLATION?

John Ellis
TH Division, CERN, CH 1211 Geneva 23, Switzerland

ABSTRACT

The future of flavour physics and CP violation in the quark, lepton and Higgs sectors are discussed, particularly from the viewpoint of physics beyond the Standard Model, such as supersymmetry. Current issues in $B \to \pi^+\pi^-, \phi K_s$ and $D^{*+}D^{*-}$, B_s physics and rare B decays are reviewed. The prospects for seeing flavour and CP violation in the charged-lepton sector are discussed, using the minimal supersymmetric seesaw model as a guide. Finally, the possible consequences of CP violation in the Higgs sector are mentioned.

1 Mea Maxima Culpa

The organizers have asked me to look towards the future, rather than summarize this meeting. Unfortunately, this is just as well, because commitments at CERN prevented me from attending most of the meeting. I am very sorry

that I missed many interesting subjects, such as factorization, J/ψ production at RHIC, charmonium, heavy-quark effective theory, $\bar{b}b$ production, b-quark fragmentation, $W \to c\bar{s}$ decay, $B \to \ell\nu\gamma$, $\mathrm{Re}(\epsilon'/\epsilon)$, $K_S \to \gamma\gamma$, CLEO-c, LHCb light, $Z \to \bar{b}b$, ΔG, x_s, $D \to \sigma, \kappa$, flavour textures, $B \to \ell^+\ell'^-$, $B_s - \bar{B}_s$ mixing, $D_0 - \bar{D}_0$ mixing, $\Delta\Gamma_s\Gamma_s$, $\tau(D_s)/\tau(D_0)$, $\tau(\Xi_c^+)/\tau(\Lambda_c^+)$, the ${}^1\mathrm{D}_2(\bar{b}b)$ and many more .... For these reasons, I could not in any case present a balanced summary of the meeting.

2 A Personal Point of View

There are three preferred experimental arenas for probing flavour dynamics and CP violation: the quark sector - where both are well established, the lepton sector - where flavour mixing has been seen among the neutrinos and CP violation is expected, and the Higgs sector - about which we have no direct experimental information. Reflecting my personal bias, I assume in discussing these sectors that supersymmetry will appear at some accessible energy.

In the quark sector, dare we hope that that the current triumph of the standard Kobayashi-Maskawa (KM) model in predicting correctly the value of $\sin 2\beta$ observed in $B_0 \to J/\psi K_s$ decays may be short-lived? As discussed at this meeting, the first rounds of data on $B \to \pi^+\pi^-, \phi K_s$ and $D^{*+}D^{*-}$ decay asymmetries do not agree very well with the KM model. Might one of these be a harbinger of new physics, such as supersymmetry? Answers to the tough questions are still in the future: does the unitarity triangle close, or is it a quadrangle? New tools for analyzing flavour dynamics in the quark sector await us: what will B_s physics or $b \to s\gamma, s\ell^+\ell^-$ tell us?

In the neutrino sector, many questions about neutrino masses and mixing remain unanswered: is the large-mixing-angle (LMA) solar solution correct? What is the value of θ_{13}? Is there a CP-violating phase δ? What are the absolute values of the neutrino masses? Beyond neutrinos, in the presence of low-energy supersymmetry we may expect a new flavour frontier to open up among the charged leptons: will $\mu \to e\gamma, \tau \to e/\mu\gamma, \mu \to 3e$ and $\tau \to 3\ell$ be observable? Do the electron and muon have measurable CP-violating electric dipole moments? What is the relation to leptogenesis?

The final frontier for studies of flavour dynamics and CP violation may be the Higgs sector, which is their origin in the Standard Model (SM). In the minimal supersymmetric extension of the Standard Model (MSSM), the masses,

mixings and couplings of the physical Higgs bosons may exhibit observable flavour- and CP-violating effects.

3 Roadmap to Physics Beyond the Standard Model

Let us first set flavour dynamics in the general context of physics beyond the SM.

The standard list of problems beyond the SM includes those of *Unification* - can one find a single simple framework for all the gauge interactions? *Flavour* - why so many different types of quarks and leptons and what explains their patterns of mixing and CP violation? and *Mass* - do particle masses really originate from a Higgs boson, and if so why are they so small, where there may be a rôle for supersymmetry? Beyond all these 'beyonds' there is the quest for a *Theory of Everything*, capable of reconciling gravity with quantum mechanics as well as solving all the above problems, perhaps via superstring or M theory?

At what energy scales might appear these examples of new physics? LEP told us that they cannot appear below 100 GeV, and quantum gravity must become strong by 10^{19} GeV at the latest. Within this range, we believe that the problem of mass must be resolved at some energy below about 1 TeV, by the discovery of a Higgs boson and/or supersymmetry. Measurements of gauge couplings give circumstantial support to supersymmetric grand unification at around 10^{16} GeV with sparticles appearing around 1 TeV. *However, we have little, if any, idea of the scale at which the flavour problem may be solved.* Perhaps only at the quantum-gravity scale $\sim 10^{19}$ GeV? perhaps at the GUT scale $\sim 10^{16}$ GeV? perhaps at some intermediate scale, as suggested by the seesaw model of neutrino masses? perhaps at the TeV scale? How far along the road will we solve flavour dynamics and the find the origin of CP violation?

4 Milestones in CP Violation

Our progress along this road can be measured by a plethora of milestones. Long after its discovery in the K^0 mass matrix via $K^0 \to \pi^+\pi^-$ decay, we have only recently passed two important ones:

- The measurement of direct CP violation in $K^0 \to 2\pi$ decay amplitudes [1], as long predicted in the KM model [2],

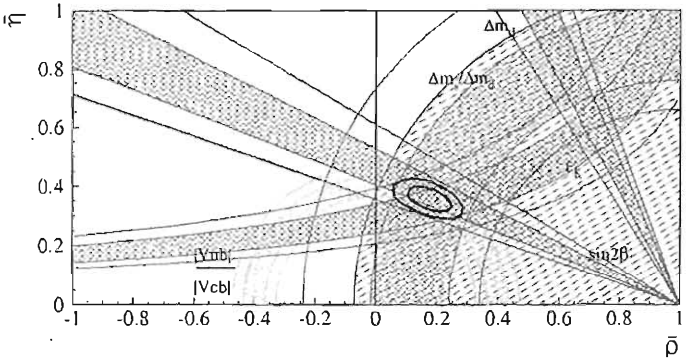

Figure 1: *A global fit to the unitarity triangle* [4], *demonstrating good agreement with the measurements of* $\sin 2\beta$ *by BaBar and Belle* [3].

• Observation of CP violation elsewhere, namely in $B^0 \to J/\psi K_s$ decay [3].

The latest NA48 and KTeV measurements of $\mathrm{Re}(\epsilon'/\epsilon)$ are now in relatively good agreement: $(14.7 \pm 2.2) \times 10^{-4}$ and $(20.7 \pm 2.8) \times 10^{-4}$, leading to the world average [1]:

$$\mathrm{Re}(\epsilon'/\epsilon) \;=\; (16.6 \pm 1.6 ... 2.3) \times 10^{-4}, \qquad (1)$$

where the first error is naive, and the second one is rescaled according to the Particle Data Group prescription. The value (1) is consistent with theoretical calculations, but these are not very accurate, because of delicate cancellations between different non-perturbative matrix elements. Measurements of $\sin 2\beta$ are already startlingly precise [3]:

$$\sin 2\beta \;=\; 0.741 \pm 0.067, \qquad (2)$$

and very consistent with KM expectations of mixing-induced CP violation, as seen in Fig. 1 [4]. However, the origin of the CP asymmetry in $B^0 \to J/\psi K_s$ decay is not yet confirmed, hence the importance of the next milestone, namely:

• The measurement of direct CP violation in $B^0 \to 2\pi$ decay amplitudes, predicted to be the angle $\alpha (= \phi_2)$ in the KM model.

As discussed later in more detail, the search for this effect [5] is currently the subject of some discussion [6]. Beyond it, many other CP-violating milestones beckon:

- CP violation in other K decays, such as $K_L^0 \to \pi^0 \bar{\nu}\nu$ decay,
- CP violation in other B decays, such as the measurement of the third unitarity angle γ,
- CP violation in D decays.

As we heard at this meeting, there is no hint of CP violation in $D^0 - \bar{D}^0$ mixing [7], which is expected only at a very low level in the SM, making it an excellent place to look for new physics beyond it. Other places to look for new sources of CP violation include

- The neutron electric dipole moment d_n,
- CP violation in neutrino oscillations via the MNS phase δ,
- T violation in lepton decays such as $\mu \to 3e$ and $\tau \to 3\ell$,
- The lepton electric dipole moments d_e, d_μ, d_τ.

Only after we pass some more of these milestones will we have a chance of pinning down the origin(s) of CP violation: is it due to the KM mechanism alone? or are there other contributions? perhaps due to θ_{QCD}? the MNS phase? supersymmetry? or ...?

5 The Next Steps along the CP Road

5.1 Quo Vadis $B^0 \to \pi^+\pi^-$?

As you know, this decay mode receives contributions from $b \to u\bar{u}d$ tree diagrams and $b \to s\bar{u}s$ penguin diagrams, which contain both a weak and a strong phase. The resulting CP-violating asymmetry contains two parts:

$$S_{\pi\pi} \sin(\Delta m_d \Delta t) \; + \; A_{\pi\pi} \cos(\Delta m_d \Delta t), \tag{3}$$

where the latter term is that due to direct CP violation. The values of $S_{\pi\pi}$ and $A_{\pi\pi}$ depend on the proportion of penguin pollution r (that may be constrained by other measurements such as $B^0 \to 2\pi^0$ and $B^+ \to K_s\pi^+$) and as well the angle α (or ϕ_2) that we seek to determine. As seen in Fig. 2 [6], the first measurements by BaBar and Belle [5] are not in good agreement, though the naive average suggests that $S_{\pi\pi} \sim -0.6, A_{\pi\pi} \sim 0.6$, which are consistent with ϕ_2 (or α) $\sim$ 110 degrees, as also seen in Fig. 2. Naive averaging may not be adequate, however, since the Belle measurement lies outside the physical boundary: $A_{\pi\pi}^2 + S_{\pi\pi}^2 = 1$, which should be taken into account in any fit.

There has recently been much progress in calculating exclusive B decay amplitudes using the QCD factorization framework [8], with error estimates

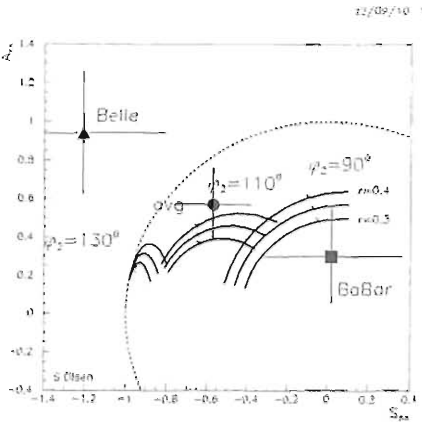

Figure 2: *The BaBar and Belle measurements of the asymmetry parameters* $S_{\pi\pi}, A_{\pi\pi}$ [5], *and their naive average, are compared with KM predictions for different values of* $\phi_2 = \alpha$, *the penguin pollution factor* r *and the strong-interaction phase. Also shown is the unitarity limit* $A_{\pi\pi}^2 + S_{\pi\pi}^2 = 1$ [6].

based on evaluations of power corrections and annihilation diagrams. This framework suggests $S_{\pi\pi} \sim -0.3$ to -0.9 [8], consistent with the naive average shown in Fig. 2. Thus there is reason to hope that $B^0 \to \pi^+\pi^-$ decay could become a valuable check on the KM model, as soon as the experimental situation settles down.

5.2 Quo Vadis $B \to \phi K_s$?

In the KM model, this decay is mediated by a strange gluonic penguin diagram: $b \to s + (g \to \bar{s}s)$, which has no intrinsic weak phase. Therefore, this decay should exhibit only mixing-induced CP violation, and should have the same asymmetry $\sin 2\beta$ as $B \to J/\psi K_s$. Other processes mediated by the same diagram include $B \to (\eta', K^+K^-)K_s$ [9], and first measurements of these decay asymmetries are consistent (within large errors) with that in $B \to J/\psi K_s$ and the KM model:

$$\eta' : \ 0.76 \pm 0.36; \ K^+K^- : \ 0.52 \pm 0.47, \tag{4}$$

whereas the decay asymmetry in $B \to \phi K_s$ looks rather different:

$$\phi: \ -0.39 \pm 0.41. \tag{5}$$

If this result holds up with more statistics, it would require new physics in the $b \to s + (g \to \bar{s}s)$ penguin diagram.

Several theoretical papers have appeared since the result (5) emerged, discussing models based on conventional R-conserving supersymmetry [10], R-violating supersymmetry [11], left-right symmetry [12] and a Z' model [13]. *Une affaire à suivre ....*

5.3 Quo Vadis $B \to D^{*+}D^{*-}$?

The dominant diagram contributing to this process is thought to be $b \to c + (W \to \bar{c}d)$, with the competing penguin diagram $b \to d + (g \to \bar{c}c)$ thought to be rather small: $|P/T| < 0.1$. A first measurement of the CP-violating asymmetry -Im(λ_+) that should conicide with $\sin 2\beta$ yields [14]:

$$-\mathrm{Im}(\lambda_+) \ = \ -0.31 \pm 0.43 \pm 0.1, \tag{6}$$

which deviates by about 2.7 σ, nominally. However, the experimentalists caution that, with the current low statistics, the errors are not Gaussian. *Une autre affaire à suivre ....*

5.4 Quo Vadis γ?

There are various isospin relations between $B \to \pi K$ amplitudes that can be used to provide information about γ: e.g., the relation between those for the charged $B^+ \to \pi^0 K^+, \pi^+ K^0$, the relation between those for the neutral $B^0 \to \pi^- K^+, \pi^0 K^0$, and the mixed relation between $B^0 \to \pi^- K^+$ and $B \to \pi^+ K^0$. The charged amplitudes may be parametrized by the two quantities [15]

$$R^c, A_0^c \ \equiv \ 2\frac{B(\pi^0 K^+) \pm B(\pi^0 K^-)}{B(\pi^+ K^0) + B(\pi^- \bar{K}^0)}, \tag{7}$$

which depend on the strong tree-to-penguin ratio $r_c(\sim 0.2?)$, the electroweak tree-to-penguin ratio $q(\sim 0.7?)$, and the difference δ_c between the tree- and penguin-diagram phases.

Fig. 3 shows the current status of measurements of R^c and A_0^c [15]. We see from the third panel that the data prefer $\gamma > 90$ degrees, whereas the global

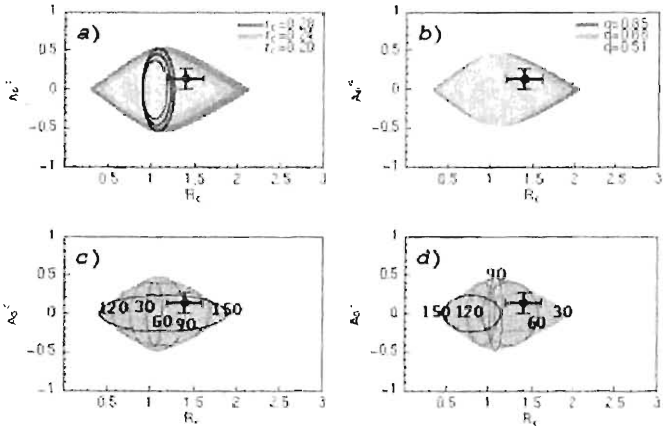

Figure 3: *Allowed regions in the R_c-A_0^c plane for charged $B \to \pi K$ decays, showing the effects of varying (a) the strong penguin pollution factor r_c, (b) the electroweak penguin pollution factor q, (c) the KM phase γ and (d) the phase difference δ_c* [15].

KM fit shown in Fig. 1 prefers $\gamma < 90$ degrees. Again, it remains to see whether this possible discrepancy is confirmed by more data on the same decay modes, and/or on other decays such as $B^- \to D^0 K^-$, $B^0 \to D^{(*)\pm}\pi^\pm$, etc.

5.5 The Road Ahead for B Factories?

Measurements of β at B factories are likely to attain an accuracy of ± 1 degree, those of α may reach ± 5 degrees, and those of γ may reach ± 25 degrees, which would correspond to a check of the unitarity triangle at the 15 % level. It would clearly be desirable to push the experimental statistical errors down until they match the theoretical systematic errors. This provides worthwhile objectives for the subsequent generation of LHCb, BTeV and super-B factory experiments.

6 The B_s Road to CP Violation

There are just three neutral-meson systems where one can reasonably expect to see mixing and CP-violating effects in the SM and its plausible extensions:

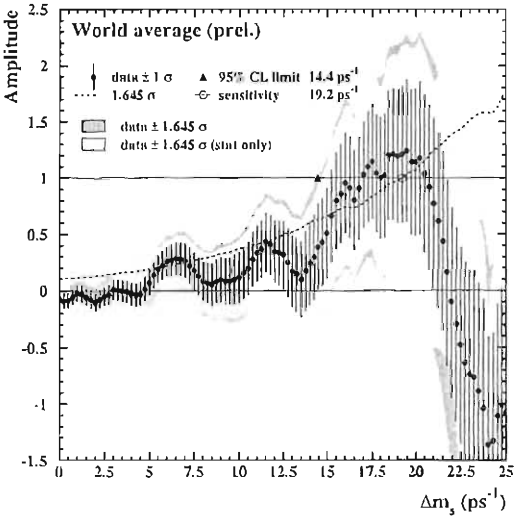

Figure 4: *Combined LEP/SLD/CDF results for Δm_s. The data are shown as points with error bars, the lines show the 95% C.L. curves, and the dotted curve shows the expected sensitivity* [16].

the $K^0 - \bar{K}^0$ system that has been explored for many decades, the $B^0 - \bar{B}^0$ system that is now being explored at B factories, and the the $B_s^0 - \bar{B}_s^0$ system. If we really do understand the SM and CP violation as well as we think, we can make many reliable predictions for the $B_s^0 - \bar{B}_s^0$ system. Conversely, this may be a valuable laboratory for testing the SM, since any deviation from these confident predictions would be good evidence for physics beyond the SM. Among these predictions, one may list [15]:

- A large mixing parameter $x_s \equiv \Delta m_s/\Gamma_s = \mathcal{O}(20)$ - this prediction may be on the verge of being confirmed, as the compilation of present experiments on $B_s^0 - \bar{B}_s^0$ mixing shown in Fig. 4 shows quite a hint of mixing with approximately the predicted value of x_s [16];
- The $B_s^0 - \bar{B}_s^0$ mixing phase should be very small: $\phi_s = \mathrm{Arg}(V_{ts}^* V_{tb}) \sim -2$ degrees;
- There may be a sizeable difference in the total decay widths of the mass

eigenstates of the $B_s^0 - \bar{B}_s^0$ system: $\Delta\Gamma_s/\Gamma_s \sim 10$ %.
Among the interesting B_s^0 decay modes, let us mention $B_s^0 \to J/\psi\phi$, whose CP-violating asymmetry should be

$$A_{CP} \simeq \sin(\Delta m_s t) \sin\phi_s, \tag{8}$$

and hence very small in the SM. This makes it a good place for new contributions to $B_s^0 - \bar{B}_s^0$ mixing, as might occur in supersymmetry, for example. Another interesting decay mode is $B_s^0 \to D_s^{\pm} K^{\mp}$, whose CP-violating asymmetry should be proportional to $\phi_s + \gamma$, and hence could (within the SM) be a good way to measure γ.

There are currently no plans to try to accumulate large samples of B_s^0 mesons at the operating B factories, so B_s^0 physics may be left as the hunting preserve of the hadronic experiments LHCb [17] and BTeV [18].

7 The Supersymmetric Flavour and CP Problems

In the supersymmetric limit, flavour mixing in the MSSM is identical to that in the SM, but supersymmetry must be broken. It is commonly thought that this occurs via gaugino masses M_a, scalar mass-squared parameters $(m_0^2)_j^i$ and trilinear couplings A_{ijk}. The gaugino mass parameters might have CP-violating phases that could show up in electric dipole moments and/or the Higgs sector, as discussed later. The big questions concerning $(m_0^2)_j^i$ and A_{ijk} are whether they are universal, or at least can be diagonalized in the same basis as the quark and lepton flavours, and whether they contain extra CP-violating phases. Is the super-CKM mixing of squarks the same as the KM mixing of quarks? If not, how does it differ, and why?

Three generic classes of options can be distinguished [19]:

- Minimal flavour violation, in which the $(m_0^2)_j^i$ and A_{ijk} *are* universal at the GUT scale, being renormalized at lower energies by the Yukawa couplings λ_{ijk}, and resulting in a super-CKM mixing pattern that is related to, and derivable from, the conventional CKM mixing;
- Extra supersymmetric loop effects, that may in general be parameterized as quark mass insertions $(\delta_{ij}^{d,u})_{LL,RR}$ [10];
- Extra tree-level effects, as could arise from generic R-violating interactions.

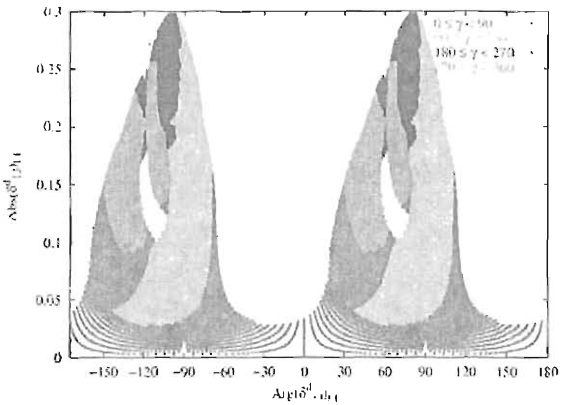

Figure 5: *Phenomenological bounds on the magnitude and phase of the insertion* $(\delta^d_{13})_{LL}$ [10].

Quite frankly, fundamental theory provides no clear guidance which option Nature might have chosen. On the other hand, the observed suppressions of flavour-changing neutral interactions put severe constraints on R-violating models, which will not be discussed further here. These constraints certainly favour models with minimal flavour violation, although the best one can do phenomenologically, in a model-independent way, is to set upper bounds on the insertions $(\delta^{d,u}_{ij})_{LL,RR}$, as exemplified in Fig. 5 [10].

If supersymmetric flavour violation is indeed minimal, one expects the squarks to be approximately degenerate, apart from the $\tilde{t}$ and possibly the $\tilde{b}$. These loopholes open up interesting opportunities in B physics. For example, there could be significant supersymmetric contributions to the mass differences Δm_d and Δm_s, though not to the ratio $\Delta m_d/\Delta m_s$. These would generate knock-on effects in the global unitarity triangle fits and B_s physics. Rare B decays already provide interesting upper limits on supersymmetric flavour violation and opportunities for the future, as we discuss next.

8 Rare B Decays

This is a very rich area [20], and just a few examples are given here.

- $b \to s\gamma$ decay: This process may receive significant contributions from

the exchanges of charged Higgs bosons $H^\pm$ and chargino spartners of the $W^\pm$ and $H^\pm$ [21], and the fact the observed decay rate agrees within errors with the SM provides important constraints on the MSSM parameters, as seen in Fig. 6 [22]. In time, one could hope to measure a CP-violating asymmetry in

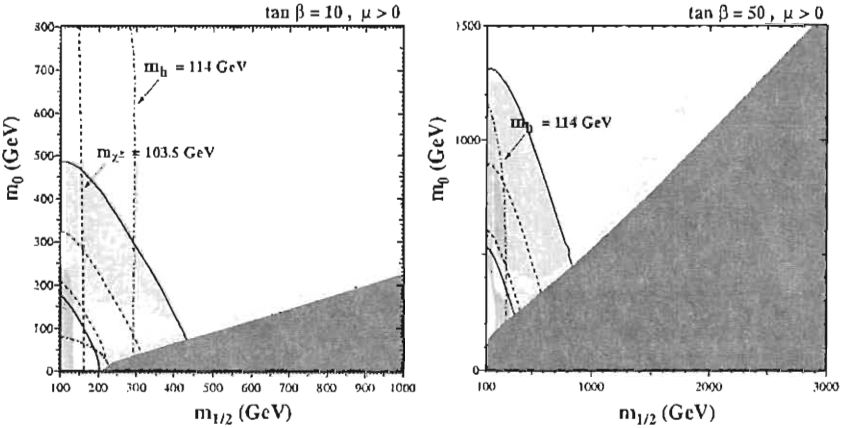

Figure 6: *Compilations of phenomenological constraints on supersymmetry for (a)* $\tan\beta = 10, \mu > 0$, *(b)* $\tan\beta = 50, \mu > 0$ [22]. *The near-vertical lines are the LEP limits* $m_{\chi^\pm} = 103.5$ *GeV (dashed and black), shown in (a) only, and* $m_h = 114$ *GeV (dotted and red). Also, in the lower left corner of (a), we show the* $m_{\tilde{e}} = 99$ *GeV contour. In the dark (brick red) shaded regions, the LSP is the charged* $\tilde{\tau}_1$, *so this region is excluded. The light (turquoise) shaded areas are the cosmologically preferred regions with* $0.1 \leq \Omega h^2 \leq 0.3$. *The shaded (pink) regions are the* $\pm 2\sigma$ *ranges of* $g_\mu - 2$.

$b \to s\gamma$ decays, and verify whether $\sin 2\beta$ measured at the loop level coincides with the value measured in the $J/\psi K_s$ decay mode.

• $b \to s\ell^+\ell^-$ decay: The case where the s quark yields a K meson has been observed, but not where it yields an excited state K^*. There could in principle be supersymmetric effects on the total decay rate, on the $\ell^+\ell^-$ mass spectrum, as seen in Fig. 7(a), and on the forward-backward asymmetry A_{FB}, as seen in Fig 7(b) [23]. Again, the question whether $\sin 2\beta$(loop) concides with $\sin 2\beta(J/\psi K_s)$ can be posed.

• $b \to s\bar{\nu}\nu$ decay: This process can also be calculated reliably in the SM,

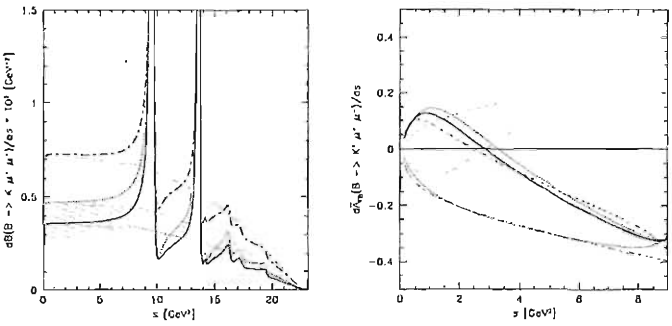

Figure 7: *Possible supersymmetric effects on (a) the invariant-mass distribution in $B \to K\mu^+\mu^-$ decay and (b) the forward-backward asymmetry in $B \to K^*\mu^+\mu^-$ decay* [23].

and observation of $B \to X_s+$ nothing would be interesting for constraining extensions of the SM.

- $B \to \mu^+\mu^-$ decay: This can receive important supersymmetric corrections [24], in particular for larger values of $\tan\beta$.
- $B \to \tau^+\tau^-$ decay: This offers some prospects for studying CP violation in the MSSM [25].
- $B \to \tau^\pm\mu^\mp, e^\pm e^\mp$ and $\mu^\pm e^\mp$ decays: These could in principle provide interesting windows on flavour violation in the lepton sector [26], which is the subject of the next section.

It may be interesting to note some of the statistics that may be provided by present and forthcoming experiments. For $B \to K^*\gamma$, we may expect 6,000 events at the B factories, 25,000 at LHCb or BTeV, and 120,000 at a super-B factory. The corresponding numbers for $B \to X_s\mu^+\mu^-$ are 120, 4,500 and 6,000, respectively, whilst for $B \to X_s\bar{\nu}\nu$ they are 8, 0 and 160, respectively. There is ample justification for another generation of B experiments even beyond LHCb and BTeV.

9 Neutrino Flavour Violation

There is no good reason why either the total lepton number L or the individual lepton flavours $L_{e,\mu,\tau}$ should be conserved. We have learnt that the only

conserved quantum numbers are those associated with exact gauge symmetries, just as the conservation of electromagnetic charge is associated with $U(1)$ gauge invariance. On the other hand, there is no exact gauge symmetry associated with any of the lepton numbers.

Moreover, neutrinos have been seen to oscillate between their different flavours [27, 28], showing that the separate lepton flavours $L_{e,\mu,\tau}$ are indeed not conserved, though the conservation of total lepton number L is still an open question. The observation of such oscillations strongly suggests that the neutrinos have different masses. Again, massless particles are generally associated with exact gauge symmetries, e.g., the photon with the $U(1)$ symmetry of the Standard Model, and the gluons with its $SU(3)$ symmetry. In the absence of any leptonic gauge symmetry, non-zero lepton masses are to be expected, in general.

The conservation of lepton number is an accidental symmetry of the renormalizable terms in the Standard Model lagrangian. However, one could easily add to the Standard Model non-renormalizable terms that would generate neutrino masses, even without introducing a 'right-handed' neutrino field. For example, a non-renormalizable term of the form [29]

$$\frac{1}{M}\nu H \cdot \nu H, \tag{9}$$

where M is some large mass beyond the scale of the Standard Model, would generate a neutrino mass term:

$$m_\nu \nu \cdot \nu : \; m_\nu \; = \; \frac{\langle 0|H|0\rangle^2}{M}. \tag{10}$$

Of course, a non-renormalizable interaction such as (9) seems unlikely to be fundamental, and one should like to understand the origin of the large mass scale M.

The minimal renormalizable model of neutrino masses requires the introduction of weak-singlet 'right-handed' neutrinos N. These will in general couple to the conventional weak-doublet left-handed neutrinos via Yukawa couplings Y_ν that yield Dirac masses $m_D \sim m_W$. In addition, these 'right-handed' neutrinos N can couple to themselves via Majorana masses M that may be $\gg m_W$, since they do not require electroweak summetry breaking. Combining

the two types of mass term, one obtains the seesaw mass matrix [30]:

$$(\nu_L, N) \begin{pmatrix} 0 & M_D \\ M_D^T & M \end{pmatrix} \begin{pmatrix} \nu_L \\ N \end{pmatrix}, \tag{11}$$

where each of the entries should be understood as a matrix in generation space.

This seesaw model can accommodate the neutrino mixing seen experimentally, and naturally explains the small differences in the masses-squared of the light neutrinos. By itself, it would lead to unobservably small transitions between the different charged-lepton flavours. However, supersymmetry may enhance greatly the rates for processes violating the different charged-lepton flavours, rendering them potentially observable, as we discuss below.

The effective mass matrix for light neutrinos in the seesaw model may be written as:

$$\mathcal{M}_\nu \;=\; Y_\nu^T \frac{1}{M} Y_\nu v^2 \left[\sin^2\beta\right] \tag{12}$$

where we have used the relation $m_D = Y_\nu v[\sin\beta]$ with $v \equiv \langle 0|H|0\rangle$, and the factors of $\sin\beta$ appear in the supersymmetric version of the seesaw model. Diagonalizing the neutrino mass matrix (12) and the charged-lepton masses introduces in general a mismatch between the mass and flavour eigenstates [31]:

$$V_{MNS} \;\equiv\; V_\ell V_\nu^\dagger, \tag{13}$$

which is reminiscent of the way the CKM matrix appears in the quark sector [2]:

$$V_{CKM} \;\equiv\; V_d V_u^\dagger, \tag{14}$$

though the difference in the ways the quark and neutrino masses (11) arise may give us some hope that the patterns of neutrino and quark mixing, V_{MNS} and V_{CKM}, could be somewhat different.

The MNS matrix describing neutrino oscillations can be written in the form

$$V \;=\; \begin{pmatrix} c_{12} & s_{12} & 0 \\ -s_{12} & c_{12} & 0 \\ 0 & 0 & 1 \end{pmatrix} \begin{pmatrix} 1 & 0 & 0 \\ 0 & c_{23} & s_{23} \\ 0 & -s_{23} & c_{23} \end{pmatrix} \begin{pmatrix} c_{13} & 0 & s_{13} \\ 0 & 1 & 0 \\ -s_{13}e^{-i\delta} & 0 & c_{13}e^{-i\delta} \end{pmatrix}, \tag{15}$$

and there are in addition two CP-violating phases that are not observable in neutrino oscillations, but appear in neutrinoless double-β decay.

The first matrix factor in (15) is measurable in solar neutrino experiments, and the recent data from SNO [28] and Super-Kamiokande [32] prefer quite

strongly the large-mixing-angle (LMA) solution to the solar neutrino problem with $\Delta m^2_{12} \sim 6 \times 10^{-5}$ eV^2 and large but non-maximal mixing: $\theta_{12} \sim 30^o$. The validity or otherwise of the LMA solution is expected to be settled quite soon by the KamLAND experiment. The second matrix factor in (15) is measurable in atmospheric neutrino experiments, and the data from Super-Kamiokande in particular [27] favour maximal mixing of atmospheric neutrinos: $\theta_{23} \sim 45^o$ and $\Delta m^2_{23} \sim 2.5 \times 10^{-3}$ eV^2. However, the third matrix factor in (15) is basically unknown, with experiments such as Chooz [33] and Super-Kamiokande only establishing upper limits on θ_{13}, and *a fortiori* providing no information on the CP-violating phase δ.

The phase δ could in principle be measured by comparing the oscillation probabilities for neutrinos and antineutrinos as seen in Fig. 8 [34]. This is possible only if Δm^2_{12} and s_{12} are large enough - as now suggested by the success of the LMA solution to the solar neutrino problem, and if s_{13} is large enough - which remains an open question.

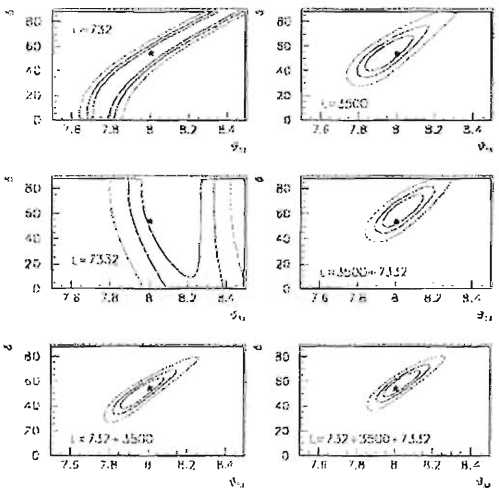

Figure 8: *A simultaneous fit to θ_{13} and δ, using a neutrino-factory beam with different baselines and detector techniques* [34], *may enable the CP-violating phase δ to be extracted.*

The effective low-energy mass matrix for the light neutrinos contains 9 parameters, 3 mass eigenvalues, 3 real mixing angles and 3 CP-violating phases.

However, these are not all the parameters in the minimal seesaw model. In fact, this model has a total of 18 parameters [35, 36]. The remaining 9 associated with the heavy-neutrino sector may be measurable via their renormalization effects on soft supersymmetry-breaking parameters, as we discuss below. The total number of CP-violating parameters is 6, including the MNS phase δ, the two Majorana phases relevant to neutrinoless double-β decay, and three extra phases that play a key rôle in leptogenesis, as we discuss later.

10 Flavour and CP Violation for Charged Leptons

Assuming that the soft supersymmetry-breaking parameters put it at the GUT scale are universal, and working in the leading-logarithmic approximation with degenerate heavy singlet neutrinos, one finds the following radiative corrections to the soft supersymmetry-breaking terms for sleptons:

$$\begin{aligned} \left(\delta m_{\tilde{L}}^2\right)_{ij} &= -\frac{1}{8\pi^2}\left(3m_0^2 + A_0^2\right)\left(Y_\nu^\dagger Y_\nu\right)_{ij} \mathrm{Ln}\left(\frac{M_{GUT}}{M}\right), \\ \left(\delta A_l\right)_{ij} &= -\frac{1}{8\pi^2} A_0 Y_{\ell_i}\left(Y_\nu^\dagger Y_\nu\right)_{ij} \mathrm{Ln}\left(\frac{M_{GUT}}{M}\right). \end{aligned} \tag{16}$$

The non-universality of the corrections (16) leads to processes that violate the different charged lepton numbers, such as $\mu \to e\gamma, \tau \to \mu\gamma, \tau \to e\gamma, \mu N \to eN, \mu \to 3e, \tau \to 3e, e2\mu, \mu 2e$ and 3 μ [36, 37]. Fig. 9(a) shows that the branching ratio for $\mu \to e\gamma$ could be close to the present experimental upper limit, and Figs. 9(b) and (c) makes the same point for the decays $\tau \to \mu\gamma$ and $\tau \to e\gamma$, respectively [38].

The electric dipole moments of the electron and muon depend sensitively on the non-degeneracy of the heavy singlet neutrinos [37, 38]. As seen in Fig. 10, they could take values as large as $d_e \sim 3 \times 10^{-30}$ e.cm and $d_\mu \sim 10^{-27}$ e.cm, to be compared with the present experimental upper limits of $d_e < 1.6 \times 10^{-27}$ e.cm [39] and $d_\mu < 10^{-18}$ e.cm [40]. An ongoing series of experiments might be able to reach $d_e \sim 3 \times 10^{-30}$ e.cm, and a type of solid-state experiment that might be sensitive to $d_e \sim 10^{-33}$ e.cm has been proposed [41]. Also, $d_\mu \sim 10^{-24}$ e.cm might be accessible with the PRISM experiment proposed for the JHF [42], and $d_\mu \sim 5 \times 10^{-26}$ e.cm might be attainable at the front end of a neutrino factory [43].

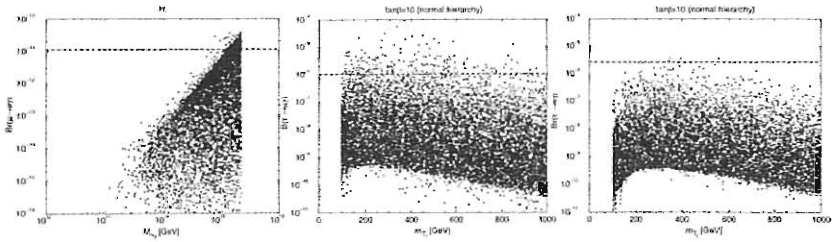

Figure 9: *Scatter plots of the branching ratios for (a) $\mu \to e\gamma$, (b) $\tau \to \mu\gamma$ and (c) $\tau \to e\gamma$ in variants of the supersymmetric seesaw model, for various values of its unknown parameters* [38].

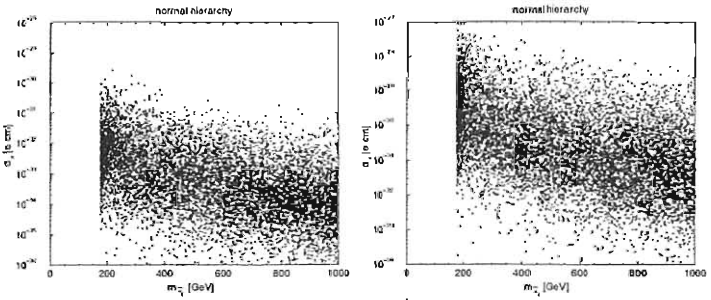

Figure 10: *Scatter plots of (a) d_e and (b) d_μ in variants of the supersymmetric seesaw model, for different values of the unknown parameters* [38].

11 Leptogenesis

One of the favoured scenarios for baryogenesis is first to generate a lepton asymmetry via CP-violating decays of heavy singlet neutrinos, which is then recycled into a baryon asymmetry via non-perturbative electroweak interactions [44]. The CP asymmetry in this leptogenesis scenario is related to the product $Y_\nu Y_\nu^\dagger$. The total decay rate of a heavy neutrino N_i may be written in the form

$$\Gamma_i \;=\; \frac{1}{8\pi}\left(Y_\nu Y_\nu^\dagger\right)_{ii} M_i, \tag{17}$$

and one-loop CP-violating diagrams involving the exchange of heavy neutrino N_j would generate an asymmetry in N_i decay of the form:

$$\epsilon_{ij} = \frac{1}{8\pi} \frac{1}{\left(Y_\nu Y_\nu^\dagger\right)_{ii}} \mathrm{Im}\left(\left(Y_\nu Y_\nu^\dagger\right)_{ij}\right)^2 f\left(\frac{M_j}{M_i}\right), \tag{18}$$

where $f(M_j/M_i)$ is a known kinematic function.

The relevant combination $Y_\nu Y_\nu^\dagger$ is independent of V_{MNS} and hence of the light neutrino mixing angles and CP-violating phases. The basic reason for this is that one makes a unitary sum over all the light lepton species in evaluating the decay asymmetry ϵ_{ij} (18). Fig. 11 shows explicitly that one can generate a lepton asymmetry even if the MNS phase δ vanishes.

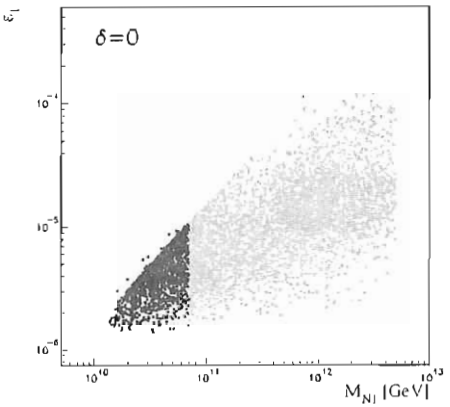

Figure 11: *Heavy singlet neutrino decay may exhibit a CP-violating asymmetry, leading to leptogenesis and hence baryogenesis, even if the neutrino oscillation phase δ vanishes* [45].

In general, one may formulate the following strategy for calculating leptogenesis in terms of laboratory observables:

- Measure the neutrino oscillation phase δ and the Majorana phases,
- Measure observables related to the renormalization of soft supersymmetry-breaking parameters, that are functions of δ, the Majorana and leptogenesis

phases,

• Extract the effects of the known values of δ and the Majorana phases, and thereby isolate the leptogenesis parameters.

12 CP Violation in the MSSM Higgs Sector

A popular alternative scenario for baryogenesis has been to generate a quark asymmetry at the electroweak scale [46]. This requires a breakdown of thermal equilibrium, necessitating a first-order electroweak phase transition. This is impossible in the SM, since LEP tells us that the Higgs boson weighs more than 114.4 GeV, whereas a first-torder electroweak phase transition is possible only if $m_H < 70$ GeV [47]. Generating a first-order phase transition would require extra light scalar bosons, as could be provided in supersymmetry, if the lighter $\tilde{t}$ is very light. This scenario would also require more CP violation than is present in the SM.

Indeed, two extra CP-violating phases appear in the MSSM, even if the soft supersymmetry-breaking parameters are universal at the input GUT scale, as assumed here. These can be taken as the (supposedly common) phases of the trilinear soft supersymmetry-breaking parameters $\mathrm{Arg}(A_{t,b})$ and the phase of the gluino mass $\mathrm{Arg}(m_{\tilde{g}})$. These generate mixing between the 'scalar'and 'pseudoscalar' MSSM Higgs bosons: at the one-loop level

$$\delta m^2_{SP} \sim \frac{m_t^4}{v^2} \frac{\mu \mathrm{Im} A_t}{32\pi^2 m^2_{susy}} + \cdots, \tag{19}$$

and a dependence on $\mathrm{Arg}(m_{\tilde{g}})$ appears at the two-loop level.

In the presence of CP violation, it is convenient to parametrize the MSSM Higgs sector in terms of m_{H^+} and $\tan\beta$. As seen in Fig. 12 [48], there may be level crossing between the two lightest neutral Higgs bosons, and the lightest Higgs H_1 may have a suppressed coupling in the process $e^+e^- \to Z + H_1$. In this case, it could be that there exists a light Higgs boson lurking below the lower limit established by LEP in the SM. The prospects that experiments at hadron colliders may be able to plug this hole are discussed in [49].

The phenomenology of CP-violating Higgs bosons is very rich, and only its surface has been scratched. A $\mu^+\mu^-$ collider - either at the energy of the lightest Higgs boson, or close to the nearby masses of the second and third neutral Higgs bosons - may be necessary one day to unravel this physics [50].

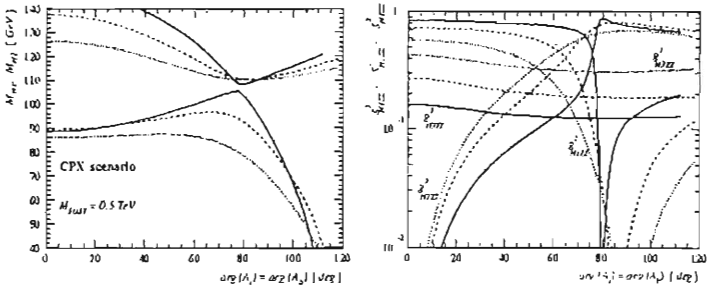

Figure 12: *In the MSSM with maximal CP violation in the Higgs sector, (a) there may be level-crossing between the lightest and second-lightest Higgs bosons, and (b) the lightest Higgs boson may have a small coupling in the process* $e^+e^- \to Z + H$ [48].

13 Some Answers

At a round-table discussion earlier this week, some central questions were raised, to which I would like to provide some personal answers.

- *Q: What is the rôle of flavour studies in providing clues about new physics?*
  A: They may cast light on the darkest corners of supersymmetry, namely its flavour and CP problems.

- *Q: What are the implications of CP studies for our understanding of baryogenesis?*
  A: Standard Model CP violation is inadequate for the task, but CP violation in either the lepton or Higgs sector could do the job. Both may be tested in future experiments.

- *Q: What are the implications of lepton mixing for unification and phenomenology?*
  A: It provides a direct window on physics at the GUT scale, and could open up a whole new arena for experiments on decays that violate the charged lepton flavours, such as $\mu \to e\gamma, \tau \to \mu\gamma, \tau \to e\gamma$ and many more.

Flavour physics and CP violation surely have a long and glorious future!

References

1. J. R. Batley *et al.* [NA48 Collaboration], Phys. Lett. B **544**, 97 (2002) [arXiv:hep-ex/0208009]; A. Alavi-Harati *et al.* [KTeV Collaboration], arXiv:hep-ex/0208007.
2. J. R. Ellis, M. K. Gaillard and D. V. Nanopoulos, Nucl. Phys. B **109**, 213 (1976).
3. K. Abe *et al.* [Belle Collaboration], Phys. Rev. D **66**, 071102 (2002) [arXiv:hep-ex/0208025]; B. Aubert *et al.* [BABAR Collaboration], arXiv:hep-ex/0207042.
4. A. Stocchi, arXiv:hep-ph/0211245.
5. K. Abe *et al.* [Belle Collaboration], Phys. Rev. Lett. **89** (2002) 071801; B. Aubert *et al.* [BABAR Collaboration], arXiv:hep-ex/0207055.
6. T. E. Browder, arXiv:hep-ex/0210012.
7. U. Egede [BABAR Collaboration], arXiv:hep-ex/0210060; A. Petrov, R. Ray, talks at this meeting, obtainable from `http://frontierscience.lnf.infn.it/2002/IWFS.html`.
8. M. Beneke, G. Buchalla, M. Neubert and C. T. Sachrajda, Nucl. Phys. B **606**, 245 (2001) [arXiv:hep-ph/0104110].
9. M. D. Sokoloff, talk at this meeting, available from `http://frontierscience.lnf.infn.it/2002/IWFS.html`.
10. L. Silvestrini, arXiv:hep-ph/0210031; and references therein.
11. A. Datta, Phys. Rev. D **66**, 071702 (2002) [arXiv:hep-ph/0208016]; B. Dutta, C. S. Kim and S. Oh, arXiv:hep-ph/0208226.
12. M. Raidal, arXiv:hep-ph/0208091.
13. G. Hiller, Phys. Rev. D **66**, 071502 (2002) [arXiv:hep-ph/0207356].
14. B. Aubert *et al.* [BABAR Collaboration], arXiv:hep-ex/0207072.
15. R. Fleischer, arXiv:hep-ph/0210323; and references therein.

16. Working group on B oscillations, http://lepbosc.web.cern.ch/LEPBOSC/.

17. N. Harnew, talk at this meeting, available from http://frontierscience.lnf.infn.it/2002/IWFS.html; The home page of this experiment is: http://lhcb.web.cern.ch/lhcb/.

18. D. Christian, talk at this meeting, available from http://frontierscience.lnf.infn.it/2002/IWFS.html.

19. A. Masiero and O. Vives, New J. Phys. 4 (2002) 4; and references therein.

20. A. Ali, arXiv:hep-ph/0201120.

21. C. Degrassi, P. Gambino and G. F. Giudice, JHEP **0012** (2000) 009 [arXiv:hep-ph/0009337]; M. Carena, D. Garcia, U. Nierste and C. E. Wagner, Phys. Lett. B **499** (2001) 141 [arXiv:hep-ph/0010003]; D. A. Demir and K. A. Olive, Phys. Rev. D **65** (2002) 034007 [arXiv:hep-ph/0107329].

22. J. Ellis, T. Falk, K. A. Olive and Y. Santoso, arXiv:hep-ph/0210205; and references therein.

23. A. Ali, P. Ball, L. T. Handoko and G. Hiller, Phys. Rev. D **61**, 074024 (2000) [arXiv:hep-ph/9910221].

24. A. Dedes, H. K. Dreiner and U. Nierste, Phys. Rev. Lett. **87**, 251804 (2001) [arXiv:hep-ph/0108037].

25. A. Dedes and A. Pilaftsis, arXiv:hep-pb/0209306.

26. A. Dedes, J. R. Ellis and M. Raidal, arXiv:hep-ph/0209207.

27. Y. Fukuda *et al.* [Super-Kamiokande Collaboration], Phys. Rev. Lett. **81**, 1562 (1998) [arXiv:hep-ex/9807003].

28. Q. R. Ahmad *et al.* [SNO Collaboration], Phys. Rev. Lett. **89**, 011301 (2002) [arXiv:nucl-ex/0204008]; Phys. Rev. Lett. **89**, 011302 (2002) [arXiv:nucl-ex/0204009].

29. R. Barbieri, J. R. Ellis and M. K. Gaillard, Phys. Lett. B **90**, 249 (1980).

30. M. Gell-Mann, P. Ramond and R. Slansky, Proceedings of the Supergravity Stony Brook Workshop, New York, 1979, eds. P. Van Nieuwenhuizen and D. Freedman (North-Holland, Amsterdam); T. Yanagida, Proceedings of the Workshop on Unified Theories and Baryon Number in the Universe, Tsukuba, Japan 1979 (edited by A. Sawada and A. Sugamoto, KEK Report No. 79-18, Tsukuba); R. Mohapatra and G. Senjanovic, Phys. Rev. Lett. **44** (1980) 912.

31. Z. Maki, M. Nakagawa and S. Sakata, Prog. Theor. Phys. **28**, 870 (1962).

32. S. Fukuda *et al.* [Super-Kamiokande Collaboration], Phys. Lett. B **539**, 179 (2002) [arXiv:hep-ex/0205075].

33. M. Apollonio *et al.* [CHOOZ Collaboration], Phys. Lett. B **466**, 415 (1999) [arXiv:hep-ex/9907037].

34. A. Cervera, A. Donini, M. B. Gavela, J. J. Gomez Cadenas, P. Hernandez, O. Mena and S. Rigolin, Nucl. Phys. B **579**, 17 (2000) [Erratum-ibid. B **593**, 731 (2001)] [arXiv:hep-ph/0002108].

35. J. A. Casas and A. Ibarra, Nucl. Phys. B **618**, 171 (2001) [arXiv:hep-ph/0103065].

36. J. R. Ellis, J. Hisano, S. Lola and M. Raidal, Nucl. Phys. B **621**, 208 (2002) [arXiv:hep-ph/0109125].

37. J. R. Ellis, J. Hisano, M. Raidal and Y. Shimizu, Phys. Lett. B **528**, 86 (2002) [arXiv:hep-ph/0111324].

38. J. R. Ellis, J. Hisano, M. Raidal and Y. Shimizu, arXiv:hep-ph/0206110.

39. B. C. Regan, E. D. Commins, C. J. Schmidt and D. DeMille, Phys. Rev. Lett. **88** (2002) 071805; B. E. Sauer, talk at this meeting, availablde from `http://frontierscience.lnf.infn.it/2002/IWFS.html`.

40. H. N. Brown *et al.* [Muon g-2 Collaboration], Phys. Rev. Lett. **86**, 2227 (2001) [arXiv:hep-ex/0102017].

41. S. K. Lamoreaux, arXiv:nucl-ex/0109014.

42. M. Furusaka *et al.*, JAERI/KEK Joint Project Proposal *The Joint Project for High-Intensity Proton Accelerators*, KEK-REPORT-99-4, JAERI-TECH-99-056.

43. J. Äystö *et al.*, *Physics with Low-Energy Muons at a Neutrino Factory Complex*, CERN-TH/2001-231, hep-ph/0109217; and references therein.

44. M. Fukugita and T. Yanagida, Phys. Lett. B **174**, 45 (1986).

45. J. R. Ellis and M. Raidal, Nucl. Phys. B **643**, 229 (2002) [arXiv:hep-ph/0206174].

46. See, for example: G. R. Farrar and M. E. Shaposhnikov, Phys. Rev. D **50**, 774 (1994) [arXiv:hep-ph/9305275].

47. M. Laine, arXiv:hep-ph/0010275.

48. M. Carena, J. R. Ellis, A. Pilaftsis and C. E. Wagner, Phys. Lett. B **495**, 155 (2000) [arXiv:hep-ph/0009212].

49. M. Carena, J. R. Ellis, S. Mrenna, A. Pilaftsis and C. E. Wagner, CERN-TH/2002-299, in preparation.

50. C. Blochinger *et al.*, arXiv:hep-ph/0202199; and references therein.

Short Communications in Plenary Session

Chairpersons: R. de Sangro, P. de Simone, M. Beriani

A. Berezhnoy	The Photonic Production of Charmed Meson Pairs
L.A. Tikhonova	Preliminary Results on Charm Production Near Threshold in pA–Interactions at 70 GeV
N. Fabiano	Two Photon Width of Heavy Pseudoscalar Mesons
M.M. Obertino	Study of the Charmonium ^3P_J States in $\bar{p}$ p Annihilations at FNAL
J. Yarba	The BTeV Electromagnetic Calorimeter Requirements for High Quality Reconstruction of Neutral Particles
V. Tayursky	The higher Precision measurement of J/Psi and Psi(2S) masses at VEPP_4M with the KEDR Detector
J. Sjölin	A Study of the LHC Experimental Sensitivity to CP Violating $gt\bar{t}$ Couplings
M. Rovere	Recent Charm Meson Branching Ratio and Lifetime Measurements from FOCUS Experiment
I. Segoni	Charmes Baryond Lifetime in FOCUS
G. Zhu	Global Analysis of B → PP, PV Decays with QCD Facorization
M. Hohlfeld	Prospect of Higgs Physics in Run 2 at the Fermilab Tevatron Collider
T. Christiansen	Searches for Leptoquarks with the DØ Detector at the Tevatron
R. Lefèvre	LHCb Level 0 Trigger
O. Shekhovtsova	Corrections to the ISR Radiative Function
K. Cho	National HEP Data Grid Projet in Korea

Frascati Physics Series Vol. XXXI (2003), pp. 409–411
FRONTIERSCIENCE 2002 – Frascati, October 6–11, 2002
Short Communication in Plenary Session

THE PHOTONIC PRODUCTION OF THE CHARMED MESON PAIRS

A.V. Berezhnoy *
Skobeltsin Institute for Nuclear Physics
of Moscow State University,
Moscow, Russia

ABSTRACT

In the framework of the constituent quark model the pair production of the charmed meson in the photonic interaction is calculated. The results are compared with the effective heavy quark theory predictions. It is shown that the light valence quark of the D-meson plays the essential role in the c-quark hadronization, as well as in the c-quark production. Moreover the light valence quark interaction with the initial photonic field is shown to be strong even for $m_Q \to \infty$. That is why the effective heavy quark theory can not be applied under the photonic interaction.

1 Charmed meson pair production in the e^+e^--annihilation

The two assumptions:

* coauthors A.K. Likhoded, V.V. Kiselev, *Institute for High Energy Physic, Protvino, Russia*

1. the interaction between the light constituent quark and photonic field can be neglected

2. the spin-spin interaction between heavy and light quark is negligible

allow to obtain the following ratio for the pair production near threshold in the e^+e^--annihilation [1]:

$$\sigma_{D\bar{D}} : \sigma_{D\bar{D}^*+\bar{D}D^*} : \sigma_{D^*\bar{D}^*} = 1 : 4 : 7. \quad (1)$$

The more detail analysis of the charmed meson pair production in the e^+e^--annihilation shows [2]:

- for the reasonable quark mass values the assumption 1 is valid;
- the assumption 2 is wrong and becomes valid only for $m_Q \to \infty$.

That is why the ratio (1) for $m_c = 1.8$ and $m_q = 0.2$ violates as follows:

$$\sigma_{D\bar{D}} : \sigma_{D\bar{D}^*+\bar{D}D^*} : \sigma_{D^*\bar{D}^*} \approx 1 : 8 : 14. \quad (2)$$

2 The photonic charmed meson pair production

The assumptions 1 and 2 allow to obtain the following ratio for the photonic pair production near threshold [3]:

$$\sigma_{D\bar{D}} : \sigma_{D\bar{D}^*+\bar{D}D^*} : \sigma_{D^*\bar{D}^*} = 1 : 0 : 3. \quad (3)$$

Nevertheless our detail analysis shows that the both assumptions are not valid for the photonic production. Moreover one can not obtain ratio (3) even for $m_Q \to \infty$. That ratio is valid only for zero charge of the light quark and $m_Q \to \infty$.

Thus, the interaction of the light valence quark of D-meson with the initial photonic field gives the essential contribution into the photonic production of the charmed meson pairs. That can be clearly seen from Fig. 1 where the cross section of the charged D-meson pair production is performed.

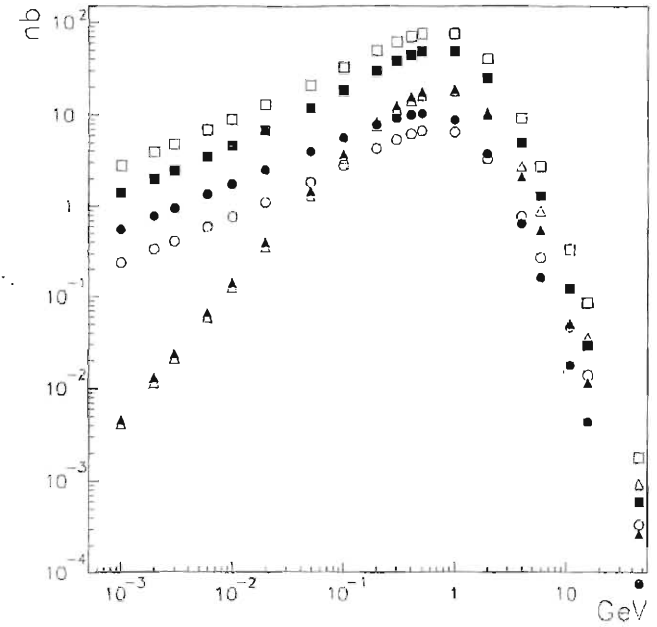

Figure 1: The exclusive photonic production cross section of the $D\bar{D}$-pairs (open circles), $D\bar{D}^*(\bar{D}D^*)$-pairs (open triangles) and $D^*\bar{D}^*$-pair (open squares) as function of the $\Delta = \sqrt{s} - \sqrt{s_{th}}$. The black markers denote the cross section values calculated without taking into account the light valence quark interaction with the initial photonic field ($m_c = 1.8$ GeV, $m_q = 0.2$ GeV).

References

1. A. De Rújula, Howard Georgi and S. L. Glashow, Phys. Rev. Lett. **37**, 398 (1976).

2. V. V. Kiselev, International Journal of Modern Physics **A10**, 465 (1995).

3. V.G. Kartvelishvili and and A. K. Likhoded, JETP Lett. **26**, 54 (1976).

Frascati Physics Series Vol. XXXI (2003), pp. 413–415
FRONTIERSCIENCE 2002 – Frascati, October 6–11, 2002
Short Communication in Plenary Session

PRELIMINARY RESULTS ON CHARM PRODUCTION NEAR THRESHOLD IN pA-INTERACTIONS AT 70 GeV

L.A. Tikhonova*
Skobeltsin Institute for Nuclear Physics, Moscow State University, RU-119899, Moscow, Russia

A study of the charmed particle production in pp and pA interactions at 70 GeV is conducted with the help of SVD setup at the Serpukhov accelerator. Main goals of the experiment are:

1.Measurement of the total charm production cross sections on Si,C and Pb targets; study of the cross section A-dependence.

2.Measurement of the differential x_F and p_t spectra and study of the leading effect for the charm mesons and baryons.

3.Study of the possible influence of the intrinsic charm in the proton on the

* On behalf of SVD-2 Collaboration members: S.G. Basiladze, G.A. Bogdanova, P.F. Ermolov, A.A. Kiryakov, A.G. Kholodenko, V.A. Kramarenko, A.V. Kubarovsky,A.N. Larichev, A.K. Leflat, P.P. Nomokonov, V.V. Popov, V.Yu. Volkov, A.P. Vorobiev

inclusive charm spectra.

The experiment was planned to perform in two stages.

At the first stage a rapid cycling liquid hydrogen bubble chamber was used as a vertex detector and estimation of the total charm production cross section in pp interactions at 70 GeV was obtained as $1.6 \pm 0.9(stat.) \pm 0.3(syst.)\mu b$ [1]. At the second stage a new high precision microstrip vertex detector with Si, C and Pb targets, Cherenkov threshold counter and gamma-detector were included into SVD-2 setup [2]. The first physical run with new vertex detector was performed in April 2002, about 53 millions of inelastic pN-events on Si, C and Pb targets were registered.

Data analysis is in progress now. For the first step, the simplest decay mode $D^0 \to K\pi$ was selected. A two body decay, formed by two tracks, was identified as a D decay, if it satisfied the following conditions:

1.Two tracks at each of ZX and ZY projections of microstrip Si-detectors into vertex detector have the impact parameter $l > 30\mu m$.

2.The decay point is outside of any nuclear target in the vertex detector.

3.These two tracks are reconstructed in magnetic spectrometer with $\chi^2 < 5$.

4.The curvatures of these tracks in the magnetic field have the different signs

5.The total momentum vector of the decay tracks points back to the primary vertex.

6.The invariant mass for the decay hypothesis $D^0 \to K\pi$ is in the range 1.8 to 2.0 GeV.

Using the number of selected $D^0 \to K\pi$ candidates, the total number of events, having 2 tracks with high impact parameter, registered in vertex detector and using the spectrometer acceptance calculated with the help of PYTHIA we can estimate the total charm production cross-section. Assuming a linear A-dependence of the total charm production cross-section we have obtained $\sigma_{c\bar{c}} \sim 1 \ldots 2\mu b$, in agreement with our previous estimation for pp-interactions, obtained with hydrogen bubble chamber at 70 GeV.

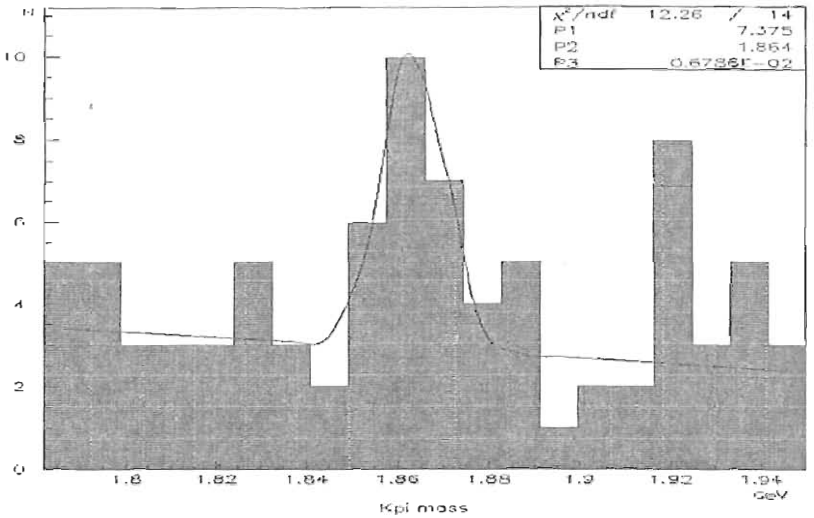

Figure 1: *Effective mass of $K\pi$-combinations. Gaussian fit is shown for illustration only.*

References

1. N.S. Amaglobeli *et al.* (SVD collaboration), Physics of Atomic Nuclei (Russian) **64**, 891 (2001).

2. A. Leflat *et al.*, Nucl. Phys. **A699**, 352 (2002).

Frascati Physics Series Vol. XXXI (2003), pp. 417–419
FRONTIERSCIENCE 2002 – Frascati, October 6–11, 2002
Short Communication in Plenary Session

TWO PHOTON WIDTH OF HEAVY PSEUDOSCALAR MESONS

Nicola Fabiano *
Perugia University and INFN, via A. Pascoli, I-06100 Perugia, Italy

1 Introduction

We discuss the partial width of the pseudoscalar charmonium state η_c and bottomonium state η_b into two photons. Predictions from potential models are examined and compared with experimental values for the η_c case. Through the NRQCD factorisation procedure results for η_c are also compared with those from J/ψ data, and results for η_b to the Υ decay data.

* coauthor Giulia Pancheri, *Laboratori Nazionali Frascati INFN, P.O.Box 13, I00044 Frascati, Italy*

2 Experimental values and relation to vector electromagnetic width

In this work we revisit the calculation of the two photon width of η_c, highlighting newest experimental results and updating the potential model calculation. Unlike the η_c, the η_b state hasn't been observed yet. We will examine various theoretical predictions for the electromagnetic decay of the lightest $b\bar{b}$ bound state. We start with the two photon decay width of a pseudoscalar quark–antiquark bound state with first order QCD corrections. The ratio of the pseudoscalar decay rate to the vector one is given by

$$\frac{\Gamma(P \to \gamma\gamma)}{\Gamma(V \to e^+e^-)} \approx 3Q^2 \frac{(1 - 3.38\alpha_s/\pi)}{(1 - 5.34\alpha_s/\pi)} = 3Q^2 \left[1 + 1.96\frac{\alpha_s}{\pi} + \mathcal{O}(\alpha_s^2)\right] . \quad (1)$$

This expression can be used to estimate the radiative width of pseudoscalar state from the measured values of the leptonic decay width of the vector state.

3 Potential models predictions for η_c and η_b $\gamma\gamma$ decay width

We present the results one can obtain for the absolute width, through the extraction of the wave function at the origin from potential models. The "prototype" potential is given by the Cornell potential model

$$V(r) = -\frac{k}{r} + \frac{r}{a^2} \quad (2)$$

which allows us to compute the Born decay width. The full expression of the pseudoscalar decay width is given by:

$$\Gamma(P \to \gamma\gamma) = \Gamma^P_{Born}\left[1 + \frac{\alpha_s}{\pi}\left(\frac{\pi^2 - 20}{3}\right)\right] \quad (3)$$

Γ^P_{Born} depends on $\psi(0)$ of the particular potential model taken into account.

4 Octet component procedure

We present after another procedure which admits other components to the meson decay beyond the one from the colour singlet picture (Bodwin, Braaten and Lepage). The decay width expression is given by means of NRQCD from the expansion

$$\Gamma = \sum_{n=1}^{2} \frac{2\Im f_n(\alpha_s)}{M^{d_n}} \langle \mathcal{O}_n \rangle \quad (4)$$

which is a sum of terms, each of which factors into a short–distance perturbative coefficient $\Im f_n$ and a long–distance nonperturbative matrix element $(\mathcal{O}_n)$. ¿From the experimental values of electromagnetic decay and light hadron of the vector state we obtain the two photon decay width of the pseudoscalar state. We compute also the decay width from the lattice calculation of the nonperturbative long–distance terms.

5 Conclusions

The $\Gamma(\eta_c \to \gamma\gamma)$ prediction gives the value 7.5 ± 1.6 keV. The $\Gamma(\eta_b \to \gamma\gamma)$ prediction gives the value 466 ± 101 eV. Prediction of the BBL procedure and other theoretical results are in good agreement with each other.

References

1. N. Fabiano, G. Pancheri, Eur. Phys. J. C **25**, 421–425, (2002), and references therein; hep-ph/0204214.

2. N. Fabiano, to appear in Eur. Phys. J. C (2002), and references therein; hep-ph/0209283.

Frascati Physics Series Vol. XXXI (2003), pp. 421–423
FRONTIERSCIENCE 2002 – Frascati, October 6–11, 2002
Short Communication in Plenary Session

STUDY OF THE CHARMONIUM ^3P_J STATES IN $\bar{p}p$ ANNIHILATIONS AT FNAL

Maria Margherita Obertino *
University of Minnesota.

1 The study ^3P_J states in $\bar{p}p$ annihilations.

The charmonium spectrum, characterized by well-spaced narrow states, is considered a rich source of tests for QCD. The study of the ^3P_J resonances in particular provides information about the spin dependence of the interaction and could yield measurements of quantities calculable in PQCD framework, leading to a determination of some of the basic parameters of the theory.
In $\bar{p}p$ annihilation the ^3P_J states can be directly formed through the exchange of two or three gluons; consequently their parameters can be extracted from the excitation curve with a precision that depends only on the knowledge of the energy of the initial state and the event statistics. The chance provided by the stochastic cooling to use dense $\bar{p}$ beams with narrow momentum spread

* On behalf of E835 collaboration

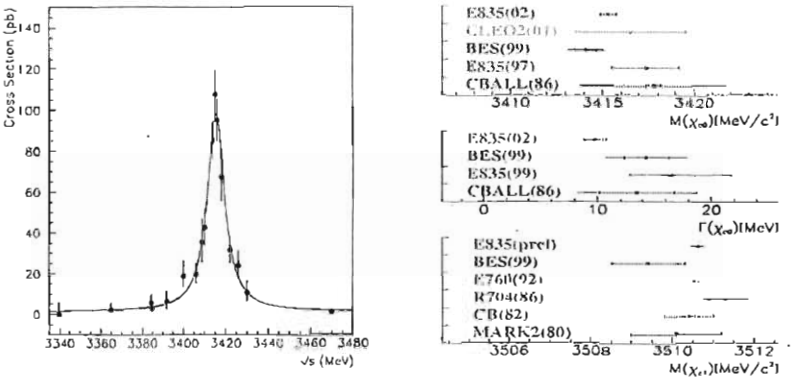

Figure 1: *Measured cross section for the reaction* $\bar{p}p \rightarrow J/\psi\gamma$ *in the* χ_{c0}*region; comparison of the experimental results on* $M_{\chi_{c0}}$, $\Gamma_{\chi_{c0}}$ *and* $M_{\chi_{c1}}$.

allows the $\bar{p}p$ experiments to obtain very precise measurements of the ^3P_J parameters. This tecnique was first applied at CERN by R704 and later used by E760 and E835 at Fermilab. We present the measurements of the χ_{c0} ($^3P_0$) and χ_{c1} ($^3P_1$) mass and width made by E835 with data collected during 2000, where both the resonances were formed and detected via the reaction

$$\bar{p}p \rightarrow \chi_{c0,1} \rightarrow J/\psi\gamma \rightarrow (e^+e^-)\gamma \qquad (1)$$

We report here only the results obtained; more information about the experimental method can be found in references [1] [2].

2 χ_{c0} parameters.

E835 collected 32.8 pb^{-1} of data in the χ_{c0} energy region($\sqrt{s} \sim 3330 \div 3470\ MeV$). The measured cross section is shown in fig. 1. The comparison between the value of the χ_{c0} mass and total width extracted from the fit of these data ($M_{\chi_0} = 3415.4 \pm 0.4 \pm 0.2 MeV/c^2$ and $\Gamma_{\chi_0} = 9.8 \pm 1.0 \pm 0.1 MeV$) [2] and the one quoted by previous experiments shows a significant improvement in the precision for both the parameters (see fig. 1).

3 χ_1 parameters.

E835 performed two scans in the χ_1 energy region ($\sqrt{s} \sim 3509 \div 3512\ MeV$) and collected a total integrated luminosity of $\sim 4\ \mathrm{pb}^{-1}$. The two sets of data were analyzed separately; the weighted average of their results is:

$$M_{\chi_1} = 3510.62 \pm 0.02 \pm 0.17 MeV/c^2 \quad \Gamma_{\chi_1} = 0.88 \pm 0.05 \pm 0.09 MeV$$

The most precise previous measurement of the χ_1 mass (see Fig. 1) and the only previous measurement of the χ_1 width were made by E760 which obtained $M_{\chi_1}^{E760} = 3510.53 \pm 0.13 MeV/c^2$ and $\Gamma_{\chi_1}^{E760} = 0.88 \pm 0.14 MeV$ [1]. The good agreement between E835 and E760 can be considered an evidence of the our understanding of the systematics on these measurements.

References

1. R. Cester and P.A. Rapidis , Annu.Rev.Nucl.Part.Sci. **44**, 329-371 (1994).

2. S .Bagnasco *et al*, Physics Letter B **533**, 237-242 (2002).

Frascati Physics Series Vol. XXXI (2003), p. 425–427
FRONTIERSCIENCE 2002 – Frascati, October 6–11, 2002
Short Communication in Plenary Session

THE BTeV ELECTROMAGNETIC CALORIMETER REQUIREMENTS FOR HIGH QUALITY RECONSTRUCTION OF NEUTRAL PARTICLES

J .Yarba *
Fermilab, P.O.Box 500, Batavia, IL 60510, USA

1 The BTeV Electromagnetic Calorimeter Requirements

The BTeV [1] experiment at Fermilab will need excellent photon detection which is crucial to study CP violations in B decays and rare decay of B's to explore physics beyond the standard model. A homogeneous electromagnetic calorimeter (ECAL) built of more than 10000 Lead Tungstate ($PbWO_4$) crystals instrumented with photomultiplier tubes will be installed to ensure excelent energy and position resolution, compact shower size to minimize the number of overlapping showers, fast signal, and radiation hardness.

With the light output of 5000 photoelectrons/MeV, one can expect the energy resolution as good as $1.7\%\sqrt{E} \oplus 0.55\%$. The spacial resolution is expected to be $3500\mu m/\sqrt{E} \oplus 200\ \mu m$, at least. With these resolutions, the π^0

* On behalf of BTeV collaboration, ECAL group

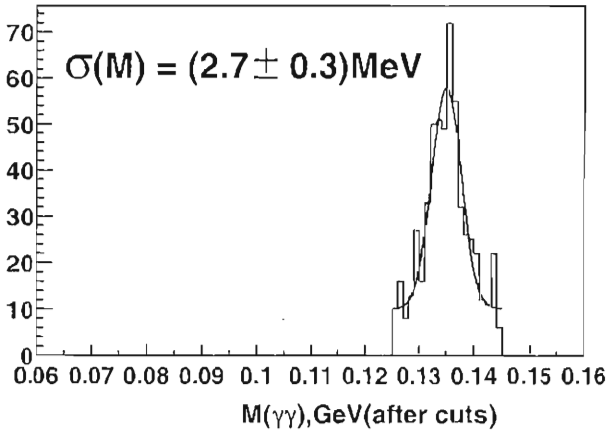

Figure 1: Invariant $\gamma\gamma$ mass for $B^0 \to \rho^+\pi^-$ events, BTeV Geant3 simulation

mass resolution will be in the range of 2÷5MeV, as exemplified in fig.1 for π^0 coming from $B^0 \to \rho^+\pi^-$ decay, simulated by Geant3; the BTeV reconstruction software were used to reconstruct photons and charged tracks. This ensures B-mass resolution in the range of 28÷40MeV.

2 Test Beam Study of the $PbWO_4$ Prototype

To prove the expectations from simulation, behavior of the crystals need to be understood for conditions which are close to what is expected in BTeV.

The BTeV ECAL prototype built of 25 $PbWO_4$ crystals instrumented with photomultiplier tubes was exposed with an e^- beam in the energy range of 1÷45GeV and with a π^- beam of 40GeV, to study energy and position resolution and to observe changes in the light output due to irradiation.

We found the energy resolution of $1.8\%\sqrt{E}\oplus$ 0.33% and the position resolution of $2800\mu m\sqrt{E}\oplus$ $160\mu m$ (fig.2); these agree well with expectations.

The irradiation of $PbWO_4$ crystals results in light output loss. However, the crystals are able to recover from radiation damage naturally by room temperature annealing. This limits the light output loss only to the point when radiation damage and recovery balance. Continuous calibration is needed to control the effect during operation of BTeV.

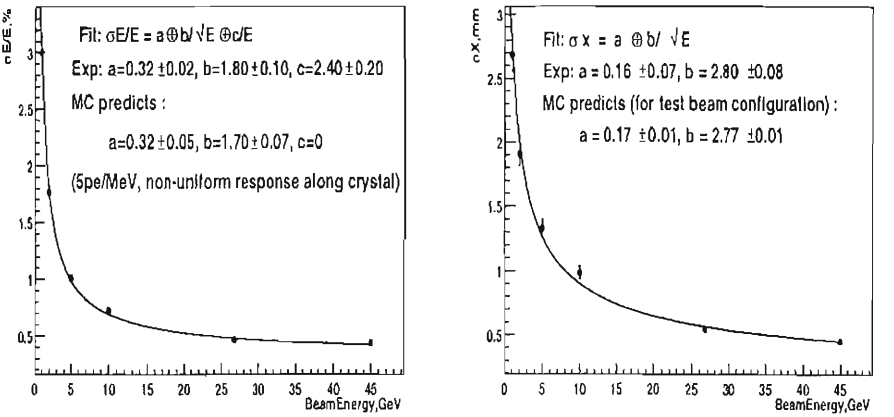

Figure 2: Measured energy and position resolution of $PbWO_4$ crystals

References

1. G.Y. Drobychev et al., Update to Proposal for an Experiment to Measure Mixing, CP Violation and Rare Decays in Charm and Beauty Particle Decays at the Fermilab Collider - BTeV, March 2002

Frascati Physics Series Vol. XXXI (2003), pp. 429
FRONTIERSCIENCE 2002 – Frascati, October 6–11, 2002
Short Communication in Plenary Session

THE HIGHER PRECISION MEASUREMENT OF J/Psi AND Psi(2S) MASSES AT VEPP-4M WITH THE KEDR DETECTOR

Valery Tayursky

Budker INP, Russia

Written contribution not received

Frascati Physics Series Vol. XXXI (2003), pp. 431–433
FRONTIERSCIENCE 2002 – Frascati, October 6–11, 2002
Short Communication in Plenary Session

A STUDY OF THE LHC EXPERIMENTAL SENSITIVITY TO CP VIOLATING $gt\bar{t}$ COUPLING

J. Sjölin
Stockholm University

1 Physics motivation

Detailed measurements of the top coupling structures will be possible at the emerging LHC experiments ATLAS and CMS. Already after one year, millions of top pairs are expected to be available for analysis from both experiments. The top quark is interesting for many reasons since the large rest mass makes it exhibit several unique properties. For example, the top quark decay time is much less than the associated hadronization time. Thus the decay is clean from non-perturbative effects, enabling direct and unmasked access to the spin properties. The large Yukawa coupling also makes it extra sensitive to the electro-weak symmetry breaking sector. As a consequence, non Standard Model (SM) CP violating phases originating from multiple higgs models or supersymmetry may be detectable in events containing top quarks. Another

factor that contributes to the sensitivity to new physics is that effects from the CP violating phase in the SM is below the experimental sensitivity by many orders of magnitude. Hence, any CP violating signal in the top sector is an indication of new physics.

2 Model independent description of CP violation

The symmetries of the SM and Lorentz invariance severely restricts the number of possible lowest order effective CP violating interactions that can be induced by physics beyond the SM, see e.g. reference [1]. Assuming small non SM contributions in the top decay, one finds only one new dominating CP violating operator in addition to the SM Lagrangian active in top quark pair events at LHC. The operator is the chromo-electric dipole moment parameterized here by D_5

$$\mathcal{L}_5 = -i\frac{D_5}{2}\bar{t}\sigma^{\mu\nu}\gamma_5 t G^a_{\mu\nu}T^a. \quad (1)$$

This means that whatever mechanism there is that might be responsible for a non SM CP violation, it will to first order induce a non-zero value of D_5. Two vertices are affected: the SM gluon-top-antitop vertex and a new gluon-gluon-top-antitop vertex. It turns out that the CP violation in this case originates from top and antitop spin correlations. That is, complete spin dependent matrix elements must be used for a correct description. Also, to first order in D_5, the total cross-section is unaffected.

3 Analysis

Spin dependent tree level matrix elements including the effects of D_5 were calculated and implemented into a MC with separate fragmentation handled by PYTHIA. The ATLAS detector at LHC was simulated by fast parameterizations. Two types of top pair events were used in the analysis: lepton + jets final states and dilepton final states. An effective and extremely robust observable used in the analysis was

$$f_2(l^+, l^-, b, \bar{b}) = \frac{1}{m_t^2}\frac{\epsilon_{\mu\nu\sigma\rho}p^\mu_{l^+}p^\nu_{l^-}p^\sigma_b p^\rho_{\bar{b}}}{(p_{l^+}\cdot p_{l^-}p_b\cdot p_{\bar{b}})^{1/2}}\ (T_N\text{-odd}). \quad (2)$$

For lepton + jets events one of the leptons were replaced by a d-type quark. The b-jet charge was found by solving the kinematics for the final states. For

the dileptons this was solved analytically and for lepton + jets a 3C-fit was solved numerically. For a complete description of the analysis see reference [2].

4 Results

The result from the analysis is that both dilepton and lepton + jets final states are about equally sensitive for the parameter D_5. The detection limit for a 5σ signal, using one of the topologies with one year of running at low luminosity, is estimated to be

$$D_5 > 5 \times 10^{-18} \text{ cm} \cdot g_s. \tag{3}$$

References

1. Jin Min Yang and Bing-Lin Young, Phys. Rev. D **56** (1997) 5907.
2. J Sjölin, *ATLAS scientific note* SN-ATLAS-2002-021.

Frascati Physics Series Vol. XXXI (2003), pp. 435–437
FRONTIERSCIENCE 2002 – Frascati, October 6–11, 2002
Short Communication in Plenary Session

RECENT CHARM MESON BRANCHING RATIO AND LIFETIME MEASUREMENTS FROM FOCUS EXPERIMENT

Marco Rovere *
Università dell' Insubria and INFN - Sezione di Milano

1 Introduction

The results presented have been obtained using the high statistics charm sample of the FOCUS experiment at Fermilab. The large amount of data available together with the very clean particle identification allowed us to obtain evidence of doubly and singly Cabibbo suppressed decays never seen before and to measure charm meson lifetimes with an unprecedented level of accuracy.

2 Branchig Ratio Measurements

Thanks to the excellent vertex resolution and particle identification of the FOCUS spectrometer we have obtained the first clear evidence of the doubly

* On behalf of the FOCUS collaboration

Cabibbo suppressed decay $D^+ \to K^+K^-K^+$ and the first evidence of the singly Cabibbo suppressed decay $D_s^+ \to K^+K^-K^+$ [1]. These signals are shown in fig. 1. We have measured their branching ratio relative to $D^+ \to K^-\pi^+\pi^+$ and $D_s^+ \to K^-K^+\pi^+$ respectively, obtaining the following results:

$$\Gamma\left(D^+ \to K^-K^+K^+\right)/\Gamma\left(D^+ \to K^-\pi^+\pi^+\right) = (9.49 \pm 2.17 \pm 0.22) \times 10^{-4} \quad (1a)$$

$$\Gamma\left(D_s^+ \to K^-K^+K^+\right)/\Gamma\left(D_s^+ \to K^-K^+\pi^+\right) = (8.95 \pm 2.12\ ^{+2.24}_{-2.31}) \times 10^{-3}, \quad (1b)$$

where the first error is statistical and the second is systematic.

Our D^+ measurement is consistent with present 90% C.L. limit from E687 [2]. The D_s^+ measurement is consistent with the previous E687 upper limit [2] and constitutes the second D_s^+ Cabibbo suppressed decay ever measured.

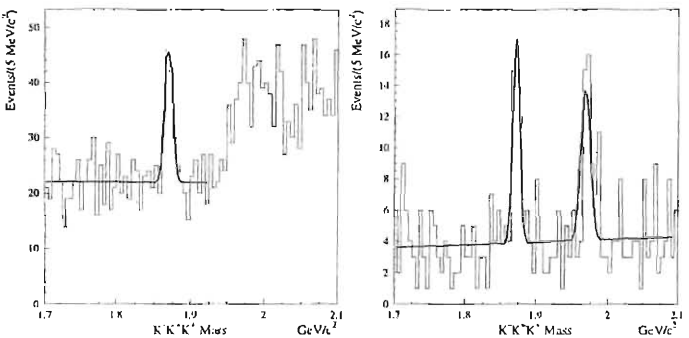

(a) (b)

Figure 1: Invariant masses. (a)$D^+ \to K^+K^-K^+$, (b)$D_s^+ \to K^+K^-K^+$

We present also new measurements of two semileptonic branchig ratios [3]. We obtain values of:

$$\Gamma\left(D^+ \to \bar{K}^0\mu^+\nu\right)/\Gamma\left(D^+ \to K^-\pi^+\pi^+\right) = (0.602 \pm 0.010 \pm 0.021) \quad (2a)$$

$$\Gamma\left(D_s^+ \to \phi\mu^+\nu\right)/\Gamma\left(D_s^+ \to \phi\pi^+\right) = (0.54 \pm 0.033 \pm 0.048) \quad (2b)$$

Our $D^+ \to \bar{K}^0\mu^+\nu$ result includes the effects of the s-wave interference discussed in Reference [4].

3 Lifetime Measurements

FOCUS has obtained the most accurate measurement to date of the lifetimes of the D^+, D^0 and D_s^+. Using about 210000 D^0 and 110000 D^+ events we obtain the following values: 409.6 ± 1.1(statistical) ± 1.5(systematic) fs for D^0, 1039.4 ± 4.3(statistical) ± 7.0(systematic) fs for D^+ and a preliminary value of 506 ± 8 fs for D_s^+. Particular attention have been dedicated to the evaluation of the systematic errors which, for such a high statistics sample, represent the main source of error. Our values are reported in Table 1 along with a comparison with the most recent published results. Our results will significantly decrease the errors in the current world average values for D^0 and D^+ lifetimes.

Table 1: *Measured lifetimes* ($\times 10^{-12}$ *s*).

Experiment	D^0	D^+
E687 [5]	$0.413 \pm 0.004 \pm 0.003$	$1.048 \pm 0.015 \pm 0.011$
CLEO II [6]	$0.4085 \pm 0.0041^{+0.0035}_{-0.0034}$	$1.0336 \pm 0.0221^{+0.0099}_{-0.0127}$
E791 [7]	$0.413 \pm 0.003 \pm 0.004$	
FOCUS [8]	$0.4096 \pm 0.0011 \pm 0.0015$	$1.0394 \pm 0.0043 \pm 0.0070$

References

1. FOCUS Collaboration, J.M. Link *et al*, Phys. Lett. **B 541**, 227 (2002).
2. E687 Collaboration, P.L. Frabetti *et al.*, Phys. Rev. Lett. **B 363**, 259 (1995).
3. FOCUS Collaboration, J.M. Link *et al*, Phys. Lett. **B 541**, 243 (2002).
4. FOCUS Collaboration, J.M. Link *et al*, Phys. Lett. **B 535**, 43 (2002).
5. E687 Collaboration, P.L. Frabetti *et al.*, Phys. Lett. **B 323** 459 (1994).
6. CLEO Collaboration, G. Bonvicini *et al.*, Phys. Rev. Lett. **82** 4586 (1999).
7. E791 Collaboration, E.M. Aitala *et al.*, Phys. Rev. Lett. **83** 32 (1999).
8. FOCUS Collaboration, J.M. Link *et al*, Phys. Lett. **B 537** 192 (2002).

Frascati Physics Series Vol. XXXI (2003), pp. 439–441
FRONTIERSCIENCE 2002 – Frascati, October 6–11, 2002
Short Communication in Plenary Session

CHARM BARYON LIFETIME IN FOCUS

Ilaria Segoni *
University of Colorado at Boulder

1 Introduction

The investigation of hadron lifetimes is a study of quark interactions. The evaluation of the decay widths is crucial to determine the parameters of strong and weak interactions [1, 2] (like the baryon wave function at the origin and the SU(3) symmetry breaking). Confrontation with experimental results is critical, as theory alone can't accomplish this task.

2 The FOCUS measurements

The FOCUS collaboration has measured all of the singly charmed baryon ground state lifetimes: Λ_c^+, Ξ_c^+, Ξ_c^0, and Ω_c^0. Each of these measurements

* On behalf of the FOCUS collaboration

was performed using a binned maximum likelihood fit method.

Using a sample of 8034 ± 122 events from the decay mode $pK^-\pi^+$ we measure $\tau(\Lambda_c^+) = 204.6 \pm 3.4$ (stat.)± 2.5 (sys.) fs [3]. Systematic effects were thoroughly investigated. The effects of time scale, acceptance, absorption, background production and resolution were studied in detail.

The Ξ_c^- total sample [4] of 532 ± 30 events derives from four different modes: $\Xi^-\pi^+\pi^+$ (in four topologies), $\Sigma^+K^-\pi^+$ (in two topologies), $pK^-\pi^+$ and $\Lambda^0K^-\pi^+\pi^+$. We measure $\tau(\Xi_c^+) = 439 \pm 22$ (stat.)± 9 (sys.) fs. We studied production, resolution, background and different fit conditions to evaluate the systematic uncertainty. We also evaluated the contribution from the two fold ambiguity in momentum in the Σ mode, due to the "kink" topology.

For the Ξ_c^0 we used 110 ± 17 events from the $\Xi^-\pi^+$ and Ω^-K^+ modes. We measure $\tau(\Xi_c^0) = 118^{+14}_{-12}$ (stat.)± 5 (sys.) fs. For the evaluation of the systematic uncertainty we investigated production, and a set of different choices for the fit conditions. Since the time resolution (50 fs) is only half as large as $\tau(\Xi_c^0)$, detailed studies have been performed to validate the lifetime technique and to investigate systematic effects. A contribution to the systematic error was included from a study using a convolved binned likelihood method.

The Ω_c^0 lifetime measurement is not yet published. We reconstruct the decay modes $\Xi^-K^-\pi^+\pi^+$ and $\Omega^-\pi^+$. Our preliminary result is $\tau(\Omega_c^0) = 79 \pm 12$ (stat.)± 9 (sys.) fs. Different fit conditions have been considered for the systematic uncertainty evaluation. We also estimate the effects due to time resolution following the same procedure that was applied for the Ξ_c^0.

3 Conclusions

FOCUS has improved the precision on the measurements of all the charm baryon lifetimes, see Table 1. As the data values are quite precise it seems likely that improvements in theory will be driven by new measurements of semileptonic branching ratios, rather than from new lifetime measurements.

References

1. B. Guberina and B. Melic, Eur. Phys. J. **C2** 697 (1998).

2. G. Bellini, I. I. Y. Bigi, P. J. Dornan, Phys. Rept. **289**, 1 (1997).

Table 1: *FOCUS results are compared with the previous world averages* [6].

	FOCUS (fs)	Previous world average (fs)
$\tau(\Lambda_c^+)$	$204.6 \pm 3.4 \pm 2.5$	206 ± 12
$\tau(\Xi_c^+)$	$439 \pm 22 \pm 9$	330^{+60}_{-40}
$\tau(\Xi_c^0)$	$118^{+14}_{-12} \pm 5$	98^{+23}_{-15}
$\tau(\Omega_c^0)$	$79 \pm 12 \pm 9$	64 ± 20

3. FOCUS Collaboration, J. M. Link *et al*, Phys. Rev. Lett. **88**, 161801 (2002).

4. FOCUS Collaboration, J. M. Link *et al*, Phys. Lett. B **523**, 53 (2001).

5. FOCUS Collaboration, J. M. Link *et al*, Phys. Lett. B **541**, 211 (2001).

6. Particle Data Group, D. E. Groom *et al*, Eur. Phys. J. C 15 (2002) 1.

Frascati Physics Series Vol. XXXI (2003), pp. 443–445
FRONTIERSCIENCE 2002 – Frascati, October 6–11, 2002
Short Communication in Plenary Session

GLOBAL ANALYSIS OF $B \to PP$, PV DECAYS WITH QCD FACTORIZATION

Guohuai Zhu
Theory Group, KEK, Tsukuba, Ibaraki 305-0801, Japan

Non-leptonic charmless B decays are crucial for the determination of CKM triangle. But theoretically it is very difficult to extract fundamental CP parameters cleanly from non-leptonic B decays due to the complex hadronization process. Three years ago, QCD factorization [1](QCDF), a novel method, was proposed. It argues that, in the heavy quark limit, non-leptonic B decays can be factorized into perturbatively-calculable hard part and soft part described by some universal non-perturbative parameters, such as form factor and light-cone distribution amplitudes(LCDA). Now BaBar and Belle have accumulated copious data on non-leptonic B decays, it should be right time to check the consistency between the QCDF predictions and the experimental measurements.

The decay amplitudes for charmless B decays depend on various parameters. The readers may refer to [2] for the details on the related input parameters. Beneke *et al.* [1] have done a global fit on $B \to \pi\pi$, πK decays, here we entend it to fourteen $B \to PP$ and PV decay modes. It is noticed that only two

new sensitive parameters (form factor $A_0^{B\rho}$ and annihilation parameter X_A^{PV}) are introduced for the extension. So we could give a much more stringent test on the consistency between QCDF and the experiments.

We implement the CkmFitter package [1] to do the global fit. It shows that the QCDF predictions are well consistent with the experimental measurements: $\chi^2_{min} = 4.2$ for fourteen decay channels. The best fit $\gamma = 79°$ is somewhat large

Table 1: The best fit values using the global analysis with and without chiral-related contributions for $B \to PP$ and PV decays. The branching ratios are in unit of 10^{-6}. The experimental data are the uncorrelated average of measurements of BaBar, Belle and CLEO.

Mode	$\pi^+\pi^-$	$\pi^+\pi^0$	$K^+\pi^-$	$K^+\pi^0$	$K^0\pi^+$
Exp.	4.77 ± 0.54	5.78 ± 0.95	18.5 ± 1.0	12.7 ± 1.2	18.1 ± 1.7
Best Fit	4.82	5.35	19.0	11.4	20.1
No chiral	5.68	3.25	18.8	12.6	20.2
Mode	π^0K^0	$\eta\pi^+$	$\rho^\pm\pi^\mp$	$\rho^0\pi^+$	$\eta\rho^+$
Exp.	10.2 ± 1.5	< 5.2	25.4 ± 4.3	8.6 ± 2.0	< 6.2
Best Fit	8.2	2.8	26.7	8.9	4.6
No chiral	7.3	1.8	29.5	8.5	3.8
Mode	ϕK^+	ϕK^0	$K^+\rho^-$	ωK^0	
Exp.	8.9 ± 1.0	8.6 ± 1.3	13.1 ± 4.7	5.9 ± 1.9	
Best Fit	8.9	8.4	12.1	6.3	
No chiral	7.1	6.7	5.1	1.2	

but still consistent with the standard CKM fit. As an illustration, in Table 1, we list the best fit values of the global analysis for the related $B \to PP$,PV decay modes with and without chiral-related contributions. It implies that the chirally enhanced corrections might be important especially for penguin-dominated PV decays. Based on the global fit, we could also give predictions on some interesting decay channels: $\mathcal{B}(B^0 \to \pi^0\pi^0) \sim 1\times10^{-6}$, this channel is very important for the CKM angle α. The pure annihilation decay $B^0 \to K^+K^-$ is favored to be around 0.8×10^{-7}. $\mathcal{B}(B^+ \to \omega K^+) \sim 6 \times 10^{-6}$ is larger than the BaBar measurement but consistent with the Belle observation. As to $B^+ \to \omega\pi^+$, it is predicted to be around 7×10^{-6}. It is also highly interesting

[1] http://ckmfitter.in2p3.fr

that the penguin-to-tree ratio for $\pi^+\pi^-$ mode is expected to be larger than 0.3. For πK^* decays, it is anticipated that further measurements with higher precision would observe smaller branching ratios. For $B \to \eta^{(\prime)} K^{(*)}$, QCDF can not give quantitative estimations at present. The readers should refer to [2] for more details.

Acknowledgements

I am grateful to D.S. Du, J.F. Sun and D.S. Yang, the work reported here is collaborated with them.

References

1. M. Beneke, G. Buchalla, M. Neubert and C.T. Sachrajda, Phys. Rev. Lett. **83**, 1914 (1999); Nucl. Phys. **B606**, 245 (2001).

2. D.S. Du, J.F. Sun, D.S. Yang and G.H. Zhu, hep-ph/0209233, submitted to Phys. Rev. **D**.

Frascati Physics Series Vol. XXXI (2003), pp. 447
FRONTIERSCIENCE 2002 – Frascati, October 6–11, 2002
Short Communication in Plenary Session

PROSPECT OF HIGGS PHYSICS IN RUN 2 AT THE FERMILAB TEVATRON COLLIDER

M. Hohlfeld

Institut für Physik - Mainz

Written contribution not received

Frascati Physics Series Vol. XXXI (2003), pp. 449–451
FRONTIERSCIENCE 2002 – Frascati, October 6–11, 2002
Short Communication in Plenary Session

SEARCHES FOR LEPTOQUARKS WITH THE DØ DETECTOR AT THE TEVATRON

T. Christiansen
LMU München, Am Coulombwall 1, D-85748 Garching, Germany

The existence of leptoquarks (LQ), color-triplets of bosons with lepton and quark quantum numbers, is predicted by different theories beyond the Standard Model. This article summarizes the DØ Run-I searches for the three different LQ generations in $p\bar{p}$ collisions at $\sqrt{s} = 1.8$ TeV and presents ongoing studies at Run II.

Limits on proton decays, on lepton flavor violation and on flavor-changing neutral currents lead to the assumption that there would be three different generations of leptoquarks, each one of them only interacting within one lepton and quark family. Figure 1 shows Feynman graphs of the dominant production processes in $p\bar{p}$ collisions.

Using about 100 pb^{-1} of $p\bar{p}$ collision data with a center-of-mass energy of $\sqrt{s} = 1.8$ GeV recorded during Run I with the DØ detector, no evidence for the existence of leptoquarks was found. The results on the leptoquark searches were combined to 95% confidence limits on the LQ-pair production cross section as a

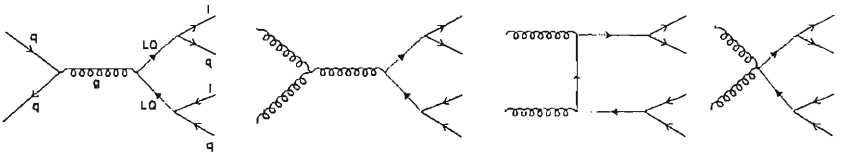

Figure 1: Leading-order diagrams for leptoquark pair production.

The lower limits for masses of 1^{st}-generation scalar leptoquarks are 225 GeV, 204 GeV and 79 GeV, assuming a branching fraction to charged leptons of $\beta = BF(LQ \to l^{\pm}q) = 1, 1/2$ and 0, respectively. [1] The corresponding limits for the 2^{nd}-generation scalar LQ masses are determined to 200 GeV, 180 GeV and 79 GeV. [2] For 3^{rd}-generation LQ masses comparable to m_{top}, the decay $LQ_3 \to t+l$ is suppressed or even forbidden. Studies of the $\nu b\bar{\nu}\bar{b}$ channel yield a lower mass limit of 94 GeV for scalar 3^{rd}-generation leptoquarks and $\beta = 0$. [3]

If both leptoquarks decay into an electron and a quark, two electrons and two jets can be reconstructed. The left diagram in figure 2 shows the di-electron mass of $eejj$ Run-II candidates collected between November 2001 and May 2002 with $\sqrt{s} \approx 2$ GeV. These 18 events, equivalent to an integrated luminosity of about 8.8 pb^{-1}, are compatible with background (15 ± 5 events expected) which is dominated by Drell-Yan Z production. Comparing the limits on the cross section for different masses m_{LQ} to NLO calculations for scalar leptoquarks, the lower limit on the mass of 1^{st}-generation leptoquarks is 113 GeV. [4] This is compatible with earlier results from Run I and reflects the lower integrated luminosity.

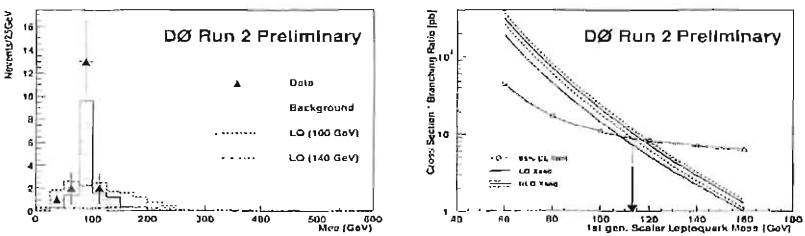

Figure 2: Search for 1^{st}-generation leptoquarks at Run II. Left: Di-electron invariant mass of $eejj$ candidate events. Right: LQ-mass dependent limits on the cross section for scalar LQ pairs assuming 100% branching fraction to charged leptons $BF(LQ \to eq) = 1$. [4]

Taking advantage of the increased collision energy and luminosity of the TeVatron for Run II, DØ will be able to extend its searches for leptoquarks to

so far inaccessible leptoquark masses. Especially for the second generation, the search for leptoquark pair production will greatly benefit from the upgraded muon spectrometer, the central tracking system with the newly installed magnetic solenoid and the new trigger system.

References

1. The DØ Collab., V.M. Abazov et al., Phys. Rev. Lett. 64, 092004 (2001).
2. The DØ Collab., B. Abbott et al., Phys. Rev. Lett. 84, 222 (2000).
3. The DØ Collab., B. Abbott et al., Phys. Rev. Lett. 81, 38 (1998).
4. M. Narain for the DØ Collaboration, *Results from the DØ Experiment at the Tevatron*, ICHEP (2002)

Frascati Physics Series Vol. XXXI (2003), pp. 453–455
FRONTIERSCIENCE 2002 – Frascati, October 6–11, 2002
Short Communication in Plenary Session

LHCb LEVEL 0 TRIGGER

R. Lefèvre *
Laboratoire de Physique Corpusculaire, 63177 Aubière Cedex, France

1 Introduction

The trigger is one of the most important system of the LHCb experiment. A high-performance trigger is indeed required to get the best benefit of the 10^5 $b\bar{b}$ pairs produced each second at the interaction point extracting the small fraction of interesting events. A four level trigger based first on large transverse momentum particles, then on displaced decay vertices and finally on full final state reconstruction is foreseen. It will achieve an overall suppression factor of 200000 (from 40 MHz down to 200 Hz). The especially challenging first trigger level, called level 0, is presented here.

* On behalf of the LHCb Collaboration

2 Level 0 global sketch

The LHCb level 0 trigger system [1] is a fully synchronous, pipelined architecture operating at 40 MHz with a fixed latency of 4 μs that will be hardware implemented making use of FPGAs. It has an global rate reduction factor of 40. It is based on simple criteria such as pile-up veto and high transverse momenta (p_T) canditates. Due to the relatively high mass of the b quark, the decay products of the B mesons have indeed a higher p_T spectrum than the other products of the pp reactions. Multiple interaction events are vetoed because they can not be efficiently fully reconstructed. The subdetectors used for the level 0 trigger are the pile-up detector which is a part of the vertex detector, the calorimeters and the muon chambers. The data coming from those three subdetectors are first processed in three independant boards. The pile-up veto one computes the primary vertices candidates while the calorimeter and the muon boards compute the highest p_T canditates. The data are then centralised in the level 0 decision unit which takes the decision.

3 Level 0 data processing

The pile-up detector is made of two R-stations silicon strip discs that allow to reconstruct the primary vertices. The pile-up veto ensures a good rejection of multiple interaction events leading to a gain of 30 % to 40 % on single $b\bar{b}$ events for the optimal luminosity: half of the 60000 single $b\bar{b}$ events produced per second at $L = 2 \times 10^{32}\ s^{-1}cm^{-2}$ can then be retained by the level 0 trigger.

The calorimeter system of LHCb is divided in four longitudinal parts that allow particle identification: a scintillating pad detector for the electron-gamma separation, a preshower for the electron-MIP separation, an electromagnetic and an hadronic calorimeter. The calorimeter trigger identifies the cluster candidates and finds the highest E_T electron, gamma, resolved π^0, merged π^0 and the two highest hadrons. The E_T cuts depend on the identification and are about few GeVs. Relatively good efficiencies are obtained: around 50 % for $B_d \rightarrow J/\Psi(e^+e^-)K_S$, from 40 % to 70 % for hadron channels.

The muon trigger finds the muon candidates looking for straight lines within the hits of the muon chambers. The p_T of each candidate is evaluated assuming that the track has been produced at the center of the interaction region. The p_T cut is about 0.6 GeV/c which leads to good efficiencies: around

85 % for $B_d \to J/\Psi(\mu^+\mu^-)K_S$, around 55 % for inclusive $B \to \mu X$.

4 Level 0 decision

The level 0 decision unit produces the level 0 decision combining all the level 0 data and therefore provides a good discriminating power to the system. In addition, it computes a block data containing the most significant level 0 information and sends it to level 1 trigger. This leads to very important enhancements of the level 1 efficiencies matching level 0 and level 1 candidates: a factor 2 for $B_d \to \pi^+\pi^-$, a factor 2.5 for $B_d \to J/\Psi(\mu^+\mu^-)K_S$. The level 0 decision unit is designed to be very flexible so that modifications and extensions of the trigger algorithm can be easily integrated to match running conditions, such as luminosity, and physic requirements.

References

1. LHCb Collaboration, LHCb Technical Proposal, CERN LHCC 98-4 (1998).

Frascati Physics Series Vol. XXXI (2003), pp. 457–459
FRONTIERSCIENCE 2002 – Frascati, October 6–11, 2002
Short Communication in Plenary Session

CORRECTIONS TO THE ISR RADIATIVE FUNCTION

O.N. Shekhovtsova*
NSC KIPT, Akademicheskaya 1, Kharkov, 61108, Ukraine

Initial state radiative events at DAΦNE

$$e^-(p_1) + e^+(p_2) \to \gamma(k) + \pi^+(p_+) + \pi^-(p_-) \tag{1}$$

allow to scan the cross section $\sigma_{e^-e^+\to\pi^+\pi^-}$ from the threshold up to M_Φ [1]. In this case the measured distribution $d\sigma(e^-e^+ \to \gamma\pi^+\pi^-)/dq^2$ and the cross section $\sigma_{e^-e^+\to\pi^+\pi^-}$ are connected by the radiative function $H(q^2, \theta_\gamma)$

$$q^2 \frac{d\sigma(e^-e^+ \to \gamma\pi^+\pi^-)}{dq^2} = H(q^2, \theta_\gamma)\sigma_{e^-e^+\to\pi^+\pi^-} \ . \tag{2}$$

To be competitive with direct scanning, $H(q^2, \theta_\gamma)$ has to be calculated with accuracy better than 1%, taking into account the realistic selection rules. This

* co-authors; V.A. Khoze - *University of Durham, Durham, DH1 3LE, UK*, G. Pancheri - *INFN Laboratori Nazionale di Frascati, Italy* L. Trentadue - *Università di Parma and INFN, Italy* M.I. Konchatnij and N.P. Merenkov - *NSC KIPT, Akademicheskaya 1, Kharkov, 61108, Ukraine*

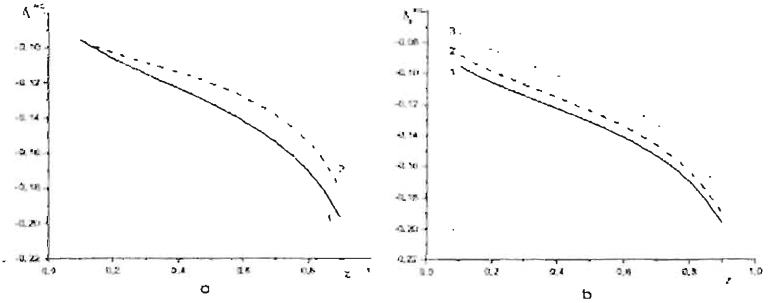

Figure 1: *z–dependence of the quantity* δ_F^{RC} *for small angle events,* $\theta_\gamma < 5°$*: Fig.1a taking into account the restriction (3) (line 2) and the restriction (4) (line 1) for* $x = 1$*; Fig.1b imposing the restriction (4):* $x = 0.2$ *(line 1),* $x = 0.4$ *(line 2),* $x = 0.8$ *(line 3)*

task is solved by means of Monte Carlo event generators, but for some *idealized* conditions the analytical calculations can be performed with high accuracy, that is a very important test for the results produced by Monte Carlo generators.

Since the emitted photon in the reaction (1) is not detected, there is the essential background caused by $\Phi \to \pi^+\pi^-\pi^0$, $\omega \to \pi^+\pi^-\pi^0$ decays. To reject this background it is enough to select the events with small difference between the lost (undetected) energy Ω and the lost 3–momentum modules $|\vec{K}|$

$$\Omega - |\vec{K}| < \eta E \ , \eta << 1 \ , \ \Omega = 2E - E_- - E_+ \ , \ |\vec{K}| = |\vec{p}_+ + \vec{p}_-| \ , \quad (3)$$

where E is the initial beam energy. For $\eta < m_\pi^2/2E^2$ the 3–pion final states are forbidden and then the quantity Ω means the total energy of all emitted photons, $|\vec{K}|$ is the momentum. Taking into account the restriction (3) the first order RC to the Born cross section for the different kinematical region has been calculated in [2] and results are presented in Fig.1a ($\delta_F^{RC} = (H - H^B)/H^B$ with H^B estimated on the Born level and H calculated with the first order photon RC's, $q^2 = 4E^2 z$). As it should be expected this RC is negative since the positive contribution caused by the real photon emission does not compensate the negative one–loop contribution.

The restriction (3) is not artificial since the track mass cut used at

DAΦNE experiments can be written in similar form

$$\Omega - |\vec{K}| < \frac{E\bar{\eta}(x)}{1+z}\ ,\ \bar{\eta}(x) = \frac{4m_\pi \Delta M_{tr}}{E^2}\frac{(x+1)^2}{4x}\ ,\ x = \frac{E_+}{E_-}. \qquad (4)$$

For rough estimation of the RC's with the restriction (4) it is enough to replace $\eta \to \frac{\bar{\eta}(x)}{1+z}$ in the corresponding formulae of [2]. The results for the collinear kinematics are presented in Fig.1b.

References

1. A.B. Arbuzov *et al*, JHEP **12**, 009 (1998); S. Spagnolo, Eur. Phys. J. C **6**, 637 (1999); S. Binner *et al*, Phys. Lett. B **459**, 279 (1999).
2. V.A. Khoze *et al*, Eur. Phys. J. C. **22**, 199 (2002)
3. The KLOE Collaboration, hep–ex/0205046

Frascati Physics Series Vol. XXXI (2003), pp. 461–463
FRONTIERSCIENCE 2002 – Frascati, October 6–11, 2002
Short Communication in Plenary Session

NATIONAL HEP DATA GRID PROJECT IN KOREA

Kihyeon Cho *
CHEP, Kyungpook National University, Daegu 702-701, Korea

1 Introduction

The Center for High Energy Physics(CHEP), Kyungpook National University in Korea plays an important role on international collaborations and cooperation programs for high energy physics in Korea. CHEP also plays a major role on the national HEP Data Grid infrastructure implementation which is supported by the Ministry of Information and Communication (MIC) through KISTI(Korea Institute of Science and Technology Information) for five years starting in 2002.

* On behalf of High Energy Physics Data Grid Working Group in Korea

Table 1: *The network between CHEP in Korea and laboratories abroad.*

Laboratory	Network	Current bandwidth	Future bandwidth
KEK (Japan)	APII	2 x 1 Gbps	10 Gbps (λ)
Fermilab (USA)	APII	45 Mbps	a Gbps level
CERN (EU)	TEIN	10 Mbps	a few Gbps(λ) level

2 The Object of HEP Data Grid Project

The object of HEP Data Grid is to construct the system to manage and process the data which will be produced in the near future. The data should be analyzed even if high energy physicists as users do not know the actual place of data. Therefore, HEP Data Grid is indispensable for future high energy physics activities. 30 high energy physicists and computer engineers in Korea are involved in HEP Data Grid project related with CDF experiment at Fermilab, AMS at the International Space Station, CMS at CERN, PHENIX at BNL and K2K at KEK.

This project also includes the goal of making a regional data center for CMS and AMS experiments and to make a DeCenteralized Analysis Farm in Korea (KCAF) for CDF experiment. CHEP will be a Tier-1 institute and other universities in Korea will be a Tier-2 institute. For networking, we use multi-leveled (Tier) hierarchy of distributed servers to provide transparent access to data. Table 1 shows the network bandwidth between CHEP in Korea and laboratories abroad. We will have the storage of 1,200 TByte Raid disk system, 3.2PByte HPSS system and 1,000 linux CPU clusters for the capability in Regional Data in 2006. This Grid project is related with CERN in EU and Fermilab in USA. The working method for the CERN side is top-down method to construct EU-Data Grid [1] directly by R&D while the working method for the Fermilab side is bottom-up method to start from Central Analysis Farm (CAF) to Fermilab CDF Grid through DeCenteralized Analysis Farm(DCAF).

3 Current Results

Currently we installed EU Data Grid software and made the infrastructure of test-beds. We have successfully tested the Grid software between CHEP and Tier 2 institute (SNU).

For the Fermilab CDF Grid, we have designed a DCAF in Korea (KCAF) as the first step. A job broker will decide at which farm the job will run at the final step. However, KCAF is much more difficult than CAF due to data files which are physically apart by more than 10,000 km. In order to run the remote data which is currently stored in Fermilab, USA, we will use SAM (Sequential data Access via Meta-data) [2] and/or GridFTP [1].

4 Summary

HEP Data Grid activities in Korea are rapidly growing along with Global HEP Data Grid. High Energy Physics Data Grid Working Group in Korea has been contributing the Global High Energy Physics Data Grid in many ways.

References

1. See http://eu-datagrid.web.cern.ch/eu-datagrid/.
2. See http://cdfdb.fnal.gov/sam/.

Participants

ACHARD Pablo	Geneva Univ.	pablo.achard@cern.ch
AGOSTINO Lorenzo	Colorado Univ.	agostino@pizero.colorado.edu
ALEXANDER Jim	Cornell Univ.	jima@lns.cornell.edu
ALFONSI Matteo	INFN-LNF	matteo.alfonsi@lnf.infn.it
ALIMONTI Gianluca	INFN Milano	gianluca.alimonti@mi.infn.it
ARTUSO Marina	Syracuse Univ.	
BASILE Emanuele	INFN-LNF	lelebasile@hotmail.com
BASINI Giuseppe	INFN-LNF	giuseppe.basini@lnf.infn.it
BATTAGLIA Marco	CERN	Marco.Battaglia@Cern.ch
BENCIVENNI Giovanni	INFN-LNF	giovanni.bencivenni@lnf.infn.it
BENUSSI Luigi	INFN-LNF	luigi.benussi@lnf.infn.it
BEREJNOI Alexandre	Moscow Univ.	berezh@al20.inr.troitsk.ru
BERTANI Monica	INFN-LNF	monica.bertani@lnf.infn.it
BERZANO Umberto	Pavia Univ.	umberto.berzano@pv.infn.it
BIANCO Stefano	INFN-LNF	stefano.bianco@lnf.infn.it
BOCCALI Tommaso	Scuola Normale Superiore, Pisa	Tommaso.Boccali@cern.ch
BUCHALLA Gerhard	Munich Univ.	Gerhard.Buchalla@physik.uni-muenchen.de
BUTLER J.	FERMILAB	butler@fnal.gov
CAPONERO Michele A.	ENEA Frascati	caponero@frascati.enea.it
CAPUSSELA Tiziana	Napoli Univ.	
CATALDI Gabriella	INFN - Sezione Lecce	
CESTER Rosanna	INFN Torino	cester@to.infn.it
CHIODINI Gabriele	INFN Milano	chiodini@fnal.gov
CHO Kihyeon	Kyungpook National Univ.	khcho@knu.ac.kr
CHRISTIAN David	FNAL	dcc@fnal.gov
CHRISTIANSEN Tim	Munich Univ.	tim@fnal.gov
CIAFFONI Orlando	INFN-LNF	orlando.ciaffoni@lnf.infn.it
COAN Thomas		
CONETTI Sergio		
COX Brad	Virginia Univ.	cox@uvahed.phys.virginia.edu
DE LUCIA Erika	INFN Roma 1	erika.delucia@roma1.infn.it
DE SANGRO Riccardo	INFN-LNF	riccardo.desangro@lnf.infn.it

DE SIMONE Patrizia	INFN-LNF	patrizia.desimone@lnf.infn.it
DENISOV Sergei	IHEP	denisov@mx.ihep.su
DI NEZZA Pasquale	INFN-LNF	Pasquale.DiNezza@lnf.infn.it
DORIGO Tommaso	INFN Padova	dorigo@pd.infn.it
DOSSELLI Umberto	INFN Padova	
EDERA Laura	Milano Univ.	laura.edera@mi.infn.it
EGEDE Ulrik	Blackett Laboratory	U.Egede@ic.ac.uk
ELLIS John	CERN	john.ellis@cern.ch
EREDITATO Antonio	INFN Napoli	antonio.ereditato@cern.ch
FABBRI Franco Luigi	INFN-LNF	franco.fabbri@lnf.infn.it
FABIANO Nicola	INFN Perugia	Nicola.Fabiano@pg.infn.it
FELLI Ferdinando	Roma 1 Univ.	ffelli@metall.ing.uniroma1.it
FERUGLIO Ferruccio	Padova Univ.	feruglio@pd.infn.it
FINOCCHIARO Giuseppe	INFN-LNF	giuseppe.finocchiaro@lnf.infn.it
FOSTER Brian	Bristol Univ.	
GARCIA BELLIDO Juan	Madrid Univ.	bellido@delta.ft.uam.es
GATTI Claudio	Pisa Univ.	
GIACOBBE Benedetto	INFN Bologna	giacobbe@bo.infn.it
GIANOTTI Paola	INFN-LNF	paola.gianotti@lnf.infn.it
GIROMINI Silvia	INFN-LNF	silvia.giromini@lnf.infn.it
GIVOLETTI M:	CAEN	
GÖBEL Carla	Fisica Inst. Uruguay	gobel@fing.edu.uy
GOSHAW A.	Duke Univ.	
GOTTSCHALK Erik	FERMILAB	erik@fnal.gov
GRIECO F.	CAEN	
HARNEW Neville	Oxford Univ.	n.harnew1@physics.ox.ac.uk
HOHLFELD Marc	Institut für Physik - Mainz	hohlfeld@fnal.gov
ISIDORI Gino	INFN-LNF	gino.isidori@lnf.infn.it
JEITLER Manfred	CERN	manfred.jeitler@cern.ch
KOZANECKI Witold	DAPNIA-SPP, CEA-Saclay	witold@hep.saclay.cea.fr
KUTSCHKE Robert	FERMILAB	kutschke@fnal.gov
KWON Youngjoon	Yonsei Univ.	kwon@phya.yonsei.ac.kr
LA MONACA Andrea	INFN-LNF	andrea.lamonaca@lnf.infn.it
LANFRANCHI Gaia	INFN-LNF	gaia.lanfranchi@lnf.infn.it
LAURELLI Paolo	INFN-LNF	

LEFEVRE Regis	Lab. Physique Corpusculaire	lefevrer@clermont.in2p3.fr
LEVTCHENKO Mikhail	INFN Milano	mikhail.levtchenko@cern.ch
LIGABUE Franco	Scuola Normale Superiore, Pisa	Franco.Ligabue@cern.ch
MAIER Andrew	Siegen Univ.	Andrew.Maier@cern.ch
MARTINELLI Guido	Roma 1 Univ.	
MARTINI Mara	CERN	mara.martini@cern.ch
MATTEUZZI Clara	INFN Milano	clara.matteuzzi@cern.ch
MCBRIDE Patty	FNAL	mcbride@fnal.gov
MELIC Blazenka	Wuerzburg Univ.	melic@physik.uni-wuerzburg.de
MENASCE Dario	INFN Milano	menasce@mi.infn.it
MEYER Andreas	Hamburg Univ.	Andreas.Meyer@desy.de
MONTAGNA Guido	INFN Pavia	Guido.Montagna@pv.infn.it
MORONI Luigi	INFN Milano	
MOULSON Matthew	INFN-LNF	matthew.moulson@lnf.infn.it
MUCCIFORA Valeria	INFN-LNF	valeria.mucciforа@lnf.infn.it
MURTAS Fabrizio	INFN-LNF	fabrizio.murtas@lnf.infn.it
NASON Paolo	INFN Milano	paolo.nason@mib.infn.it
OBERTINO Maria M.	Torino Univ.	obertino@fnal.gov
ORTH Herbert	GSI	h.orth@gsi.de
PACE Elisabetta	INFN-LNF	elisabetta.pace@lnf.infn.it
PALLOTTA Massimo	INFN-LNF	pallotta@lnf.infn.it
PANCHERI Giulia	INFN-LNF	pancheri@lnf.infn.it
PAOLOZZI Antonio	Roma 1 Univ.	
PATEL Popat M.	McGill Univ.	patel@hep.physics.mcgill.ca
PATTERI Piero	INFN-LNF	piero.patteri@lnf.infn.it
PEDRINI Daniele	INFN Milano	
PERFETTO Francesco	Napoli Univ.	
PETRONZIO Roberto	INFN Roma 2	petronzio@roma2.infn.it
PETROV Alexey	Wayne State Univ.	apetrov@physics.wayne.edu
PICCOLO Marcello	INFN-LNF	marcello.piccolo@lnf.infn.it
POLI LENER Marco	INFN-LNF	marco.polilener@lnf.infn.it
RATTI Sergio	INFN Pavia	Sergio.Ratti@pv.infn.it
RAY Ronald	FERMILAB	rray@fnal.gov
REIS Alberto	CBPF	alberto@cbpf.br

ROSS Graham	Oxford Univ.	g.ross1@physics.ox.ac.uk
ROVERE Marco	INFN Milano	marco.rovere@mi.infn.it
RUMERIO Paolo	Northwestern Univ.	rumerio@fnal.gov
RUSS James	Carnegie Mellon Univ.	russ@cmphys.phys.cmu.edu
SAITO Naohito	Kyoto Univ.	saito@nh.scphys.kyoto-u.ac.jp
SALA Silvano	INFN Milano	silvano.sala@mi.infn.it
SAUER Benjamin E.	Sussex Univ.	b.e.sauer@sussex.ac.uk
SAXON David	Glasgow Univ.	d.saxon@physics.gla.ac.uk
SCHMITT Lars	TU-München, Physik, E18	Lars.Schmitt@ph.tum.de
SCHNEIDER Olivier	Lausanne Univ.	Olivier.Schneider@iphe.unil.ch
SCHUNE Marie Helene	LAL	schunem@lal.in2p3.fr
SEGONI Ilaria	Colorado Univ.	segoni@pizero.colorado.edu
SETH Kamal	Northwestern Univ.	KSETH@northwestern.edu
SHEKHOVTSOVA Olga	NSC KIPT	shekhovtsova@kipt.kharkov.ua
SHELDON Paul	Vanderbilt Univ.	paul.sheldon@vanderbilt.edu
SJOLIN Jorgen	Stockholm Univ.	sjolin@physto.se
SOBEL Henry	California Univ.	hsobel@uci.edu
SOKOLOFF Michael D.	Cincinnati Univ.	sokoloff@physics.uc.edu
SPADA Francesca	CERN	francesca.spada@cern.ch
SPADARO Tommaso	INFN-LNF	tommaso.spadaro@lnf.infn.it
STONE Sheldon	Syracuse Univ.	
TIKHONOVA Larissa	SINP MSU	larisa@sinp.msu.su, larisa@npi.msu.su
TOMASSINI Sandro	INFN-LNF	sandro.tomassini@lnf.infn.it
UPLEGGER Lorenzo	INFN Milano	
URALTSEV Nikolai	INFN Milano	Nikolai.Uraltsev@mib.infn.it
VALENTE Paolo	Roma 1 Univ. INFN-LNF	paolo.valente@lnf.infn.it
YAMANAKA Taku	4Osaka Univ.	taku@hep.sci.osaka-u.ac.jp
YARBA Julia	FERMILAB	yarba_j@fnal.gov
YIP Kin	Brookhaven National Lab.	kinyip@bnl.gov
ZALLO Adriano	INFN-LNF	adriano.zallo@lnf.infn.it
ZHU Guohuai	KEK	zhugh@post.kek.jp
ZICHICHI Antonino	Bologna Univ.	

Frascati Physics Series Volumes

Volume I
Heavy Quarks at Fixed Target
Eds. S. Bianco and F.L. Fabbri
Frascati, May 31-June 2, 1993
ISBN 88-86409-00-1

Volume II –Special Issue
Les Rencontres de Physique de la Vallée d'Aoste - Results and Perspectives in Particle Physics
Ed. M. Greco
La Thuile, Aosta Valley, March 5 -11, 1995
ISBN 88-86409-03-6

Volume III
Heavy Quarks at Fixed Target
Ed. B. Cox
University of Virginia, Charlottesville
October 7-10, 1994,
ISBN 88-86409-04-4

Volume IV
Workshop on Physics and Detectors for DAΦNE
Eds. R. Baldini, F. Bossi, G. Capon, G. Pancheri
Frascati, April 4-7, 1995
ISBN 88-86409-05-2

Volume V – Special Issue
Les Rencontres de Physique de la Vallée d'Aoste - Results and Perspectives in Particle Physics
Ed. M. Greco
La Thuile, Aosta Valley, March 3-9, 1996
ISBN 88-86409-07-9

Volume VI
Calorimetry in High Energy Physics
Eds. A. Antonelli, S. Bianco, A. Calcaterra, F.L. Fabbri
Frascati, June 8-14, 1996
ISBN 88-86409-10-9

Volume VII
Heavy Quarks at Fixed Target
Ed. L. Köpke
Rhinefels Castle, St. Goar, October 3-6, 1996
ISBN 88-86409-11-7

Volume VIII
ADONE a milestone on the particle way
Ed. V. Valente – 1997
ISBN 88-86409-12-5

Volume IX – Special Issue
Les Rencontres de Physique de la Vallée d'Aoste – Results and Perspectives in Particle Physics
Ed. M. Greco
La Thuile, Aosta Valley, March 2-8, 1997
ISBN-88-86409-13-3

Volume X
Advanced ICFA Beam Dynamics
Workshop on Beam Dynamics Issue for e^+e^- Factories
Eds. L. Palumbo, G. Vignola
Frascati, October 20-25, 1997
ISBN 88-86409-14-1

Volume XI
Proceedings of the XVIII International Conference on Physics in Collision
Eds. S. Bianco, A. Calcaterra, P. De Simone, F. L. Fabbri
Frascati, June 17-19, 1998
ISBN 88-86409-15-X

Volume XII – Special Issue
Les Rencontres de Physique de la Vallée d'Aoste Results and Perspectives in Particle Physics
Ed. M. Greco
La Thuile, Aosta Valley, March 1-7, 1998
ISBN 88-86409-16-8

Volume XIII
Bruno Touschek and the Birth of the e^+e^-
Ed. G. Isidori
Frascati, 16 November, 1998
ISBN 88-86409-17-6

Volume XIV – Special Issue
Les Rencontres de Physique de la Vallée d'Aoste - Results and Perspectives in Particle Physics
Ed. M. Greco
La Thuile, Aosta Valley, February 28-March 6, 1999
ISBN 88-86409-18-4

Volume XV
Workshop on Hadron Spectroscopy
Eds. T. Bressani, A. Feliciello, A. Filippi
Frascati, March 8–2 1999
ISBN 88-86409-19-2

Volume XVI
Physics and Detectors for DAΦNE
Eds. S. Bianco, F. Bossi, G. Capon, F.L. Fabbri, P. Gianotti, G. Isidori, F. Murtas
Frascati, November 16-19, 1999
ISBN 88-86409-21-4

Volume XVII – Special Issue
Les Rencontres de Physique de la Vallée d'Aoste - Results and Perspectives in Particle Physics
Ed. M. Greco
La Thuile, Aosta Valley, February 27 –March 4, 2000
ISBN 88-86409-23-0

Volume XVIII
LNF Spring School
Ed. G. Pancheri
Frascati 15-20 May, 2000
ISBN 88-86409-24-9

Volume XIX
XX Physics in Collision
Ed. G. Barreira
Lisbon June 29-July 1st. 2000
ISBN 88-86409-25-7

Volume XX
Heavy Quarks at Fixed Target
Eds. I. Bediaga, J. Miranda, A. Reis
Rio de Janeiro, Brasil, October 9-12, 2000
ISBN 88-86409-26-5

Volume XXI
IX International Conference on Calorimetry in High Energy Physics
Eds. B. Aubert, J. Colas, P. Nédélec, L. Poggioli
Annecy Le Vieux Cedex, France, October 9-14, 2000
ISBN 88-86409-27-3

Volume XXII –Special Issue
Les Rencontres de Physique de la Vallée d'Aoste - Results and Perspectives in Particle Physics
Ed. M. Greco
La Thuile, Aosta Valley, March 4-10 , 2001
ISBN 88-86409-28-1

Volume XXIII
XXI Physics in Collision
Ed. Soo-Bong Kim
Seoul, Korea, June 28 –30, 2001
ISBN 88-86409-30-3

Volume XXIV
International School of Space Science –2001 Course on: Astroparticle and Gamma-ray Physics in Space
Eds. A. Morselli, P. Picozza
L'Aquila, Italy, August 30 –September 7, 2000
ISBN 88-86409-31-1

Volume XXV
TRDs for the 3rd Millennium Workshop on Advanced Transition Radiation Detectors for Accelerator and Space Applications
Eds. N. Giglietto, P. Spinelli
Bari, Italy, September 20-23, 2001
ISBN 88-86409-32-X

Volume XXVI
KAON 2001
International Conference on CP Violation
Eds. F. Costantini, G. Isidori, M. Sozzi
Pisa Italy, June 12th –17th, 2001
ISBN 88-86409-33-8

Volume XXVII – Special Issue
Les Rencontres de Physique de la Vallée d'Aoste - Results and Perspectives in Particle Physics
Ed. M. Greco
La Thuile, Aosta Valley, March 3-9, 2002
ISBN 88-86409-34-6

Volume XXVIII
Heavy Quarks at Leptons 2002
Eds. G. Cataldi, F. Grancagnolo, R. Perrino, S. Spagnolo
Vietri sul mare (Italy), May 27th – June 1st, 2002
ISBN 88-86409-35-4

Volume XXIX
Workshop on Radiation Dosimetry: Basic Technologies, Medical Applications, Environmental Applications
Ed. A. Zanini
Rome (Italy), February 5–6, 2002
88-86409-36-2

Volume XXX Special Issue
Les Rencontres de Physique de la Vallée d'Aoste - Results and Perspectives in Particle Physics
M. Greco
La Thuile, Aosta Valley, March 9-15, 2003
in progress